MATHEMATICAL MODELING OF ENDOCRINE SYSTEMS

EDITED BY: Darko Stefanovski, Giovanni Pacini and Ray Boston
PUBLISHED IN: Frontiers in Endocrinology

frontiers Research Topics

ISSN 1664-8714
ISBN 978-2-88971-942-6
DOI 10.3389/978-2-88971-942-6

About Frontiers

Frontiers is more than just an open-access publisher of scholarly articles: it is a pioneering approach to the world of academia, radically improving the way scholarly research is managed. The grand vision of Frontiers is a world where all people have an equal opportunity to seek, share and generate knowledge. Frontiers provides immediate and permanent online open access to all its publications, but this alone is not enough to realize our grand goals.

Frontiers Journal Series

The Frontiers Journal Series is a multi-tier and interdisciplinary set of open-access, online journals, promising a paradigm shift from the current review, selection and dissemination processes in academic publishing. All Frontiers journals are driven by researchers for researchers; therefore, they constitute a service to the scholarly community. At the same time, the Frontiers Journal Series operates on a revolutionary invention, the tiered publishing system, initially addressing specific communities of scholars, and gradually climbing up to broader public understanding, thus serving the interests of the lay society, too.

Dedication to Quality

Each Frontiers article is a landmark of the highest quality, thanks to genuinely collaborative interactions between authors and review editors, who include some of the world's best academicians. Research must be certified by peers before entering a stream of knowledge that may eventually reach the public - and shape society; therefore, Frontiers only applies the most rigorous and unbiased reviews.
Frontiers revolutionizes research publishing by freely delivering the most outstanding research, evaluated with no bias from both the academic and social point of view. By applying the most advanced information technologies, Frontiers is catapulting scholarly publishing into a new generation.

What are Frontiers Research Topics?

Frontiers Research Topics are very popular trademarks of the Frontiers Journals Series: they are collections of at least ten articles, all centered on a particular subject. With their unique mix of varied contributions from Original Research to Review Articles, Frontiers Research Topics unify the most influential researchers, the latest key findings and historical advances in a hot research area! Find out more on how to host your own Frontiers Research Topic or contribute to one as an author by contacting the Frontiers Editorial Office: frontiersin.org/about/contact

MATHEMATICAL MODELING OF ENDOCRINE SYSTEMS

Topic Editors:
Darko Stefanovski, University of Pennsylvania, United States
Giovanni Pacini, Institute of Neurosciences, Italian National Research Council, Italy
Ray Boston, University of Pennsylvania, United States

Citation: Stefanovski, D., Pacini, G., Boston, R., eds. (2021). Mathematical Modeling of Endocrine Systems. Lausanne: Frontiers Media SA.
doi: 10.3389/978-2-88971-942-6

Table of Contents

04 ***Editorial: Mathematical Modeling of Endocrine Systems***
Darko Stefanovski, Giovanni Pacini and Ray C. Boston

06 ***Origins and History of the Minimal Model of Glucose Regulation***
Richard N. Bergman

18 ***Mathematical Modeling and Simulation Provides Evidence for New Strategies of Ovarian Stimulation***
Sophie Fischer, Rainald Ehrig, Stefan Schäfer, Enrico Tronci, Toni Mancini, Marcel Egli, Fabian Ille, Tillmann H. C. Krüger, Brigitte Leeners and Susanna Röblitz

28 ***Model-Based Assessment of C-Peptide Secretion and Kinetics in Post Gastric Bypass Individuals Experiencing Postprandial Hyperinsulinemic Hypoglycemia***
Michele Schiavon, David Herzig, Matthias Hepprich, Marc Y. Donath, Lia Bally and Chiara Dalla Man

38 ***Insulin Action, Glucose Homeostasis and Free Fatty Acid Metabolism: Insights From a Novel Model***
Darko Stefanovski, Naresh M. Punjabi, Raymond C. Boston and Richard M. Watanabe

46 ***Mathematical Model of Glucagon Kinetics for the Assessment of Insulin-Mediated Glucagon Inhibition During an Oral Glucose Tolerance Test***
Micaela Morettini, Laura Burattini, Christian Göbl, Giovanni Pacini, Bo Ahrén and Andrea Tura

57 ***An Analysis of Glucose Effectiveness in Subjects With or Without Type 2 Diabetes* via *Hierarchical Modeling***
Shihao Hu, Yuzhi Lu, Andrea Tura, Giovanni Pacini and David Z. D'Argenio

68 ***Selenium Kinetics in Humans Change Following 2 Years of Supplementation With Selenomethionine***
Blossom H. Patterson, Gerald F. Combs Jr, Philip R. Taylor, Kristine Y. Patterson, James E. Moler and Meryl E. Wastney

79 ***Modeling Challenge Data to Quantify Endogenous Lactate Production***
Darko Stefanovski, Pamela A. Wilkins and Raymond C. Boston

87 ***Adapting Protocols or Models for Use in Insulin-Requiring Diabetes and Islet Transplant Recipients***
Glenn M. Ward, Jacqueline M. Walters, Judith L. Gooley and Raymond C. Boston

frontiers in Endocrinology

EDITORIAL
published: 04 November 2021
doi: 10.3389/fendo.2021.789386

Editorial: Mathematical Modeling of Endocrine Systems

Darko Stefanovski[1]*, *Giovanni Pacini*[2] *and Ray C. Boston*[3]

[1] Clinical Studies-New Bolton Center, School of Veterinary Medicine, University of Pennsylvania, Philadelphia, PA, United States, [2] Institute of Neurosciences, Italian National Research Council, Padova, Italy, [3] University of Pennsylvania, Philadelphia, PA, United States

Keywords: mathematical modeling and simulation, selenium, free fatty acid (FA) metabolism, glucose metabolism, glucagon kinetics, ovarian simulations, insulin secretion, minimal model of glucose metabolism

Editorial on the Research Topic:

Mathematical Modeling of Endocrine Systems

Mathematical modeling is a process for formulating a set of equations to simultaneously represent a system's structure and behavior. While in the majority of cases, the equations of the mathematical model are non-linear and designated using ordinary differential equations (ODEs), this does not exclude either models that are as simple as a single linear equation or even a more complex set of hundreds of partial differential equations (PDEs). A "system" that is subjected to modeling can include several organ systems or be as limited to focusing only on a specific interaction between cells. Sometimes the model can even focus on a single cell, or on an entire cell line.

Commonly, in scientific endeavors, the inception of models starts with observations: or more specifically, with a set of samples taken over time from a single entity (subject, animal, tissue sample, or cells) or perhaps following the system's response to a perturbation. The aim is inevitably to build a mathematical account that responds to the observed data of the underlying biological system. Thus, models offer insights into the mechanisms and signal transduction pathways, and provide the bedrock for hypothesis-generating research. Furthermore, the parameters of the model may conveniently serve as biomarkers of specific biological mechanisms, or of patho-physiological states.

We are very enthusiastic to have in this special modeling edition a vibrant and informative historical account of the development of one of the most successful and widely used mathematical models of a biological system: i.e., the Minimal Model of Glucose Kinetics. The original developer, Dr. Richard N. Bergman, outlines the merits of the model, which indeed the great majority of the investigators from the listed authors of this Research Topic have, for more than 15 years, used in their metabolic research projects. Some have also been responsible (the three editors included) for the release of automated computational tools to perform frequently sampled IVGTT data analyses for the rapid, and precise, estimation of Insulin Sensitivity and Glucose Effectiveness.

As the title of this Research Topic suggests, the aim of this collection of papers is to provide interesting and novel information on various facets of mathematical modeling of endocrine systems. Four articles focus on various aspects of mathematical modeling of endocrine control of glucose metabolism. Morettini et al. investigate glucagon kinetics and its relationship with insulin during an oral glucose challenge (OGTT); using the output from a simple model, they are able to assess pancreatic alpha-cell sensitivity to insulin. Schiavon et al. describe the issues encountered with modeling insulin secretion using a model of C-peptide kinetics in post gastric bypass patients with Type 2 Diabetes. Ward et al. describe the modifications needed in mathematical models of insulin

OPEN ACCESS

Edited and reviewed by:
Ruth Andrew,
University of Edinburgh,
United Kingdom

***Correspondence:**
Darko Stefanovski
sdarko@vet.upenn.edu

Specialty section:
This article was submitted to Systems Endocrinology, a section of the journal Frontiers in Endocrinology

Received: *04 October 2021*
Accepted: *21 October 2021*
Published: *04 November 2021*

Citation:
Stefanovski D, Pacini G and Boston RC (2021) Editorial: Mathematical Modeling of Endocrine Systems. Front. Endocrinol. 12:789386. doi: 10.3389/fendo.2021.789386

secretion/kinetics, and in glucose metabolism, to use data obtained with islet transplant recipients with Type 1 Diabetes. The work by Hu et al. (D'Argenio's group) focuses on the successful integration of mathematical models, and hierarchical statistical models, to obtain more accurate population estimates of Glucose Effectiveness, which – together with Insulin Sensitivity – characterizes the glucose dynamics during glucose challenges.

An article from Boston's group delves into problems linked to automatically, and accurately quantifying the manifest features of lactate infusions: these are essential to gain insights into the persistence of both exogenous and endogenous lactate in conjunction with such challenges.

Work by Stefanovski et al. describes the development of a novel model of whole-body FFA kinetics, and this enables the estimation of insulin action in regard to adipose tissue. Indeed, the model actually quantifies the ability of insulin to rapidly suppress lipolysis during the frequently sampled IVGTT.

The article from Patterson et al. covers the development of a model of Selenium (Se), in regard to both endocrine, and to immune, systems. The report estimates the kinetics of Se before and after 2 years of Se administration.

The work of Fischer et al. outlines previously developed models of the menstrual cycle that are capable of simulating control administrations, including, for example, ovarian contraception pills, and GnRH analogs. These can then be used for *in-silico* experiments that may help to improve ovarian stimulation.

We sincerely hope that the contributions outlined above will show how your own future interests in applying mathematical modeling methods might help advance new challenges in kinetic investigations for you. Looking forward to these efforts, we would also like to remind you of the importance of using mathematical models *per se* … while simulation and additional *in-vivo* studies can provide evidence of the validity and repetability of a model, it is the continuous use of models by the general scientific community that will assure their reliability and robustness.

AUTHOR CONTRIBUTIONS

All authors listed have made a substantial, direct, and intellectual contribution to the work and approved it for publication.

Conflict of Interest: The authors declare that the research was conducted in the absence of any commercial or financial relationships that could be construed as a potential conflict of interest.

Publisher's Note: All claims expressed in this article are solely those of the authors and do not necessarily represent those of their affiliated organizations, or those of the publisher, the editors and the reviewers. Any product that may be evaluated in this article, or claim that may be made by its manufacturer, is not guaranteed or endorsed by the publisher.

frontiers in Endocrinology

ORIGINAL RESEARCH
published: 15 February 2021
doi: 10.3389/fendo.2020.583016

Origins and History of the Minimal Model of Glucose Regulation

Richard N. Bergman *

Diabetes and Obesity Research Institute, Cedars-Sinai Medical Center, Los Angeles, CA, United States

It has long been hoped that our understanding of the pathogenesis of diabetes would be helped by the use of mathematical modeling. In 1979 Richard Bergman and Claudio Cobelli worked together to find a "minimal model" based upon experimental data from Bergman's laboratory. Model was chosen as the simplest representation based upon physiology known at the time. The model itself is two quasi-linear differential equations; one representing insulin kinetics in plasma, and a second representing the effects of insulin and glucose itself on restoration of the glucose after perturbation by intravenous injection. Model would only be sufficient if it included a delay in insulin action; that is, insulin had to enter a remote compartment, which was interstitial fluid (ISF). Insulin suppressed endogenous glucose output (by liver) slowly. Delay proved to be due to initial suppression of lipolysis; resultant lowering of free fatty acids reduced liver glucose output. Modeling also demanded that normalization of glucose after injection included an effect of glucose itself on glucose disposal and endogenous glucose production – these effects were termed "glucose effectiveness." Insulin sensitivity was calculated from fitting the model to intravenous glucose tolerance test data; the resulting insulin sensitivity index, SI, was validated with the glucose clamp method in human subjects. Model allowed us to examine the relationship between insulin sensitivity and insulin secretion. Relationship was described by a rectangular hyperbola, such that Insulin Secretion x Insulin Sensitivity = Disposition Index (DI). Latter term represents ability of the pancreatic beta-cells to compensate for insulin resistance due to factors such as obesity, pregnancy, or puberty. DI has a genetic basis, and predicts the onset of Type 2 diabetes. An additional factor was clearance of insulin by the liver. Clearance varies significantly among animal or human populations; using the model, clearance was shown to be lower in African Americans than Whites (adults and children), and may be a factor accounting for greater diabetes prevalence in African Americans. The research outlined in the manuscript emphasizes the powerful approach by which hypothesis testing, experimental studies, and mathematical modeling can work together to explain the pathogenesis of metabolic disease.

Keywords: diabetes, metabolism, mathematical model, disposition index, insulin clearance, glucose effectiveness

OPEN ACCESS

Edited by:
Darko Stefanovski, University of Pennsylvania, United States

Reviewed by:
Kalyan C. Vinnakota, Gilbert Family Foundation, United States
Adrian Vella, Mayo Clinic, United States

***Correspondence:**
Richard N. Bergman
richard.bergman@cshs.org

Specialty section:
This article was submitted to Systems Endocrinology, a section of the journal Frontiers in Endocrinology

Received: *13 July 2020*
Accepted: *22 December 2020*
Published: *15 February 2021*

Citation:
Bergman RN (2021) Origins and History of the Minimal Model of Glucose Regulation. Front. Endocrinol. 11:583016. doi: 10.3389/fendo.2020.583016

EARLY THOUGHTS AND PERSONAL ISSUES

Mathematical modeling of physiological systems gained interest in the early 1950's. One of the earliest models in the metabolic field was that of Bolie, who represented the glucose/insulin relationship in terms of two simple equations (1). During the same period, more complex models were introduced. One example is Guyton's model of the cardiovascular system (2). It was Guyton's goal to include all (at the time) known information regarding the known physiology of the cardiovascular system, and he included additional interactions which emanated from his own work (**Figure 1**). While Guyton and colleagues were able to gain much insight from this work, the model was not usable by the scientific or medical communities, in view of its great complexity.

My own background was as an electrical engineer. I was virtually without training in the biological sciences. This changed due to interaction with Professor Oscar Hechter (my uncle by marriage) of the Worcester Foundation of Experimental Biology. Hechter suggested I contact John Urquhart of the University of Pittsburgh; John along with F. Eugene Yates, were pioneers of modeling of endocrine systems. Their electromechanical model of the adrenocortical system remains a classic (3). I joined Urquhart's lab despite my lack of education in the biological sciences. He was patient, and he taught me much about experimental physiology. At Pitt, I came in contact with I. Arthur Mirsky, who was a giant of the field of carbohydrate metabolism. I made a major life decision; I believed that mathematical modeling of carbohydrate metabolism could in the end be even more important for patient care.

I therefore chose to study, for my PhD thesis, not modeling of the adrenocortical system, but modeling of the endocrine pancreas. I developed the cross-perfused pancreas system so I could measure the *dynamics* of insulin release from the endocrine pancreas (4). In fact, I believe that we were the first to discover that insulin release from the isolated pancreas was *biphasic* (**Figure 2**). Gerald Grodsky confirmed this result in the rat (5). For my PhD thesis, I developed one of the first mathematical models of pancreatic insulin secretion (**Figure 3**).

I was unfortunate (probably fortunate) that my PhD advisor abandoned our lab, setting me out for the first time as a truly independent investigator, although I was still a 22-year-old graduate student. I later followed John Urquhart to the University of Southern California Department of Biomedical Engineering. (It was very difficult to publish modeling papers in the standard endocrine or physiology literature at the time).

ORIGIN OF THE MINIMAL MODEL

In the context of "Frontiers in Physiology," it is of interest to remember the resistance of the endocrine community to models in general. In fact, Departments of Physiology (at least in the United States) were highly suspicious of modeling studies in the 1970s. In part, this was due to a history of investigators who would propose models, but not test them in the laboratory (6); such models often "died on the vine". Personally, I was determined to combine modeling with rigorous experimental testing—an approach our laboratory continues to apply to this day. (I identified with George Gershwin, dedicated to make a "Gentleman out of Jazz". Maybe we could help make a "Gentleman out of Modeling" in carbohydrate regulation).

During the first decade of my independent laboratory (1971–1980), we introduced several disparate models, such as a differential equation model of insulin secretion (discussed above), a "random hit" statistical representation of hormone binding and activation (7), and a differential equation model of

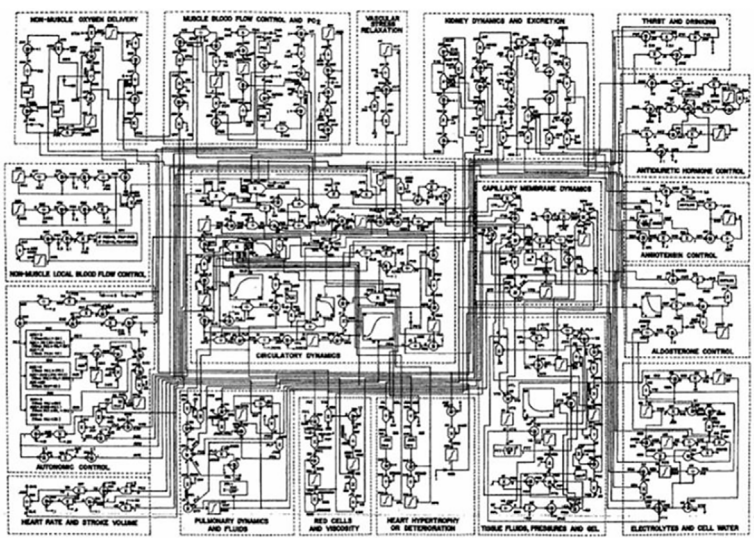

FIGURE 1 | Guyton model of the cardiovascular system.

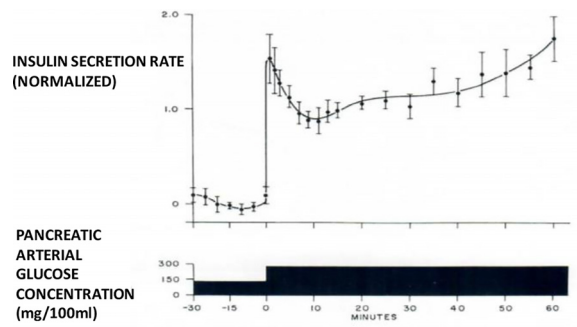

FIGURE 2 | Biphasic insulin release from perfused pancreas.

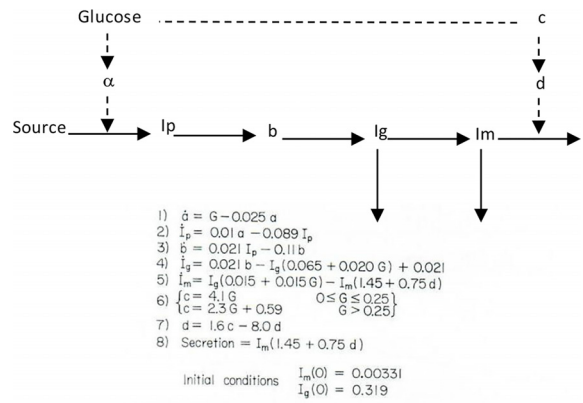

FIGURE 3 | Bergman model of insulin secretion.

liver glycogen metabolism (8). However, one model that has survived the test of time is the so-called "minimal model" of carbohydrate metabolism.

I was approached by Alberto Salvan at the International Endocrine Society meeting in Copenhagen and invited to visit Padova, Italy. Alberto was sent by Claudio Cobelli, the young "star" of the Bioengineering Department at the University of Padova. I went to Padova and introduced Claudio to my original concept—I argued that previous models of physiological systems (particularly carbohydrate metabolism) were less than useful because they were either too complex (their parameters could not be uniquely specified from data) or too simplistic to accurately account for the data available. I also argued that the effort had not yet been put forth to obtain data which made it possible to make intelligent model design. Thus, in my laboratory at Northwestern University (I was there in Bioengineering from 1976 to 1979), I encouraged my graduate student, Y. Ziya Ider, to obtain a data set which we could use as a *basis* for modeling the regulation of the glucose level. At the time, the clinical tests of metabolism included the oral glucose tolerance test and the intravenous glucose tolerance test (IVGTT); both included glucose ingestion—oral or intravenous infusion—with infrequent (~1/h) sampling. We reasoned that more frequent sampling was necessary to reveal the actual patterns of glucose and insulin which resulted from carbohydrate administration. Indeed, performing the IVGTT and *sampling every minute for 180 min* (**Figure 4**) revealed that the time course of glucose and insulin after intravenous administration was more complex than revealed by the previously used hourly sampling (9). This choice of frequent sampling after glucose injection was a critical choice. It revealed that the return of glucose to basal (by 180 min) could be described by four temporal phases (**Figure 5**): a mixing phase of glucose in plasma, a quasi-exponential phase (see below, "glucose effectiveness") an *acceleration* of the glucose decline (reflecting the action of insulin) followed by glucose's return to pre-injection value (10).

CONCEPTS UNDERLYING THE MINIMAL MODEL

With this limited data base (**Figure 4**), Claudio Cobelli came to Evanston IL, and we began to build the model. This was a critical period; the manuscript emerging from the 6 weeks of work in the summer of 1978 was entitled "Quantitative estimation of insulin sensitivity (9)". It is of interest that this seminal paper has been cited over 2,000 times; ironically, it remained virtually uncited for the first 10 years after publication.

Our basic goal was to find a "minimal model". This would be a mathematical construct which was 1) based upon known physiological principles, 2) sufficiently complex to account for the intravenous data we obtained in our laboratory, and 3) simple enough that the model parameters could be calculated *from a single IVGTT performed in a single individual.*

PARTITION ANALYSIS

We envisioned glucose regulation as a closed loop system (**Figure 6**), including glucose production and uptake, and insulin release from the pancreatic β-cells. Glucagon was not included in our original representation. However, we faced a serious dilemma: we knew from our previous work that it would be a great challenge to model insulin release from the endocrine pancreas. Therefore, we applied the principle of "partition analysis (11)"; we would treat the plasma insulin concentration as an "input" to the tissues producing and utilizing glucose, and the plasma glucose as the "output," reflecting the effect of the known insulin on the turnover of glucose. This approach allowed us to model just the insulin-sensitive tissues, while obviating the difficult problem of modeling insulin secretion from the β-cells.

CHOICE OF THE MODEL

Two approaches were possible—defining a complex model (representing all known physiology) and simplifying it, or choosing the simplest conceptual model, asking if it could account for the known data (**Figure 4**), and systematically introducing complexity until a best model could be found. The

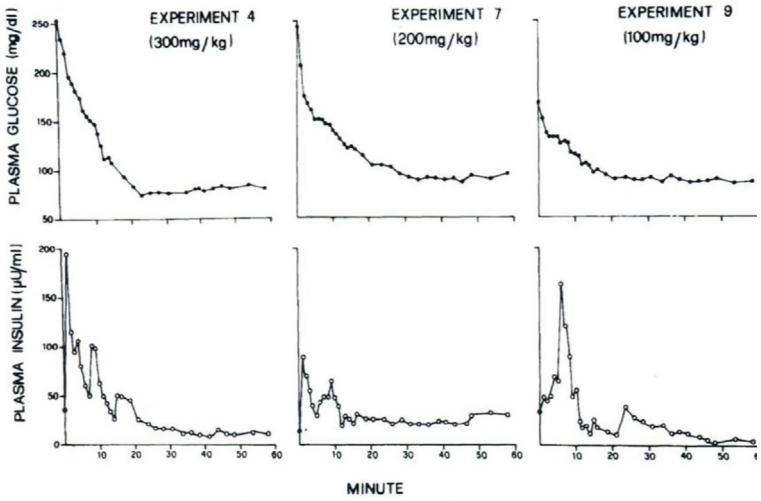

FIGURE 4 | Early IVGTTs with frequent blood sampling.

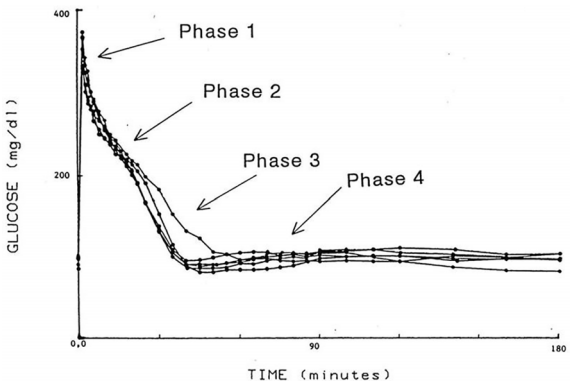

FIGURE 5 | IVGTT phases.

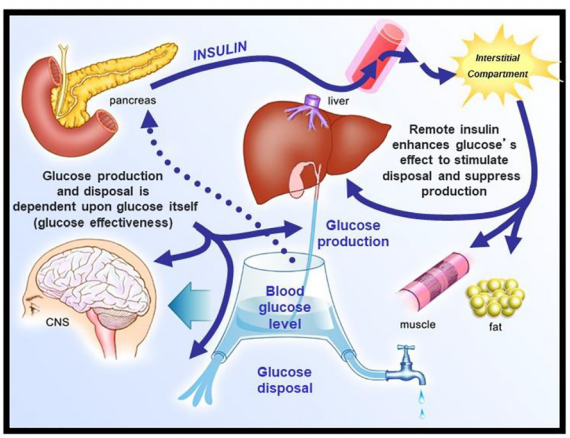

FIGURE 6 | Closed loop system of glucose regulation.

models we tested are in **Figure 7**. Note that the simplest model was glucose first order decay with no explicit insulin action; in Model 2 Michaelis Menten disappearance was added. Two compartment glucose distribution was added in Model 3. When we attempted to account for insulin glucose dynamics, we learned something very important: *it was not possible to account for glucose kinetics without a delay in insulin's effects to increase glucose utilization and suppress glucose production*. As we shall see, further experimental studies which resulted from this realization that insulin's effects were delayed in time had very important ramifications regarding insulin action *in vivo*. The model we finally chose, Number 6 in **Figure 7**, was therefore accepted as the minimal model of glucose utilization, and it remains the accepted model to this day.

Equations of the minimal model can be explained as follows (**Figure 8**): the model accounts for the return of glucose to the basal value after injection. As we had discovered that insulin's effect had to be delayed, we assumed that insulin acts from a compartment *remote from plasma*. We hypothesized that the delay in insulin action could be due to a slow rate of movement of insulin from plasma to interstitial fluid (ISF), the latter bathing skeletal muscle. To test this concept, we performed a series of euglycemic clamp experiments in which we measured insulin in blood and in skeletal muscle lymph fluid, the latter as a surrogate of ISF (12–14). We discovered that the rate of glucose disposal was directly related to ISF insulin level, proving that the delay in insulin action *in vivo* is indeed explained by the slow transport of the hormone from the blood to the ISF (**Figure 9**).

One question that arose was why the modeling was acceptable with delays not only in insulin stimulation of glucose disposal (mediated by interstitial insulin) but also with *slow insulin suppression of endogenous glucose production (EGP)*. It was

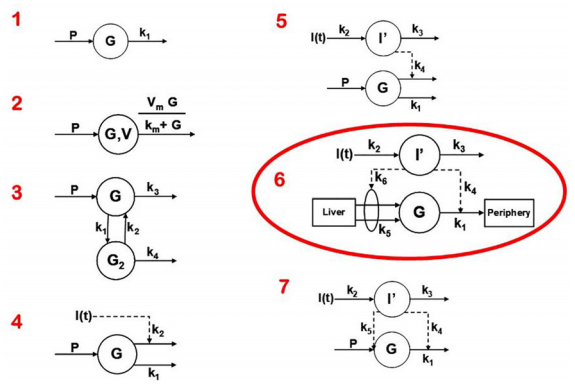

FIGURE 7 | Models tested to determine "optimal" degree of complexity. Model 6 was chosen and was designated the "minimal model."

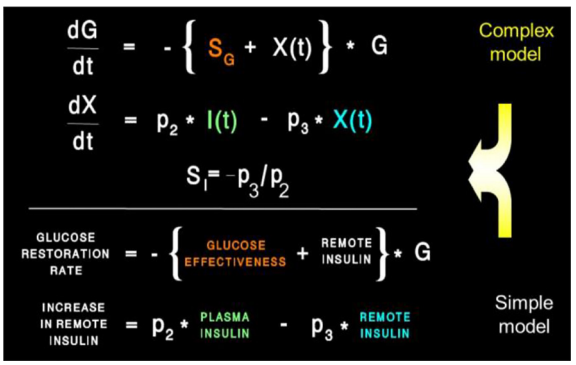

FIGURE 8 | Equations of the minimal model and their "translation."

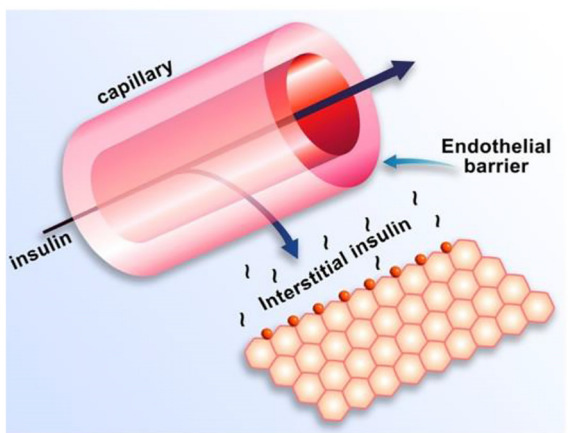

FIGURE 9 | Schematic of insulin transport from blood to interstitial fluid.

known at the time that the binding of insulin to liver was very rapid. Why, then, was the effect of insulin to suppress glucose production similarly retarded as the disposal effect (15)? Possibly, insulin acted to suppress the liver not directly, but *indirectly via* a tissue remote from the liver. In fact, we hypothesized that insulin's effect on the liver was mediated by free fatty acids (FFA); once insulin is infused, the hormone suppressed lipolysis in adipose tissue, and the resulting lowering of FFA acted to lower liver glucose production. In a series of studies carried out by Kerstin Rebrin and Garry Steil, we showed that not only was there a strong correlation between FFA suppression and the suppression of EGP, but that preventing the FFA suppression by infusion of intralipid prevented the decline in EGP (16, 17). Thus, we believe that the slow movement of insulin into ISF in adipose tissue was rate-limiting for the effect of insulin to suppress EGP; therefore, it was not necessary to include rapid suppression of EGP in the model to account for glucose dynamics *in vivo*.

Insulin kinetics in the minimal model are represented by equation 2; this first-order equation assumes that secreted insulin enters the ISF compartment where it is represented by variable "X," which we now know to represent interstitial insulin. ISF insulin then exits the remote compartment by a first-order process. Glucose dynamics are represented in the first equation; the rate of return of glucose to basal following injection was envisioned to have an insulin-dependent component [in proportion to variable X(t), or ISF insulin]. Also, to model the data, it was *requisite* that glucose could return to basal also in proportion to its own concentration, driven by a term we referred to as parameter S_G, which we named "glucose effectiveness." *Glucose effectiveness is the ability of glucose* per se *to normalize its own concentration*. We showed that the minimal model was able to account for the dynamics of glucose observed after injection.

INSULIN RESISTANCE

There has been a debate, going back decades, regarding the relative importance of insulin resistance versus β-cell failure in the pathogenesis of Type 2 diabetes mellitus. To address this issue, we felt it necessary to attempt to measure these factors from the glucose tolerance test. Applying the minimal model to the IVGTT, is it possible to access a measure of insulin resistance? Examination of the model (**Figure 8**) showed that two factors determined the ability of glucose to normalize after glucose injection—insulin action, represented by the parameter S_I, and glucose effectiveness (S_G), which accounts for glucose's ability to self-normalize. Represented mathematically, insulin sensitivity is given as the partial derivative of glucose disappearance on glucose and insulin. It was easy to demonstrate that this relationship results in the ratio of two parameters of the minimal model: p3/p2. Thus, we showed S_I, the "insulin sensitivity index", to be equal to the ratio of these parameters from the minimal model. This index appears in over 2,000 publications.

INSULIN SENSITIVITY INDEX: IS IT ACCURATE?

The accuracy of the S_I was questioned by Reaven and colleagues (18). They claimed that in insulin resistant subjects, particularly insulin resistant patients with inadequate insulin response, the insulin sensitivity index from the minimal model correlated poorly with insulin sensitivity calculated from the euglycemic glucose clamp. Reaven's manuscript, which appeared to be a blow to the minimal model method, was actually a godsend. We realized that a greater insulin pattern in blood would be necessary to accurately calculate insulin sensitivity from the IVGTT in resistant subjects. We therefore modified the IVGTT profile by adding an injection of the insulin secretagogue tolbutamide 20 min after glucose (**Figure 10**). Later the protocol was changed to inject insulin itself at 20 min after glucose, rather than tolbutamide (19).

VALIDATION OF S_I

It is generally assumed that the euglycemic glucose clamp (EGC) is the "gold standard" for the estimation of insulin sensitivity. Because most endocrinologists are not familiar with mathematical modeling, and may not trust modeling, it was of interest to validate the insulin sensitivity of the minimal model experimentally versus the clamp.

Validation studies were first carried out in the dog, where a significant correlation was observed between S_I and insulin sensitivity calculated from the EGC [r = 0.82, (20)]. This result was confirmed in human volunteers by Beard et al. (21). These studies alone supported the use of the IVGTT-based S_I for a *relative* measure of insulin sensitivity. However, the question naturally arose as to whether the IVGTT was measuring the *same physiological process* as the glucose clamp. Therefore, in collaboration with Jerrold Olefsky and colleagues, we compared minimal model values against the clamp (22). More important, we asked whether we could determine the IVGTT sensitivity values for a cohort of human subjects, and then determine what the clamp-based measures were in the same subjects. The strong correlation between IVGTT and clamp not only validated the IVGTT method, *but also demonstrated equivalency with the clamp*, when data from the two methods were expressed in identical units. We showed that insulin sensitivity from the clamp, defined as change in glucose disposal (ΔRd) induced with a measured change in plasma insulin (ΔI) per steady state glucose value [= ΔRd/(ΔI x G)], normalized by body surface area, was directly comparable to minimal model-derived S_I times the body distribution volume (S_I x V_D). In fact, correlation in a group of individuals of varying body mass index was excellent; more important, the relationship had a slope not different from 1.0, and the regression line passed through the origin, demonstrating a lack of bias (**Figure 11**). These multiple validation studies supported the use of the IVGTT with minimal modeling as a potent tool to be used to study insulin action *in vivo* in large animals or human volunteers.

THE DISPOSITION INDEX (DI)

As previously stated, a debate regarding the relative importance of insulin resistance versus β-cell dysfunction in the pathogenesis of Type 2 diabetes raged for decades (23, 24). With the minimal model in hand, we hoped to contribute to help resolve this debate. We became interested not only in the measurement of insulin sensitivity and insulin release, *but the relationship between the two*. We hypothesized that in the face of insulin

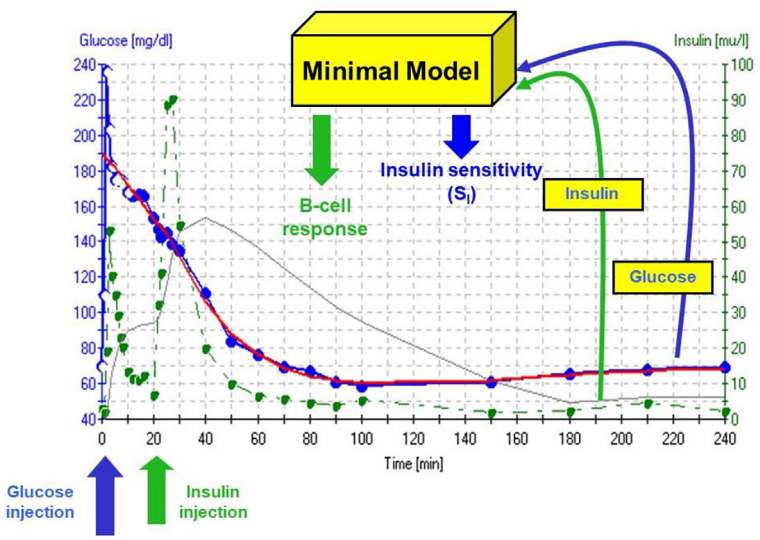

FIGURE 10 | IVGTT protocol and minimal model output. Insulin data are"input" to the minimal model, which determines the best fit of the glucose dynamics and model parameters for that IVGTT.

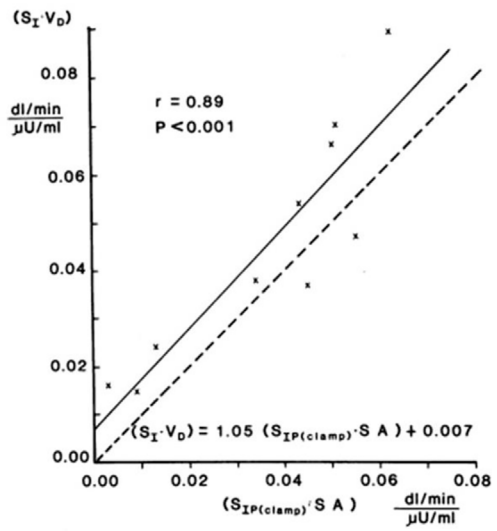

FIGURE 11 | S_I equivalence between minimal model and clamp.

resistance, β-cell function would improve, and thus resist any change in glucose tolerance (**Figure 12**). We quantified this hypothesis as what became known as the "Hyperbolic Law of Glucose Tolerance (25)".

This law can be stated as the following equation of a rectangular hyperbola:

$$S_I \times AIR_{glucose} = DI$$

in which S_I is insulin sensitivity, as discussed above, $AIR_{glucose}$ is the first phase response of plasma insulin to the glucose injection, and DI was named the "Disposition Index".

After defining the hyperbolic relationship, we applied it to human subjects (26). It was shown that the *product* of insulin secretory response (which can be assessed as the first phase insulin response to glucose injection) multiplied by insulin sensitivity would be approximately constant in normal individuals. While initially controversial, the DI has now been accepted overwhelmingly by the diabetes community as the most accurate measure of β-cell function, and it has been cited in almost 1,000 publications as of this writing (**Figure 13**).

The DI represents the ability of the islet cells to *compensate* for insulin resistance. The resistance can be due to a variety of environmental changes, including obesity, pregnancy, and PCOS. The β-cells act to compensate, and under normal conditions prevent the frankly diabetic state. This is shown clearly in pregnancy, where severe insulin resistance in the third trimester is compensated by a massive islet cell response; glucose tolerance remains normal (27). Epidemiological studies have demonstrated that lower DI is a strong predictor of future diabetes (28, 29), and genetic studies have identified predictive variants related to DI (30). Weyer and colleagues showed in Pimas that lower DI predicts decline to Type 2 diabetes, whereas higher DI is protective [**Figure 14**; (31)]. It is of interest to remember that the DI emerged as a "child" of the minimal model itself; once it was possible to measure insulin sensitivity from the IVGTT, it was only natural to consider the relation to pancreatic islet cell function.

An unanswered question that remains is the underlying mechanism accounting for the hyperbolic relationship. We followed the development of enhanced insulin secretory response in normal dogs, demonstrating that the hyperbolic relationship is a *dynamic* one, as insulin response increased in proportion to insulin resistance (32). Experiments to identify the blood-borne signal responsible for the increase in insulin response suggested that nocturnal free fatty acids, peaking in the middle of the night, might provoke the enhanced secretory response, since blocking the nocturnal rise prevented the increment in the islet response (33); a similar mechanism is apparent in human volunteers (34). More data are needed to

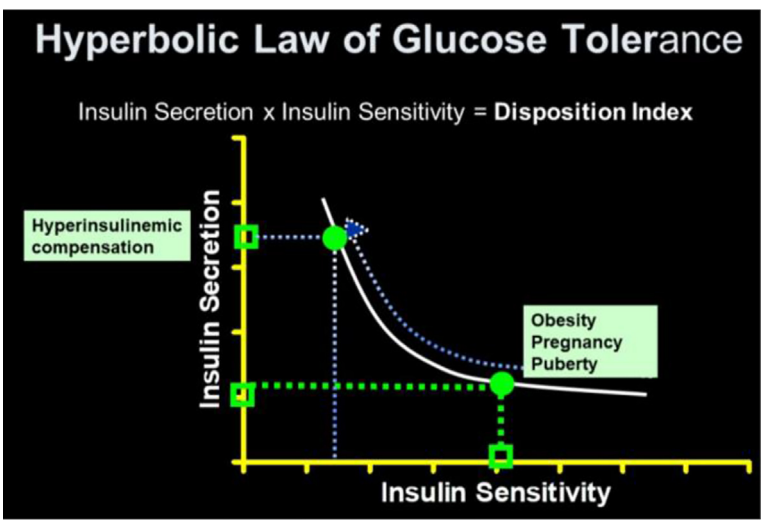

FIGURE 12 | Disposition index (DI).

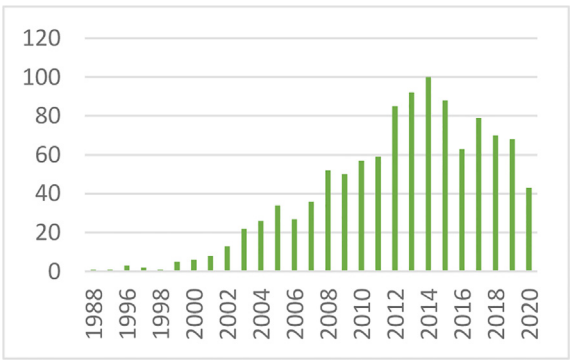

FIGURE 13 | Cited publications pertaining to the DI.

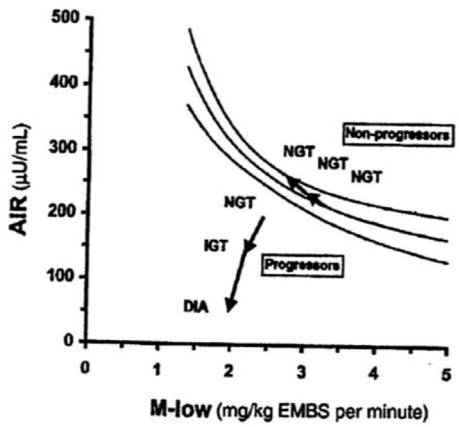

FIGURE 14 | Predictive impact of DI on diabetes risk.

confirm or deny this latter mechanism in animals and in human subjects.

ADDITIONAL FACTORS

While historically focus was on insulin resistance and islet cell response, other factors can play a major role in the ability of the organism to utilize carbohydrate efficiently. Additional factors include insulin clearance and "glucose effectiveness" [**Figure 15**; (35, 36)]. Our laboratory has recently focused more on these additional factors. (Because our research has been based upon intravenous glucose administration, we have focused less on gastrointestinal agents such as GLP-1 and GIP).

INSULIN CLEARANCE

Insulin is degraded primarily by liver and kidney. In fact, once secreted from the pancreas, about half the insulin presented to

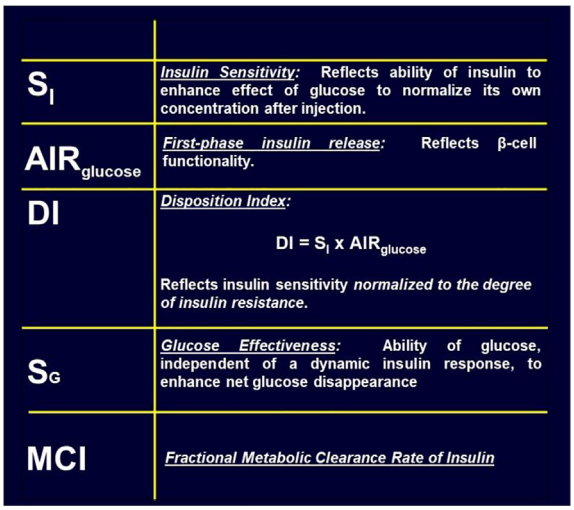

FIGURE 15 | Factors contributing to glucose tolerance.

the liver *via* the portal vein is degraded and does not enter the systemic circulation. Our laboratory has recently considered the following question: "why would evolution choose to degrade half the secreted insulin before it has a chance to act to enhance glucose utilization by skeletal muscle and other tissues?" Working with the canine model allowed us to measure insulin clearance directly by comparing insulin infusion into the portal vein with systemic insulin infusion. Given matched infusion rates, the former route would result in less systemic insulin concentrations. By comparing insulin levels resulting from different routes of insulin administration, an accurate assessment of insulin clearance can be calculated (37, 38). We were surprised to discover a substantial variance in insulin degradation rates, even in normal animals; rates varied from 22 to 77% of portally presented insulin degraded during the initial pass through the liver (37).

Working with David Polidori of Janssen Research, and Francesca Piccinini in our laboratory, we developed a new non-invasive model which allowed for estimation of first-pass hepatic clearance of insulin in human volunteers [**Figure 16**; (39)]. We were fortunate to obtain data from Drs. Barbara Gower and Jose Fernandez of the University of Alabama at Birmingham, which allowed us to apply our model to a human cohort from different ethnic groups (White, Hispanic American, African American), including nondiabetic adults and children, ages 7–13 years. In both adults and children, we confirmed that insulin clearance rates were significantly lower in African Americans than in Whites (40, 41). This lower insulin clearance can explain the hyperinsulinemia of African Americans (adults and children), which may contribute to the higher risk of Type 2 diabetes in those individuals. In our laboratory, we continue to examine the importance of variations in insulin clearance rates to diabetes risk, and mechanisms underlying the variations in clearance across different populations. While the mechanisms of insulin clearance, particularly in the liver, remain to be more

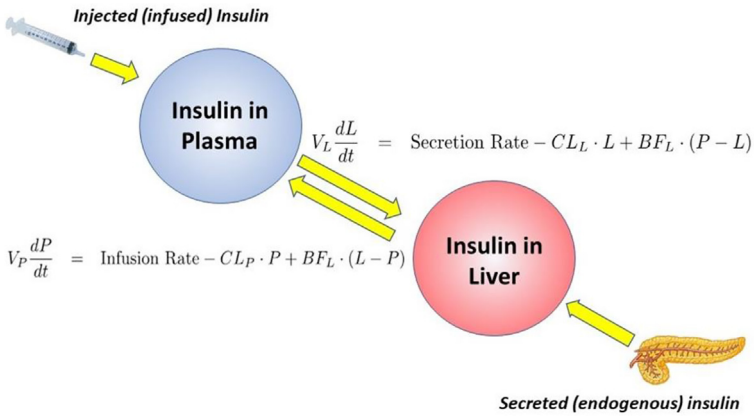

FIGURE 16 | Model of insulin clearance.

clearly defined, it is apparent that insulin degrading enzyme (IDE) and CEACAM1 may both be involved (42). We have hypothesized that reduction in insulin clearance, particularly in liver, might be one cause of Type 2 diabetes, at least in some individuals. The concept is illustrated in **Figure 17**. Lower hepatic insulin clearance (in African Americans, for example) would result in a larger proportion of secreted insulin bypassing first-pass degradation of the hormone. This would result in systemic hyperinsulinemia, both at fasting and after nutrient intake. Hyperinsulinemia has been shown to downregulate insulin action in skeletal muscle (43, 44). The resulting insulin resistance would stress the pancreatic β-cells, potentially leading to prediabetes or diabetes itself (lower clearance, insulin resistance, and reduced β-cell function). While the putative importance of this hypothetical mechanism of diabetes pathogenesis remains to be proven, very recent data emerging from the NIH studies of diabetes in the Pima Nation appear to support this hypothesis. The NIH investigators, led by Douglas Chang, have very recently reported that in a study of 570 Pimas, followed over a period of 8 years, lower insulin clearance (measured by the glucose clamp) was a strong predictor of conversion from prediabetes to Type 2 diabetes mellitus, and this effect of lower insulin clearance was apparently independent of other factors (45). The NIH study appears to be a direct confirmation of the lower clearance hypothesis. However, further studies of the importance of insulin clearance in pathogenesis of

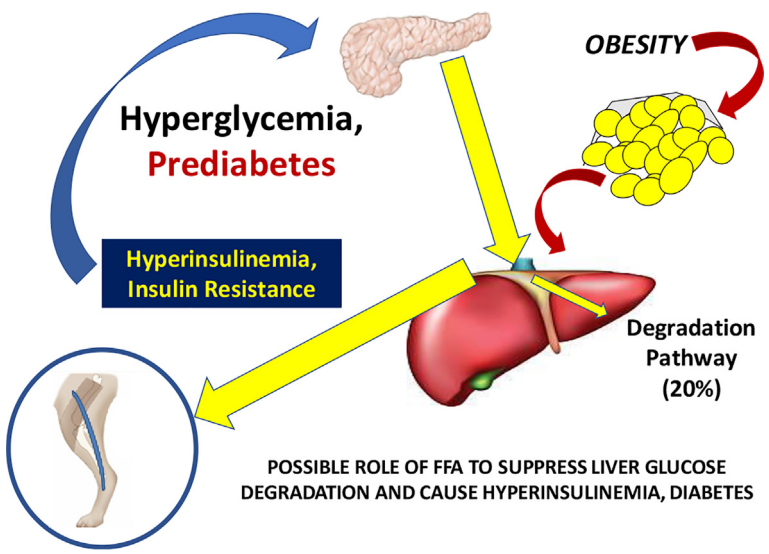

FIGURE 17 | Hypothesis of the pathogenesis of Type 2 diabetes. It is suggested that increased plasma free fatty acids cause a reduction in hepatic insulin clearance, possibly by downregulation of IDE. A large proportion of insulin secreted by the β-cells therefore bypasses first-pass degradation, resulting in peripheral hyperinsulinemia. Higher plasma insulin downregulates skeletal muscle insulin sensitivity, stressing β-cells, and resulting in diabetes.

diabetes remain to be done. Of particular interest is whether lower clearance is predictive in other ethnic groups, and what fraction of those who convert from prediabetes to diabetes may be due to reduced clearance, or other factors.

GLUCOSE EFFECTIVENESS

In the original choice of the minimal model (discussed above), we could only account for glucose normalization by including two fundamental processes: the effects of insulin to enhance glucose utilization (represented by factor S_I) and a second term S_G, which is the *effect of glucose per se to enhance glucose utilization independent of a dynamic insulin response.* We coined the term "glucose effectiveness" to describe this process, and while it is not totally understood, we continue to examine it. Marilyn Ader, in our laboratory, demonstrated the importance of S_G in experimental animals in studies where she demonstrated glucose's ability to self-normalize (after injection) even if the dynamic insulin response is blocked (46).

The importance of S_G remains under investigation; we have proposed that it is a second defense for those at risk for Type 2 diabetes. Individuals with a combination of reduced insulin response and insulin resistance together can be protected from frank diabetes by a maintained glucose effectiveness. There has been some debate regarding the measurement of glucose effectiveness from analysis of the intravenous glucose tolerance test using the minimal model (47, 48). Inclusion of the secondary secretagogue, or insulin injection itself, during the test clearly improved the assessment of S_I but possible incorrect estimation of S_G is still a possibility. To improve this estimation, we have developed a new approach. The mechanisms underlying glucose effectiveness remain unclear, but we have proposed that much of the insulin-independent glucose utilization after carbohydrate intake is due to activation of hepatic glucokinase, resulting in a greater rate of glucose phosphorylation, glycogen deposition, and release of three-carbon intermediates from liver (predominately lactate). We have therefore developed a simple model of the liver, relating glucose uptake to lactate output from the liver (**Figure 18**). This model can be analyzed using data from the IVGTT, yielding an estimate of S_G independent of the traditional minimal model analysis of the IVGTT. We are presently evaluating the precision and accuracy of the "lactate model" approach (49).

COMMENTARY

It can no longer be doubted that mathematical modeling can have a great impact on our understanding of metabolic regulation. The minimal model is but one part of an extensive number of mathematical representations that have enabled the scientific community to understand metabolic physiology, to predict the time course of development of metabolic disease, and to design devices to more effectively regulate the blood sugar.

The interaction among hypothesis, predictions, modeling and experimental testing of the models has characterized our work

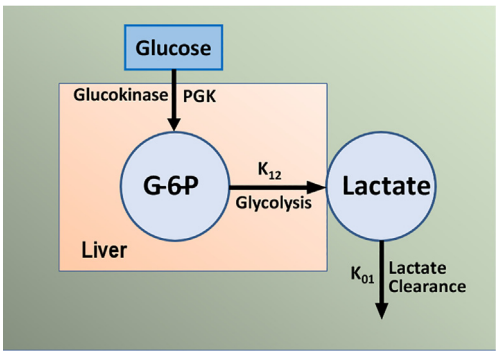

FIGURE 18 | Simple model of glucose/lactate kinetics. Glucose enters hepatocytes, independent of insulin, and follows the glycolytic pathway via glucokinase. Lactate exits the liver and is a surrogate for glucokinase activation and "glucose effectiveness".

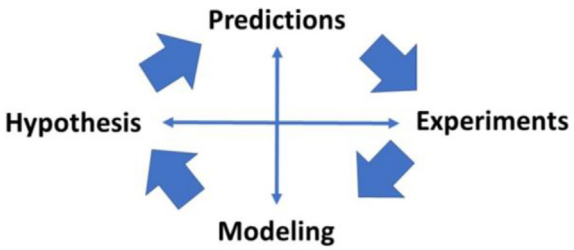

FIGURE 19 | Importance of modeling in the scientific method.

(**Figure 19**) and the work of other productive laboratories. It is of interest that investigations may begin at various points in the interactions shown in the figure; the minimal model itself began first with experimental data, then the model was proposed, and predictions of the model were tested in experimental models. In some cases, the model resulted in predictions (e.g., slow effect of insulin) which were examined in new experimental models (sampling of interstitial fluid). The possible role of insulin clearance in pathogenesis of Type 2 diabetes began with a hypothesis (lower clearance predicted diabetes) and examined with population studies (lower clearance in African American adults and children). Thus we have enjoyed, and we recommend, studying the interaction among these four activities to further our understanding of the mechanisms underlying metabolic disease at the organ level.

We were fortunate to have in our armamentarium the ability to model using modern computer techniques, and the availability of our laboratory to test our hypotheses directly. We were lucky to assemble a group of colleagues, drawn from biomedical engineering, mathematics, experimental physiology and molecular biology, to do our work. We can only thank them and the scientists with whom they worked for our modest success in helping to understand the complex but fascinating story of the regulation of carbohydrate metabolism in the intact organism.

DATA AVAILABILITY STATEMENT

The original contributions presented in the study are included in the article/supplementary material. Further inquiries can be directed to the corresponding author.

ETHICS STATEMENT

The studies involving human participants were reviewed and approved by University of Alabama Human Subjects Committee. Written informed consent to participate in this study was provided by the participants' legal guardian/next of kin. Animal studies were reviewed and approved by USC IACUC and Cedars IACUC.

AUTHOR CONTRIBUTIONS

The author confirms being the sole contributor of this work and has approved it for publication.

FUNDING

This research was supported by research grants to Richard N. Bergman from the National Institutes of Health (DK 29867, DK 27619).

REFERENCES

1. Bolie VW. Coefficients of normal blood glucose regulation. *J Appl Physiol* (1961) 16:783–8. doi: 10.1152/jappl.1961.16.5.783
2. Guyton AC, Coleman TG, Granger HJ. Circulation: overall regulation. *Annu Rev Physiol* (1972) 34:13–46. doi: 10.1146/annurev.ph.34.030172.000305
3. Yates FE, Urquhart J. Control of plasma concentrations of adrenocortical hormones. *Physiol Rev* (1962) 42:359–433. doi: 10.1152/physrev.1962.42.3.359
4. Bergman RN, Urquhart J. The pilot gland approach to the study of insulin secretory dynamics. *Recent Prog Horm Res* (1971) 27:583–605. doi: 10.1016/B978-0-12-571127-2.50039-0
5. Gerich JE, Charles MA, Grodsky GM. Characterization of the effects of arginine and glucose on glucagon and insulin release from the perfused rat pancreas. *J Clin Invest* (1974) 54:833–41. doi: 10.1172/JCI107823
6. Rashevsky N. *Advances and applications of mathematical biology*. Chicago: University of Chicago Press (1940). doi: 10.2307/1439087
7. Bergman RN, Hechter O. A random-hit matrix model for coupling in a hormone-sensitive adenylate cyclase system. *J Biol Chem* (1978) 253:3238–50. doi: 10.1016/S0021-9258(17)40828-3
8. Bergman RN, El Refai M. Dynamic control of hepatic glucose metabolism: studies by experiment and computer simulation. *Ann BioMed Eng* (1975) 3:411–32. doi: 10.1007/BF02409326
9. Bergman RN, Ider YZ, Bowden CR, Cobelli C. Quantitative estimation of insulin sensitivity. *Am J Physiol* (1979) 236:E667–77. doi: 10.1152/ajpendo.1979.236.6.E667
10. Ader M. Physiologic principles underlying glucose effectiveness. In: RN Bergman, JC Lovejoy, editors. *The Minimal Model Approach and Determinants of Glucose Tolerance*. Baton Rouge: Louisiana State University Press (1997).
11. Bergman RN, Cobelli C. Minimal modeling, partition analysis and the estimation of insulin sensitivity. *Fed Proc* (1980) 39:110–5.
12. Bergman RN, Bradley DC, Ader M. On insulin action in vivo: the single gateway hypothesis. *Adv Exp Med Biol* (1993) 334:181–98. doi: 10.1007/978-1-4615-2910-1_13
13. Steil GM, Ader M, Moore DM, Rebrin K, Bergman RN. Transendothelial insulin transport is not saturable in vivo: no evidence for a receptor-mediated process. *J Clin Invest* (1996) 97:1497–503. doi: 10.1172/JCI118572
14. Yang YJ, Hope ID, Ader M, Bergman RN. Insulin transport across capillaries is rate limiting for insulin action in dogs. *J Clin Invest* (1989) 84:1620–8. doi: 10.1172/JCI114339
15. Bradley DC, Poulin RA, Bergman RN. Dynamics of hepatic and peripheral insulin effects suggest common rate-limiting step in vivo. *Diabetes* (1992) 42:296–306. doi: 10.2337/diabetes.42.2.296
16. Rebrin K, Steil GM, Getty L, Bergman RN. Free fatty acid as a link in the regulation of hepatic glucose output by peripheral insulin. *Diabetes* (1995) 44:1038–45. doi: 10.2337/diab.44.9.1038
17. Rebrin K, Steil GM, Mittelman S, Bergman RN. Causal linkage between insulin regulation of lipolysis and liver glucose output. *J Clin Invest* (1996) 98:741–9. doi: 10.1172/JCI118846
18. Donner CC, Fraze E, Chen YDI, Hollenbeck CB, Foley JE, Reaven GM. Presentation of a new method for specific measurement of in vivo insulin-stimulated glucose disposal in humans: comparison of this approach with the insulin clamp and minimal model techniques. *J Clin Endocrinol Metab* (1985) 60:723–6. doi: 10.1210/jcem-60-4-723
19. Welch S, Gebhart SSP, Bergman RN, Phillips LS. Minimal model analysis of intravenous glucose tolerance test-derived insulin sensitivity in diabetic subjects. *J Clin Endocrinol Metab* (1990) 71:1508–18. doi: 10.1210/jcem-71-6-1508
20. Finegood DT, Pacini G, Bergman RN. The insulin sensitivity index. Correlation in dogs between values determined from the intravenous glucose tolerance test and the euglycemic glucose clamp. *Diabetes* (1984) 33:362–8. doi: 10.2337/diabetes.33.4.362
21. Beard JC, Bergman RN, Ward WK, Porte DJr. The insulin sensitivity index in nondiabetic man: correlation between clamp-derived and IVGTT-derived values. *Diabetes* (1986) 35:362–9. doi: 10.2337/diabetes.35.3.362
22. Bergman RN, Prager R, Volund A, Olefsky JM. Equivalence of the insulin sensitivity index in man derived by the minimal model method and the euglycemic glucose clamp. *J Clin Invest* (1987) 79:790–800. doi: 10.1172/JCI112886
23. Perley M, Kipnis DM. Plasma insulin responses to glucose and tolbutamide of normal weight and obese diabetic and nondiabetic subjects. *Diabetes* (1966) 15:867–74. doi: 10.2337/diab.15.12.867
24. Shen SW, Reaven GM, Farquhar JW. Comparison of impedance to insulin-mediated glucose uptake in normal subjects and in subjects with latent diabetes. *J Clin Invest* (1970) 49:2151–60. doi: 10.1172/JCI106433
25. Stumvoll M, Tataranni PA, Bogardus C. The hyperbolic law – a 25-year perspective. *Diabetologia* (2005) 48:207–9. doi: 10.1007/s00125-004-1657-3
26. Bergman RN, Phillips LS, Cobelli C. Physiologic evaluation of factors controlling glucose tolerance in man: measurement of insulin sensitivity and B-cell glucose sensitivity from the response to intravenous glucose. *J Clin Invest* (1981) 68:1456–67. doi: 10.1172/JCI110398
27. Buchanan TA, Metzger BE, Freinkel N, Bergman RN. Insulin sensitivity and B-cell responsiveness to glucose during late pregnancy in lean and moderately obese women with normal glucose tolerance or mild gestational diabetes. *Am J Obstet Gynecol* (1990) 162:1008–14. doi: 10.1016/0002-9378(90)91306-W
28. Holder T, Giannini C, Santoro N, Pierpont B, Shaw M, Duran E, et al. A low disposition index in adolescent offspring of mothers with gestational diabetes: a risk marker for the development of impaired glucose tolerance in youth. *Diabetologia* (2014) 57:2413–20. doi: 10.1007/s00125-014-3345-2
29. Lorenzo C, Wagenknecht LE, Rewers MJ, Karter AJ, Bergman RN, Hanley AJ, et al. Disposition index, glucose effectiveness, and conversion to type 2 diabetes: the Insulin Resistance Atherosclerosis Study (IRAS). *Diabetes Care* (2010) 33:2098–103. doi: 10.2337/dc10-0165
30. Palmer JP, Langefeld CD, Campbell JK, Williams AH, Saad M, Norris JM, et al. Genetic mapping of disposition index and acute insulin response loci on chromosome 11q: The Insulin Resistance Atherosclerosis Study (IRAS) Family Study. *Diabetes* (2006) 55:911–8. doi: 10.2337/diabetes.55.04.06.db05-0813

31. Weyer C, Hanson K, Bogardus C, Pratley RE. Long-term changes in insulin action and insulin secretion associated with gain, loss, regain and maintenance of body weight. *Diabetologia* (2000) 43:36–46. doi: 10.1007/s001250050005
32. Stefanovski D, Richey JM, Woolcott O, Lottati M, Zheng D, Harrison LN, et al. Consistency of the disposition index in the face of diet-induced insulin resistance: potential role of FFA. *PloS One* (2011) 6(3):e18134. doi: 10.1371/journal.pone.0018134
33. Broussard JL, Kolka CM, Castro AVB, Asare Bediako I, Paskiewicz RL, Szczepaniak EW, et al. Elevated nocturnal NEFA are an early signal for hyperinsulinaemic compensation during diet-induced insulin resistance in dogs. *Diabetologia* (2015) 58:2663–70. doi: 10.1007/s00125-015-3721-6
34. Broussard JL, Chaptot F, Abraham V, Day A, Delebecque F, Whitmore HR, et al. Sleep restriction increases free fatty acids in healthy men. *Diabetologia* (2015) 58:791–8. doi: 10.1007/s00125-015-3500-4
35. Bergman RN, Piccinini F, Kabir M, Kolka CM, Ader M. Hypothesis: Role of reduced hepatic insulin clearance in the pathogenesis of type 2 diabetes. *Diabetes* (2019) 68:1709–16. doi: 10.2337/db19-0098
36. Best JD, Kahn SE, Ader M, Watanabe RM, Ni T-C, Bergman RN. Role of glucose effectiveness in the determination of glucose tolerance. *Diabetes Care* (1996) 19:1018–30. doi: 10.2337/diacare.19.9.1018
37. Asare Bediako I, Paszkiewicz RL, Kim SP, Woolcott OO, Kolka CM, Burch MA, et al. Variability of directly measured first-pass hepatic insulin extraction and its association with insulin sensitivity and plasma insulin. *Diabetes* (2018) 67:1495–503. doi: 10.2337/db17-1520
38. Kim SP, Ellmerer M, Kirkman EL, Bergman RN. Beta-cell "rest" accompanies reduced first-pass hepatic insulin extraction in the insulin resistant, fat-fed canine model. *Am J Physiol* (2007) 292:1581–9. doi: 10.1152/ajpendo.00351.2006
39. Polidori DC, Bergman RN, Chung ST, Sumner AE. Hepatic and extrahepatic insulin clearance are differentially regulated: results from a novel model-based analysis of intravenous glucose tolerance data. *Diabetes* (2016) 65:1556–64. doi: 10.2337/db15-1373
40. Piccinini F, Polidori DC, Gower BA, Bergman RN. Hepatic but not extrahepatic insulin clearance is lower in African American than in European American women. *Diabetes* (2017) 66:2564–70. doi: 10.2337/db17-0413
41. Piccinini F, Polidori DC, Gower BA, Fernandez J, Bergman RN. Dissection of hepatic and extra-hepatic insulin clearance: ethnic differences in childhood. *Diabetes Obes Metab* (2018) 12:2869–75. doi: 10.1111/dom.13471
42. Najjar SM, Perdomo G. Hepatic insulin clearance: mechanism and physiology. *Physiology* (2019) 34:198–215. doi: 10.1152/physiol.00048.2018
43. Catalano KJ, Maddux BA, Szary J, Youngren JF, Goldfine ID, Schaufele F. Insulin resistance induced by hyperinsulinemia coincides with a persistent alteration at the insulin receptor tyrosine kinase domain. *PloS One* (2014) 9:e108693. doi: 10.1371/journal.pone.0108693
44. Rizza RA, Mandarino LJ, Genest J, Baker BA, Gerich JE. Production of insulin resistance by hyperinsulinemia in man. *Diabetologia* (1985) 28:70–5 doi: 10.1007/BF00279918
45. Shah MH, Piaggi P, Looker HC, Paddock E, Krakoff J, Chang DC. Lower insulin clearance is associated with increased risk of Type 2 diabetes in Native Americans. *Diabetologia* (2021) [online ahead of print]. doi: 10.1007/s00125-020-05348-5
46. Ader M, Pacini G, Yang YJ, Bergman RN. Importance of glucose per se to intravenous glucose tolerance: comparison of the minimal model prediction with direct measurements. *Diabetes* (1985) 34:1092–103. doi: 10.2337/diabetes.34.11.1092
47. McDonald C, Dunaif A, Finegood DT. Minimal-model estimates of insulin sensitivity are insensitive to errors in glucose effectiveness. *J Clin Endocrinol Metab* (2000) 85:2504–8. doi: 10.1210/jc.85.7.2504
48. Quon MJ, Cochran C, Taylor SI, Eastman RC. Non-insulin-mediated glucose disappearance in subjects with IDDM: discordance between experimental results and minimal model analysis. *Diabetes* (1994) 43:890–6. doi: 10.2337/diabetes.43.7.890
49. Stefanovski D, Youn JH, Rees M, Watanabe RM, Ader M, Ionut V, et al. Estimating hepatic glucokinase activity using a simple model of lactate kinetics. *Diabetes Care* (2012) 35:1015–20. doi: 10.2337/dc11-1540

Conflict of Interest: The author declares that the research was conducted in the absence of any commercial or financial relationships that could be construed as a potential conflict of interest.

frontiers in Endocrinology

ORIGINAL RESEARCH
published: 11 March 2021
doi: 10.3389/fendo.2021.613048

Mathematical Modeling and Simulation Provides Evidence for New Strategies of Ovarian Stimulation

Sophie Fischer[1], Rainald Ehrig[2], Stefan Schäfer[3], Enrico Tronci[4], Toni Mancini[4], Marcel Egli[5], Fabian Ille[5], Tillmann H. C. Krüger[6], Brigitte Leeners[7†] and Susanna Röblitz[1†]*

[1] Computational Biology Unit, Department of Informatics, University of Bergen, Bergen, Norway, [2] Computational Systems Biology Group, Zuse Institute Berlin (ZIB), Berlin, Germany, [3] Department of Microstructure and Residual Stress Analysis, Helmholtz Centre Berlin for Materials and Energy, Berlin, Germany, [4] Department of Computer Science, University of Rome "La Sapienza", Rome, Italy, [5] Centre of Competence in Aerospace Biomedical Science & Technology, Lucerne University of Applied Sciences and Arts, Lucerne, Switzerland, [6] Department of Psychiatry, Social Psychiatry and Psychotherapy, Hannover Medical School, Hannover, Germany, [7] Department of Reproductive Medicine, University Hospital Zurich, Zurich, Switzerland

OPEN ACCESS

Edited by:
Ray Boston, University of Pennsylvania, United States

Reviewed by:
Duncan MacGregor, University of Edinburgh, United Kingdom
Chiara Dalla Man, University of Padua, Italy

***Correspondence:**
Susanna Röblitz
susanna.roblitz@uib.no

[†]*These authors share senior authorship*

Specialty section:
This article was submitted to Systems Endocrinology, a section of the journal Frontiers in Endocrinology

Received: *01 October 2020*
Accepted: *26 January 2021*
Published: *11 March 2021*

Citation:
Fischer S, Ehrig R, Schäfer S, Tronci E, Mancini T, Egli M, Ille F, Krüger THC, Leeners B and Röblitz S (2021) Mathematical Modeling and Simulation Provides Evidence for New Strategies of Ovarian Stimulation. Front. Endocrinol. 12:613048. doi: 10.3389/fendo.2021.613048

New approaches to ovarian stimulation protocols, such as luteal start, random start or double stimulation, allow for flexibility in ovarian stimulation at different phases of the menstrual cycle. It has been proposed that the success of these methods is based on the continuous growth of multiple cohorts ("waves") of follicles throughout the menstrual cycle which leads to the availability of ovarian follicles for ovarian controlled stimulation at several time points. Though several preliminary studies have been published, their scientific evidence has not been considered as being strong enough to integrate these results into routine clinical practice. This work aims at adding further scientific evidence about the efficiency of variable-start protocols and underpinning the theory of follicular waves by using mathematical modeling and numerical simulations. For this purpose, we have modified and coupled two previously published models, one describing the time course of hormones and one describing competitive follicular growth in a normal menstrual cycle. The coupled model is used to test ovarian stimulation protocols *in silico*. Simulation results show the occurrence of follicles in a wave-like manner during a normal menstrual cycle and qualitatively predict the outcome of ovarian stimulation initiated at different time points of the menstrual cycle.

Keywords: endocrinological networks, systems biology, follicular dynamics, ordinary differential equations, assisted reproductive technologies

INTRODUCTION

Infertility is a worldwide problem. According to the World Health Organization, about 48.5 million couples worldwide were affected by unwanted childlessness in 2010, and the number continues to grow (1). Men and women are just as likely to contribute to the couple's infertility (2). Infertility as a disease of the female reproductive system affects approximately 10% of women of reproductive age

worldwide (3). Unbalanced hormone levels are one cause, in a wide range of conditions, leading to infertility. For many couples, unwanted childlessness is a burden. Assisted reproductive technologies (ART) provide strategies to deal with infertility. Both unwanted childlessness and ART increase the risk for negative psycho-social functioning, such as depression and anxiety disorders (4–6), whereby the treatment burden has fallen mainly on women (2). Therefore, new ART approaches deserve to be highlighted. We want to add further scientific evidence for the efficiency of those new approaches by using mathematical modeling and numerical simulations.

Female reproduction is essentially enabled by a feedback mechanism between ovarian hormones, mainly progesterone (P4) and estradiol (E2), and the pituitary hormones luteinizing hormone (LH) and follicular stimulating hormone (FSH), see **Figure 1**. The hormone interaction network is important for regulating folliculogenesis. While the initial recruitment of follicles does not depend on gonadotropins (7, 8), the growth of cohorts of larger follicles relies on a stimulatory effect of FSH. FSH signaling is mediated by the expression of FSH receptors on granulosa cells (9, 10). The gonadodropins LH and FSH are responsible for follicular estradiol production. LH stimulates androstenedione production, which is the substrate for the FSH stimulated aromatase reaction producing estradiol (8, 11, 12). Around mid-cycle, usually one dominant follicle ovulates and releases an oocyte. The remaining parts of the dominant follicle transform into the corpus luteum, which has a key role in preparing the body for a possible pregnancy. If the oocyte is not fertilized, the corpus luteum decays and a new cycle starts (13–15). Interruptions in the feedback system are one reason for infertility.

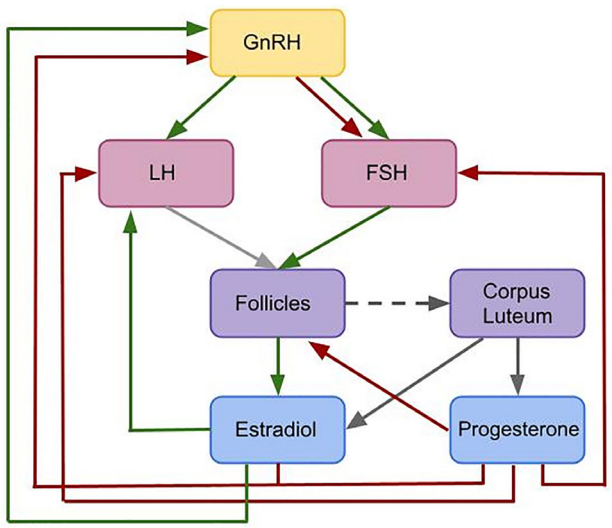

FIGURE 1 | Flowchart illustrating the interactions included in the given model. This is a simplified feedback interactions network for the hormonal control of the female menstrual cycle. Green arrows indicate positive feedback effects, while red arrows express negative feedback interactions. Gray arrows show other types of interactions. The pulsatile release of GnRH stimulates the release of the pituitary hormones LH and FSH. These hormones effect follicular maturation. Growing follicles produce E2 which has a positive feedback effect on the LH concentration. A high LH concentration triggers the ovulation of one selected follicle (light gray arrow) followed by the formation of the corpus luteum (dark gray dashed arrow). The simultaneous release of E2 and P4 by the corpus luteum (dark gray arrows) inhibits the release of GnRH. Additionally, P4 has an inhibitory effect on LH and FSH. While P4 only has an inhibitory effect on GnRH, E2 has either a stimulatory or an inhibitory effect on GnRH, depending on the E2 level.

Modern assisted reproductive technologies like *in vitro* fertilization (IVF) or intracytoplasmic sperm injection (ICSI) have increased the chance for pregnancy. Ovarian stimulation, which aims at obtaining multiple fertilizable oocytes, is a critical step in ART (16). Since the 1980s, the long gonadotropin-releasing hormone (GnRH) agonist protocol has been commonly used to prepare for oocyte retrieval and in-vitro fertilization (17, 18). This protocol starts around mid-luteal phase with GnRH agonist administration for about 14 days. Right after the beginning of GnRH agonist administration, a short period of gonadotropin (FSH and LH) hypersecretion is observable. The treatment leads to GnRH-receptor down-regulation in the pituitary (19, 20). In the next step, the growth of multiple follicles is stimulated by FSH administration alone, e.g. with recombinant FSH (rFSH), or by a combination of FSH and LH, e.g. with human menopausal gonadotropin (hMG). Continuation of GnRH agonist administration during the stimulation phase prevents an LH surge and hence ovulation. In the final step, ovulation is induced by injecting human chorionic gonadotropin (hCG) (18). Patient-specific and clinic-dependent modifications of these general procedures are common. The two most common alternatives are the short GnRH agonist protocol and the antagonist protocol. Both protocols work without downregulation, though some clinics perform a pre-treatment phase for 10 to 25 days with a P4 antagonist that inhibits ovulation.

The stimulation phase in the short GnRH agonist protocol is the same as in the long protocol. It includes the stimulation with hMG or rFSH and the concurrent administration of a GnRH agonist. The antagonist protocol also includes the stimulation with hMG or rFSH but, in contrast to the agonist protocols, a GnRH antagonist is administered from day 5 of the stimulation period. The final step in all protocols is the induction of ovulation by hCG.

In general, infertility treatment is a long-term and expensive therapy with high dropout rates (21), mainly because it imposes physical, mental, and emotional burdens (22). Often, life has to be subordinated to medical procedures. Therefore, treatment alternatives are of interest. Both the short and the antagonist protocol are less time-consuming than the long protocol. However, the stimulation phase in these protocols conventionally starts in the early follicular phase. This constraint could cause too long waiting times, e.g. for women requiring emergency fertility preservation. Hence, the advancement of a new class of ovarian stimulation approaches called random - and luteal phase-start ovarian stimulation protocol (23) has progressed. In recent years, several studies investigating ovarian stimulation

protocols with various starting points have been published (24–26). Originally, these protocols were invented for fertility preservation in cancer patients, where time is a limiting factor (27). However, they might be beneficial for patients outside an oncological setting (23), though there is an ongoing debate whether the oocyte quality differs between protocols. Other approaches like the double ovarian stimulation, where two waves within one cycle are stimulated, might help to increase the number of accumulated oocytes within one treatment cycle (28). That strategy could be of particular interest for the therapy of poor ovarian response patients (29, 30).

One possible explanation for the success of stimulation initiated in different phases of the cycle is the "wave" theory. The use of high-resolution transvaginal ultrasonography has underpinned the hypothesis that, similar to ruminants, follicular growth and development in human is characterized by waves (31, 32), whereby each wave involves the recruitment of a cohort of follicles and the possible selection of a dominant follicle. Given that multiple waves of follicles appear each cycle, there are multiple time points during one cycle that are suitable to start ovarian stimulation.

The mathematical model underlying this study simulates the time-evolution of key hormones and growth behavior of multiple follicles. In particular, we test the hypothesis that random recruitment of follicles leads to the emergence of follicular waves. Based on the occurrence of follicular waves that we observe in our simulation results, we study variable-start ovarian stimulation protocols in silico. We demonstrate simulation results for two protocols, namely (i) stimulation initiated in the late follicular phase and (ii) stimulation initiated in the luteal phase. We analyze statistics of treatment duration and numbers of follicles in our simulation results and compare them with the literature.

MATERIALS AND METHODS

Mathematical Modeling of the Female Menstrual Cycle

Mathematical modeling is a useful tool to better understand the human menstrual cycle by validating or testing hypothesis in silico, and predicting possible dynamics. A first mathematical model for the human menstrual cycle was introduced in a series of articles by Schlosser, Selgrade, and Harris-Clark (33). Their model allows to simulate the time course of hormones and follicular maturation stages over several cycles and is able to display multiple follicular waves (34). This model was extended by pharmacokinetic sub-models to simulate the administration of drugs, including ovarian contraceptive pills (35, 36) and GnRH analogs (37). These pharmacokinetic-pharmacodynamic (PKPD) models allow to study the influence of dose and time point of administration of various drugs on the cycle dynamics.

All those models are based on ordinary or delay differential equations since they allow to simulate the time evolution of hormone concentrations and follicles. Hill functions have been used to characterize stimulatory and inhibitory effects, as it is common practice for modeling regulatory networks. The model by Röblitz et al. (37) consists of 33 ordinary differential equations that describe the feedback mechanisms between the hormones that are of particular importance for the female menstrual cycle (GnRH, FSH, LH, E2, P4, inhibin A, inhibin B) and the development of follicles and corpus luteum throughout consecutive cycles. Compared to previous models, it does not use delay differential equations and consists of fewer equations and parameters. However, all those models have in common that follicular growth is described in terms of activity levels of different follicular maturation stages, but not in terms of follicle numbers and sizes. Thus, the simulation results cannot be compared with ultrasound data.

A mathematical model that quantifies the time evolution of the sizes of multiple follicles comparable to observations by ultrasound measurements in mono-ovulatory species was presented by (38). This model contains a separate differential equation for each follicle, whereby the structure of this equation is the same for all follicles, but the initial follicle sizes are different. The equations are coupled *via* a term that accounts for competitive interactions between follicles. Together with the model by (37) a previous version of the model by (38) formed the basis for the development of computational tools to enable in silico clinical trials in reproductive endocrinology (39, 40). In particular, by introducing variability into model parameters (41–43), the authors could analyze inter-individual variability in the cycle and automatically synthesize, by means of artificial intelligence guided by patient digital twins, optimal personalized treatments for the patients at hand (44). However, the tools could only be applied to the downregulation phase before follicular stimulation, because the feedback mechanisms from the ovaries to the pituitary were not implemented in the modified model. This drawback motivated the development of the fully coupled model as presented in this work. To our knowledge, this is the first mathematical model that allows for the simulation of stimulation protocols that start at different time points in the cycle.

Model Construction and Assumptions

The mathematical model underlying this work is the result of modifying and coupling the two previously published models by Röblitz et al. (37) and Lange et al. (38). In a first step, the model by Röblitz et al. (37) was reduced by removing the equations for the development of follicles and the corpus luteum and the hormones produced by them (inhibin A, inhibin B, E2, P4). In addition, we removed the equations for LH receptor binding mechanisms, since they were not needed for our purpose. The remaining equations were kept exactly as in (37), except for the FSH synthesis rate. In the new model, this rate is inhibited by P4 instead of inhibin A and B [**Eq. (S5) in the Supplement**], since P4 reaches its peak in the mid-luteal phase exactly as inhibin A. The influence of inhibin B could be neglected without any consequences for the qualitative behavior of the model. In addition, we have introduced a new equation for the amount of FSH that reaches the follicles [**Eq. (S9) in the Supplement**] to account for delays caused by transportation and for changes in concentration caused by different volumes. In contrast to (37), the equations for FSH receptor binding now take into account

FSH in the ovaries instead of the FSH blood concentration [**Eqs. (S10)–(S12) in the Supplement**].

Instead of re-introducing a corpus luteum into the model equations, we decided to use algebraic equations to directly model the amounts of E2 and P4 produced in the luteal phase of the cycle [**Eqs. (S23) and (S25) in Supplement S1**]. The model describes E2 and P4 levels in the luteal phase by Gaussian-shaped curves with fixed parameters based on fits to experimental data (for P4 see **Figure S1 in Supplement S3**). This simplification is based on the observation that the variability in the length of the luteal phase is significantly lower than the variability in the length of the follicular phase (45).

We modified the follicle equation introduced by (38) in a way that the hormone dynamics in the system have a direct effect on the follicular growth behavior [**Eqs. (S20)-(S22) in Supplement S1**]. The maturation of each follicle is modeled by a separate ODE. All ODEs have the same structure and include both shared and follicle specific parameters. Each follicle carries two random properties that are follicle specific, hence there are two follicle specific parameters: the time point at which a follicle is recruited, and its FSH sensitivity. The following assumptions are made about these two parameters:

- The time point at which a follicle is recruited and starts growing is follicle-specific and follows a Poisson process. The overall number of follicles that are recruited within a specific time interval is a Poisson random variable. The parameter of this distribution, in the following named Poisson parameter, corresponds to the probability that a given number of follicles is recruited in a fixed time interval. In the model, the Poisson parameter is modulated by the FSH concentration: if the FSH concentration is above a certain threshold, more follicles are recruited.
- The second property is a follicle specific FSH value, referred to as FSH sensitivity threshold value, which has to be exceeded in order to stimulate the follicle's growth. This refers to the biological finding that follicle growth does not occur below a certain level of FSH (46), and that any two follicles might respond differently to FSH, even if the two have the same size, because they differ in the FSH receptor density. The distribution of the FSH sensitivity threshold values in the population of follicles is assumed to follow a normal distribution. Follicles that are more sensitive to FSH, i.e. which require less FSH to start growing, have a competitive advantage for being selected as the dominant follicle. Whether a follicle becomes dominant, however, depends on both its FSH sensitivity and its recruitment time point.

The competition between follicles, which is represented by a common parameter [**Eq. (S22) in Supplement S1**], is inhibited by FSH concentrations above a certain threshold, taking into account the "FSH window concept" (47–49). This concept is based on the observation that the period of time during which FSH is above a certain threshold effects the number of follicles reaching the dominant follicle's size (50, 51). Moreover, we assume that the follicular growth rate is inhibited by P4 and stimulated by the FSH receptor complex level in a threshold dependent way [**Eq. (S21) in Supplement S1**] (52).

Growing follicles are the main source of E2 in the female body and the dominant follicle produces the most E2 (12, 53, 54). Estradiol is produced by granulosa cells, which proliferate and form a multilayered structure. This is included in the model by an additional term in E2 production which is dependent on the follicular size [**Eqs. (S24) and (S25) in Supplement S1**].

To sum up, the coupling between the hormone dynamics model and the follicular growth model is realized as follows (compare **Figure 1**). The levels of FSH in the blood and of the FSH receptor complex enter into the equations for the follicles in a threshold dependent way. In addition, the LH level plays a role in determining the time point of ovulation. Ovulation of a follicle that exceeds the size threshold occurs 12 h after the LH level is higher than a certain threshold. The levels of E2 and P4 in the luteal phase depend on the time point of the last ovulation. E2 and P4 levels enter into the equations for LH and FSH synthesis and for the frequency and mass of GnRH, in the same way as in (37). The coupled model contains in total 72 parameters, i.e. less than the two original models taken together (114 parameters in (37) and 5 parameters in (38). We adopted 44 parameters from (37) and only changed the values of three of them. A detailed parameter list can be found in the Supplement. The model has been implemented in MATLAB and numerical simulations were performed using the ODE solver *ode15s*. The code is available at https://github.com/SoFiwork/GynCycle.

Ovarian Stimulation Protocols

Stimulation protocols are introduced to the model by a pharmacokinetic approach. The dosing concentrations of the administered drug, as used in the ovarian stimulation protocols, are calculated during the simulation based on three drug specific pharmacokinetic parameters using the information given by (55) [**Eq. (S26) in Supplement S1**]. In order to study treatment outcomes, two different stimulation protocols were implemented. The two studies were selected based on the accessibility of results, the size of study cohorts and the physiological stage of patients. Each study includes data from more than 100 women. Patients were at the age of 18 to 40 years with a body mass index of 18 to 30 kg/m^3. All women showed spontaneous ovulation.

Stimulation Initiated in the Late Follicular Phase

Our simulated treatment protocol for ovarian stimulation during the late follicular phase follows the description in Zhu and Fu (24). As a simplification, we did not vary the administered hMG dose during the first days of stimulation. The stimulation starts with a daily administration of 150 IU hMG when at least one follicle measures 14 mm in diameter. After 6 days, the daily dose is increased to 225 IU per day. We chose day 6 to change the hMG concentration because re-examination and dose adjustment in the clinical trial took place after 5 - 7 days. The stimulation stops whenever at least 3 follicles reach a diameter of at least 18 mm. The ovulation of a dominant follicle during the stimulation phase is characteristic for this protocol.

Stimulation Initiated in the Luteal Phase

The protocol described in (26) served as a reference to simulate the stimulation of multiple follicular growth during the luteal phase. In this clinical trial, the drug administration in the simulation starts between day 1 and 3 after ovulation under the condition that there exist follicles smaller than 8 mm. Follicular growth is stimulated by the daily administration of 225 IU hMG. The stimulation terminates if at least three follicles have reached a diameter of 18 mm.

RESULTS

Unstimulated Cycle

As indicated in **Figure 2**, the model generates quasi-periodic solutions for all four hormones. Due to the individual growth behavior of follicles implemented in the model, variations in cycle length and number of follicles per cycle occur. Simulations for a normal cycle were performed for more than 1000 time steps in order to get an idea of the variability in the model outcome. In total, 42 simulated menstrual cycles (here, one menstrual cycle is defined from one ovulation to the next one) were used for a statistical analysis. In the simulations, the average cycle length was 30.56 days, with a standard deviation of 7.00 days (**Figure S2 in Supplement**). On average, 16.19 follicles greater than 4 mm were detected during one cycle, with a standard deviation of 3.08 follicles. The results were tested for normality using the Shapiro-Wilk test with a 95 confidence interval. A correlation between the cycle length and the follicular count was not observed.

The simulated hormone curves are supposed to be comparable to serum hormone concentration profiles in terms of shape and peak values. **Figures 2A–E** display consecutive menstrual cycles in the time period between day 50 and day 130 from one simulation run. The time evolution of all four hormone profiles is illustrated, and the described interplay between hormones and follicles is apparent.

The wave-like growth behavior of the follicles (**Figure 2E**) is generated by the model itself and is not enforced by the implementation. **Figure 2G** shows an example of the ovulation of a dominant follicle that occurs 12 h after LH reached its peak concentration. This 12-h gap is accomplished by the way the ovulation event is defined in our model (see *Discussion*). Once ovulation is detected during the run time of the simulation, the ovulated follicle is taken out from the cohort of follicles

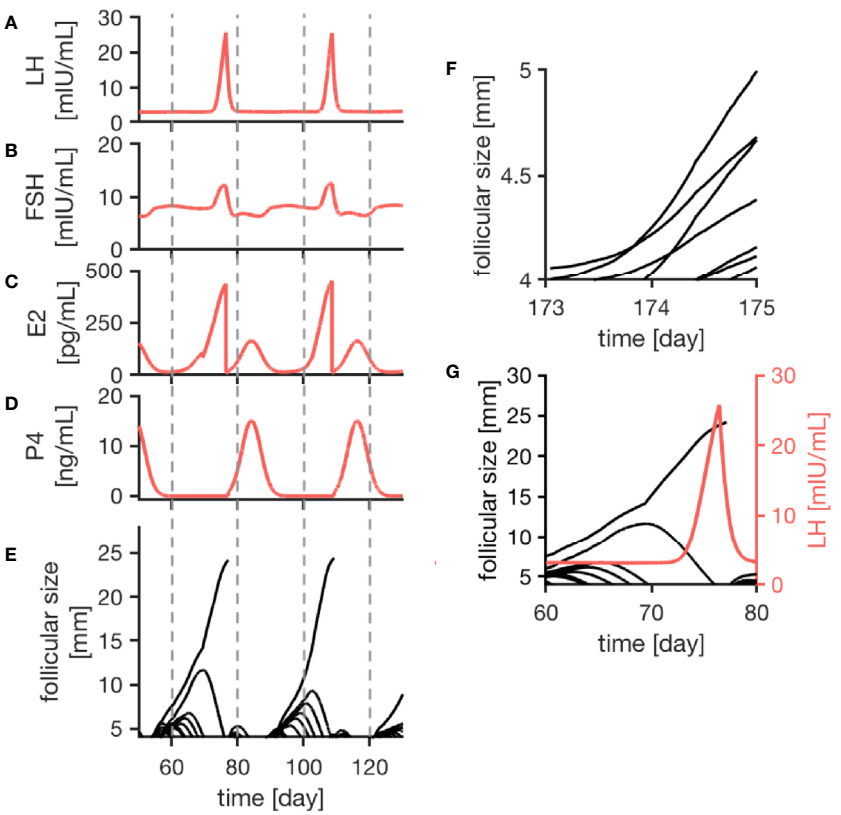

FIGURE 2 | Simulation results of the female menstrual cycle model are displayed. The left column illustrates the simulation outcome for two menstrual cycles and the right column zooms into details. Here, one cycle is defined from one ovulation to the next one. Sub-figures **(A–D)** represent the simulated hormone concentration profiles for LH, FSH, E2 and P4. **(E)** portrays growth trajectories of follicles >4 mm. The ovulation of a dominant follicle is indicated by terminating trajectories, as seen for example around day 80 of the simulation. **(F)** illustrates competition between follicles indicated by crossing growth trajectories. **(G)** Points out that the ovulation of a dominant follicle occurs 12 h after the LH peak concentration as a result of the way the ovulation process is implemented in the model.

(indicated by the terminating trajectory in **Figure 2G**). This follicle no longer contributes to steroid production. Keeping it in the simulation would needlessly increase computational time. The growth behavior of follicles causes variation in the length of the follicular phase. In contrast to that, the luteal phase has a constant length of 14 days due to its implementation.

The follicular growth equation, as introduced by (38) and modified for the given model, includes a term addressing the competition for dominance between follicles. In the simulation results, its effect is visible by crossing growth trajectories (**Figure 2F**). This crossing only is possible because each follicle has its specific parameters. As it can be seen in **Figure 2**, competition is stronger during the early follicular phase before a dominant follicle emerges.

Ovarian Stimulation

The simulations of ovarian stimulation initiated in the luteal phase or the late follicular phase are characterized by the growth of multiple follicles. Additionally, the ovulation of a dominant follicle during a stimulation protocol occurs only during stimulation in the late follicular phase. In the model, the competition term is inhibited by high FSH concentrations, enabling the growth of multiple follicles under stimulatory treatment.

Figure 3 exemplarily displays hormone concentration profiles and follicle development for one simulation of each treatment approach. Additionally, error bars at four characteristic time points (one day before treatment, one day after first drug administration, six days after first drug administration, last day of drug administration) indicate the variability in the hormone levels between 20 simulations using the same treatment conditions. The characteristic time points where chosen in a way that the results are easily comparable to the clinical data. In both cases, the FSH concentration rises with each day of the treatment. Due to the growth of multiple large follicles, which are the main source of E2, the E2 level increases significantly during ovarian stimulation. The levels are almost ten times higher compared to the normal cycle (**Figure 2C**).

Simulations of an ovarian stimulation during the luteal phase are dominated by high P4 levels during the stimulation with hMG. The high P4 concentration prevents the ovulation of

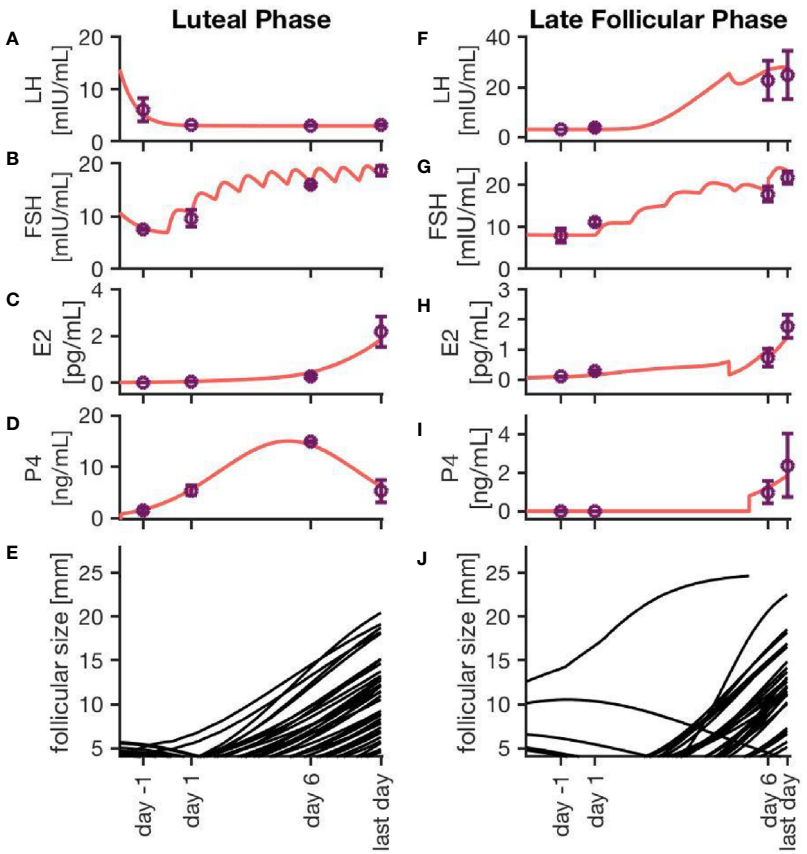

FIGURE 3 | Simulation results for two different ovarian stimulation protocols. The growth of multiple large follicles, caused by the stimulation treatment, is characteristic for both strategies. The left column represents simulation results from a luteal phase stimulation protocol, while the right column shows the effect of a stimulation during the late follicular phase. Sub-figures **(A–D, F–I)** exemplary represent hormone profiles originating from one simulation in red. Purple dots and error bars represent mean values and variances, respectively, from 20 simulations at four characteristic time points: 1 day before the stimulation treatment starts, 1 day after starting the treatment, 6 days after starting the treatment, and the last day of treatment. Sub-figures **(E, J)** illustrate the growth trajectories of the follicles.

follicles (through the negative feedback mechanisms of P4 on LH). The concentrations of LH, FSH, P4 and E2 in **Figures 3A–D** are comparable to observations by (26).

Figure 3J illustrates the follicular growth behavior under stimulation in the late follicular phase, initiated after the occurrence of a dominant follicle. The ovulation of the dominant follicle is followed by an increase in P4 concentration comparable to non-treated conditions. The E2 level decreases after the ovulation of the dominant follicle but starts to increase again. This increase is caused by multiple large follicles as a result of the stimulation.

Figure 4 represents the individual outcomes (treatment duration and follicular count) of 20 simulations per treatment protocol. The mean and standard deviation of these results are given in **Table 1**. The simulation results for ovarian stimulation initiated in the luteal phase match the observations from Kuang et al. (26). The simulated treatment duration for the late follicular phase stimulation approach is noticeably lower than the clinical observations, which goes along with comparably low counts of follicles >14 mm. **Figure 4** convincingly shows that simulations differ among each other even if non-follicular parameters are the same in all simulations. Hence, the individual growth behaviors of the follicles have a major effect on treatment simulations and outcomes.

DISCUSSION

The mathematical model developed in this work addresses the interplay between pituitary hormones, ovarian hormones and follicular growth. Simulation results for the unstimulated cycle agree qualitatively and quantitatively with observations reported in literature. In particular:

- The time evolution of the four hormone profiles for LH, FSH, P4 and E2 is consistent with the scientific literature (56).
- An average cycle length of around 29 days, ranging from cycles with a duration of 22–25 up to 36 days, is reported in experimental studies (56–58). The simulation results are in line with these observations.
- In the literature, it is described that the variability in the length of the follicular phase is significantly higher than for the luteal phase (58, 59). The given simulation results fulfill the same property.
- The observed intra-cycle variability of 7 days is comparable to experimental results by (58).
- (32) observed the emergence of two to three waves carrying 4 to 14 follicles greater than 4 mm. The given simulation results of 16.19 ± 3.08 follicles in two waves per cycle match their experimental investigations.

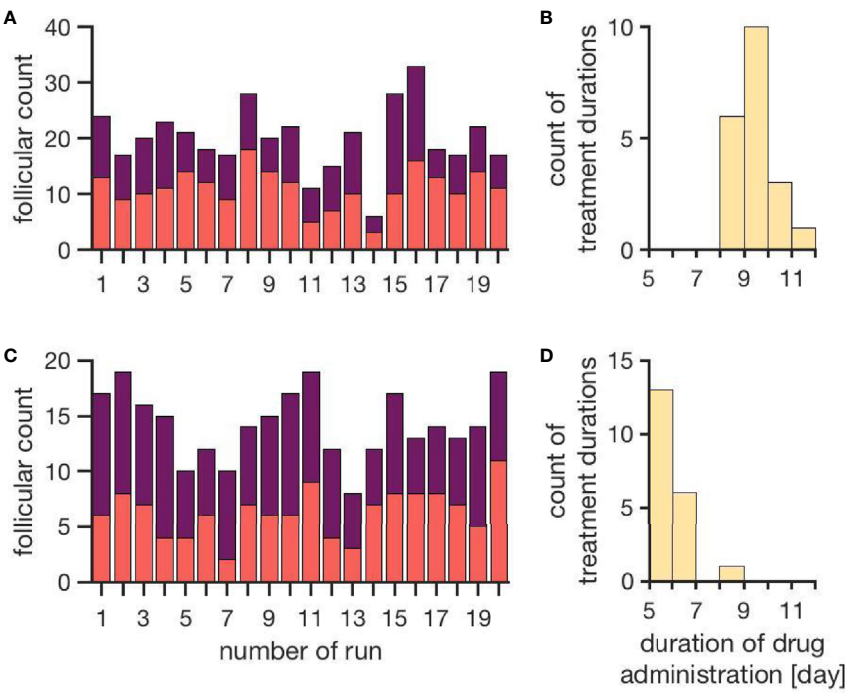

FIGURE 4 | Simulation outcomes of 20 independent cycles for each treatment: ovarian stimulation induced either during the luteal phase (top, **A, B**) or the late follicular phase (bottom, **C, D**). In the upper row **(A, B)**, follicular counts and treatment duration for the luteal phase stimulation approach are displayed (red: follicles 10–14 mm; purple: follicles >14 mm). On average, 11.1 ± 3.5 follicles with a diameter of 10 to 14 mm and 8.9 ± 3.7 follicles with a diameter >14 mm are observed. The average treatment duration is 9.4 ± 0.7 days. The lower row **(C, D)** shows follicular counts and treatment durations for simulated stimulations in the late follicular phase. A treatment cycle takes about 6.0 ± 0.7 days. The average count of follicles with diameters 10 - 14 mm is 6.3 ± 2.2 and the one for follicles >14 mm is 8.0 ± 2.2. (Numbers refer to mean ± standard deviation.)

TABLE 1 | Comparison between simulation results and clinical observations.

	Luteal phase ovarian stimulation		Late follicular phase ovarian stimulation	
	Kuang et al. (26)	Simulation	Zhu and Fu (24)	Simulation
Num. of follicles with diameter 10 - 14 mm	13.9 ± 7.8	11.1 ± 3.5		6.3 ± 2.2
Num. of follicles with diameter > 14 mm	11.1 ± 5.5	8.9 ± 3.7	11.7 ± 6.2	8.0 ± 2.2
Duration of treatment with hMG	10.2 ± 1.6	9.4 ± 0.7	10.93 ± 1.66	6.0 ± 0.7

Ovarian stimulation is induced either during the luteal phase or the late follicular phase. Each of the two studies includes data from more than 100 woman. Patients were at the age of 18 – 40 years with a body mass index of 18 – 30 kg/m^3. All woman showed spontaneous ovulation.

The discontinuity in the profile of the E2 curve (**Figure 2** at day 85 of the simulation) is related to the growth behavior of the follicles and is caused by atresia of larger sub-dominant follicles.

By comparing the results in Table 4, it is visible that variations in the experimental data are higher than in the simulation results. That indicates the fact that the inter-individual variability in human is higher than the variability between simulations sharing one set of non-follicular parameters. The stochastic growth behavior of follicles is the only source of variability between simulations. According to (24), the LH concentration under stimulatory treatment in the late follicular phase is not supposed to increase after the ovulation of the dominant follicle due to the inhibitory effect of P4. However, this effect is not visible in the simulation results (**Figures 3F–J**). This might be due to the comparably lower P4 concentrations in the simulation results. Here, the P4 concentration at day 6 is about 0.99 ± 0.6 ng/mL, whereas the figures published by (24) indicate P4 concentrations up to more than five times as high. In the present model, the P4 concentration is linked to the formation of the corpus luteum as the only source of P4. Minor P4 sources such as the adrenal cortex are neglected. However, the equations for the P4 concentration matches experimental measurements quite well (**Figure S1 in Supplementary Material**). A relation between the high LH concentrations, the low P4 concentrations and the follicular growth behavior are conceivable as well. Since the simulated treatment duration is several days shorter than those in the clinical observations, it appears that follicles are growing too fast during the simulation of ovarian stimulation. If this is the reason for the mismatch between the simulation results and the observations by (24), two explanations are credible: (i) the model parameters should have other values, or (ii) at least one mechanism is missing. However, at this point it was not possible to compare the simulated follicular growth under treatment to detailed experimental investigations since ultrasound measurement data were not available from literature.

Another reason for the mismatch could be that we could not simulate the clinical treatment procedures in full detail. In a clinical setting the dose is adjusted according to the treatment response, which is based on an evaluation of follicular growth during the stimulation procedure. Since the criteria for dose adjustment were not described in the available publications, we did not implement adjustments in our model.

We have not yet simulated double ovarian stimulation due to technical difficulties with the model implementation. However, we will do this in future work in order to address some of the problems that are still unsolved (60), for example the choice of the best day to start the second stimulation or the necessity of using a GnRH antagonist during the second stimulation.

Finally, we want to point out that clinical data are mainly reported as summary statistics, usually in terms of means and standard deviations, and for very few indicators, e.g. treatment duration or number and sizes of follicles on certain treatment days. However, with our model-based approach we could go beyond a simple comparison of moments. Since the model simulations generate distributions, we could compare them with data from literature if the publications about clinical trial outcomes reported the complete data distributions.

CONCLUSION

This study demonstrates how mathematical modeling and simulations can contribute to enhance our mechanistic understanding of ovarian stimulation protocols. In particular, our approach allows to study the extend of variability in both treated and untreated cycles. The model simulations confirm that follicular size is not a reliable parameter for determining treatment outcome since the receptor status of each individual follicle (modeled by the FSH sensitivity threshold) and the timing of growth matter. However, we cannot (yet) make use of that knowledge in a clinical setting as long as the receptor status cannot be inferred from measurements. Making predictions on the level of individuals, either in-vivo or in-silico, will therefore remain notoriously difficult. However, models that include random effects can be used to quantify uncertainties in the predictions. Even though these uncertainties might be large, being aware of what could happen as well as identifying outliers can assist in making decisions. Moreover, the model presented here could be used to compare the outcome of different treatment strategies in terms of specific success criteria (e.g. average number of follicles larger than a threshold size at the end of the stimulation), similar to the approach in (39). This requires to first validate the model with data from other stimulation protocols. For example, in order to compare the two protocols simulated here with the three currently most often used protocols (long, short, and antagonist), we would need data on each protocol from cohorts that are comparable in terms of size and physiological stage (e.g. race, age, BMI). We therefore invite clinicians to share their data and to join interdisciplinary research projects with the ultimate goal to develop model-based clinical decision support systems.

DATA AVAILABILITY STATEMENT

The original contributions presented in the study are included in the article/**Supplementary Material**. Further inquiries can be directed to the corresponding author.

AUTHOR CONTRIBUTIONS

SF and SR conceived the study. ET, TM, ME, FI, TK, BL, and SR obtained the funding. BL collected the data. SF, RE, SS, BL, and SR analyzed and interpreted the data. SF, RE, SS, and SR developed the mathematical model. SF and SS implemented the model and performed the simulations. All authors contributed to the article and approved the submitted version.

FUNDING

The work of SF and SR was supported by the Trond Mohn Foundation (BSF, https://www.mohnfoundation.no/), grant no. BFS2017TMT01. The funder had no role in study design, data collection and analysis, decision to publish, or preparation of the manuscript.

SUPPLEMENTARY MATERIAL

The Supplementary Material for this article can be found online at: https://www.frontiersin.org/articles/10.3389/fendo.2021.613048/full#supplementary-material

REFERENCES

1. Mascarenhas M, Flaxman S, Boerma T, Vanderpoel S, Stevens G. National, regional, and global trends in infertility prevalence since 1990: a systematic analysis of 277 health surveys. *PloS Med* (2012) 9:e1001356. doi: 10.1371/journal.pmed.1001356
2. Turner KA, Rambhatla A, Schon S, Agarwal A, Krawetz SA, Dupree JM, et al. Male infertility is a women's health issue – Research and clinical evaluation of male infertility is needed. *Cells* (2020) 9:990. doi: 10.3390/cells9040990
3. Yatsenko SA, Rajkovic A. Genetics of human female infertility. *Biol Reprod* (2019) 101:549–66. doi: 10.1093/biolre/ioz084
4. Wischmann T, Stammer H, Scherg H, Gerhard I, Verres R. Psychosocial characteristics of infertile couples: a study by the 'Heidelberg Fertility Consultation Service'. *Hum Reprod* (2001) 16:1753–61. doi: 10.1093/humrep/16.8.1753
5. Quesnel-Vallée A, Maximova K. Mental health consequences of unintended childlessness and unplanned births: Gender differences and life course dynamics. *Soc Sci Med* (2009) 68:850–7. doi: 10.1016/j.socscimed.2008.11.012
6. Suthersan D, Kennedy S, Chapman M. Physical symptoms throughout ivf cycles. *Hum Fertil* (2011) 14:122–8. doi: 10.3109/14647273.2011.571748
7. Oktay K, Briggs D, Gosden RG. Ontogeny of follicle-stimulating hormone receptor gene expression in isolated human ovarian follicles. *J Clin Endocrinol Metab* (1997) 82:3748–51. doi: 10.1210/jc.82.11.3748
8. McGee EA, Hsueh AJ. Initial and cyclic recruitment of ovarian follicles. *Endocr Rev* (2000) 21:200–14. doi: 10.1210/edrv.21.2.0394
9. Gougeon A. Regulation of ovarian follicular development in primates: facts and hypotheses. *Endocr Rev* (1996) 17:121–55. doi: 10.1210/edrv-17-2-121
10. Filicori M. The role of luteinizing hormone in folliculogenesis and ovulation induction. *Fertil Steril* (1999) 71:405–14. doi: 10.1016/S0015-0282(98)00482-8
11. Erickson GF, Shimasaki S. The physiology of folliculogenesis: the role of novel growth factors. *Fertil Steril* (2001) 76:943–9. doi: 10.1016/S0015-0282(01)02859-X
12. Hiller SG, Reichert JR LE, Van Hall EV. Control of preovulatory follicular estrogen biosynthesis in the human ovary. *J Clin Endocrinol Metab* (1981) 52:847–56. doi: 10.1210/jcem-52-5-847
13. Henzl M, Segre E. Physiology of human menstrual cycle and early pregnancy. A review of recent investigations. *Contraception* (1970) 1:315–38. doi: 10.1016/0010-7824(70)90017-X
14. Odell W. The reproductive system in women. In: DeGroot LJ, ed. *Endocrinology Vol 3*. New York: Grune & Stratton (1979). 3:1383–400.
15. Franz W3rd. Basic review: Endocrinology of the normal menstrual cycle. *Prim Care* (1988) 15:607.
16. Arslan M, Bocca S, Mirkin S, Barroso G, Stadtmauer L, Oehninger S. Controlled ovarian hyperstimulation protocols for in vitro fertilization: two decades of experience after the birth of Elizabeth Carr. *Fertil Steril* (2005) 84:555–69. doi: 10.1016/j.fertnstert.2005.02.053
17. Shrestha D, La X, Feng HL. Comparison of different stimulation protocols used in in vitro fertilization: A review. *Ann Trans Med* (2015) 3:137. doi: 10.3978/j.issn.2305-5839.2015.04.09
18. Lai Q, Zhang H, Zhu G, Li Y, Jin L, He L, et al. Comparison of the GnRH agonist and antagonist protocol on the same patients in assisted reproduction during controlled ovarian stimulation cycles. *Int J Clin Exp Pathol* (2013) 6:1903–10.
19. Huirne J, Homburg R, Lambalk C. Are GnRH antagonists comparable to agonists for use in IVF? *Hum Reprod* (2007) 22:2805–13. doi: 10.1093/humrep/dem270
20. Khalaf M, Mittre H, Levallet J, Hanoux V, Denoual C, Herlicoviez M, et al. GnRH agonist and GnRH antagonist protocols in ovarian stimulation: differential regulation pathway of aromatase expression in human granulosa cells. *Reprod Biomed Online* (2010) 21:56–65. doi: 10.1016/j.rbmo.2010.03.017
21. Domar A. Impact of psychological factors on dropout rates in insured infertility patients. *Fertil Steril* (2004) 81:271–3. doi: 10.1016/j.fertnstert.2003.08.013
22. Pasch LA, Holley SR, Bleil ME, Shehab D, Katz PP, Adler NE. Addressing the needs of fertility treatment patients and their partners: are they informed of and do they receive mental health services? *Fertil Steril* (2016) 106:209–15.e2. doi: 10.1016/j.fertnstert.2016.03.006
23. Sighinolfi G, Grisendi V, La Marca A. How to personalize ovarian stimulation in clinical practice. *J Turk Ger Gynecol Assoc* (2017) 18:148. doi: 10.4274/jtgga.2017.0058
24. Zhu X, Fu Y. Evaluation of ovarian stimulation initiated from the late follicular phase using human menopausal gonadotropin alone in normo-ovulatory women for treatment of infertility: A retrospective cohort study. *Front Endocrinol* (2019) 10:448. doi: 10.3389/fendo.2019.00448
25. Kim JH, Kim SK, Lee HJ, Lee JR, Jee BC, Suh CS, et al. Efficacy of random-start controlled ovarian stimulation in cancer patients. *J Korean Med Sci* (2015) 30:290–5. doi: 10.3346/jkms.2015.30.3.290
26. Kuang Y, Hong Q, Chen Q, Lyu Q, Ai A, Fu Y, et al. Luteal-phase ovarian stimulation is feasible for producing competent oocytes in women undergoing in vitro fertilization/intracytoplasmic sperm injection treatment, with optimal pregnancy outcomes in frozen-thawed embryo transfer cycles. *Fertil Steril* (2014b) 101:105–11. doi: 10.1016/j.fertnstert.2013.09.007
27. Cakmak H, Rosen M. Ovarian stimulation in cancer patients. *Fertil Steril* (2013) 99:1476–84. doi: 10.1016/j.fertnstert.2013.03.029
28. Moffat R, Pirtea P, Gayet V, Wolf JP, Chapron C, de Ziegler D. Dual ovarian stimulation is a new viable option for enhancing the oocyte yield when the time for assisted reproductive technnology is limited. *Reprod Biomed Online* (2014) 29:659–61. doi: 10.1016/j.rbmo.2014.08.010
29. Kuang Y, Chen Q, Hong Q, Lyu Q, Ai A, Fu Y, et al. Double stimulations during the follicular and luteal phases of poor responders in IVF/ICSI programmes (Shanghai Protocol). *Reprod Biomed Online* (2014a) 29:684–91. doi: 10.1016/j.rbmo.2014.08.009
30. de Almeida Cardoso MC, Evangelista A, Sartório C, Vaz G, Werneck CLV, Guimarães FM, et al. Can ovarian double-stimulation in the same menstrual cycle improve IVF outcomes? *JBRA Assist Reprod* (2017) 21:217. doi: 10.5935/1518-0557.20170042
31. Baerwald A, Adams G, Pierson R. Characterization of ovarian follicular wave dynamics in women. *Biol Reprod* (2003a) 69:1023–31. doi: 10.1095/biolreprod.103.017772

32. Baerwald A, Adams G, Pierson R. A new model for ovarian follicular development during the human menstrual cycle. *Fertil Steril* (2003b) 80:116–22. doi: 10.1016/S0015-0282(03)00544-2
33. Harris-Clark L, Schlosser P, Selgrade J. Multiple stable periodic solutions in a model for hormonal control of the menstrual cycle. *Bull Math Biol* (2003) 65:157–73. doi: 10.1006/bulm.2002.0326
34. Panza N, Wright A, Selgrade J. A delay differential equation model of follicle waves in women. *J Biol Dyn* (2016) 10:200–21. doi: 10.1080/17513758.2015.1115564
35. Reinecke I, Deuflhard P. A complex mathematical model of the human menstrual cycle. *J Theor Biol* (2007) 247:303–30. doi: 10.1016/j.jtbi.2007.03.011
36. Reinecke I. *Mathematical modeling and simulation of the female menstrual cycle. Ph.D. thesis, PhD thesis*. Freie Universität Berlin (2009).
37. Röblitz S, Stötzel C, Deuflhard P, Jones HM, Azulay D-O, van der Graaf PH, et al. A mathematical model of the human menstrual cycle for the administration of GnRH analogues. *J Theor Biol* (2013) 321:8–27. doi: 10.1016/j.jtbi.2012.11.020
38. Lange A, Schwieger R, Plöntzke J, Schäfer S, Röblitz S. Follicular competition in cows: the selection of dominant follicles as a synergistic effect. *J Math Biol* (2018) 78(3):579–606. doi: 10.1007/s00285-018-1284-0
39. Ehrig R, Dierkes T, Schäfer S, Röblitz S, Tronci E, Mancini T, et al. *An Integrative Approach for Model Driven Computation of Treatments in Reproductive Medicine*. ZIB report 16-04, Berlin: Zuse Institute (2016). Available at: https://opus4.kobv.de/opus4-zib/frontdoor/index/index/docId/5710.
40. Mancini T, Mari F, Massini A, Melatti I, Salvo I, Sinisi S, et al. Computing personalised treatments through in silico clinical trials. A case study on downregulation in assisted reproduction. In: *Proceedings of 25th RCRA International Workshop on Experimental Evaluation of Algorithms for Solving Problems with Combinatorial Explosion. EasyChair* (2018). doi: 10.29007/g864
41. Tronci E, Mancini T, Salvo I, Sinisi S, Mari F, Melatti I, et al. Patient-specific models from inter-patient biological models and clinical records. In: *Proceedings of 14th Conference in Formal Methods in Computer-Aided Design (FMCAD 2014)*. IEEE (2014). p. 207–14. doi: 10.1109/FMCAD.2014.6987615
42. Mancini T, Tronci E, Salvo I, Mari F, Massini A, Melatti I. Computing biological model parameters by parallel statistical model checking. In: *Proceedings of the 3rd International Conference on Bioinformatics and Biomedical Engineering (IWBBIO 2015) (Springer), vol. 9044 of Lecture Notes in Computer Science*. Springer (2015). p. 542–54. doi: 10.1007/978-3-319-16480-9_52
43. Sinisi S, Alimguzhin V, Mancini T, Tronci E, Leeners B. Complete populations of virtual patients for in silico clinical trials. *Bioinformatics* (2020a). doi: 10.1093/bioinformatics/btaa1026
44. Sinisi S, Alimguzhin V, Mancini T, Tronci E, Mari F, Leeners B. Optimal personalised treatment computation through in silico clinical trials on patient digital twins. *Fundam Inform* (2020b) 174:283–310. doi: 10.3233/FI-2020-1943
45. Waller K, Swan SH, Windham GC, Fenster L, Elkin EP, Lasley BL. Use of urine biomarkers to evaluate menstrual function in healthy premenopausal women. *Am J Epidemiol* (1998) 147:1071–80. doi: 10.1093/oxfordjournals.aje.a009401
46. Brown J. Pituitary control of ovarian function—concepts derived from gonadotrophin therapy. *Aust New Z J Obstet Gynaecol* (1978) 18:47–54. doi: 10.1111/j.1479-828X.1978.tb00011.x
47. Baerwald A, Adams G, Pierson R. Ovarian antral folliculogenesis during the human menstrual cycle: A review. *Hum Reprod Update* (2011) 18:73–91. doi: 10.1093/humupd/dmr039
48. Fauser BB, van Heusden AM. Manipulation of human ovarian function: physiological concepts and clinical consequences. *Endocr Rev* (1997) 18 (1):71–106. doi: 10.1210/edrv.18.1.0290
49. Adams G, Kot K, Smith C, Ginther O. Selection of a dominant follicle and suppression of follicular growth in heifers. *Anim Reprod Sci* (1993) 30:259–71. doi: 10.1016/0378-4320(93)90076-4
50. Schipper I, Hop WC, Fauser BC. The follicle-stimulating hormone (FSH) threshold/window concept examined by different interventions with exogenous FSH during the follicular phase of the normal menstrual cycle: duration, rather than magnitude, of fsh increase affects follicle development. *J Clin Endocrinol Metab* (1998) 83:1292–8. doi: 10.1210/jc.83.4.1292
51. Baird D. The selection of the follicle of the month. In: *From Ovulation to Implantation Proceedings of the VII Regnier de Graaf Symposium*. Maastricht, the Netherlands: Excerpta Medica (1990).
52. Baird DT, Bäckström T, McNeilly AS, Smith SK, Wathen CG. Effect of enucleation of the corpus luteum at different stages of the luteal phase of the human menstrual cycle on subsequent follicular development. *J Reprod Fertil* (1984) 70:615–24. doi: 10.1530/jrf.0.0700615
53. Baird D, Fraser I. Concentration of oestrone and oestradiol in follicular fluid and ovarian venous blood of women. *Clin Endocrinol* (1975) 4:259–66. doi: 10.1111/j.1365-2265.1975.tb01533.x
54. McNatty K, Baird D, Bolton A, Chambers P, Corker C, McLean H. Concentration of oestrogens and androgens in human ovarian venous plasma and follicular fluid throughout the menstrual cycle. *J Endocrinol* (1976) 71:77–85. doi: 10.1677/joe.0.0710077
55. Dataset Kompendium. *Arzneimittelkompendium der Schweiz* (2020). Available at: https://compendium.ch/ (Accessed 10 June 2020).
56. Landgren B-M, Unden A-L, Diczfalusy E. Hormonal profile of the cycle in 68 normally menstruating women. *Eur J Endocrinol* (1980) 94:89–98. doi: 10.1530/acta.0.0940089
57. Cole L, Ladner D, Byrn F. The normal variabilities of the menstrual cycle. *Fertil Steril* (2009) 91:522–7. doi: 10.1016/j.fertnstert.2007.11.073
58. Fehring RJ, Schneider M, Raviele K. Variability in the phases of the menstrual cycle. *J Obstet Gynecol Neonatal Nurs* (2006) 35:376–84. doi: 10.1111/j.1552-6909.2006.00051.x
59. Lenton EA, Landgren B-M, Sexton L. Normal variation in the length of the luteal phase of the menstrual cycle: identification of the short luteal phase. *BJOG* (1984) 91:685–9. doi: 10.1111/j.1471-0528.1984.tb04831.x
60. Sighinolfi G, Sunkara SK, La Marca A. New strategies of ovarian stimulation based on the concept of ovarian follicular waves: from conventional to random and double stimulation. *Reprod Biomed Online* (2018) 37:489–97. doi: 10.1016/j.rbmo.2018.07.006

Conflict of Interest: The authors declare that the research was conducted in the absence of any commercial or financial relationships that could be construed as a potential conflict of interest.

frontiers in Endocrinology

ORIGINAL RESEARCH
published: 15 March 2021
doi: 10.3389/fendo.2021.611253

Model-Based Assessment of C-Peptide Secretion and Kinetics in Post Gastric Bypass Individuals Experiencing Postprandial Hyperinsulinemic Hypoglycemia

*Michele Schiavon[1], David Herzig[2], Matthias Hepprich[3], Marc Y. Donath[3], Lia Bally[2] and Chiara Dalla Man[1]**

[1] Department of Information Engineering, University of Padova, Padova, Italy, [2] Department of Diabetes, Endocrinology, Nutritional Medicine and Metabolism, Inselspital, Bern University Hospital, University of Bern, Bern, Switzerland, [3] Division of Endocrinology, Diabetes and Metabolism, University Hospital Basel, Basel, Switzerland

OPEN ACCESS

Edited by:
Darko Stefanovski,
University of Pennsylvania,
United States

Reviewed by:
Amit Tirosh,
Sheba Medical Center, Israel
Michael Rickels,
University of Pennsylvania,
United States

***Correspondence:**
Chiara Dalla Man
dallaman@dei.unipd.it

Specialty section:
This article was submitted to Systems Endocrinology, a section of the journal Frontiers in Endocrinology

Received: 28 September 2020
Accepted: 19 January 2021
Published: 15 March 2021

Citation:
Schiavon M, Herzig D, Hepprich M, Donath MY, Bally L and Dalla Man C (2021) Model-Based Assessment of C-Peptide Secretion and Kinetics in Post Gastric Bypass Individuals Experiencing Postprandial Hyperinsulinemic Hypoglycemia. Front. Endocrinol. 12:611253. doi: 10.3389/fendo.2021.611253

Assessment of insulin secretion is key to diagnose postprandial hyperinsulinemic hypoglycemia (PHH), an increasingly recognized complication following bariatric surgery. To this end, the Oral C-peptide Minimal Model (OCMM) can be used. This usually requires fixing C-peptide (CP) kinetics to the ones derived from the Van Cauter population model (VCPM), which has never been validated in PHH individuals. The objective of this work was to test the validity of the OCMM coupled with the VCPM in PHH subjects and propose a method to overcome the observed limitations. Two cohorts of adults with PHH after gastric bypass (GB) underwent either a 75 g oral glucose (9F/3M; age=42±9 y; BMI=28.3±6.9 kg/m^2) or a 60 g mixed-meal (7F/3M; age = 43 ± 11 y; BMI=27.5±4.2 kg/m^2) tolerance test. The OCMM was identified on CP concentration data with CP kinetics fixed to VCPM (VC approach). In both groups, the VC approach underestimated CP-peak and overestimated CP-tail suggesting CP kinetics predicted by VCPM to be inaccurate in this population. Thus, the OCMM was identified using CP kinetics estimated from the data (DB approach) using a Bayesian Maximum a Posteriori estimator. CP data were well predicted in all the subjects using the DB approach, highlighting a significantly faster CP kinetics in patients with PHH compared to the one predicted by VCPM. Finally, a simulation study was used to validate the proposed approach. The present findings question the applicability of the VCPM in patients with PHH after GB and call for CP bolus experiments to develop a reliable CP kinetic model in this population.

Keywords: model identification, parameter estimation, obesity, insulin secretion, oral minimal model, OGTT, mixed meal

INTRODUCTION

Postprandial hyperinsulinemic hypoglycemia is an increasingly recognized metabolic complication affecting up to a third of patients following gastric bypass surgery (1, 2). While the underlying mechanisms remain to be fully elucidated (3), excessive postprandial insulin exposure due to exaggerated insulin secretion and/or diminished insulin clearance are key pathophysiological hallmarks of postprandial hyperinsulinemic hypoglycemia (4–6). Thus, reliable estimation of insulin secretion is fundamental to improve our understanding and diagnostic armamentarium of this complex condition.

Insulin secretion is not directly measurable *in vivo* but can be reconstructed from plasma C-peptide concentrations using non-parametric, e.g., deconvolution (7), or parametric approaches, e.g., structural models (8–11). Nevertheless, both approaches require the knowledge of C-peptide kinetics, usually described by a linear two-compartment model (12).

The direct measurement of C-peptide kinetics requires the injection of a C-peptide bolus under somatostatin infusion to block its endogenous secretion (13). However, to reduce patient burden and costs associated with additional experiments, C-peptide kinetic parameters predicted by the Van Cauter population model (14) can be used. The Van Cauter population model was originally validated in normal, obese, and non-insulin-dependent diabetic individuals and its use within approaches to estimate insulin secretion was shown to yield similar average estimates in the target population as when individual estimates from C-peptide bolus data are used (15, 16). However, this might not hold true when the Van Cauter population model is applied to different populations, such as patients having undergone bariatric surgery, procedures that substantially alter glucose kinetics and secretion of gluco-regulatory hormones (17). Since inaccuracy in C-peptide kinetics may negatively affect the estimation of insulin secretion, the applicability of the Van Cauter population model to predict C-peptide kinetics in patients suffering from postprandial hyperinsulinemic hypoglycemia must be investigated.

The aim of this work was to assess the validity of the Van Cauter population model in post-gastric bypass individuals suffering from postprandial hyperinsulinemic hypoglycemia. This was done by coupling it with a model for the estimation of C-peptide secretion. Among the models proposed in the literature, here the so-called Oral C-peptide Minimal Model (OCMM) (11, 18) was used. In a second step, a new methodology was proposed to overcome the observed limitations when using the Van Cauter population model in these subjects. Finally, the validity of this new methodology was tested by means of an *in silico* experiment.

DATABASE AND METHODS

Databases

Data from twenty-two post-gastric bypass individuals suffering from postprandial hyperinsulinemic hypoglycemia gathered during two separate clinical trials were used in this work.

Twelve subjects (Cohort 1 - OGTT) (9F; age = 42±9 y; BMI = 28.3±6.9 kg/m^2) were studied at the University Hospital Bern, Bern, Switzerland (NCT03609632). Participants arrived at the clinical research facility at 0800 after an overnight fast. An intravenous cannula was inserted in one arm for blood sampling and kept open with a saline infusion. Participants underwent a standard oral glucose tolerance test (OGTT) consisting in the ingestion of 75 g of dextrose and the frequent sampling for plasma glucose, insulin and C-peptide concentrations for 210 min after glucose ingestion. Samples were taken every 15 min until 60 min after glucose ingestion and every 30 min subsequently. Hypoglycemia, defined as plasma glucose level < 2.8 mmol/L, was treated using intravenous dextrose (10%) to reach euglycaemia. Plasma glucose was determined from venous blood using the Biosen C-line analyser (IGZ Instruments AG, Zurich, Switzerland). Insulin and C-peptide concentration were measured by conventional immunoassays (Roche Diagnostics, Mannheim, Germany).

The other 10 subjects (Cohort 2 - MMTT) (7F; age = 43±11 y; BMI = 27.5±4.2 kg/m^2) were studied at the University Hospital Basel, Basel, Switzerland (NCT03200782). Subjects participated in a double-blind, double-dummy placebo controlled, randomized, cross-over trial where each subject underwent a standardized liquid mixed-meal tolerance test (MMTT, 300 ml Ensure plus®, Abbott, 60 g carbohydrates, 450 kcal) on three occasions receiving either a placebo, a SGLT2-inhibitor or a IL-1 receptor agonist. For the purpose of this work, only data from the placebo visit were used. More details on the study protocol can be found in (19). Plasma glucose, insulin and C-peptide concentrations were sampled every 30 min for 180 min after mixed-meal ingestion. In case of symptomatic hypoglycemia, defined by the Whipple's triad with plasma glucose < 2.5 mmol/L, immediate glucose measurement and blood sampling was performed followed by the administration of 10 g glucose (orally or intravenously).

In **Figure 1**, mean ± standard error (SE) of plasma glucose (top) and C-peptide (bottom) concentrations of the two studies are reported.

Methods

The Oral C-Peptide Minimal Model (OCMM)

The oral C-peptide minimal model (OCMM, **Figure 2**) (11, 18) interprets plasma C-peptide concentration in relation to the observed changes in glucose concentration and provides a quantification of β-cell responsivity to glucose.

C-peptide kinetics are described by the well-known two-compartment model (12) (**Figure 2**, right panel):

$$\begin{cases} \dot{CP_1}(t) = -(k_{01} + k_{21}) \cdot CP_1(t) + k_{12} \cdot CP_2(t) + SR(t) & CP_1(0) = 0 \\ \dot{CP_2}(t) = -k_{12} \cdot CP_2(t) + k_{21} \cdot CP_1(t) & CP_2(0) = 0 \end{cases} \quad (1)$$

where CP_1 and CP_2 (pmol/L) are the above-basal C-peptide concentrations in the first (central) and second (peripheral) compartments respectively, k_{ij} (min^{-1}) the C-peptide kinetic parameters, with k_{01} representing the C-peptide fractional metabolic clearance rate (MCR, min^{-1}) and SR (pmol/L/min)

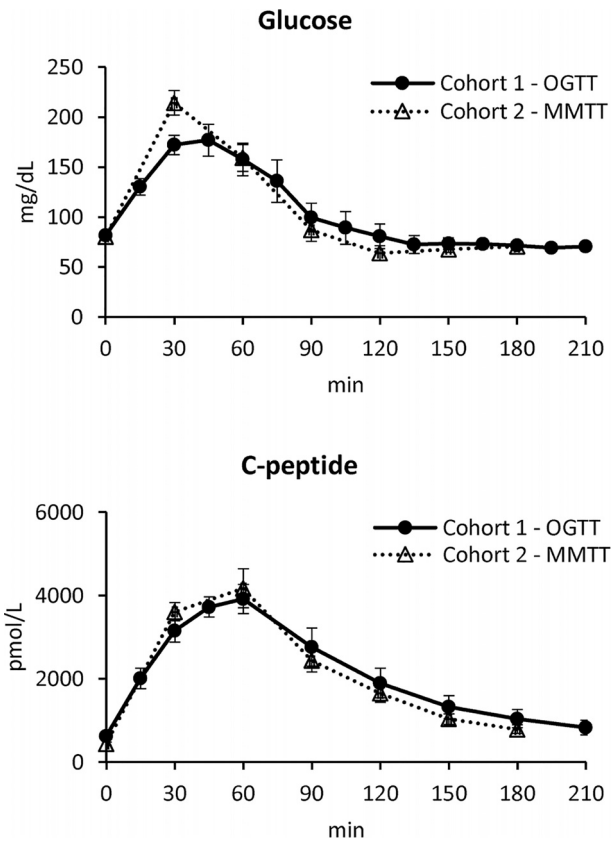

FIGURE 1 | Plasma glucose (top) and C-peptide (bottom) concentrations in Cohort 1 – OGTT (continuous line with black circles) and Cohort 2 – MMTT (dotted line with triangles) (mean ± SE).

the above basal pancreatic secretion normalized by the volume of distribution of the first compartment.

SR is modeled as the sum of two components controlled by glucose concentration (static component, SR_s) and its rate of increase (dynamic component, SR_d) (**Figure 2**, left panel):

$$SR(t) = SR_s(t) + SR_d(t) \tag{2}$$

In particular, SR_s represents the provision of new releasable insulin Y(t) (pmol/L/min):

$$SR_s(t) = Y(t) \tag{3}$$

which is controlled by glucose concentration (G, mmol/L) according to:

$$\dot{Y}(t) = -\alpha[Y(t) - \beta \cdot [G(t) - h]\,] \;\; Y(0) = 0 \tag{4}$$

Thus, SR_s is dynamically related to glucose concentration and tends toward a steady-state value with a time constant $1/\alpha$ (min). The steady-state value is linearly dependent from glucose concentration above a threshold level h (mmol/L), here fixed to pre-meal (basal) glucose level G_b (20), through a parameter β (min^{-1}). SR_d represents the secretion of promptly releasable insulin and is proportional, through a parameter k_d (dimensionless), to the rate of glucose increase:

$$SR_d(t) = \begin{cases} k_d \cdot \dot{G}(t) & if\ \dot{G}(t) > 0 \\ 0 & if\ \dot{G}(t) \le 0 \end{cases} \tag{5}$$

Basal insulin secretion (SR_b) can be calculated as:

$$SR_b = k_{01} \cdot CP_{1b} \tag{6}$$

where CP_{1b} is the basal C-peptide concentration in the first compartment.

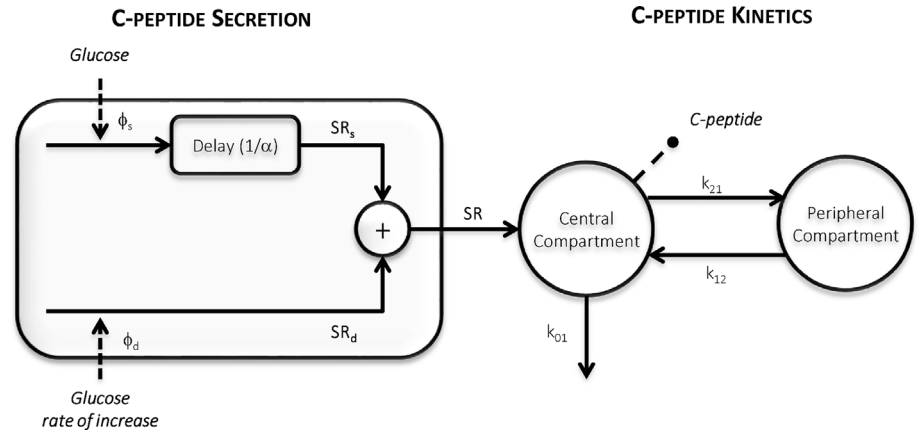

FIGURE 2 | The Oral C-peptide Minimal Model (OCMM) (11, 18) with its secretion (left) and kinetics (right) components. SR is the pancreatic secretion, Φ_s and Φ_d static and dynamic β-cell responsivity indices respectively, $1/\alpha$ time constant of the static component, and k_{01}, k_{12}, and k_{21} C-peptide kinetic parameters.

From model parameters, indices of static ($\Phi_s = \beta$, 10^{-9} min^{-1}), dynamic ($\Phi_d = k_d$, 10^{-9}) and basal β-cell responsiveness ($\Phi_b = SR_b/G_b$, 10^{-9} min^{-1}) can be derived. Finally, an index of total β-cell responsiveness to glucose (Φ_{tot}, 10^{-9} min^{-1}) (11) can be calculated as:

$$\phi_{tot} = \frac{\int_0^T [SR(t) + SR_b]dt}{\int_0^T G(t)dt}$$

$$= \frac{\phi_d \cdot (G_{max} - G_b) + \phi_s \cdot \int_0^T [G(t) - h]dt + T \cdot \phi_b \cdot G_b}{\int_0^T G(t)dt} \quad (7)$$

where T (min) is the time at which the system is assumed to return to steady-state conditions after the perturbation (here assumed T=300 min).

Model Identification

The OCMM is *a priori* uniquely identifiable if the measured C-peptide data are assumed as model output and the measured glucose concentrations as known input (21, 22). Parameters were estimated with a Bayesian Maximum a Posteriori (MAP) estimator (23), which requires the maximization of the *a posteriori* probability density function of the parameter vector $\boldsymbol{p} = [k_d, \alpha, \beta, k_{01}, k_{12}, k_{21}]$:

$$\hat{\boldsymbol{p}}_{MAP} = \arg\max_{\boldsymbol{p}} f_{\boldsymbol{p}|\boldsymbol{z}}(\boldsymbol{p}|\boldsymbol{z}) \quad (8)$$

which, by recalling the Bayes theorem, can be rewritten as

$$\hat{\boldsymbol{p}}_{MAP} = \arg\max_{\boldsymbol{p}} \frac{f_{\boldsymbol{z}|\boldsymbol{p}}(\boldsymbol{z}|\boldsymbol{p}) f_{\boldsymbol{p}}(\boldsymbol{p})}{f_{\boldsymbol{z}}(\boldsymbol{z})} \quad (9)$$

where $f_{\boldsymbol{z}|\boldsymbol{p}}$ $(\boldsymbol{z}|\boldsymbol{p})$ is the likelihood of the data, $f_{\boldsymbol{z}}$ $(\boldsymbol{z})$ is the probability density function of the data vector $\boldsymbol{z}$, which can be ignored in the maximization problem since it does not depend on $\boldsymbol{p}$, and $f_{\boldsymbol{p}}$ $(\boldsymbol{p})$ is the *a priori* probability density function of $\boldsymbol{p}$. The definition of $f_{\boldsymbol{p}}$ $(\boldsymbol{p})$ differs depending on the adopted identification approach, as detailed below.

C-Peptide Kinetics Fixed to Van Cauter Population Model (VC Approach)

Here, we assumed $\boldsymbol{p}=[\boldsymbol{p_1}, \boldsymbol{p_2}]$ with $\boldsymbol{p_1}=[k_d, \alpha, \beta]$ and $\boldsymbol{p_2}=[k_{01}, k_{12}, k_{21}]$. The *a priori* probability density function f_{p1} $(\boldsymbol{p}_1)$ was assumed to be noninformative for all the parameters except for α to improve the numerical identifiability of the model (11), especially when a limited number of samples is available. The C-peptide kinetic parameters $(\boldsymbol{p_2})$ were fixed to those predicted by the Van Cauter (VC) population model (**Table 1**) (14). In that study, a method was proposed to estimate the kinetics parameters of the two-compartment model of C-peptide kinetics (12) from patient demographics. The model was originally validated in a large database of normal, obese, and non-insulin-dependent individuals with diabetes. However, it has never been validated in PHH subjects.

The VC approach provided unsatisfactory results in terms of model ability to predict the data in this population (see Results section). Therefore, another identification approach was tested (DB approach). Finally, a simulation study was also performed to test the accuracy of this method. An overview of the workflow is shown in **Figure 3**.

C-Peptide Kinetics Estimated from the Data (DB Approach)

Here, the C-peptide kinetic parameters $(\boldsymbol{p_2})$ were estimated, together with the secretion parameters $(\boldsymbol{p_1})$ from the C-peptide data (data-based, DB) using the MAP estimator of eqs. 8 and 9. The *a priori* probability density function $f_{\boldsymbol{p}1}$ $(\boldsymbol{p}_1)$ was the same as the one adopted in the VC approach, while $f_{\boldsymbol{p}2}$ $(\boldsymbol{p}_2)$ was derived from the Van Cauter population model (14).

For both approaches (VC and DB), measurement error of C-peptide concentration was assumed to be independent, Gaussian, with zero mean and variance dependent on C-peptide concentrations (24). Glucose concentration and its time derivative were used as error-free model inputs. Here, the time derivative of glucose concentration was calculated using a stochastic regularized deconvolution method (25), particularly suitable in case of noisy signals. The precision of model parameter estimates was quantified by its coefficient of variation (CV, %) (23). Parameter estimation and statistical analyses were carried out using Matlab® (R2016a); differential equations were integrated using a method based on an explicit

TABLE 1 | Procedure to obtain the c-peptide kinetic parameters using the Van Cauter population model (14).

Step 1:	Determine subject's type: normal, obese, non-insulin dependent diabetes (NIDDM)				
Step 2:	Determine C-peptide short half-life (*a*) and fraction (*f*) parameters				
			Normal	*Obese*	*NIDDM*
	Short half-life (*a*)	[min]	4.95	4.55	4.52
	Fraction (*F*)	[dimensionless]	0.76	0.78	0.78
Step 3:	Derive the long half-life (*b*) parameter according to the equation				
	Long half-life (*b*)	[min]		0.14·(*age* [*year*] + 29.2)	
Step 4:	Determine the C-peptide kinetic parameters as follows				
	k_{12}	[min^{-1}]		F·(ln(2)/*b*) + (1–F)·(ln(2)/*a*)	
	k_{01}	[min^{-1}]		(ln(2)/*a*)·(ln(2)/*b*)/k_{12})	
	k_{21}	[min^{-1}]		(ln(2)/*a*) + (ln(2)/*b*) – k_{01} – k_{12}	

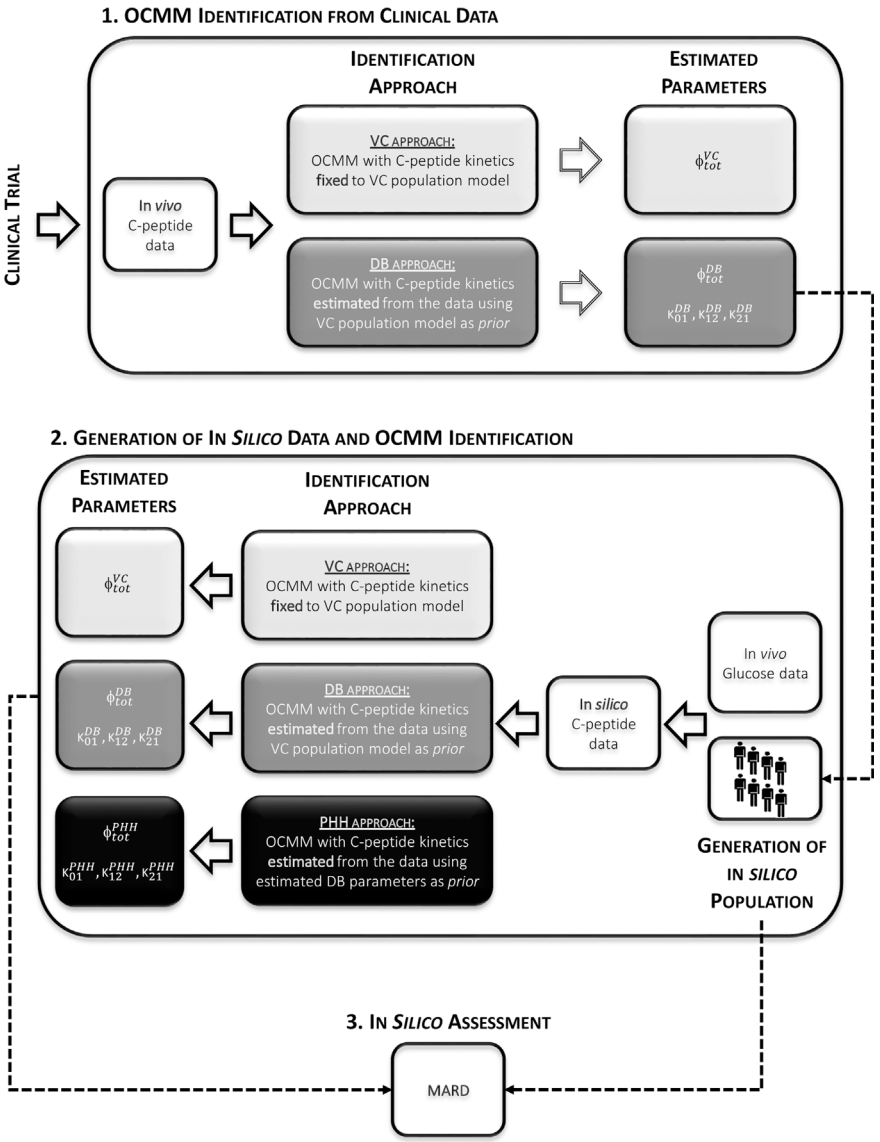

FIGURE 3 | Overview of the study workflow. 1: Identification of the OCMM by both the VC and the proposed DB approach from *in vivo* data. 2: Use of estimated parameters with the DB approach to randomly generate the in *silico* population from which C-peptide concentration curves were simulated. Identification of the OCMM using the VC, DB, and PHH approach using in *silico* data. 3: Calculation of mean absolute relative difference (MARD) for the assessment of the proposed methodology using *in silico* results.

Runge-Kutta (4^{th}–5^{th} order) pair formula implemented in the Matlab function *ode45* (26).

In Silico Assessment

The ability of the proposed DB approach to accurately estimate the kinetic and secretion parameters of the OCMM was assessed by computer simulation.

To set up the simulation, we first used the C-peptide kinetic parameters estimated with the DB approach to derive the joint C-peptide kinetic parameter distribution in our PHH subjects. Specifically, similarly to what done in (27), the kinetic parameters were assumed to be log-normally distributed with mean ($\boldsymbol{\mu_{p2}}$) and covariance matrix ($\boldsymbol{\Sigma_{p2}}$):

$$\boldsymbol{\mu_{p2}} = [mean(\ln k_{01}), mean(\ln k_{12}), mean(\ln k_{21})] \tag{10}$$

$$\Sigma_{p2} = \begin{bmatrix} var(\ln k_{01}) & covar(\ln k_{01}, \ln k_{12}) & covar(\ln k_{01}, \ln k_{21}) \\ covar(\ln k_{01}, \ln k_{12}) & var(\ln k_{12}) & covar(\ln k_{12}, \ln k_{21}) \\ covar(\ln k_{01}, \ln k_{21}) & covar(\ln k_{12}, \ln k_{21}) & var(\ln k_{21}) \end{bmatrix} \tag{11}$$

From the above distribution, we randomly extracted 1,100 kinetic parameter vectors $\boldsymbol{p_2}=[k_{01}, k_{12}, k_{21}]$. In particular, for each of the 22 subjects in our database, 50 triplets ($\boldsymbol{p_2}$) were randomly generated and coupled to the set of estimated secretion

parameters ($\boldsymbol{p_1}$) together with the corresponding glucose curve. This allowed us to create 1,100 *in silico* (virtual) subjects, with known kinetic and secretion parameters, for which the C-peptide concentration after an oral test was simulated using the subject-specific glucose curve as input signal. Such *in silico* C-peptide profiles were then sampled and corrupted by an additive Gaussian random noise with zero mean and variance as in (24). Finally, the OCMM was identified using both the VC and DB approach, as described in Section 2.2.2. In addition, we tested to what extent the final parameter estimates were affected by the choice of the *a priori* information. To do so, the model was also identified using as *prior* information the C-peptide kinetic parameters estimated with the DB approach (PHH approach).

Statistical Analysis

Normality of variable distributions was assessed by Lilliefors test and, since some of the variable of interest were not normally distributed, nonparametric tests were used. In particular, for the parameters estimated from *in vivo* (clinical) data, differences between the VC and the DB approaches, within the same cohort, were assessed using a Wilcoxon signed-rank test; while a Mann-Whitney-U test was used to compare cohorts (Cohort 1-OGTT vs. Cohort 2-MMTT). For the results of the *in silico* experiment, mean absolute relative differences (MARD) between the estimated parameters from the respective approach and the known parameters were calculated in order to assess the validity of the approaches. Differences in MARD among identification approaches (VC vs. DB vs. PHH) were then assessed by Kruskal-Wallis test and post-hoc analysis was performed using Dunn-Sidak correction for multiple comparison (26). Results are reported as median [25^{th}, 75^{th}] percentile unless otherwise specified. A p-value <0.05 was considered statistically significant.

RESULTS

Model Identification

In both cohorts, the VC approach underestimated C-peptide peak and overestimated C-peptide tail, while the DB accurately predicted C-peptide data in all subjects (**Figure 4**). Individual estimates of the key parameters Φ_{tot} and MCR are reported in **Figure 5**.

For both cohorts, a statistically significant difference between the VC and the DB approach was observed for Φ_{tot} (**Figure 5**, top) and MCR (**Figure 5**, bottom). No statistically significant differences between cohorts were observed for both variables within the VC and DB approach, respectively. When pooling data from both cohorts, a significantly higher Φ_{tot} (16.1 [13.5, 20.0] 10^{-9} min^{-1} vs. 15.4 [11.6, 17.7] 10^{-9} min^{-1}, p<0.01) was observed with the DB than the VC approach, which was accompanied by a significantly higher C-peptide MCR (0.068 [0.061, 0.074] min^{-1} vs. 0.059 [0.057, 0.061] min^{-1}, p<0.001) in the DB vs. VC approach. All parameters were estimated with precision: CV among parameters was 19 [14, 24] % using the DB approach and 9 [5, 17] % using the VC approach.

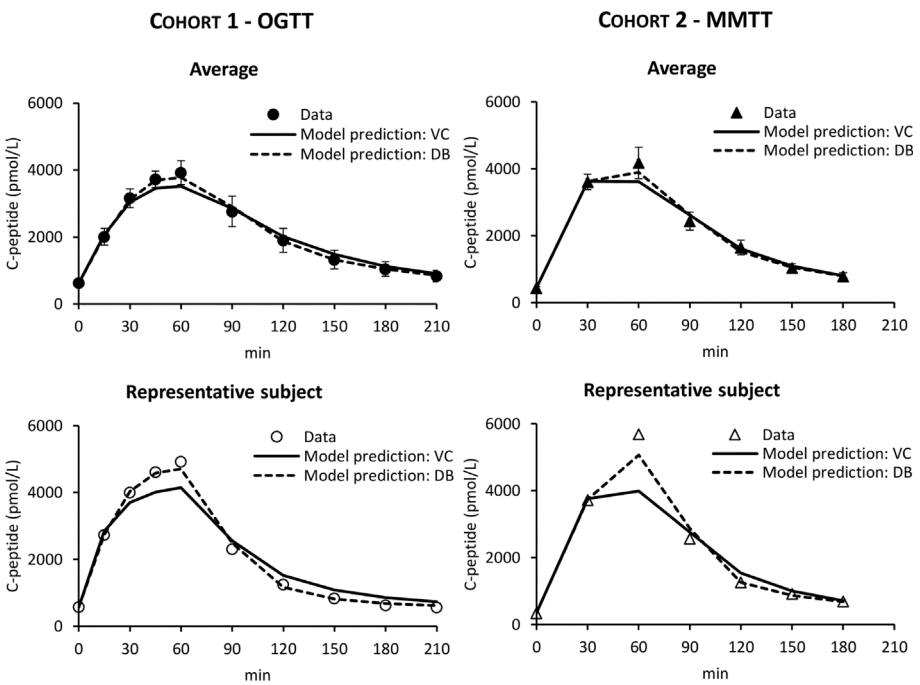

FIGURE 4 | C-peptide data in Cohort 1 – OGTT (left panels, circles) and Cohort 2 – MMTT (right panels, triangles) vs. model predictions obtained with VC (continuous line) and DB (dashed line) approach. Mean ± SE are reported in the top panels while representative subjects in the bottom panels.

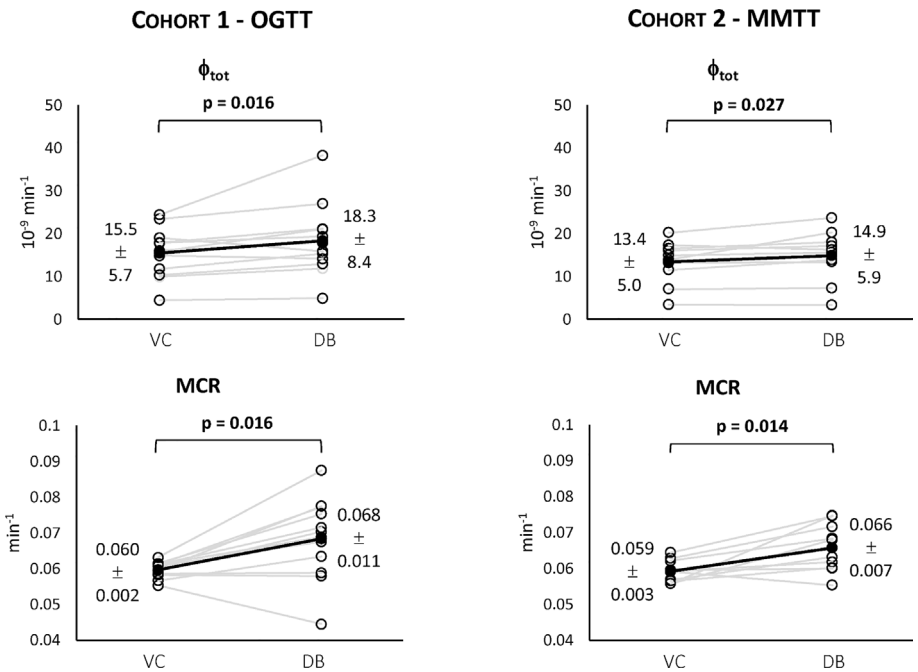

FIGURE 5 | Individual estimates of the index of total β-cell responsivity to glucose (Φ_{tot}, top) and C-peptide metabolic clearance rate (MCR, bottom) for both Cohort 1 – OGTT (left) and Cohort 2 – MMTT (right).

In Silico Assessment

The distributions of the simulated vs. real C-peptide concentrations were very similar for both cohorts (**Figure 6**). Model parameters were estimated with precision in almost all the subjects with CV of 8 [5, 16] %, 19 [15, 24] %, and 17 [13, 25] % for the VC, DB, and PHH approach, respectively.

The MARD of estimated vs. true Φ_{tot} and MCR are reported in **Figure 7**. MARD for Φ_{tot} was 14 [7, 22] % with the VC, 11 [5, 17] % with the DB and 9 [5, 16] % with the PHH approach. MARD for MCR was 13 [7, 20] % with the VC, 9 [5, 15] % with the DB and 8 [4, 14] % with the PHH approach. For both parameters, the Kruskal-Wallis test highlighted a significant difference in MARD among the identification approaches. The post-hoc analysis revealed a significant difference of VC vs. DB and PHH, but not between DB vs. PHH approaches. Moreover, the overall MARD, calculated by pooling all the estimated parameters, was 23 [11, 44] % vs. 14 [6, 24] % vs. 14 [6, 25] % with the VC vs. DB vs. PHH approach, respectively. Also in this case, Kruskal-Wallis test detected a significant difference between approaches which was confirmed by post-hoc analysis only when comparing VC vs. DB and PHH approach.

DISCUSSION

In this work, we tested the validity of the OCMM (11, 18) coupled with the Van Cauter population model for C-peptide kinetics in post-gastric bypass surgery individuals suffering from postprandial hyperinsulinemic hypoglycemia. We observed unsatisfactory results in terms of the model ability to predict the data (**Figure 4**). We hypothesized that this could be due to a mismatch between the actual C-peptide kinetics of the specific population under study and those predicted by the Van Cauter population model. To overcome this limitation, we used a Bayesian approach to estimate C-peptide kinetics from the data and tested the performance of the two different approaches using an *in silico* experiment.

While the OCMM prediction with the VC approach underestimated the C-peptide peak and overestimated the C-peptide tail, model fit of the data was satisfactory in all subjects with the DB approach (**Figure 4**). Our results, as illustrated by the higher C-peptide MCR with the DB vs. VC approach (**Figure 5** bottom), are suggestive of faster C-peptide kinetics in post-gastric bypass patients suffering from postprandial hyperinsulinemic hypoglycemia compared to values predicted by the Van Cauter population model (14).

The better model prediction achieved with the DB approach was expected since, unlike the VC approach, the C-peptide kinetic parameters are allowed to adapt to the specific data. However, this does not demonstrate that the estimated kinetic and secretion parameters are closer to the true ones. To assess the validity of the proposed approach, a simulation study was performed. Results showed that the MARD of estimated vs. true parameters was significantly lower with the DB vs. VC approach for both Φ_{tot} and MCR (**Figure 7**), suggesting that the DB approach, despite exploiting the *a priori* information derived from the VC model, allows to estimate model parameters closer to the true ones than the VC approach. Similar results were also

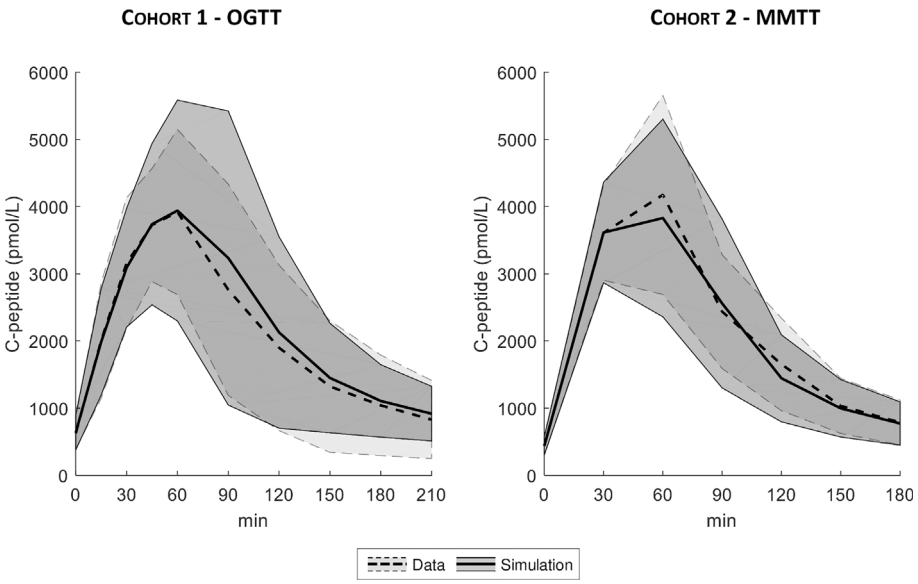

FIGURE 6 | Mean ± SD of true (dashed line with light shaded area) vs. simulated data (continuous line with dark shaded area), for both Cohort 1- OGTT (left) and Cohort 2 - MMTT (right).

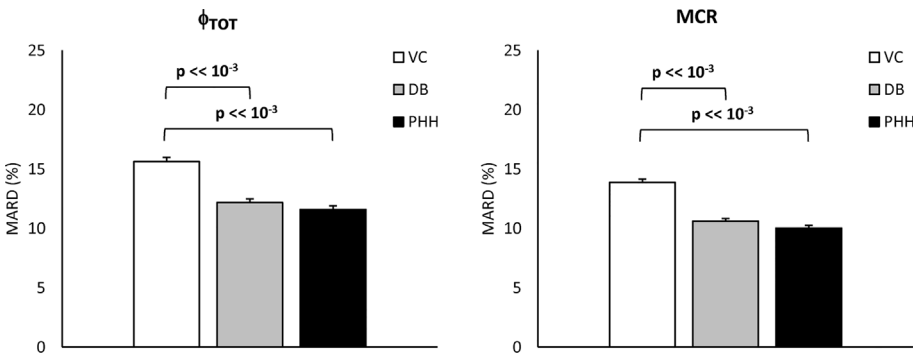

FIGURE 7 | Mean Absolute Relative Difference (MARD) of estimated vs. true Φ_{tot} and MCR (left and right, respectively) for the VC, DB, and PHH approach calculated from the 1100 simulated C-peptide traces (mean ± SE).

obtained when using a *prior* better reflecting the characteristics of the population under study (PHH approach), indicating that final results are minimally affected by the specific choice of the *prior*.

A limitation of the present study is the use of only one of the possible C-peptide secretion models available in the literature (11) and we imputed the unsatisfactorily prediction of the data to a mismatch of C-peptide kinetics while this could also be due to inadequacy of the model for the specific population. Using other models, e.g., (8–10), could lead to different conclusions depending on model structure and *a priori/a posteriori* identifiability properties. However, the C-peptide secretion model adopted here (11) has been used in many studies either on different populations, e.g., healthy (28), prediabetes (29), and subjects with type 2 diabetes (30), and experimental conditions, e.g., testing the effects of pharmacological treatments (31, 32), while always showing its ability to describe the data with C-peptide kinetic parameters fixed to the ones predicted by the Van Cauter population model. Another limitation is that the proposed DB approach was validated in a simulation framework only, while a C-peptide bolus experiment in the same subjects or inclusion of a control group with previous assessment of C-peptide kinetics would be required. In other words, the higher C-peptide MCR suggested by our results need to be confirmed by the current gold-standard experiment using C-peptide bolus under somatostatin infusion. Nevertheless, we would like to point out that the methodology outlined in this work is applicable beyond the study of insulin secretion in this population. The described approach will allow to study insulin secretion also in other metabolic disorders possibly affecting C-

peptide kinetics (e.g., renal diseases) or to study secretion of other hormones for which a population model of the kinetics is not yet available (e.g., glucagon). Noteworthy, as a first step to study this population, we focused on C-peptide secretion and kinetics only. However, assessing insulin kinetics and hepatic insulin extraction is also of great interest. To do so, we will apply this methodology to estimate insulin kinetics and hepatic insulin extraction in future works.

In conclusion, the results of the present study show the limitations of the OCMM coupled to the Van Cauter population model to accurately describe C-peptide data in post-gastric bypass individuals suffering from postprandial hyperinsulinemic hypoglycemia. Consequently, its validity to study insulin secretion and β-cell function in this population is limited. To overcome this limitation, we propose an alternative approach by estimating C-peptide kinetics from the data using a Bayesian approach. This opens new possibilities for the study of hormones for which population kinetic models are unavailable. Overall, our results suggest faster C-peptide metabolic clearance rate in post-gastric bypass individuals suffering from postprandial hyperinsulinemic hypoglycemia compared to previously studied populations. While the ability of the new approach to describe C-peptide data was tested *in silico*, further confirmation using *in vivo* experiments are warranted.

DATA AVAILABILITY STATEMENT

The original contributions presented in the study are included in the article. Further inquiries can be directed to the corresponding author.

ETHICS STATEMENT

The studies involving human participants were reviewed and approved by Local ethics committee (Kantonale Ethikommission Bern, Bern, Switzerland for NCT03609632 and Ethikkommission Nordwest- und Zentralschweiz, Basel, Switzerland for NCT03200782). Study related procedures were performed in accordance with the local ethics standards and with the Declaration of Helsinki. The patients/participants provided their written informed consent to participate in this study.

AUTHOR CONTRIBUTIONS

All authors contributed to the article and approved the submitted version. MS performed the analysis, contributed to the discussion and wrote the manuscript. DH and LB provided the data, contributed to the discussion and writing the manuscript. MH and MD provided the data, contributed to the discussion, and edited the manuscript. CDM reviewed data analysis, contributed to results interpretation and writing the manuscript. CDM is the guarantor of this work and, as such, had full access to all the data in the study and takes responsibility for the integrity of the data and the accuracy of the data analysis.

FUNDING

This work was supported by MIUR (Italian Minister for Education) under the initiative "Departments of Excellence" (Law 232/2016), University of Padova under the initiative "SID-Networking Project 2019", the Swiss National Science Foundation (PCEGP3_186978) and the Scientific Fund of the Department of Diabetes, Endocrinology, Nutritional Medicine, Inselspital as well as the Diabetes Center Bern and the University Hospital in Basel.

ACKNOWLEDGMENTS

We would like to thank Sjaam Jainandunsing and Nicole Hunkeler for their assistance during the experiments in Bern.

REFERENCES

1. Lee CJ, Brown TT, Schweitzer M, Magnuson T, Clark JM. The incidence and risk factors associated with developing symptoms of hypoglycemia after bariatric surgery. *Surg Obes Relat Dis* (2018) 14(6):797–802. doi: 10.1016/j.soard.2018.01.028
2. Capristo E, Panunzi S, De Gaetano A, Spuntarelli V, Bellantone R, Giustacchini P, et al. Incidence of hypoglycemia after gastric bypass vs sleeve gastrectomy: a randomized trial. *J Clin Endocrinol Metab* (2018) 103:2136–46. doi: 10.1210/jc.2017-01695
3. Jørgensen NB, Dirksen C, Bojsen-Møller KN, Jacobsen SH, Worm D, Hansen DL, et al. Exaggerated glucagon-like peptide 1 response is important for improved beta-cell function and glucose tolerance after Roux-en-Y gastric bypass in patients with type 2 diabetes. *Diabetes* (2013) 9:3044–52. doi: 10.2337/db13-0022
4. Honka H, Salehi M. Postprandial hypoglycemia after gastric bypass surgery: from pathogenesis to diagnosis and treatment. *Curr Opin Clin Nutr Metab Care* (2019) 22(4):295–302. doi: 10.1097/MCO.0000000000000574
5. Goldfine AB, Mun EC, Devine E, Bernier R, Baz-Hecht M, Jones DB, et al. Patients with neuroglycopenia after gastric bypass surgery have exaggerated incretin and insulin secretory responses to a mixed meal. *J Clin Endocrinol Metab* (2007) 12:4678–85. doi: 10.1210/jc.2007-0918
6. Shah A, Holter MM, Rimawi F, Mark V, Dutia R, McGinty J, et al. Insulin clearance after oral and intravenous glucose following gastric bypass and gastric banding weight loss. *Diabetes Care* (2019) 2:311–7. doi: 10.2337/dc18-1036
7. Pillonetto G, Sparacino G, Cobelli C. Reconstructing insulin secretion rate after glucose stimulus by an improved stochastic deconvolution method. *IEEE Trans BioMed Eng* (2001) 48(11):1352–4. doi: 10.1109/10.959332
8. Hovorka R, Chassin L, Luzio SD, Playle R, Owens DR. Pancreatic β-cell responsiveness during meal tolerance test: model assessment in normal subjects and subjects with newly diagnosed noninsulin-dependent diabetes mellitus. *J Clin Endocrinol Metab* (1998) 83:744–50. doi: 10.1210/jc.83.3.744
9. Cretti A, Lehtovirta M, Bonora E, Brunato B, Zenti MG, Tosi F, et al. Assessment of β-cell function during the oral glucose tolerance test by a minimal model of insulin secretion. *Eur J Clin Invest* (2001) 31:405–16. doi: 10.1046/j.1365-2362.2001.00827.x

10. Mari A, Schmitz O, Gastaldelli A, Oestergaard T, Nyholm B, Ferrannini E. Meal and oral glucose tests for assessment of beta-cell function: modeling analysis in normal subjects. *Am J Physiol Endocrinol Metab* (2002) 283:1159–66. doi: 10.1152/ajpendo.00093.2002
11. Breda E, Toffolo G, Polonsky KS, Cobelli C. Insulin release in impair glucose tolerance. Oral minimal model predicts normal sensitivity to glucose but defective response times. *Diabetes* (2002) 51:227–33. doi: 10.2337/diabetes.51.2007.S227
12. Eaton RP, Allen RC, Schade DS, Erickson KM, Standefer J. Prehepatic insulin production in man: kinetic analysis using peripheral connecting peptide behavior. *J Clin Endocrinol Metab* (1980) 51:520–8. doi: 10.1210/jcem-51-3-520
13. Polonsky KS, Licinio-Paxiao J, Given BD, Pugh W, Rue P, Galloway J, et al. Use of biosynthetic human C-peptide in the measurement of insulin secretion rates in normal volunteers and type 1 diabetics. *J Clin Invest* (1986) 77:98–105. doi: 10.1172/JCI112308
14. Van Cauter E, Mestrez F, Sturie J, Polonsky KS. Estimation of insulin secretion rated from C-peptide levels: comparison of individual and standard kinetic parameters from C-peptide clearance. *Diabetes* (1992) 41:368–77. doi: 10.2337/diabetes.41.3.368
15. Magni P, Sparacino G, Bellazzi R, Toffolo G, Cobelli C. Insulin minimal model indexes and secretion: proper handling of uncertainity by a Bayesian approach. *Ann Biomed Eng* (2004) 32(7):1027–37. doi: 10.1023/B:ABME.0000032465.75888.91
16. Varghese RT, Dalla Man C, Laurenti MC, Piccinini F, Sharma A, Shah M, et al. Performance of individually measured population-based C-peptide kinetics to asses β-cell function in the presence and absence of acute insulin resistance. *Diabetes Obes Metab* (2018) 20(3):549–55. doi: 10.1111/dom.13106
17. Svane MS, Bosjen-Møller KN, Martinussen C, Dirksen C, Madsen JL, Reitelseder S, et al. Postprandial nutrient handling and gastrointestinal hormone secretion after Roux-en-Y gastric bypass vs sleeve gastrectomy. *Gastroenterology* (2019) 156:1627–41. doi: 10.1053/j.gastro.2019.01.262
18. Cobelli C, Dalla Man C, Toffolo G, Basu R, Vella A, Rizza R. The oral minimal model method. *Diabetes* (2014) 63:1203–13. doi: 10.2337/db13-1198
19. Hepprich M, Wiedermann SJ, Schelker BL, Trinh B, Stäerkle A, Geigges M, et al. Postprandial hypoglycemia in patients after bariatric surgery is mediated by glucose-induced IL-1β. *Cell Metab* (2020) 31(4):699–709. doi: 10.1016/j.cmet.2020.02.013
20. Dalla Man C, Campioni M, Polonsky KS, Basu R, Rizza RA, Toffolo G, et al. Two-hour seven-sample oral glucose tolerance test and meal protocol. *Diabetes* (2005) 54:3265–73. doi: 10.2337/diabetes.54.11.3265
21. Cobelli C, Foster D, Toffolo G. *Tracer kinetic in Biomedical Research: from Data to Model*. New York: Kluwer Academic/Plenum (2000).
22. Bellu G, Saccomani MP, Audoly S, D'Angiò L. DAISY: A new software tool to test global identifiability of biological and physiological systems. *Comput Methods Programs Biomed* (2007) 88(1):52–61. doi: 10.1016/j.cmpb.2007.07.002
23. Carson ER, Cobelli C. *Modeling methodology in physiology and medicine. 2nd ed*. San Diego, CA, USA: Academic Press (2013).
24. Toffolo G, Campioni M, Basu R, Rizza RA, Cobelli C. A minimal model of insulin secretion and kinetics to assess hepatic insulin extraction. *Am J Physiol Endocrinol Metab* (2006) 290:169–76. doi: 10.1152/ajpendo.00473.2004
25. De Nicolao G, Sparacino G, Cobelli C. Nonparametric input estimation in physiological systems: Problems, methods, case studies. *Automatica* (1997) 33:851–70. doi: 10.1016/S0005-1098(96)00254-3
26. *Matlab, version 9.0.0.341360 (R2016a)*. Natick, Massachusetts: The MathWorks Inc (2016).
27. Visentin R, Campos-Náñez E, Schiavon M, Lv D, Vettoretti M, Breton M, et al. The UVA/Padova type 1 diabetes simulator goes from single meal to single day. *J Diabetes Sci Technol* (2018) 12(2):273–81. doi: 10.1177/1932296818757747
28. Basu R, Dalla Man C, Campioni M, Basu A, Klee G, Toffolo G, et al. Effects of age and sex on postprandial glucose metabolism. *Diabetes* (2006) 55:2001–14. doi: 10.2337/db05-1692
29. Konopka AR, Esponda RR, Robinson MM, Johnson ML, Carter RE, Schiavon M, et al. Hyperglucagonemia mitigates the effect of metformin on glucose production in prediabetes. *Cell Rep* (2016) 15:1394–400. doi: 10.1016/j.celrep.2016.04.024
30. Basu A, Dalla Man C, Basu R, Toffolo G, Cobelli C, Rizza RA. Effect of type 2 diabetes on insulin secretion, insulin action, glucose effectiveness, and postprandial glucose metabolism. *Diabetes Care* (2009) 32:866–72. doi: 10.2337/dc08-1826
31. Hinshaw L, Schiavon M, Mallad A, Dalla Man C, Basu R, Bharucha AE, et al. Effects of delayed gastric emptying on postprandial glucose kinetics, insulin sensitivity, and β-cell function. *Am J Physiol Endocrinol Metab* (2014) 307:494–502. doi: 10.1152/ajpendo.00199.2014
32. Visentin R, Schiavon M, Gobel B, Riz M, Cobelli C, Klabunde T, et al. Dual glucagon-like peptide-1 receptor/glucagon receptor agonist SAR425899 improves beta-cell function in type 2 diabetes. *Diabetes Obes Metab* (2020) 22:640–7. doi: 10.1111/dom.13939

Conflict of Interest: The authors declare that the research was conducted in the absence of any commercial or financial relationships that could be construed as a potential conflict of interest.

frontiers in Endocrinology

ORIGINAL RESEARCH
published: 16 March 2021
doi: 10.3389/fendo.2021.625701

Insulin Action, Glucose Homeostasis and Free Fatty Acid Metabolism: Insights From a Novel Model

Darko Stefanovski[1*], *Naresh M. Punjabi*[2], *Raymond C. Boston*[1†] *and Richard M. Watanabe*[3†]

[1] School of Veterinary Medicine, University of Pennsylvania, New Bolton Center, PA, United States, [2] Division of Pulmonary and Critical Care Medicine, Johns Hopkins University School of Medicine, Baltimore, MD, United States, [3] Department of Preventive Medicine, Keck School of Medicine of USC, Los Angeles, CA, United States

Glucose and free fatty acids (FFA) are essential nutrients that are both partly regulated by insulin. Impaired insulin secretion and insulin resistance are hallmarks of aberrant glucose disposal, and type 2 diabetes (T2DM). In the current study, a novel model of FFA kinetics is proposed to estimate the role insulin action on FFA lipolysis and oxidation allowing estimation of adipose tissue insulin sensitivity (S_{IFFA}). Twenty-five normal volunteers were recruited for the current study. To participate, volunteers had to be less than 40 years of age and have a body mass index (BMI) < 30 kg/m^2, and be free of medical comorbidity. The proposed model of FFA kinetics was used to analyze the data derived from the insulin-modified FSIGT. Mean fractional standard deviations of the parameter estimates were all less than 20%. Standardized residuals of the fit of the model to the FFA temporal data were randomly distributed, with only one estimated point lying outside the 2-standard deviation range, suggesting an acceptable fit of the model to the FFA data. The current study describes a novel one-compartment non-linear model of FFA kinetics during an FSIGT that provides an FFA metabolism insulin sensitivity parameter (S_{IFFA}). Furthermore, the models suggest a new role of glucose as the modulator of FFA disposal. Estimates of S_{IFFA} confirmed previous findings that FFA metabolism is more sensitive to changes in insulin than glucose metabolism. Novel derived indices of insulin sensitivity of FFA (S_{IFFA}) were correlated with minimal model indices. These associations suggest a cooperative rather than competitive interplay between the two primary nutrients (glucose and FFA) and allude to the FFA acting as the buffer, such that glucose homeostasis is maintained.

Keywords: free fatty acids (FFA), insulin action, FFA metabolism, glucose, lipolysis

OPEN ACCESS

Edited by:
Marcus M. Seldin, University of California, Irvine, United States

Reviewed by:
Xia Lei, Oklahoma State University, United States
Maia Angelova, Deakin University, Australia

***Correspondence:**
Darko Stefanovski
sdarko@vet.upenn.edu

[†]These authors have contributed equally to this work

Specialty section:
This article was submitted to Systems Endocrinology, a section of the journal Frontiers in Endocrinology

Received: *03 November 2020*
Accepted: *01 February 2021*
Published: *16 March 2021*

Citation:
Stefanovski D, Punjabi NM, Boston RC and Watanabe RM (2021) Insulin Action, Glucose Homeostasis and Free Fatty Acid Metabolism: Insights From a Novel Model. Front. Endocrinol. 12:625701. doi: 10.3389/fendo.2021.625701

INTRODUCTION

Glucose and free fatty acids (FFA) are essential nutrients that are both partly regulated by insulin. While insulin's role in glucose metabolism promotes disposal in peripheral tissues such as muscle, insulin action in the adipose tissue, mainly suppresses lipolysis. In individuals with obesity or type 2 diabetes suffer from insulin resistance, a state where insulin is inefficient in performing the above outlined roles (1). Furthermore, there is evidence that many of the adverse metabolic effects of

glucose intolerance, such as insulin resistance and type 2 diabetes, may be mediated by FFA and have termed lipotoxicity (2). It has been proposed that type 2 diabetes is a consequence of aberrant lipid metabolism (2–4), which supports the concept of interaction between insulin, glucose and FFA homeostasis. Hence, identifying methods that combine simple experimental protocols that yield data that can be used to estimate indices of insulin sensitivity on the level of adipose tissue is of great importance. Furthermore, it will be beneficial if these strategies simultaneously quantify the interaction between glucose and FFAs.

There is no agreement on the best methodology for estimating insulin sensitivity (5). Previous approaches that estimate adipocyte level insulin sensitivity can be loosely divided into 3 classes. First, previously a method has been developed that uses simple experimental data (postabsorptive FFA and insulin) and simple calculations adipose tissue insulin resistance index [Adipo-IR (6)]. This method is the analog of the previously developed index of homeostatic model assessment (HOMA) of whole-body glucose insulin resistance [HOMA-IR (7)]. One potential problem with this model is that while fasting glucose is maintained within a narrow range by a feedback loop mechanism involving insulin, no such mechanism is known relating to FFA homeostasis (5). Thus, Adipo-IR may be a less reliable estimate of adipose insulin resistance. Second, the multistep pancreatic clamp experimental protocol provides methodology for estimating adipose tissue insulin sensitivity, whereby using somatostatin to keep endogenous insulin concentration fully suppressed, the exogenously imposed insulin concentration that provides 50% suppression of lipolysis (IC_{50}) yields the desired index of adipose tissue insulin resistance. However, the complexity and the time involved in performing the multistep pancreatic clamp makes its adaptation difficult (8). Third and final are the methodologies that use simple experimental protocols such as the frequently sampled intravenous glucose tolerance test (FSIGTT) or the oral glucose tolerance test (OGTT) and sophisticated mathematical models that based on the data provide estimates of indices of insulin sensitivity. While these models have been found to be based on experimental data that is more physiologically plausible, they rely on set of simplifying assumptions regarding the kinetics of the system which may not be fully validated to approaches that do not rely on such underlying assumptions (5). The methodology presented here belongs to the third class of approaches of estimating adipose tissue insulin sensitivity.

Previously, several models of FFA kinetics have been proposed that address the bidirectional interaction between insulin and FFA either directly or indirectly (9–15). Many of these available models are limited in that they have complex mechanisms requiring multiple parameters with assumed values, are dependent upon experimental protocols not commonly utilized in the clinical setting (9), are based on underlying assumptions that and not based on observations (11), or only partially use the available data (10, 12). In contrast to previous models, our novel model of FFA kinetics was specifically designed to provide quantitative measures of sensitivity of FFA to the actions of insulin and oxidation allowing estimation of insulin sensitivity on FFA metabolism (S_{IFFA}). Another unique feature of our novel model is that it estimates the contribution of plasma glucose as a regulator of FFA oxidation. Estimates derived from the novel model of FFA kinetics are compared with other model-based approaches and with previously published experimental parameters of FFA metabolism.

METHODS

Model Development

The primary objective was to develop a parsimonious model (16) that would characterize plasma FFA kinetics during a frequently sample intravenous glucose tolerance test (FSIGT). The following assumptions were made in the development of the model: (a) plasma insulin does not directly influence FFA kinetics, but acts through a "remote" compartment to exert its action; (b) insulin action controls the rate of lipolysis; (c) plasma glucose regulates FFA disposal in proportional manner; (d) suppression of FFA is at its maximum at the time of the insulin bolus at 20 minutes. The model acceptance criteria were that, on per subject basis, the model will accurately recreate the FFA time profile where the standardized residuals do not exhibit any systemic deviation and are within the range of two standard deviations. Furthermore, all parameters of the proposed model had to be uniquely identified with fractional standard deviations (FSD) below 0.5.

Mathematical Model of FFA Kinetics During an FSIGT Test

Figure 1A depicts the full FFA model, which was then reduced. The proposed model of plasma FFA kinetics during an FSIGT (**Figure 1B**) is described with the following set of differential equations.

$$\frac{dFFA}{dt} = -(S_{FFA} \cdot \alpha \cdot FFG(t)) \cdot FFA(t) + (S_{FFA} - X_{FFA}(t)) \cdot FFA_b;\ FFA(0)\,\mathrm{pt} = FFA_b \quad (1)$$

$$\frac{dX_{FFA}}{dt} = -P_{XFCR} \cdot X_{FFA}(t) + P_{X\alpha} \cdot (I(t) - I_b); X_{FFA}(0) = 0 \quad (2)$$

Where *FFG(t)* is linear interpolation of glucose plasma concentration at time *t*. S_{FFA} is the fractional FFA disposal rate with units 1/min. Parameter α serves dual purpose as a unit conversion and scaling factor for the effect of plasma glucose, *FFG(t)*, on the disposal of FFA with units 1/mmol/l. It is assumed that the FFA plasma concentration at time 0, *FFA(0)*, is equal to the fasting FFA concentration, FFA_b.

Plasma FFA kinetics (*FFA(t)*) are linked to insulin action on FFA ($X_{FFA}(t)$) kinetics and glucose homeostasis *via* equation 1. Insulin action is defined in equation 2, where plasma insulin increment above basal (I(t) – Ib) contributes to insulin action similar to minimal model (16) and we assume insulin action at steady-state is equal to zero. Parameters P_{XFCR} and P_{Xa} are also

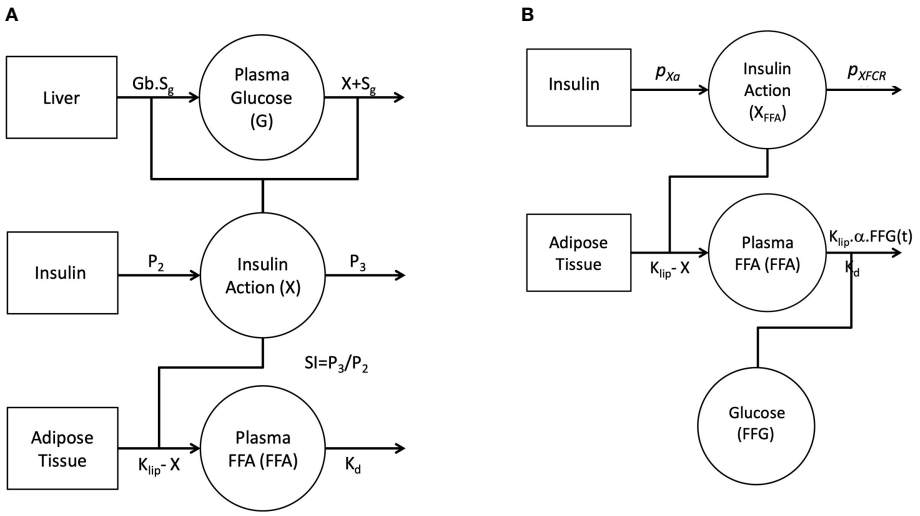

FIGURE 1 | Graphical depiction of the initial single-pool non-linear models of Glucose and FFA **(A)**. Insulin in the remote compartment (*X*, insulin action with units 1/min) regulates the appearance and elimination of plasma glucose and FFA lipolysis rate. Final non-linear single pool FFA model where insulin action on FFA (X_{FFA}, units 1/min) modulates the rate of lipolysis and plasma glucose (*FFG*, units mg/dl) regulates the disposal of FFA **(B)**.

analogous to the P_2 and P_3 parameters of the minimal model. Parameter P_{XFCR} is the fractional disposal rate of insulin from the remote compartment with units 1/min. The parameter P_{Xa} also serves a dual function as a unit conversion and a fractional transfer rate with units $1/min^2$.mU/l. The Adipose Tissue insulin sensitivity parameter (SI_{FFA}) is calculated as the ratio between P_{XFCR} and P_{Xa},

$$\mathrm{SI}_{FFA} = \frac{P_{XFCR}}{P_{X_\alpha}} \tag{3}$$

Study Sample

Normal healthy volunteers were recruited from the local Baltimore-Washington area as previously outlined (**Table 1**) (17). Briefly, after institutional review board (IRB) study approval, eligibility for participation required a BMI < 30 kg/m^2 and absence of the following physician diagnosed conditions: type 2 diabetes mellitus, angina, myocardial infarction, coronary revascularization, congestive heart failure, stroke, obstructive lung disease, renal or hepatic dysfunction, or neurologic disease. After an initial telephone screening, eligible volunteers were required to complete a serologic screen to confirm absence of an abnormal fasting glucose. Informed consent was obtained from each volunteer and the study protocol was approved by the local institutional review board.

Study Protocol

The FSIGT was performed as previously described (13). An intravenous line was placed in the right and left antecubital veins for blood sampling and kept patent with a continuous infusion of 0.9% saline. The intravenous line in the dominant arm was used for blood sampling while glucose and insulin were administered through the contralateral intravenous line. Basal sampling occurred at −15, −10, −5, and −1 min before glucose administration. Glucose (50% dextrose, 0.3 g/kg) was administered intravenously at time zero over one minute followed by infusion of normal saline. Twenty minutes after the glucose injection, regular insulin (0.03 U/kg) was injected. Blood samples were collected at 2, 3, 4, 5, 6, 8, 10, 12, 14, 16, 19, 22, 24, 25, 27, 30, 40, 50, 60, 70, 80, 90, 100, 120, 140, 160, and 180 min post-glucose injection.

Glucose was measured enzymatically in duplicate using a Glucose Analyzer II (Beckman Instruments, Fullerton, CA). Insulin concentrations were determined in duplicate by radioimmunoassay using standard commercial kits (Linco Research; St Charles, MO). Free fatty acids (NEFA C, Wako Pure Chemical Industries; Richmond, VA, USA) were measured using colorimetric methods in commercially available kits.

Statistical Analysis

Model parameter estimation was performed using WinSAAM (University of Pennsylvania, Kennett Square, PA), which uses modified Chu-Berman numerical integrator for solving the model equations and a variant of the generalized non-linear weighted least squares version of the Gauss-Newton optimizer (18). Weights were computed as the inverse variance from the FFA assay and invoked in the data fitting step as fractional standard deviations of 5%. Parameter estimates of the mathematical model were obtained by fitting (obtaining point estimates) FFA estimated temporal profile to the observed FFA concentrations for each individual subject.

Statistical analysis was performed using Stata 15MP (StataCorp, College Station TX). All descriptive statistics of the observed data are shown as mean ± SEM unless otherwise stated. Normality testing was used to assess the skweness of the data. Correlation analysis was performed using Spearman rank correlation. In order to establish equivalence between *X* and

TABLE 1 | Mean ± SE subject characteristics (n = 25).

Age (years)	25.2 ± 4.7
BMI (kg/m^2)	23.6 ± 2.7
Fasting Glucose [mM]	5.25 ± 0.07
Fasting Insulin [pM]	45.11 ± 3.13
Free Fatty Acids [μM]	325.84 ± 23.5

X_{FFA}, t-test was used to assess the similarity between the peaks in the insulin actions. All findings were deemed significant at the level of α=0.05 for the probability of a Type I error.

RESULTS

Kinetic Analysis of Insulin Modified FSIGT

It was initially assumed that insulin action (X(t)) was identical for both glucose and FFA and a model was constructed incorporating this feature (**Figure 1A**). Similar to minimal model, the model of FFA kinetics was developed as a non-linear model of FFA kinetics during FSIGT. As graphically depicted in **Figure 1A**, it was assumed the changes in insulin action were due to change in plasma glucose and FFA during an FSIGT. In the novel FFA model, Insulin Action (X) modulated the suppression of lipolysis in adipose tissue. However, when all six parameters of the model were simultaneously fitted using FSIGT data from the 25 healthy volunteers, parameter estimates were poor with FSDs exceeding 50% and the glucose and insulin time predicted profiles showed significant systematic deviations from the data. These results suggest that the mechanism of insulin action is likely different for FFA compared to glucose. We made two significant changes to the model of FFA in order to improve the fit of the model to the observed data. First, we formulate a novel mathematical construct termed FFA insulin action (X_{FFA}). Analogues to insulin action, X_{FFA} arises as a result of changes in plasma FFA concentration alone and regulates the suppression of lipolysis, **Figure 1B**. Second and final, the plasma FFA rather than being estimated independent of glucose, is a subject to being controlled by it (glucose is another input to the new model) *via* the suppression of FFA disposal.

Results for the analysis of the FSIGT data on the 25 health volunteers using the final model of FFA kinetics is shown in **Table 2** and **Figure 2**. **Figure 2A** illustrates the fit of the model to the average temporal profile of plasma FFA concentration. It can be seen that in the period of 45 to 100 minutes, there is a modest systemic deviation of the model from the observed data. The average temporal profile of plasma FFA suggests a faster increase plasma concentration than the one suggested by the model followed by phase (100 to the end of the experiment) with slower rate of increase in FFA plasma levels. Upon visual inspection of the individual FFA temporal profiles (data not shown) it was established that this was due to a subset of observation in the above-mentioned interval present in 4 subjects (16%). Nevertheless, standardized residuals of the fit of the model to the FFA temporal data appeared randomly distributed, with only one estimated point lying outside the 2-standard deviation range, suggesting an acceptable fit of the model to the FFA data (**Figure 2B**). Mean fractional standard deviations of the parameter estimates were all less than 20% (**Table 2**), consistent with the model being identifiable from the data.

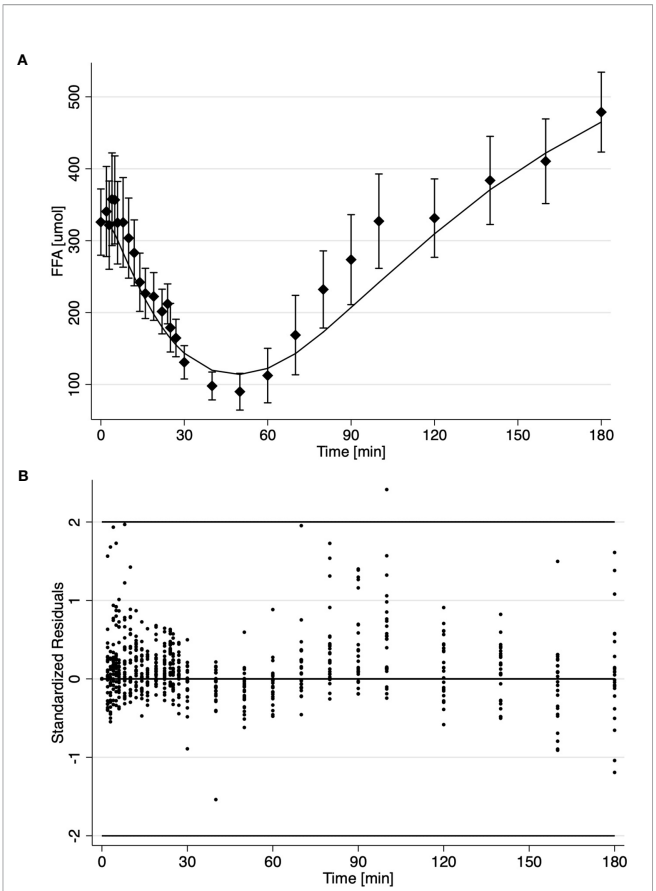

FIGURE 2 | Time course of the average ± SE (solid diamonds) and estimates (solid line) of FFA data **(A)**; Standardized residuals where each dot is one observation from different subject **(B)**.

TABLE 2 | Mean ± SE parameter estimates (n=25).

Parameter	Value ± SE	Units	FSD ± SE
α	1.0E-01 ± 1.0E-02	mmol/l^{-1}	0.09 ± 0.02
S_{FFA}	2.0E-02 ± 2.0E-03	min^{-1}	0.11 ± 0.01
p_{XFCR}	6.0E-02 ± 1.0E-02	min^{-1}	0.17 ± 0.02
p_{Xa}	3.4E-05 ± 1.1E-05	pmol/l^{-1}.min^{-2}	0.08 ± 0.01
SI_{FFA}	5.3E+00 ± 7.8E-01	10^{-4}.pmol/l^{-1}.min^{-1}	0.11 ± 0.02

The associations between parameter estimates from the proposed FFA model and metabolic indices from the traditional minimal model were assessed (**Table 3**) to examine similarities of the underlying mechanisms quantifying the various indices of the model. These results showed that the S_I from the minimal model was moderately correlated with S_{IFFA} (ρ=0.53, P=0.006, **Table 3**). There was also a strong inverse correlation between acute insulin response to glucose (*AIRg*) estimated by the minimal model and S_{IFFA} (ρ = −0.76, P≤0.0001, **Table 3**). Not surprisingly, the *DI* estimated from the minimal model, product of *AIRg* and S_I, was also correlated with S_{IFFA} (ρ = −0.55, P=0.005, **Table 3**). The observed correlations of

TABLE 3 | Spearman's rank correlation between MINMOD and novel FFA model parameter estimates (n=25).

	α	S_{FFA}	p_{XFCR}	p_{Xa}	SI_{FFA}
S_I	–0.01	–0.06	0.16	**0.52**	**0.53**
P	0.965	0.773	0.434	**0.007**	**0.006**
Sg	–0.23	–0.25	0.21	–0.12	–0.23
P	0.272	0.236	0.312	0.580	0.265
AIRg	0.04	–0.15	–0.35	**–0.84**	**–0.76**
P	0.861	0.473	0.083	**≤0.0001**	**≤0.0001**
DI	0.01	–0.16	–0.08	**–0.57**	**–0.55**
P	0.962	0.447	0.712	**0.003**	**0.005**
G_0	–0.14	–0.17	0.03	–0.12	–0.18
P	0.493	0.408	0.884	0.570	0.400
p_2	–0.06	0.07	0.35	0.34	0.06
P	0.787	0.735	0.082	0.098	0.776
p_3	–.04	–0.05	0.28	**0.51**	0.38
P	0.864	0.808	0.170	**0.010**	0.063

Bolded values are statistically significant (P<0.05).

S_{IFFA} with various indices of the minimal model were probably due to their observed association with p_{Xa} (**Table 3**) because S_{IFFA} is calculated as the ratio between p_{Xa} and p_{XFCR} parameters (analogs to the original minimal model parameters P_3 and P_2). No additional significant correlations were observed between minimal model indices and parameters of our novel FFA model.

While X_{FFA} and X are analogues to their model specification, **Figure 3** reveals major difference between the two. On average, FFAs first experience the effect of insulin action (X_{FFA}) at approximately 4 min post challenge. Endogenous glucose insulin action averaged (X, first smaller peak in **Figure 3**) peaked on average at 12 minutes. Interestingly, there was no significant difference between the magnitude of the two insulin actions (Peak insulin action on glucose, X_{max} was not significantly different from Peak insulin action on FFA, $X_{maxFFA,}$ (0.0086 min^{-1}, $p > 0.05$). The profile of X_{FFA} closely resembled the profile of plasma Insulin in the first 10 minutes.

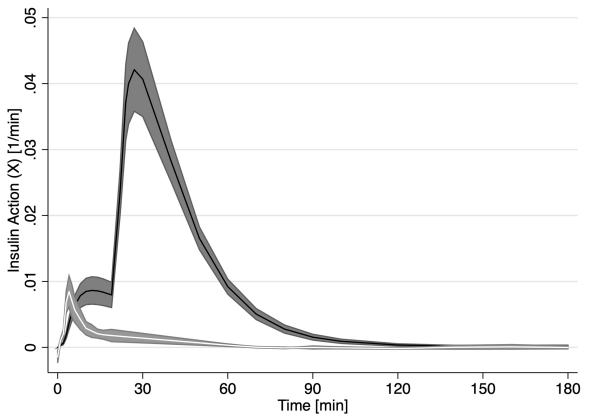

FIGURE 3 | Time course of estimated insulin action (X, solid black line) estimated by the minimal model and FFA insulin action (X_{FFA}, solid white line) from our novel model of FFA kinetics. Grey areas represent the SEM.

DISCUSSION

Since the seminal work by Randle et al. (19), there has been a bias towards casting FFAs as "metabolic villains" (20). In fact, previous work has shown that acute elevation in plasma FFA leads to impaired hepatic gluconeogenesis and overall decreased glucose tolerance (21–24). Increased plasma FFA is also associated with reduced hepatic insulin clearance (25). Furthermore, intravenous intralipid/heparin infusions result in increased intramyocellular lipid, which has been related to insulin resistance. These observations highlight the various metabolic aberrations associated with increased supply of FFA (26).

Recently it has been recognized that impaired FFA disposal may be as important in the accumulation of fat in non-adipose tissue increased FFA uptake (27). By contrast, other studies suggest increased plasma FFA are associated with compensatory insulin secretion responsible for maintaining almost unchanged glucose tolerance in the face of increasing insulin resistance (28–30). Finally, it has been proposed that type 2 diabetes perhaps results from aberrant lipid metabolism (2–4). In animal models, it has been shown that obesity, which is often associated with chronically elevated levels of insulin, leads to decreased FFA oxidation in the resting state (31). Thus, to delineate the role of FFA in glucose metabolism and glucose control over FFA homeostasis will indeed require a better understanding of insulin's influence on FFA metabolism.

The FSIGT is a widely-accepted approach for assessing glucose homeostasis that does not require the use of tracers. The purpose of the novel FFA model was to extend the usability of the FSIGT experimental approach so it provides a more comprehensive metabolic picture. Recently, the insulin-modified FSIGT has been used to study the kinetics of plasma FFA (13). The current study reveals that the plasma FFAs have very rich dynamic highly amenable to mathematical modeling. Previously, several models that explain the time course of FFA during an FSIGT have been developed (10–12, 32). The model by Thomaseth and Pavian (6) attempts to explain the profile of plasma FFA during the FSIGT. One of the features of their model is that the plasma FFA at the end of the FSIGT returns to pre-glucose injection levels (11). The latter assumption severely hinders the usability of their model, because it has been well established that plasma FFA levels at the end of the FSIGT may exceed the basal FFA concentrations by as much as 50% due to a rebound effect (13). Furthermore, and as we stated in the introduction, while glucose is under a strong feedback loop control, no such mechanism has been established for FFA (5). Hence any mathematical model that tends to accurately represent FFA kinetics must provide a formulation that permits for different equilibrium point from the assumed starting equilibrium. In contrast, models developed by Roy and Parker (17) and Periwal

and colleagues (22) make no assumptions regarding the final FFA concentrations. However, neither of these models utilize measurements from the last 60 minutes of the FSIGT, presumably because they cannot estimate the data during this interval (12). Our novel model is also capable of resolving the full temporal profile of plasma FFA regardless of the final concentration of FFAs. Furthermore, in simulation studies not shown here we observed that the model was capable of reaching a new equilibrium state and thus indicating that our novel mathematical model is stable. Interestingly, all three models previously mentioned use glucose, FFA and insulin data to simultaneously estimate both glucose and FFA. The model by Boston and Moate departs from this paradigm and utilizes only the glucose to resolve the profile of plasma FFA (32). In their model, glucose reaches a "remote" compartment *via* a time delay before it exerts its action on FFA lipolysis. This "remote" compartment is considered to be either a proxy for the action of insulin on lipolysis or the direct effect of elevated glucose levels in the "remote" compartment on the rate of lipolysis (33). Thus, their model assumes that any impairment of glucose metabolism will concordantly impact FFA metabolism. Nevertheless, the model by Boston and Moate was not intended to quantify the effect of insulin such as insulin sensitivity of FFA metabolism (S_{IFFA}).

The model of FFA kinetics during an FSIGT proposed herein was based on three simplifying assumptions. First, insulin does not directly influence FFA kinetics. Identical to the concept of the remote insulin effect (16), it was assumed that insulin had to survive transcapillary transport, which is the rate-limiting step for insulin action, to exert its effects on FFA kinetics. Insulin can take up to 20 min to traverse the transendothelial space and exert its effect on glucose kinetics (34). This time corresponded well with previously identified first phase in the plasma FFA time profile (also known as the plateau) during which there is no noticeable change in the plasma FFA concentration (13). Furthermore, this period also corresponded well to the time delay parameter, τ, in the model by Boston and Moate (32). Second, a new set of parameters were defined for insulin action on FFA based on the framework for remote insulin action from the minimal model and estimated independently of insulin action on glucose (see Equations 1 and 2, and **Figure 3**). The notion that insulin action has different kinetics for FFA is not new. Jensen and colleagues have shown that the suppression of FFA lipolysis *via* HSL is extremely sensitive to insulin (35). Furthermore, two other models of FFA kinetics also define different actions of insulin on FFA and glucose (10, 12). Third, insulin influences the suppression of FFA lipolysis, while glucose controls FFA oxidation. Previous models have assumed that FFA disappearance from plasma is mainly driven by decreased lipolysis, while FFA oxidation remains constant (12, 32). The mathematical formulation of the FFA model presented in the current study implies that FFA utilization is under a direct and proportional control of glucose. Previously, it has been shown that when carbohydrates are in abundance, the liver does not only primarily utilize glucose but also converts it to FFA. In hepatocytes, FFAs are readily esterified with glycerol 3-phosphate to generate TAG or combined with cholesterol to produce cholesterol esters (36). Because of the enhanced hepatic FFA metabolism, plasma FFA concentration falls. While much of the literature has been dedicated to the competitive nature of the association between FFA and glucose, our formulation embraces the concept of a coordinated nature of the association between these two substrates previously reported in human muscle (37). Fourth, the insulin administered during the insulin-modified FSIGT has no influence on FFA disposal. Porte and colleagues have shown the additional insulin dose is above the threshold of activation for extra receptors and hence does not play a significant role in insulin-dependent FFA disposal (38). Sumner and colleagues have shown the multiphasic response of FFA during an FSIGT is non-responsive to exogenous insulin (13). Additionally, Jensen and colleagues have shown that the difference in insulin action on lipolysis between obese, insulin resistant, and insulin sensitive is not in the rate at which lipolysis is suppressed, but more at the level of suppression suggesting that insulin suppression of lipolysis is saturable process (35). Therefore, it is highly likely that by the time the insulin bolus takes its full effect in the remote compartment, lipolysis is already maximally suppressed.

Comparing the estimates of our model parameters to previously published estimates show that our estimates were consistently smaller. Previous studies that utilized isotopic tracer to estimate endogenous lipolysis rate report a rate of 3.13 μmol/kg/min compared to our estimate of average lipolysis of 1.24 ± 0.14 μmol/kg/min for our cohort (39). Horowitz and colleagues determined FFA oxidation to be between 1.13 and 1.6 μmol/kg/min using isotopic tracer methods, which is higher compared to our average estimate of 0.72 ± 0.14 μmol/kg/min (39). Contrasting the literature-derived values of lipolysis and FFA oxidation show almost 2:1 relationship respectively between these rates, which is precisely the relationship of our estimates of lipolysis and FFA disposal. One possible reason for the discrepancy may be that our cohort consisted of healthy young volunteers which is in marked contrast to other studies that have enrolled older individuals. Nevertheless, it is encouraging that the ratio between lipolysis and FFA oxidation was similar to what has been previously observed.

The statistically significant correlations in **Table 3** indicate that S_{IFFA} is associated with all the minmod indices through p_{Xa}. From the specification of the model in **Figure 1B**, p_{Xa} is defined as being the index of the rate of appearance of insulin in the remote compartment, insulin action. It has been previously shown that insulin resistance is associated with decreased trans-endothelial transport (40). Therefore, it appears that the restricted access of insulin to the interstitial space is also limiting the supply of insulin required to suppress FFA lipolysis. Interestingly, p_{Xa} is also inversely correlated to *DI*. It is worth noting that we have not observed the same trend with p_3 from the minimal model. The association between *DI* and p_{Xa} may indicate that as the glucose tolerance increases, the fraction of insulin partitioned as X_{FFA} is decreasing. As such it only emphasizes the role of coordinated metabolism between FFA and glucose where FFA serves as a buffer fuel absorbing and dampening disturbances in glucose metabolism to promote stable glucose homeostasis. Future studies will be required to quantify more precisely this relationship.

In conclusion, the current study describes a novel one-compartment non-linear model of FFA kinetics during an FSIGT that, for the first time, provides an FFA metabolism insulin sensitivity parameter (S_{IFFA}). Estimates of S_{IFFA} confirmed previous findings that FFA metabolism is more sensitive to changes in insulin than glucose metabolism. Novel derived indices of insulin sensitivity of FFA (S_{IFFA}) were correlated with previous Bergman's minimal model indices. These associations propose a cooperative rather than competitive relationship between the two primary nutrients (glucose and FFA) and allude to the FFA acting as the buffer, such that glucose homeostasis is maintained. The new model proposed in this study is likely to shed useful insights into the changes in FFA metabolism during development of insulin resistance and type 2 diabetes.

DATA AVAILABILITY STATEMENT

The raw data supporting the conclusions of this article will be made available by the authors, without undue reservation.

ETHICS STATEMENT

The studies involving human participants were reviewed and approved by IRB Johns Hopkins University. The patients/participants provided their written informed consent to participate in this study.

AUTHOR CONTRIBUTIONS

DS contributed to the study concept, analyzed the data, and drafted the manuscript. NP contributed to the study design, collected the data, drafted and reviewed the manuscript. RB contributed to the mathematical modeling concepts, statistical analysis, drafted and reviewed the manuscript. RW contributed to the study concept, analyzed the data, drafted and reviewed the manuscript. DS is the guarantor of this work and, as such, had full access to all the data in the study and takes responsibility for the integrity of the data and the accuracy of the data analysis. All authors contributed to the article and approved the submitted version.

FUNDING

NP has received grant support from the National Institutes of Health (HL075078 and HL117167) for this work.

ACKNOWLEDGMENTS

The authors would like to thank Angelo Avogaro and Giovanni Pacini for collecting and sharing with us the FSIGT data on which part of the development of this model was based.

REFERENCES

1. Groop LC, Bonadonna RC, DelPrato S, Ratheiser K, Zyck K, Ferrannini E, et al. Glucose and free fatty acid metabolism in non-insulin-dependent diabetes mellitus. Evidence for multiple sites of insulin resistance. *J Clin Invest* (1989) 84:205–13. doi: 10.1172/JCI114142
2. DeFronzo RA. Dysfunctional fat cells, lipotoxicity and type 2 diabetes. *Int J Clin Pract Suppl* (2004) (143):9–21. doi: 10.1111/j.1368-504X.2004.00389.x
3. Raz I, Eldor R, Cernea S, Shafrir E. Diabetes: insulin resistance and derangements in lipid metabolism. Cure through intervention in fat transport and storage. *Diabetes Metab Res Rev* (2005) 21:3–14. doi: 10.1002/dmrr.493
4. Carmena R. Type 2 diabetes, dyslipidemia, and vascular risk: rationale and evidence for correcting the lipid imbalance. *Am Heart J* (2005) 150:859–70. doi: 10.1016/j.ahj.2005.04.027
5. Søndergaard E, Jensen MD. Quantification of adipose tissue insulin sensitivity. *J Invest Med* (2016) 64:989–91. doi: 10.1136/jim-2016-000098
6. Gastaldelli A, Harrison SA, Belfort-Aguilar R, Hardies LJ, Balas B, Schenker S, et al. Importance of changes in adipose tissue insulin resistance to histological response during thiazolidinedione treatment of patients with nonalcoholic steatohepatitis. *Hepatology* (2009) 50:1087–93. doi: 10.1002/hep.23116
7. Matthews DR, Hosker JP, Rudenski AS, Naylor BA, Treacher DF, Turner RC. Homeostasis model assessment: insulin resistance and beta-cell function from fasting plasma glucose and insulin concentrations in man. *Diabetologia* (1985) 28:412–9. doi: 10.1007/BF00280883
8. Søndergaard E, Espinosa De Ycaza AE, Morgan-Bathke M, Jensen MD. How to Measure Adipose Tissue Insulin Sensitivity. *J Clin Endocrinol Metab* (2017) 102:1193–9. doi: 10.1210/jc.2017-00047
9. Srinivasan R, Kadish AH, Sridhar R. A mathematical model for the control mechanism of free fatty acid-glucose metabolism in normal humans. *Comput BioMed Res* (1970) 3:146–65. doi: 10.1016/0010-4809(70)90021-2
10. Roy A, Parker RS. Dynamic modeling of free fatty acid, glucose, and insulin: an extended "minimal model". *Diabetes Technol Ther* (2006) 8:617–26. doi: 10.1089/dia.2006.8.617
11. Thomaseth K, Pavan A. "Model-based analysis of glucose and free fatty acid kinetics during glucose tolerance tests". In: *Mathematical Modeling in Nutrition and Toxicology*, Athens GA: Mathematical Biology Press (2003). p. 21–40.
12. Periwal V, Chow CC, Bergman RN, Ricks M, Vega GL, Sumner AE. Evaluation of quantitative models of the effect of insulin on lipolysis and glucose disposal. *Am J Physiol Regul Integr Comp Physiol* (2008) 295:R1089–1096. doi: 10.1152/ajpregu.90426.2008
13. Sumner AE, Bergman RN, Vega GL, Genovese DJ, Cochran CS, Pacak K, et al. The multiphasic profile of free fatty acids during the intravenous glucose tolerance test is unresponsive to exogenous insulin. *Metab Clin Exp* (2004) 53:1202–7. doi: 10.1016/j.metabol.2004.03.020
14. Ramos-Roman MA, Lapidot SA, Phair RD, Parks EJ. Insulin activation of plasma nonesterified fatty acid uptake in metabolic syndrome. *Arterioscler Thromb Vasc Biol* (2012) 32:1799–808. doi: 10.1161/ATVBAHA.112.250019
15. Morbiducci U, Di Benedetto G, Kautzky-Willer A, Deriu MA, Pacini G, Tura A. Identification of a model of non-esterified fatty acids dynamics through genetic algorithms: The case of women with a history of gestational diabetes. *Comput Biol Med* (2011) 41:146–53. doi: 10.1016/j.compbiomed.2011.01.004
16. Bergman RN, Ider YZ, Bowden CR, Cobelli C. Quantitative estimation of insulin sensitivity. *Am J Physiol* (1979) 236:E667–77. doi: 10.1152/ajpendo.1979.236.6.E667
17. Punjabi NM, Beamer BA. Alterations in Glucose Disposal in Sleep-disordered Breathing. *Am J Respir Crit Care Med* (2009) 179:235–40. doi: 10.1164/rccm.200809-1392OC
18. Seber GAF, Wilde CJ. *Nonlinear Regression*. New York, NY: Wiley (1989).
19. Randle PJ, Garland PB, Hales CN, Newholmes EA. The glucose fatty-acid cycle. Its role in insulin sensitivity and the metabolic disturbances of diabetes mellitus. *Lancet* (1963) 1:785–9. doi: 10.1016/S0140-6736(63)91500-9
20. Karpe F, Dickmann JR, Frayn KN. Fatty acids, obesity, and insulin resistance: time for a reevaluation. *Diabetes* (2011) 60:2441–9. doi: 10.2337/db11-0425
21. Boden G, Chen X, Ruiz J, White JV, Rossetti L. Mechanisms of fatty acid-induced inhibition of glucose uptake. *J Clin Invest* (1994) 93:2438–46. doi: 10.1172/JCI117252

22. Roden M, Stingl H, Chandramouli V, Schumann WC, Hofer A, Landau BR, et al. Effects of free fatty acid elevation on postabsorptive endogenous glucose production and gluconeogenesis in humans. *Diabetes* (2000) 49:701–7. doi: 10.2337/diabetes.49.5.701
23. Shah P, Vella A, Basu A, Basu R, Adkins A, Schwenk WF, et al. Elevated free fatty acids impair glucose metabolism in women: decreased stimulation of muscle glucose uptake and suppression of splanchnic glucose production during combined hyperinsulinemia and hyperglycemia. *Diabetes* (2003) 52:38–42. doi: 10.2337/diabetes.52.1.38
24. Staehr P, Hother-Nielsen O, Landau BR, Chandramouli V, Holst JJ, Beck-Nielsen H. Effects of free fatty acids per se on glucose production, gluconeogenesis, and glycogenolysis. *Diabetes* (2003) 52:260–7. doi: 10.2337/diabetes.52.2.260
25. Wiesenthal SR, Sandhu H, McCall RH, Tchipashvili V, Yoshii H, Polonsky K, et al. Free fatty acids impair hepatic insulin extraction in vivo. *Diabetes* (1999) 48:766–74. doi: 10.2337/diabetes.48.4.766
26. Bachmann OP, Dahl DB, Brechtel K, Machann J, Haap M, Maier T, et al. Effects of intravenous and dietary lipid challenge on intramyocellular lipid content and the relation with insulin sensitivity in humans. *Diabetes* (2001) 50:2579–84. doi: 10.2337/diabetes.50.11.2579
27. Kelley DE. Skeletal muscle fat oxidation: timing and flexibility are everything. *J Clin Invest* (2005) 115:1699–702. doi: 10.1172/JCI25758
28. Andreotti AC, Lanzi R, Manzoni MF, Caumo A, Moreschi A, Pontiroli AE. Acute pharmacologic blockade of lipolysis normalizes nocturnal growth hormone levels and pulsatility in obese subjects. *Metab Clin Exp* (1994) 43:1207–13. doi: 10.1016/0026-0495(94)90212-7
29. Kim SP, Catalano KJ, Hsu IR, Chiu JD, Richey JM, Bergman RN. Nocturnal free fatty acids are uniquely elevated in the longitudinal development of diet-induced insulin resistance and hyperinsulinemia. *Am J Physiol Endocrinol Metab* (2007) 292:E1590–8. doi: 10.1152/ajpendo.00669.2006
30. Mittelman SD, Van Citters GW, Kim SP, Davis DA, Dea MK, Hamilton-Wessler M, et al. Longitudinal compensation for fat-induced insulin resistance includes reduced insulin clearance and enhanced beta-cell response. *Diabetes* (2000) 49:2116–25. doi: 10.2337/diabetes.49.12.2116
31. Herling AW, Kilp S, Elvert R, Haschke G, Kramer W. Increased energy expenditure contributes more to the body weight-reducing effect of rimonabant than reduced food intake in candy-fed wistar rats. *Endocrinology* (2008) 149:2557–66. doi: 10.1210/en.2007-1515
32. Boston RC, Moate PJ. A novel minimal model to describe NEFA kinetics following an intravenous glucose challenge. *Am J Physiol Regul Integr Comp Physiol* (2008) 294:R1140–1147. doi: 10.1152/ajpregu.00749.2007
33. Boston RC, Roche JR, Ward GM, Moate PJ. A novel minimal model to describe non-esterified fatty acid kinetics in Holstein dairy cows. *J Dairy Res* (2008) 75:13–8. doi: 10.1017/S0022029907002853
34. Vincent MA, Clerk LH, Lindner JR, Klibanov AL, Clark MG, Rattigan S, et al. Microvascular recruitment is an early insulin effect that regulates skeletal muscle glucose uptake in vivo. *Diabetes* (2004) 53:1418–23. doi: 10.2337/diabetes.53.6.1418
35. Jensen MD, Caruso M, Heiling V, Miles JM. Insulin regulation of lipolysis in nondiabetic and IDDM subjects. *Diabetes* (1989) 38:1595–601. doi: 10.2337/diab.38.12.1595
36. Rui L. Energy Metabolism in the Liver. *Compr Physiol* (2014) 4:177–97. doi: 10.1002/cphy.c130024
37. Kelley DE, Mokan M, Simoneau JA, Mandarino LJ. Interaction between glucose and free fatty acid metabolism in human skeletal muscle. *J Clin Invest* (1993) 92:91–8. doi: 10.1172/JCI116603
38. Prigeon RL, Røder ME, Porte DJr, Kahn SE. The effect of insulin dose on the measurement of insulin sensitivity by the minimal model technique. Evidence for saturable insulin transport in humans. *J Clin Invest* (1996) 97:501–7. doi: 10.1172/JCI118441
39. Horowitz JF, Braudy RJ, Martin WH 3rd, Klein S. Endurance exercise training does not alter lipolytic or adipose tissue blood flow sensitivity to epinephrine. *Am J Physiol* (1999) 277:E325–31. doi: 10.1152/ajpendo.1999.277.2.E325
40. Yang YJ, Hope ID, Ader M, Bergman RN. Importance of transcapillary insulin transport to dynamics of insulin action after intravenous glucose. *Am J Physiol* (1994) 266:E17–25. doi: 10.1152/ajpendo.1994.266.1.E17

Conflict of Interest: The authors declare that the research was conducted in the absence of any commercial or financial relationships that could be construed as a potential conflict of interest.

frontiers in Endocrinology

ORIGINAL RESEARCH
published: 22 March 2021
doi: 10.3389/fendo.2021.611147

Mathematical Model of Glucagon Kinetics for the Assessment of Insulin-Mediated Glucagon Inhibition During an Oral Glucose Tolerance Test

Micaela Morettini[1], Laura Burattini[1], Christian Göbl[2], Giovanni Pacini[3], Bo Ahrén[4] and Andrea Tura[3]*

[1] Department of Information Engineering, Università Politecnica delle Marche, Ancona, Italy, [2] Division of Obstetrics and Feto-Maternal Medicine, Department of Obstetrics and Gynecology, Medical University of Vienna, Vienna, Austria, [3] Metabolic Unit, CNR Institute of Neuroscience, Padova, Italy, [4] Department of Clinical Sciences, Faculty of Medicine, Lund University, Lund, Sweden

OPEN ACCESS

Edited by:
Antonio Brunetti, University of Catanzaro, Italy

Reviewed by:
Nicolai Jacob Wewer Albrechtsen, Rigshospitalet, Denmark
Robert Wagner, Tübingen University Hospital, Germany

***Correspondence:**
Micaela Morettini
m.morettini@univpm.it

Specialty section:
This article was submitted to Systems Endocrinology, a section of the journal Frontiers in Endocrinology

Received: *28 September 2020*
Accepted: *26 January 2021*
Published: *22 March 2021*

Citation:
Morettini M, Burattini L, Göbl C, Pacini G, Ahrén B and Tura A (2021) Mathematical Model of Glucagon Kinetics for the Assessment of Insulin-Mediated Glucagon Inhibition During an Oral Glucose Tolerance Test. Front. Endocrinol. 12:611147. doi: 10.3389/fendo.2021.611147

Glucagon is secreted from the pancreatic alpha cells and plays an important role in the maintenance of glucose homeostasis, by interacting with insulin. The plasma glucose levels determine whether glucagon secretion or insulin secretion is activated or inhibited. Despite its relevance, some aspects of glucagon secretion and kinetics remain unclear. To gain insight into this, we aimed to develop a mathematical model of the glucagon kinetics during an oral glucose tolerance test, which is sufficiently simple to be used in the clinical practice. The proposed model included two first-order differential equations -one describing glucagon and the other describing C-peptide in a compartment remote from plasma - and yielded a parameter of possible clinical relevance (i.e., $S_{GLUCA}(t)$, glucagon-inhibition sensitivity to glucose-induced insulin secretion). Model was validated on mean glucagon data derived from the scientific literature, yielding values for $S_{GLUCA}(t)$ ranging from -15.03 to 2.75 (ng of glucagon·nmol of C-peptide^{-1}). A further validation on a total of 100 virtual subjects provided reliable results (mean residuals between -1.5 and 1.5 ng·L^{-1}) and a negative significant linear correlation ($r = -0.74$, $p < 0.0001$, 95% CI: -0.82 – -0.64) between $S_{GLUCA}(t)$ and the ratio between the areas under the curve of suprabasal remote C-peptide and glucagon. Model reliability was also proven by the ability to capture different patterns in glucagon kinetics. In conclusion, the proposed model reliably reproduces glucagon kinetics and is characterized by sufficient simplicity to be possibly used in the clinical practice, for the estimation in the single individual of some glucagon-related parameters.

Keywords: alpha-cell insulin sensitivity, glucagon secretion, glucose challenge, minimal model, parameter estimation, glucose homeostasis

INTRODUCTION

Glucagon is secreted from the pancreatic alpha cells and plays an important role in the maintenance of glucose homeostasis. In fact, glucagon and insulin interact to maintain euglycemia. The plasma glucose levels determine whether glucagon secretion or insulin secretion is activated or inhibited. Low plasma glucose and related decrease in plasma insulin stimulates glucagon secretion, which in turn promotes hepatic glucose production, through gluconeogenesis and glycogenolysis, to normalize the glucose levels (1–3). As reviewed in (4), regulation of glucagon secretion is a complex phenomenon and involves endocrine/paracrine mechanisms—the so-called "intra-islet interaction" (5, 6)—as well as intrinsic mechanisms in the alpha cell related to glucose sensing.

Glucagon also plays a role in the pathophysiology of type 2 diabetes (T2DM). Indeed, in patients with T2DM elevated plasma glucagon levels have been observed in the fasting state, and defective suppression of glucagon secretion exists in the postprandial state, resulting in elevated plasma glucagon levels (7), which have been shown to reflect an altered insulin inhibition of alpha-cell glucagon exocytosis (8). Such kind of alterations appears already at an early stage of T2DM development. In fact, defective suppression has been also found in impaired glucose tolerance (9). Moreover, increased fasting glucagon and delayed glucagon suppression have been shown to go along with insulin resistance in individuals with normal and impaired glucose regulation (10). The interest for the study of glucagon is also due to the reason that in patients with diabetes suffering for severe hypoglycemic events the administration of glucagon, by either injection or nasal intake, is an important therapeutic option (11). However, despite the relevance of glucagon in glucose metabolism and as pharmacological agent in glucometabolic diseases, some aspects of its secretion and kinetics remain unclear. To gain insight into this, we aimed to develop a mathematical model, with features adequate for possible use in the clinical settings.

A relatively large set of mathematical models were developed with focus on glucagon secretion at cellular level (12–21). Other models were developed for whole-body analyses, but they were complex and with the inclusion of several parameters hard to assess in the single individual, thus useful for simulation purposes rather than for clinical applications (22, 23). Similar considerations hold for studies where a glucagon model was included as a block of a more general model of blood glucose regulation, such as in studies (24, 25).

Studies presenting models analyzing glucagon kinetics for possible clinical applications are rare. One study analyzed the kinetics of glucagon administered exogenously (26), without however accounting for the interplay with insulin or glucose; another study performed similar analyses for the case of therapy based on glucagon (plus insulin) infusion (27). Some other studies developed models for the analysis of the glucagon challenge test, which is however not widely used (28, 29). The study (30) had purposes more similar to those of our study, but the developed model analyzed glucagon kinetics during an intravenous glucose tolerance test (IVGTT), or an insulin-infusion test. To our knowledge, no study has been focused on modeling the glucagon kinetics during an oral glucose tolerance test (OGTT), despite the fact that OGTT has remarkable advantages compared to the IVGTT (or other glucose tolerance tests) in terms of simplicity, and hence applicability in the clinical context.

The specific aim of this study was therefore to develop a mathematical model of the glucagon kinetics during an OGTT, which is sufficiently simple to be used in the clinical practice. For the model development, we exploited glucagon data derived from the study (31). In more details, our main aim was to develop a "minimal model" allowing estimation of glucagon-related parameters in single individuals, with specific interest for one parameter with considerable potential for clinical applications, i.e., the sensitivity to glucose-induced insulin secretion of the glucagon inhibition. This may be denoted as alpha-cell insulin sensitivity.

Abbreviations: OGTT, oral glucose tolerance test; T2DM, type 2 diabetes; IVGTT, intravenous glucose tolerance test; SD, standard deviation; CI, confidence interval.

MATERIALS AND METHODS

Model Formulation

Model Equations

The proposed mathematical model of glucagon kinetics during an OGTT is based on the hypothesis of the "intra-islet interaction" (5, 6). This hypothesis assumes that inhibition of glucagon secretion during an OGTT—which reflects at plasma level in a suppression of plasma glucagon concentration—is mainly determined by glucose-induced insulin secretion. To model insulin secretion, plasma C-peptide concentration has been exploited, since plasma C-peptide is the best marker of insulin secretion at plasma level. In fact, C-peptide is co-secreted with insulin by the beta cells but, differently from insulin, it is not significantly affected by degradation operated by the liver.

The model (**Figure 1**) is composed by two compartments, namely plasma glucagon compartment and remote (from plasma) C-peptide compartment, described by the following two ordinary differential equations:

$$\frac{dGluca(t)}{dt} = -K_{GLUCA} \cdot Gluca(t) - S_{GLUCA}(t) \cdot \frac{d\Delta CP_{remote}(t)}{dt} \qquad Gluca(0) = Gluca_b \tag{1}$$

$$\frac{d\Delta CP_{remote}(t)}{dt} = -K_{\Delta CPREM} \cdot \Delta CP_{remote}(t) + (CP_{plasma}(t) - Cp_b) \qquad \Delta CP_{remote}(0) = 0 \tag{2}$$

where Gluca(t) ($ng \cdot L^{-1}$) is the glucagon concentration in the plasma compartment, $S_{GLUCA}(t)$ (ng of glucagon·nmol of C-peptide^{-1}) is a time-varying parameter expressing glucagon-inhibition sensitivity to glucose-induced insulin secretion during the test (i.e., alpha-cell insulin sensitivity) and K_{GLUCA} (min^{-1}) represents the glucagon elimination rate from plasma due to clearance operated by liver and

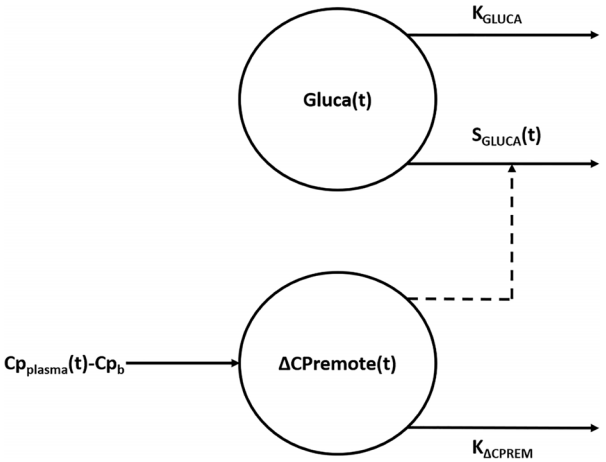

FIGURE 1 | Compartmental representation of the model. The model is composed by two compartments, namely plasma glucagon compartment and remote (from plasma) C-peptide compartment. Suprabasal C-peptide concentration in the remote compartment [$\Delta CP_{remote}(t)$], used to model insulin secretion, exerts a control action on the concentration of glucagon in the plasma compartment [Gluca(t)] through the time-varying parameter $S_{GLUCA}(t)$. K_{GLUCA} represents the glucagon elimination rate from plasma whereas $K_{\Delta CPREM}$ is the C-peptide elimination rate from the remote compartment. $\Delta CP_{remote}(t)$ represents a delayed version of suprabasal plasma C-peptide concentration measured during the test ($CP_{plasma}(t)$ - Cp_b).

kidneys (32, 33); $Gluca_b$ represents the basal plasma glucagon concentration measured during the test. $\Delta CP_{remote}(t)$ (nmol·L^{-1}) is the suprabasal C-peptide concentration in a compartment remote from plasma, which represents a delayed version of suprabasal plasma C-peptide concentration measured during the test, CP_{plasma} (t) (nmol·L^{-1}), with Cp_b being its basal value; $K_{\Delta CPREM}$ (min^{-1}) is the C-peptide elimination rate from the remote compartment. The parameters to be estimated in the model in the single individual are: K_{GLUCA}, $S_{GLUCA}(t)$, $K_{\Delta CPREM}$.

Structural Identifiability Analysis

Structural (*a priori*) identifiability of the model was tested by using DAISY (Differential Algebra for Identifiability of SYstems), a software tool that performs structural identifiability analysis for linear and nonlinear dynamic models described by polynomial or rational ordinary differential equations with either known or unknown initial conditions (34).

Model Implementation

All the steps for model implementation are outlined in **Supplementary Figure 1**. Model has been implemented in MATLAB® R2017b as a discrete-time system (considering *n* time points, equally spaced) and its response in terms of glucagon and remote C-peptide concentrations has been obtained using the *ltitr* built-in function. Model parameter vector p = [K_{GLUCA}, $S_{GLUCA}(t)$, $K_{\Delta CPREM}$] has been estimated by solving, through the *lsqnonlin* function, the following nonlinear least-squares curve fitting problem:

$$\min_p \|f(p)\|_2^2 = \min_p [RSS + K_{GLUCA} + w_1 \cdot S_{GLUCA}{}''(t) + w_2 \cdot (S_{GLUCA}(t) < 0)] \quad (3)$$

where the first term represents the residual sum of squares (being the residuals the differences between model glucagon response and glucagon curve measured during the OGTT), whereas all the others are regularization terms added as constraints to provide more information to the problem and facilitate practical (*a posteriori*) identifiability. In particular, the second term has been added on the consideration that, during the OGTT, the main contribution to glucagon suppression is given by C-peptide action and not by glucagon clearance, thus K_{GLUCA} has to be small; the third and the last term, weighted through w_1 and w_2, have been added to limit $S_{GLUCA}(t)$ rapid changes during the test and the number of samples where $S_{GLUCA}(t)$ becomes negative, respectively.

The optimal values of w_1 and w_2 were selected by an iterative procedure in which 100 possible combinations of values - considering 10 different values for w_1 and 10 different values for w_2, randomly generated - were tested. A combination of values for w_1 and w_2 was considered acceptable if it provided mean residual values lower that 10%, otherwise was discarded. Such threshold was chosen on the consideration of the uncertainty on the glucagon measurements [10% in fact is a suitable value for the inter- and intra-assay coefficient of variation for glucagon (35)]. The optimal combination, among all the combinations tested, was the one that provided the lowest mean residual.

To find the global minimum among several possible local minima, a total of 10 runs of the *lsqnonlin* local solver from different starting point (randomly generated, between 0 and 1) have been performed using the *MultiStart* algorithm (36), which repeatedly runs the solver of the model starting from different initial values of the parameters, to improve the possibility of reaching the optimal solution.

The *trust-region-reflective* algorithm has been used by *lsqnonlin* to solve the problem and the following lower and upper bounds have been applied to the parameters: (0;1) for K_{GLUCA} and $K_{\Delta CPREM}$; (-∞; +∞) for $S_{GLUCA}(t)$. Function and step-size tolerances have been set to 10^{-6}.

K_{GLUCA} and $K_{\Delta CPREM}$ estimates have been obtained considering the two parameters as constant for the whole test duration, whereas estimates have been obtained for $S_{GLUCA}(t)$ corresponding to the time samples where plasma glucagon and C-peptide concentrations have been measured. For all model parameters, the 95% CIs for the parameter estimates have been computed by using the *nlparci* function.

Model Validation

Reported Mean Experimental Data

Mean experimental data reported by Pepino et al. (31) have been used to initially validate the model. The original study by Pepino et al. (31), from which the mean data have been drawn, included a total of seventeen non-diabetic subjects undergoing a 5-h 75-g OGTT. Plasma C-peptide and glucagon concentrations at 2 min before (considered as 0 min) and at 10, 20, 30, 60, 90, 120, 150, 180,

240, and 300 min after glucose ingestion have been considered. As indicated by Pepino et al. (31), plasma glucagon was measured by a direct, double-antibody radioimmunoassay (Millipore).

Virtual Population Generation

Starting from mean and standard deviation (SD) values reported by Pepino et al. (31), a total of 100 virtual subjects have been generated using sort of Monte Carlo approach (37). Each virtual subject is characterized by glucagon and C-peptide curves in response to an OGTT, in which glucagon and C-peptide concentrations at each time sample were randomly generated, based on normal distributions with mean and SD values derived by the study of Pepino et al. (31) (considering all samples within the 95% confidence interval, CI). Furthermore, in order to obtain curves that are physiologically plausible, some additional constraints have been added [e.g., sign of the derivative between two time samples equal to that of the reference curves (31)].

Ability of the Model to Capture Different Patterns in Glucagon Kinetics

The ability of the model to capture different patterns in glucagon kinetics was tested on four characteristics mean glucagon curves in response to a five-point 75g - OGTT reported by Gar et al. (38), as representative of the four clusters identified in glucagon curve shapes of individuals with different metabolic phenotypes (i.e., normal glucose tolerance, prediabetes, type 2 diabetes). The four clusters are characterized as follow: 1) Cluster 1 had high mean fasting glucagon and delayed suppression; 2) Cluster 2 had high mean fasting glucagon and rapid suppression; 3) Cluster 3 had low mean fasting glucagon and rapid suppression; 4) Cluster 4 had low mean fasting glucagon and a rising curve after glucose ingestion. For each cluster, mean glucagon and C-peptide concentrations measured at 0 min and at 30, 60, 90, 120 after glucose ingestion have been considered. As indicated by Gar et al. (38), plasma glucagon was measured with an ELISA (Glucagon ELISA; Mercodia, Uppsala, Sweden; catalog no: 10-1271-01).

Sensitivity to OGTT Duration

In order to test sensitivity of the $S_{GLUCA}(t)$ estimation to test duration, in the 100 virtual subjects, the $S_{GLUCA}(t)$ mediated on the full 5-h OGTT has been compared to $S_{GLUCA}(t)$ mediated considering shorter OGTTs (limiting the 5-h OGTT to 2-h and 3-h).

Calculations and Statistical Analysis

The Kolmogorov-Smirnov test was used to evaluate the hypothesis that each variable had a normal distribution with unspecified mean and variance. Values were reported as mean ± SD.

Over the 100 virtual subjects, linear regression analysis has been performed between mean $S_{GLUCA}(t)$ during the OGTT and the ratio between the suprabasal area under the curve of remote C-peptide ($AUC_{\Delta CPremote}$) to the area of glucagon below the basal condition (AUC_{Gluca}); also, Pearson correlation coefficient (r) has been reported. In the case of skewed distributions tests were applied to the log-transformed values.

As regards the estimation of $S_{GLUCA}(t)$ according to the different OGTT durations, comparisons have been performed by means of a paired Student t-test in case of normally distributed variables or Wilcoxon signed-rank test in case of skewed distributed variables. The two-sided significance level was set at 5% ($p < 0.05$).

RESULTS

Analysis of structural (*a priori*) identifiability provided that the model was *a priori* identifiable (locally). Model validation on mean experimental data reported by Pepino et al. (31) provided the best fit shown in **Figure 2** and the parameter estimates (with related CIs) reported in **Table 1**. Trend of $S_{GLUCA}(t)$ during the whole OGTT is reported in **Figure 3**.

Glucagon and C-peptide curves in the 100 virtual subjects are shown in **Figure 4**. Model validation on the virtual subjects provided the mean best fit and the related residuals shown in **Figure 5**. Distribution of values for K_{GLUCA} and $K_{\Delta CPREM}$ over the virtual subjects is shown in **Figure 6**, whereas the $S_{GLUCA}(t)$ patterns are reported in **Figure 7**. A negative significant linear correlation ($r = -0.74$, $p < 0.0001$, 95% CI: -0.82 – -0.64) has been found between the log-transformed values of $S_{GLUCA}(t)$ and $AUC_{\Delta CPremote}$ to AUC_{Gluca} ratio over the 100 virtual subjects. Regression plot is reported in **Figure 8**. Regression line slope and intercept was -0.6215 (95% CI: -0.7346 – -0.5084) and 0.2987 (95% CI: 0.2017–0.3956), respectively.

No significant difference has been found between average $S_{GLUCA}(t)$ over the full 5-h OGTT and the 3-h OGTT ($p = 0.08$); in contrast, average $S_{GLUCA}(t)$ over the 2-h OGTT has been found significantly different compared to that over the full 5-h OGTT ($p < 0.0001$).

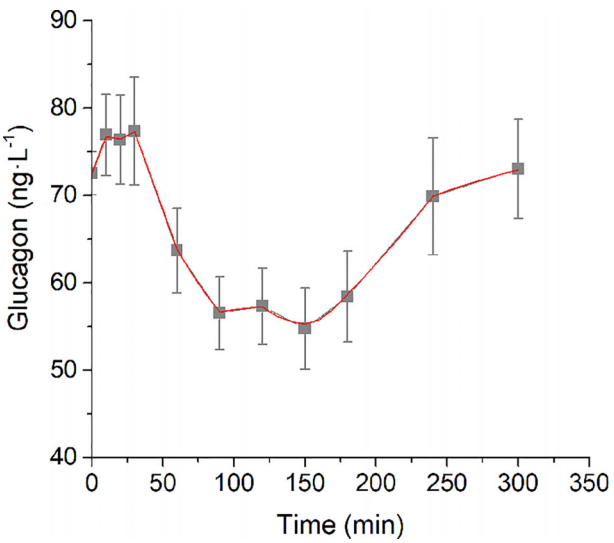

FIGURE 2 | Best-fit results for model validation on reference mean experimental data by Pepino et al. (31). Grey squares are the reference experimental values (mean ± SD); red line is the model prediction.

TABLE 1 | Values and 95% CIs for the estimates of K_{GLUCA} (min^{-1}), $K_{\Delta CPREM}$ (min^{-1}), $S_{GLUCA}(t)$ (ng of glucagon·nmol of C-peptide^{-1}) on reference mean experimental data by Pepino et al. (31).

Estimated parameter	Value	95% CI
K_{GLUCA}	0.005	-0.002–0.013
$K_{\Delta CPREM}$	0.155	0.119–0.191
S_{GLUCA1}	-15.03	-18.25 – -11.80
S_{GLUCA2}	-0.11	-0.78–0.66
S_{GLUCA3}	-0.73	-1.23 – -0.22
S_{GLUCA4}	2.34	2.17–2.60
S_{GLUCA5}	1.53	1.30–1.75
S_{GLUCA6}	-0.58	-1.24–0.07
S_{GLUCA7}	1.62	0.42–2.81
S_{GLUCA8}	2.75	2.13–3.37
S_{GLUCA9}	2.51	1.88–3.14
$S_{GLUCA10}$	1.07	0.22–1.93

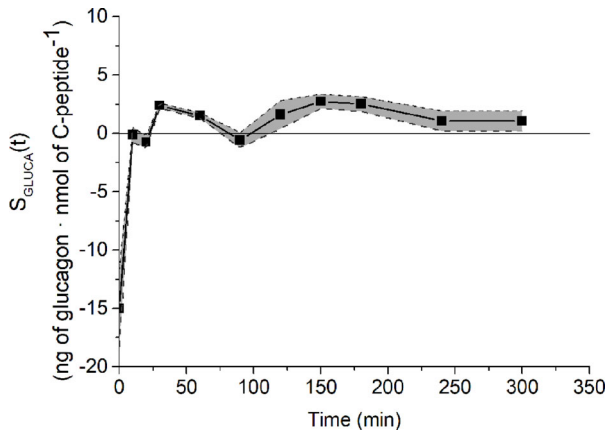

FIGURE 3 | $S_{GLUCA}(t)$ temporal estimates on reference mean experimental data by Pepino et al. (31) (closed squares) and related CIs (dashed lines).

Mean glucagon and C-peptide concentrations for the four clusters, used to assess the ability of the model to capture different patterns in glucagon kinetics, are shown in **Figure 9**. Best-fit results and $S_{GLUCA}(t)$ patterns for the four clusters are reported in **Figure 10**.

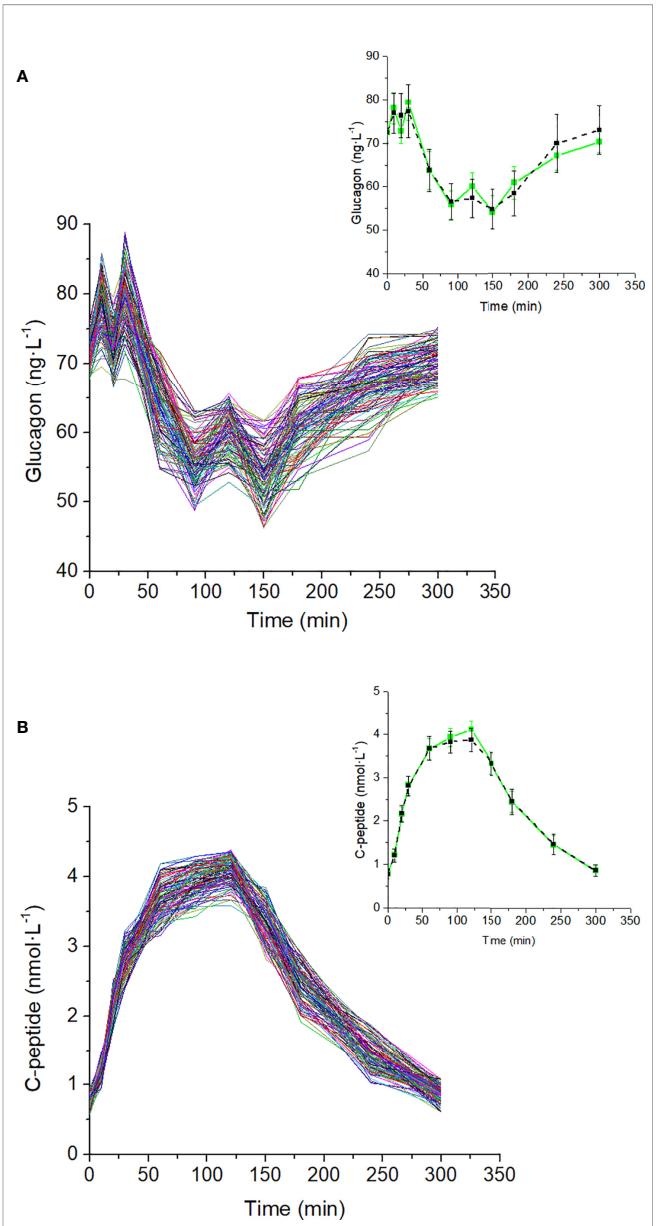

FIGURE 4 | Glucagon **(A)** and C-peptide **(B)** curves in the 100 virtual subjects (spaghetti plot). In the related inset plots, green continuous lines represent the mean (± SD) over the 100 curves; black dashed lines represent mean (± SD) taken from Pepino et al. (31), from which the virtual subjects were derived.

DISCUSSION

In this study, we developed a mathematical model of glucagon kinetics during an OGTT, which is a test widely used in the clinical practice for its simplicity, compared to other metabolic tests. The specific characteristics of the model were including parameters with clear physiological meaning and that can be estimated in a single individual, the latter being a crucial feature for potential applications in the clinical context.

Our mathematical model is based on the hypothesis that inhibition of glucagon secretion during an OGTT is mainly determined by glucose-induced insulin secretion due to an intra-islet interaction (5, 6). This led to a simplified description of glucagon regulation, thus disregarding other important regulation mechanisms, one of which is a possible direct effect of glucose (i.e., not only mediated by insulin) (39). Moreover, recent evidence supports the concept of the liver–alpha-cell axis, in which hepatic amino acid metabolism and glucagon secretion are linked in a feedback cycle (40, 41). There is also evidence for insulin secretion being regulated by glucagon action *via* glucagon-like peptide 1 (GLP-1) and glucagon receptors on beta cells (42, 43). Possible regulators of insulin secretion, such as GLP-1, have been considered in other models [also proposed by us (44, 45)] but in the present model we considered insulin

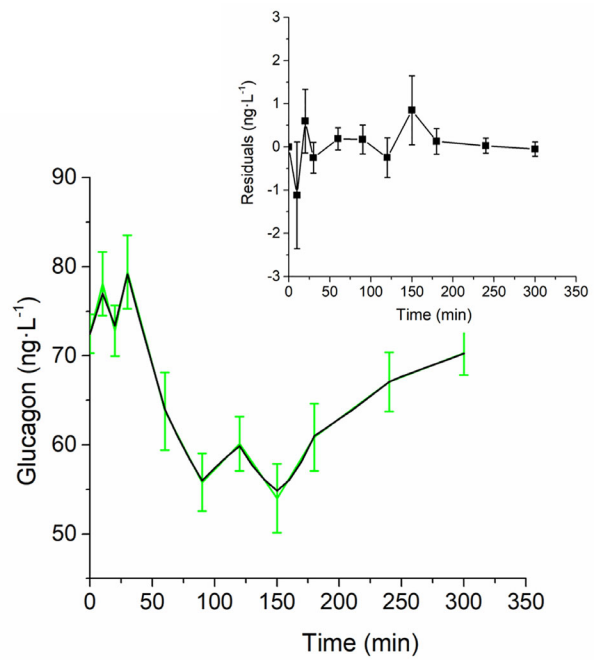

FIGURE 5 | Best-fit results for model validation on the 100 virtual subjects. Green continuous line represents the mean (± SD) over the 100 generated curves; black continuous line represents the mean predicted glucagon curve. Mean residuals over the 100 curves are displayed in the inset plot.

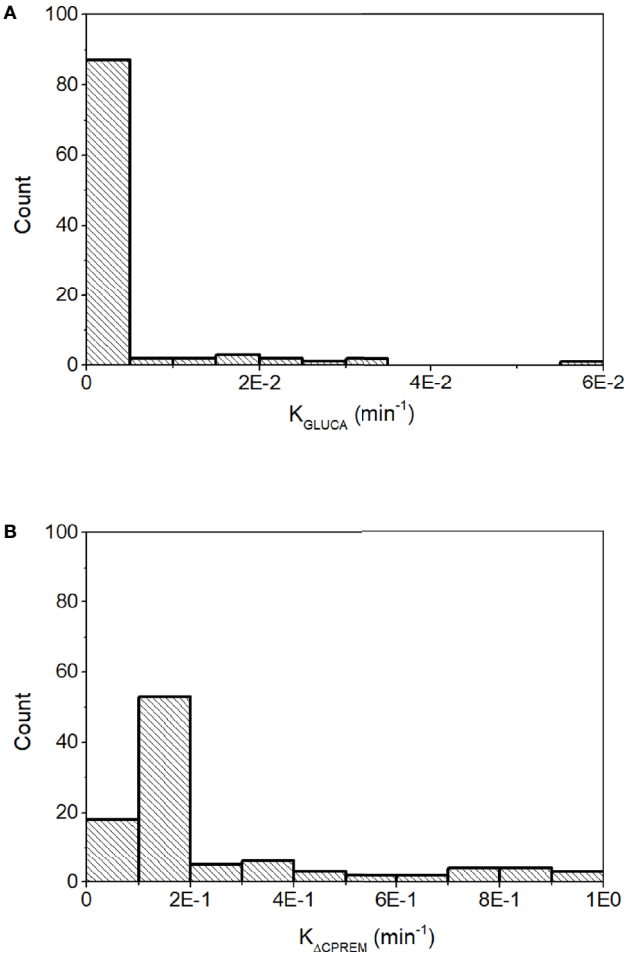

FIGURE 6 | Distribution of K_{GLUCA} **(A)** and $K_{\Delta CPREM}$ **(B)** over the 100 virtual subjects.

secretion as an input signal, regardless of how it has been generated. This simplification, both in the input and in the description of feedback mechanisms, was necessary to achieve our aim to propose a "minimal model", allowing estimation of glucagon-related parameters in single individuals.

In the study of glucose metabolism, established methodologies exist for the assessment of metabolic aspects of major relevance, such as insulin sensitivity, insulin secretion and possible incretin-based enhancement, and insulin clearance, as assessed for instance in some of our previous OGTT-based studies (45–47). The model of glucagon kinetics presented in this study will have the potential to complement the information derived from an OGTT, provided from the indicated established methodologies. Such new model will add information related to the role of glucagon in maintaining the glucose homeostasis, thus yielding to a more complete picture of the glucometabolic condition of the subjects under study. To our knowledge, this is the first study describing a mathematical model of glucagon kinetics during an OGTT.

Our model of glucagon kinetics simply requires the measure of plasma glucagon and C-peptide. It is based on two ordinary differential equations, and it includes two parameters with specific physiological meaning: the glucagon clearance from plasma, K_{GLUCA}, mainly due to liver and kidneys (32, 33), and the sensitivity of the glucagon secretion from the pancreatic alpha cells to the inhibitory effect of insulin, $S_{GLUCA}(t)$. In short, this can be named as sensitivity to glucose-induced insulin secretion of the glucagon inhibition and can be denoted as alpha-cell insulin sensitivity. This may parallel the concepts of sensitivities of the beta cells, such as the established concept of beta-cell glucose sensitivity (48), and the more recently proposed beta-cell incretin sensitivity (49).

In addition to $S_{GLUCA}(t)$, the model also includes one further parameter, i.e., the clearance of C-peptide from a compartment remote with respect to plasma. It should be acknowledged that the physiological interpretation of this parameter may not be possible, since such remote compartment cannot be defined precisely. In fact, the concept of a compartment remote from plasma is not new in mathematical models of glucose metabolism, being used as an example in the well-known original Minimal Model (for the assessment of insulin sensitivity and glucose effectiveness from an IVGTT) (50), and more recently in other models, such as our model for the assessment of non-esterified fatty acids kinetics (51). However, though it is sometimes believed that the compartment remote from plasma may be identified in the interstitial fluid, this may not be totally correct. Indeed, the remote compartment should be seen as a mathematical trick, without strict physiological meaning, which is useful to introduce a time delay between the

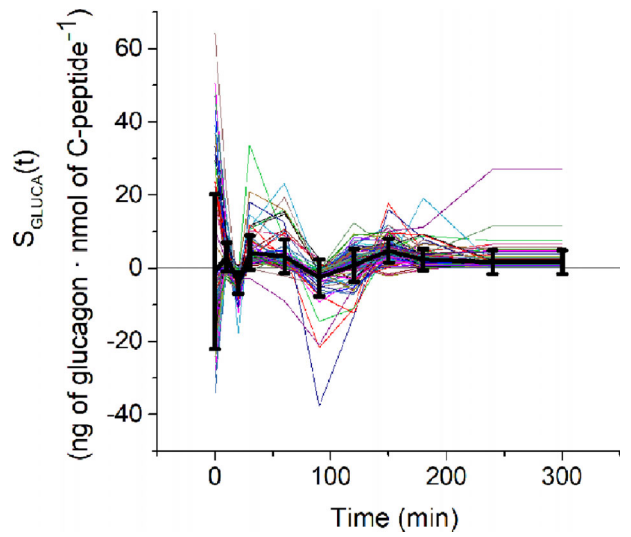

FIGURE 7 | $S_{GLUCA}(t)$ estimates over the 100 virtual subjects (spaghetti plot). Black continuous line represents the mean (± SD) $S_{GLUCA}(t)$.

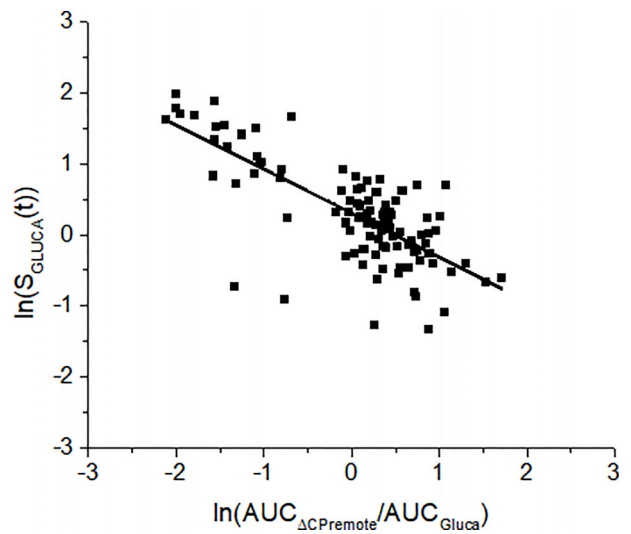

FIGURE 8 | Linear regression analysis between $S_{GLUCA}(t)$ and the ratio between the areas under the curve of the remote C-peptide and glucagon ($AUC_{\Delta CPremote}/AUC_{Gluca}$) over the 100 virtual subjects. Analysis has been performed on the log-transformed values. Regression line equation is: y= -0.6215·x+0.2987. This means that a change of 1 unit in log transformed $AUC_{\Delta CPremote}/AUC_{Gluca}$ causes a change of log transformed $S_{GLUCA}(t)$ by 0.6215.

action of the input/forcing variable and the effect on the output variable (i.e., C-peptide and glucagon, respectively, in the presented model), for a better description of the system under analysis. Therefore, $K_{\Delta CPREM}$ has precise physiological meaning (clearance), but it is applied to a variable (remote C-peptide) that is not clearly physiologically defined.

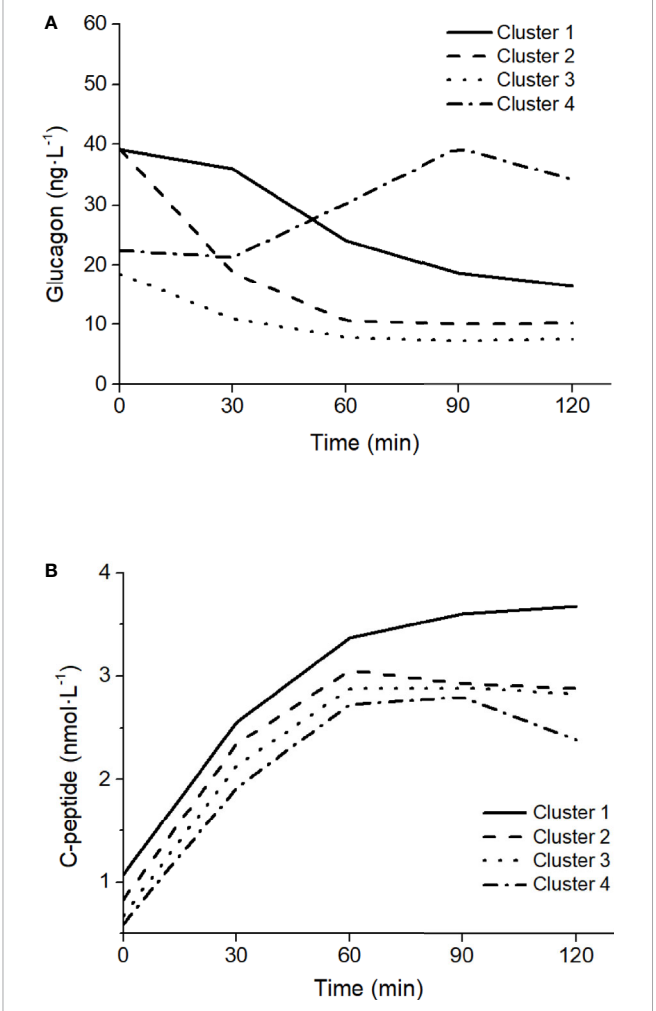

FIGURE 9 | Glucagon **(A)** and C-peptide **(B)** curves in the four clusters of patterns in glucagon kinetics, modified from Gar et al. (38).

In our approach, we hypothesized that the glucagon inhibition during the OGTT is due to the action of the secreted insulin, as suggested in several studies and summarized in some reviews, such as (4). However, in the model we exploited plasma C-peptide, rather than insulin. This is due to the reason that C-peptide may be more accurate than insulin for the assessment of insulin secretion, since they are secreted equimolarly, but the former does not significantly undergo partial degradation from the liver. Thus, we hypothesized that plasma C-peptide may be more adequate than insulin as marker of insulin secretion, i.e., to assess its inhibitory effect on glucagon. This appeared confirmed by the data of the study (31). Indeed, in linear regression analysis over the average data of the analyzed population in study (31), we verified that C-peptide time samples were significantly inversely related to those of glucagon, whereas those of insulin (as well as those of glucose) were not. In addition, surprisingly, insulin secretion values, as assessed in study (31) were similarly not related to glucagon. This may be due to limitations in the method used for insulin secretion assessment, and/or to the fact that we

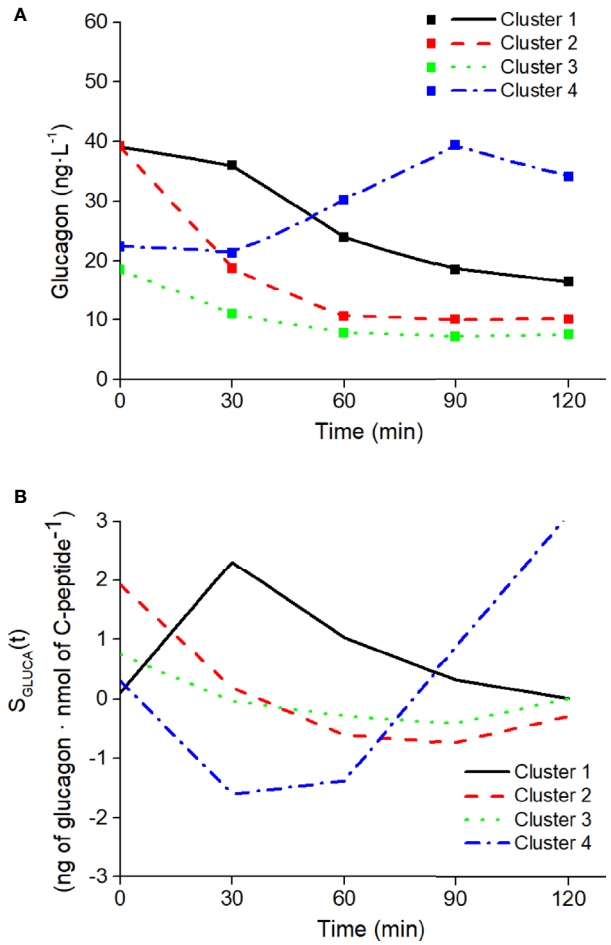

FIGURE 10 | Best-fit results **(A)** and $S_{GLUCA}(t)$ estimates **(B)** on the four clusters of patterns in glucagon kinetics. Squares in panel **(A)** are the reference experimental values; lines are the model predictions.

analyzed average curves, rather than individual curves that were not available. Moreover, it should be acknowledged that insulin may inhibit glucagon secretion by stimulation of somatostatin secretion rather than through a direct effect on the alpha cells (52). Nonetheless, above all, the reported findings suggest that the choice of plasma C-peptide as marker of the insulin effect on glucagon may be the most reasonable option: on one hand, not requiring further mathematical modeling for the calculation (as it is for insulin secretion assessment), and on the other hand showing more strict relationship with glucagon compared to both plasma insulin and insulin secretion.

In our model, sensitivity to insulin of glucagon inhibition was defined as a time-variant parameter, $S_{GLUCA}(t)$, differently to glucagon and remote C-peptide clearance, K_{GLUCA} and $K_{\Delta CPREM}$, respectively, which were assumed constant during the OGTT. This choice was based on the consideration that estimating an average clearance of glucagon (and of remote C-peptide) during the OGTT is sufficient for our purposes, whereas at contrast the sensitivity to insulin of glucagon inhibition has to be assessed with higher accuracy, being the parameter of major interest in our approach. Thus, S_{GLUCA} was defined as varying at each time sample of the OGTT reported in the study (31). This choice may arise questions about the identifiability of our model parameters, which is a crucial issue for the possibility to estimate the parameters in single individuals and hence for the potential clinical applicability of the model. To this purpose, we first performed *a priori* identifiability analysis. We found that, if the model assumes constant S_{GLUCA}, absolute *a priori* identifiability is obtained. If the model assumes the time variant S_{GLUCA}, absolute identifiability is lost, but still local identifiability is reached, meaning that there is a finite number of solutions of the minimization problem for the estimation of the parameters. Moreover, to further reducing the uncertainty in parameters estimation, we exploited the concept of regularization, that is, the process of adding information for the solution of a possibly ill-posed problem thus preventing overfitting (53), similarly to what was done in previous studies (45, 48). Indeed, in the cost function minimized by the nonlinear least-squares solver we included further factors, in addition to the traditional sum of squares of the difference between data and model prediction (fit). First, we assumed that $S_{GLUCA}(t)$ cannot undergo excessively rapid variations, as this would be unphysiological: thus, in the cost function we added a term to penalize the entity of $S_{GLUCA}(t)$ second-order derivatives. In addition, we assumed that $S_{GLUCA}(t)$ should typically show positive values, though some negative values are sometimes possible: thus, we included a term penalizing the number of $S_{GLUCA}(t)$ negative values. Furthermore, among the regularization factors we included K_{GLUCA}. This means having assumed that during the OGTT the clearance of glucagon is small, based on the reasonable hypothesis that, during the test, the sensitivity to insulin of glucagon inhibition has more influence than glucagon clearance for glucagon disappearance. Of note, such constraint explains the small values observed for K_{GLUCA}. The described regularization strategy allowed us to overcome the problem of incomplete *a priori* identifiability, and to include physiologically-based constraints for greater reliability and improved meaning of the estimated model parameters [especially with regard to $S_{GLUCA}(t)$].

Despite negative values of $S_{GLUCA}(t)$ are penalized, they are allowed in our model approach, this meaning that glucagon inhibition by insulin may not be effective in some time periods. This appears in fact clearly indicated by the inspection of average curves of study (31). Indeed, such curves suggest that during an OGTT glucagon may increase in some time periods, though slightly, whereas C-peptide (as well as insulin) is not decreasing as one would expect, thus indicating that in those periods the relationship between insulin action and glucagon variations is lost. A clear explanation for this phenomenon is still elusive, but non-suppressed (increasing glucagon) during OGTT may surprisingly be associated to even healthier metabolic phenotype (less hepatic fat, higher insulin sensitivity) according to some studies, such as (54).This may be also due to reason that, despite insulin is often reported as the major determinant of glucagon inhibition (4), other studies suggest a possible direct effect of glucose (i.e., not only mediated by insulin) (39), as well as several other factors (4, 39). It should

also be observed that in different glucose tolerance tests, such as a mixed meal test, the effect of such factors other than insulin may be even more relevant. From this point of view our model, accounting for possibly negative values of the sensitivity to insulin of glucagon inhibition, appears adequate for future model developments, also including other factors that may influence glucagon inhibition (though adding further variables may affect the clinical applicability, and hence should be considered with caution).

Another aspect that we addressed in the model development is the choice of the initial condition of the parameters to be estimated. To this purpose, we exploited the MultiStart algorithm (36). We are aware that other approaches may be possible such as genetic algorithm strategy, as done in some of our previous studies (55–57). In this study, we opted for the indicated approach, as it appeared somehow simpler to implement. Similar problem was the choice of the optimal weights of the regularization factors. However, since for some technical difficulties it appeared hard to exploit the MultiStart algorithm for such aspect as well, in this case we simply randomly generated different values for the weights.

In our study, we also computed the 95% CI of the estimated parameters [though for brevity we presented results only for the case of the data derived from the study (31)]. We found that CI of $K_{\Delta CPREM}$ did not include the zero value, probably due to its small estimated values, whereas K_{GLUCA} did. As regards $S_{GLUCA}(t)$, during the OGTT the algorithm estimated six positive values and four negative values. For the positive values, the CI did not include zero, thus indicating the robustness of the positive value estimations. For the negative values, two did not include zero as well, whereas the other two included, this indicating that for those two values the estimation was somehow uncertain. On the other hand, it should be acknowledged that these findings are related to average data, rather than actual individual human data, and this may have an effect on CI calculation. In addition, as the used method for CI calculation required the exploitation of the Jacobian matrix provided by the solver, it cannot be excluded that the tolerance in the matrix accuracy numeric (rather than analytic) calculation may have an effect as well.

Our model proved to perform properly, as indicated by the good fit for each virtual subject (considering the tolerance that we assumed in relation to the accuracy and precision of plasma glucagon measurement), and by the physiologically plausible values of the estimated parameters, varying within a range appearing reasonable, especially with reference to $S_{GLUCA}(t)$. In addition, it should be noted that, as expected, we found significant relationship between mean $S_{GLUCA}(t)$ and mean C-peptide to glucagon ratio, this further indicating reliability and robustness of our model approach. Our model approach can also be easily extended to the study of subjects characterized by different metabolic phenotypes. In fact, the model was successfully tested on characteristic OGTT curves as representative of different clusters of glucagon kinetics (low or high fasting glucagon; rapid or delayed suppression).

We also found interesting results regarding the model performances in relation to different OGTT durations. Indeed, data used in our study are related to a 5h-OGTT (31), which is not usually performed in clinical settings. However, when testing sensitivity of the $S_{GLUCA}(t)$ estimation to OGTT duration, in the population of virtual subjects our approach provided comparable results with data limited to 3h-OGTT; in contrast, it appears that the present approach cannot be extended to shorter OGTT (2h). Analysis over 2 h limits glucagon kinetics only to the suppression phase, thus neglecting the phase in which glucagon restores to the basal conditions, thus it is not surprising that 2h-OGTT did not provide results comparable to those of the 5-h OGTT. Nonetheless, since our model is not constrained to work with a specific OGTT duration, we tested it on five time-point 2h OGTT curves, which have been identified by Gar et al. as representative of different clusters of glucagon kinetics (38). As shown, our model was able to reproduce all characteristic patterns observed during the five time-point OGTT. Thus, if we aim to consider the complete glucagon kinetics we have to resort to 3h-OGTT, but if we are interested only to the suppression phase we can limit analysis to 2h-OGTT, and to five time-point only (*i.e.*, the typical 2h-OGTT time samples: 0, 30, 60, 90, 120 min).

Comparison of our findings to those of previous studies is difficult. As previously outlined, some mathematical models were developed with the aim to investigate glucagon secretion at cellular level (12–21), whereas other models, more similarly to ours, were developed for whole-body analyses, but mainly for simulation purposes rather than for clinical applications (22–25). Other studies presented models of glucagon kinetics for possible clinical applications, but they were focused on the analysis of glucagon administered exogenously, or for the analysis of the not common glucagon challenge test (26–29). The study having more aspects in common with ours is that of Kelly et al. (30). In that study, a comprehensive model of glucagon kinetics and dynamics was developed for possible clinical applications, i.e., for possible assessment of model parameters in individuals. That model has merits in the details of the physiological phenomena analyzed. For instance, the model allows to address aspects not analyzed in our study, such as the ability of glucagon to promote hepatic glucose production, sometimes denoted in study (30) as glucagon sensitivity. However, that model, which is to some extent an extension of the traditional Minimal Model (50), applies to glucose tolerance tests other than the OGTT, such as the IVGTT (consistently with the field of application of the Minimal Model). In addition, both the model versions (based on nonlinear or linear relationships between glucose, glucagon and insulin) are relatively complex and including several parameters (five equations with 11 unknown parameters, and four equations with 10 unknown parameters, for nonlinear and linear model versions, respectively). Thus, doubts may arise whether all these parameters are identifiable in a single individual. Of note, analyses of model identifiability were not presented. As regards the concept of sensitivity to insulin of glucagon inhibition, which is the focus of our study, it has to be acknowledged that the study (30) addresses the issue as well, though it does not appear the aspect of major interest in the presented analyses. In fact, one parameter similar our $S_{GLUCA}(t)$ is presented, defined as the maximum rate at which insulin suppresses glucagon secretion. However, in study (30) the parameter is assumed constant, thus not considering its possible variations during a test. In addition, and most importantly, study (30) presents simulations where such

parameter was varied in a given interval, whereas the estimation of the parameter based on glucagon and insulin data is not reported, and hence it was not proved that the model may allow estimation of such parameter. Thus, to our knowledge our study is the first showing the possibility to assess the sensitivity to insulin of glucagon inhibition in single individuals, having proved the feasibility of $S_{GLUCA}(t)$ estimation with individual data curves.

In conclusion, we developed a model of glucagon kinetics during the OGTT, with special interest for the sensitivity to insulin of glucagon inhibition, denoted as alpha-cell insulin sensitivity. Strength of our model is simplicity and the possibility to estimate parameters with clear physiological meaning (i.e., the parameters of glucagon kinetics) in a single individual, thus being potentially adequate for use in clinical settings. Future investigations may consider the option to introduce some model improvements, including description of further factors possibly affecting glucagon suppression during the OGTT, but paying attention to avoid model approaches not adequate for possible clinical applications. Another aspect for future studies will be the assessment of the actual clinical relevance of our model approach, by studying populations including subjects with different degree of glucometabolic impairment.

DATA AVAILABILITY STATEMENT

The datasets for this study include already published data and virtually generated data. The virtually generated data are available upon request to the corresponding author.

AUTHOR CONTRIBUTIONS

MM and AT conceived and designed the study. MM, and AT analyzed and interpreted the data. LB, CG, BA, and GP validated the analysis. MM and AT wrote the first draft of the manuscript. LB, CG, and BA critically revised the manuscript. All authors contributed to the article and approved the submitted version.

SUPPLEMENTARY MATERIAL

The Supplementary Material for this article can be found online at: https://www.frontiersin.org/articles/10.3389/fendo.2021.611147/full#supplementary-material

REFERENCES

1. Cherrington AD, Liljenquist JE, Shulman GI, Williams PE, Lacy WW. Importance of hypoglycemia-induced glucose production during isolated glucagon deficiency. *Am J Physiol Metab* (1979) 236:E263. doi: 10.1152/ajpendo.1979.236.3.E263
2. Jiang G, Zhang BB. Glucagon and regulation of glucose metabolism. *Am J Physiol Metab* (2003) 284:E671–8. doi: 10.1152/ajpendo.00492.2002
3. Senthil VPSIJ. *Physiology, Glucagon*. StatPearls. Treasure Island (FL: StatPearls Publishing (2020). Available at: https://www.ncbi.nlm.nih.gov/books/NBK537082/.
4. Gromada J, Chabosseau P, Rutter GA. The α-cell in diabetes mellitus. *Nat Rev Endocrinol* (2018) 14:694–704. doi: 10.1038/s41574-018-0097-y
5. Banarer S, McGregor VP, Cryer PE. Intraislet hyperinsulinemia prevents the glucagon response to hypoglycemia despite an intact autonomic response. *Diabetes* (2002) 51:958–65. doi: 10.2337/diabetes.51.4.958
6. Meier JJ, Kjems LL, Veldhuis JD, Lefèbvre P, Butler PC. Postprandial suppression of glucagon secretion depends on intact pulsatile insulin secretion: further evidence for the intraislet insulin hypothesis. *Diabetes* (2006) 55:1051–6. doi: 10.2337/diabetes.55.04.06.db05-1449
7. Dunning BE, Gerich JE. The role of alpha-cell dysregulation in fasting and postprandial hyperglycemia in type 2 diabetes and therapeutic implications. *Endocr Rev* (2007) 28:253–83. doi: 10.1210/er.2006-0026
8. Omar-Hmeadi M, Lund PE, Gandasi NR, Tengholm A, Barg S. Paracrine control of α-cell glucagon exocytosis is compromised in human type-2 diabetes. *Nat Commun* (2020) 11:1–11. doi: 10.1038/s41467-020-15717-8
9. Ahrén B, Larsson H. Impaired glucose tolerance (IGT) is associated with reduced insulin-induced suppression of glucagon concentrations. *Diabetologia* (2001) 44:1998–2003. doi: 10.1007/s001250100003
10. Færch K, Vistisen D, Pacini G, Torekov SS, Johansen NB, Witte DR, et al. Insulin resistance is accompanied by increased fasting glucagon and delayed glucagon suppression in individuals with normal and impaired glucose regulation. *Diabetes* (2016) 65:3473–81. doi: 10.2337/db16-0240
11. Thieu VT, Mitchell BD, Varnado OJ, Frier BM. Treatment and prevention of severe hypoglycaemia in people with diabetes: Current and new formulations of glucagon. *Diabetes Obes Metab* (2020) 22:469–79. doi: 10.1111/dom.13941
12. Grubelnik V, Markovič R, Lipovšek S, Leitinger G, Gosak M, Dolenšek J, et al. Modelling of dysregulated glucagon secretion in type 2 diabetes by considering mitochondrial alterations in pancreatic α-cells. *R Soc Open Sci* (2020) 7:191171. doi: 10.1098/rsos.191171
13. Grubelnik V, Zmazek J, Markovič R, Gosak M, Marhl M. Modelling of energy-driven switch for glucagon and insulin secretion. *J Theor Biol* (2020) 493:110213. doi: 10.1016/j.jtbi.2020.110213
14. Montefusco F, Cortese G, Pedersen MG. Heterogeneous alpha-cell population modeling of glucose-induced inhibition of electrical activity. *J Theor Biol* (2020) 485:110036. doi: 10.1016/j.jtbi.2019.110036
15. Edlund A, Pedersen MG, Lindqvist A, Wierup N, Flodström-Tullberg M, Eliasson L. CFTR is involved in the regulation of glucagon secretion in human and rodent alpha cells. *Sci Rep* (2017) 7:90. doi: 10.1038/s41598-017-00098-8
16. Pedersen MG, Ahlstedt I, El Hachmane MF, Göpel SO. Dapagliflozin stimulates glucagon secretion at high glucose: experiments and mathematical simulations of human A-cells. *Sci Rep* (2016) 6:31214. doi: 10.1038/srep31214
17. Briant L, Salehi A, Vergari E, Zhang Q, Rorsman P. Glucagon secretion from pancreatic α-cells. *Ups J Med Sci* (2016) 121:113–9. doi: 10.3109/03009734.2016.1156789
18. Watts M, Ha J, Kimchi O, Sherman A. Paracrine regulation of glucagon secretion: the β/α/δ model. *Am J Physiol Metab* (2016) 310:E597–611. doi: 10.1152/ajpendo.00415.2015
19. Montefusco F, Pedersen MG. Mathematical modelling of local calcium and regulated exocytosis during inhibition and stimulation of glucagon secretion from pancreatic alpha-cells. *J Physiol* (2015) 593:4519–30. doi: 10.1113/JP270777
20. Watts M, Sherman A. Modeling the pancreatic α-cell: dual mechanisms of glucose suppression of glucagon secretion. *Biophys J* (2014) 106:741–51. doi: 10.1016/j.bpj.2013.11.4504
21. Fridlyand LE, Philipson LH. A computational systems analysis of factors regulating α cell glucagon secretion. *Islets* (2012) 4:262–83. doi: 10.4161/isl.22193
22. Wendt SL, Ranjan A, Møller JK, Schmidt S, Knudsen CB, Holst JJ, et al. Cross-validation of a glucose-insulin-glucagon pharmacodynamics model for simulation using data from patients with type 1 diabetes. *J Diabetes Sci Technol* (2017) 11:1101–11. doi: 10.1177/1932296817693254
23. Farhy LS, McCall AL. Models of glucagon secretion, their application to the analysis of the defects in glucagon counterregulation and potential extension to approximate glucagon action. *J Diabetes Sci Technol* (2010) 4:1345–56. doi: 10.1177/193229681000400608

24. Palumbo MC, Morettini M, Tieri P, Diele F, Sacchetti M, Castiglione F. Personalizing physical exercise in a computational model of fuel homeostasis. *PloS Comput Biol* (2018) 14:e1006073. doi: 10.1371/journal.pcbi.1006073
25. Vahidi O, Kwok KE, Gopaluni RB, Knop FK. A comprehensive compartmental model of blood glucose regulation for healthy and type 2 diabetic subjects. *Med Biol Eng Comput* (2016) 54:1383–98. doi: 10.1007/s11517-015-1406-4
26. Lv D, Breton MD, Farhy LS. Pharmacokinetics modeling of exogenous glucagon in type 1 diabetes mellitus patients. *Diabetes Technol Ther* (2013) 15:935–41. doi: 10.1089/dia.2013.0150
27. Shirin A, Della Rossa F, Klickstein I, Russell J, Sorrentino F. Optimal regulation of blood glucose level in Type I diabetes using insulin and glucagon. *PloS One* (2019) 14:e0213665. doi: 10.1371/journal.pone.0213665
28. Masroor S, van Dongen MGJ, Alvarez-Jimenez R, Burggraaf K, Peletier LA, Peletier MA. Mathematical modeling of the glucagon challenge test. *J Pharmacokinet Pharmacodyn* (2019) 46:553–64. doi: 10.1007/s10928-019-09655-2
29. Mojto V, Rausova Z, Chrenova J, Dedik L. Short-term glucagon stimulation test of C-peptide effect on glucose utilization in patients with type 1 diabetes mellitus. *Med Biol Eng Comput* (2015) 53:1361–9. doi: 10.1007/s11517-015-1416-2
30. Kelly RA, Fitches MJ, Webb SD, Pop SR, Chidlow SJ. Modelling the effects of glucagon during glucose tolerance testing. *Theor Biol Med Model* (2019) 16:21. doi: 10.1186/s12976-019-0115-3
31. Pepino MY, Tiemann CD, Patterson BW, Wice BM, Klein S. Sucralose affects glycemic and hormonal responses to an oral glucose load. *Diabetes Care* (2013) 36:2530–5. doi: 10.2337/dc12-2221
32. Herold KC, Jaspan JB. Hepatic glucagon clearance during insulin induced hypoglycemia. *Horm Metab Res* (1986) 18:431–5. doi: 10.1055/s-2007-1012339
33. Assan R, Tchobroutsky G, Derot M. Intervention of kidney and liver in glucagon catabolism and clearance from plasma. *Acta Isot (Padova)* (1970) 10:285–94.
34. Bellu G, Saccomani MP, Audoly S, D'Angiò L. DAISY: A new software tool to test global identifiability of biological and physiological systems. *Comput Methods Prog BioMed* (2007) 88:52–61. doi: 10.1016/j.cmpb.2007.07.002
35. MERCK. *GLUCAGON RIA KIT* . Available at: https://www.merckmillipore.com/IT/it/product/Glucagon-RIA,MM_NF-GL-32K (Accessed August 7, 2020).
36. Ugray Z, Lasdon L, Plummer J, Glover F, Kelly J, Martí R. Scatter Search and Local NLP Solvers: A Multistart Framework for Global Optimization. *INFORMS J Comput* (2007) 19:328–40. doi: 10.1287/ijoc.1060.0175
37. Bekisz S, Holder-Pearson L, Chase JG, Desaive T. In silico validation of a new model-based oral-subcutaneous insulin sensitivity testing through Monte Carlo sensitivity analyses. *BioMed Signal Process Control* (2020) 61:102030. doi: 10.1016/j.bspc.2020.102030
38. Gar C, Rottenkolber M, Sacco V, Moschko S, Banning F, Hesse N, et al. Patterns of plasma glucagon dynamics do not match metabolic phenotypes in young women. *J Clin Endocrinol Metab* (2018) 103:972–82. doi: 10.1210/jc.2017-02014
39. Yu Q, Shuai H, Ahooghalandari P, Gylfe E, Tengholm A. Glucose controls glucagon secretion by directly modulating cAMP in alpha cells. *Diabetologia* (2019) 62:1212–24. doi: 10.1007/s00125-019-4857-6
40. Knop FK. EJE PRIZE 2018: A gut feeling about glucagon. *Eur J Endocrinol* (2018) 178:R267–80. doi: 10.1530/EJE-18-0197
41. Wewer Albrechtsen NJ, Færch K, Jensen TM, Witte DR, Pedersen J, Mahendran Y, et al. Evidence of a liver–alpha cell axis in humans: hepatic insulin resistance attenuates relationship between fasting plasma glucagon and glucagonotropic amino acids. *Diabetologia* (2018) 61:671–80. doi: 10.1007/s00125-017-4535-5
42. Sandoval D. Updating the Role of α-Cell Preproglucagon products on GLP-1 receptor–mediated insulin secretion. *Diabetes* (2020) 69:2238–45. doi: 10.2337/dbi19-0027
43. Ahrén B, Yamada Y, Seino Y. The mediation by GLP-1 receptors of glucagon-induced insulin secretion revisited in GLP-1 receptor knockout mice. *Peptides* (2021) 135:170434. doi: 10.1016/j.peptides.2020.170434
44. Burattini R, Morettini M. Identification of an integrated mathematical model of standard oral glucose tolerance test for characterization of insulin potentiation in health. *Comput Methods Prog BioMed* (2012) 107:248–61. doi: 10.1016/j.cmpb.2011.07.002
45. Tura A, Muscelli E, Gastaldelli A, Ferrannini E, Mari A. Altered pattern of the incretin effect as assessed by modelling in individuals with glucose tolerance ranging from normal to diabetic. *Diabetologia* (2014) 57:1199–203. doi: 10.1007/s00125-014-3219-7
46. Tura A, Chemello G, Szendroedi J, Göbl C, Færch K, Vrbíková J, et al. Prediction of clamp-derived insulin sensitivity from the oral glucose insulin sensitivity index. *Diabetologia* (2018) 61:1135–41. doi: 10.1007/s00125-018-4568-4
47. Tura A, Göbl C, Morettini M, Burattini L, Kautzky-Willer A, Pacini G. Insulin clearance is altered in women with a history of gestational diabetes progressing to type 2 diabetes. *Nutr Metab Cardiovasc Dis* (2020) 30:1272–80. doi: 10.1016/j.numecd.2020.04.004
48. Mari A, Tura A, Gastaldelli A, Ferrannini E. Assessing Insulin Secretion by Modeling in Multiple-Meal Tests: Role of Potentiation. *Diabetes* (2002) 51: S221–6. doi: 10.2337/diabetes.51.2007.S221
49. Tura A, Bagger JI, Ferrannini E, Holst JJ, Knop FK, Vilsbøll T, et al. Impaired beta cell sensitivity to incretins in type 2 diabetes is insufficiently compensated by higher incretin response. *Nutr Metab Cardiovasc Dis* (2017) 27:1123–9. doi: 10.1016/j.numecd.2017.10.006
50. Pacini G, Bergman RN. MINMOD: a computer program to calculate insulin sensitivity and pancreatic responsivity from the frequently sampled intravenous glucose tolerance test. *Comput Methods Prog BioMed* (1986) 23:113–22. doi: 10.1016/0169-2607(86)90106-9
51. Tura A, Pacini G, Winhofer Y, Bozkurt L, Di Benedetto G, Morbiducci U, et al. Non-esterified fatty acid dynamics during oral glucose tolerance test in women with former gestational diabetes. *Diabetes Med* (2012) 29:351–8. doi: 10.1111/j.1464-5491.2011.03477.x
52. Vergari E, Knudsen JG, Ramracheya R, Salehi A, Zhang Q, Adam J, et al. Insulin inhibits glucagon release by SGLT2-induced stimulation of somatostatin secretion. *Nat Commun* (2019) 10:1–11. doi: 10.1038/s41467-018-08193-8
53. López CDC, Barz T, Körkel S, Wozny G. Nonlinear ill-posed problem analysis in model-based parameter estimation and experimental design. *Comput Chem Eng* (2015) 77:24–42. doi: 10.1016/j.compchemeng.2015.03.002
54. Wagner R, Hakaste LH, Ahlqvist E, Heni M, Machann J, Schick F, et al. Nonsuppressed glucagon after glucose challenge as a potential predictor for glucose tolerance. *Diabetes* (2017) 66:1373–9. doi: 10.2337/db16-0354
55. Morbiducci U, Di Benedetto G, Kautzky-Willer A, Deriu MA, Pacini G, Tura A. Identification of a model of non-esterified fatty acids dynamics through genetic algorithms: The case of women with a history of gestational diabetes. *Comput Biol Med* (2011) 41:146–53. doi: 10.1016/j.compbiomed.2011.01.004
56. Morbiducci U, Di Benedetto G, Kautzky-Willer A, Pacini G, Tura A. Improved usability of the minimal model of insulin sensitivity based on an automated approach and genetic algorithms for parameter estimation. *Clin Sci* (2007) 112:257–63. doi: 10.1042/CS20060203
57. Morbiducci U, Tura A, Grigioni M. Genetic algorithms for parameter estimation in mathematical modeling of glucose metabolism. *Comput Biol Med* (2005) 35:862–74. doi: 10.1016/j.compbiomed.2004.07.005

Conflict of Interest: The authors declare that the research was conducted in the absence of any commercial or financial relationships that could be construed as a potential conflict of interest.

frontiers in Endocrinology

ORIGINAL RESEARCH
published: 29 March 2021
doi: 10.3389/fendo.2021.641713

An Analysis of Glucose Effectiveness in Subjects With or Without Type 2 Diabetes *via* Hierarchical Modeling

Shihao Hu[1], *Yuzhi Lu*[1], *Andrea Tura*[2], *Giovanni Pacini*[3] *and David Z. D'Argenio*[1]*

[1] Department of Biomedical Engineering, University of Southern California, Los Angeles, CA, United States, [2] Metabolic Unit, CNR Institute of Neuroscience, Padova, Italy, [3] Independent Researcher, Padova, Italy

Glucose effectiveness, defined as the ability of glucose itself to increase glucose utilization and inhibit hepatic glucose production, is an important mechanism maintaining normoglycemia. We conducted a minimal modeling analysis of glucose effectiveness at zero insulin (*GEZI*) using intravenous glucose tolerance test data from subjects with type 2 diabetes (T2D, n=154) and non-diabetic (ND) subjects (n=343). A hierarchical statistical analysis was performed, which provided a formal mechanism for pooling the data from all study subjects, to yield a single composite population model that quantifies the role of subject specific characteristics such as weight, height, age, sex, and glucose tolerance. Based on the resulting composite population model, *GEZI* was reduced from 0.021 min^{-1} (standard error – 0.00078 min^{-1}) in the ND population to 0.011 min^{-1} (standard error – 0.00045 min^{-1}) in T2D. The resulting model was also employed to calculate the proportion of the non–insulin-dependent net glucose uptake in each subject receiving an intravenous glucose load. Based on individual parameter estimates, the fraction of total glucose disposal independent of insulin was 72.8% ± 12.0% in the 238 ND subjects over the course of the experiment, indicating the major contribution to the whole-body glucose clearance under non-diabetic conditions. This fraction was significantly reduced to 48.8% ± 16.9% in the 30 T2D subjects, although still accounting for approximately half of the total in the T2D population based on our modeling analysis. Given the potential application of glucose effectiveness as a predictor of glucose intolerance and as a potential therapeutic target for treating diabetes, more investigations of glucose effectiveness in other disease conditions can be conducted using the hierarchical modeling framework reported herein.

Keywords: intravenous glucose tolerance test, glucose-insulin, minimal model, insulin sensitivity, EM algorithm

OPEN ACCESS

Edited by:
Krasimira Tsaneva-Atanasova, University of Exeter, United Kingdom

Reviewed by:
Evan Baker, University of Exeter, United Kingdom
Glenn Ward, The University of Melbourne, Australia

***Correspondence:**
David Z. D'Argenio
dargenio@usc.edu

Specialty section:
This article was submitted to Systems Endocrinology, a section of the journal Frontiers in Endocrinology

Received: *14 December 2020*
Accepted: *24 February 2021*
Published: *29 March 2021*

Citation:
Hu S, Lu Y, Tura A, Pacini G and D'Argenio DZ (2021) An Analysis of Glucose Effectiveness in Subjects With or Without Type 2 Diabetes via Hierarchical Modeling. Front. Endocrinol. 12:641713. doi: 10.3389/fendo.2021.641713

INTRODUCTION

Glucose homeostasis is governed by the interaction of many processes, central among these are insulin secretion, insulin action, insulin clearance and glucose effectiveness. Glucose effectiveness, defined as the ability of glucose itself to increase glucose utilization and inhibit hepatic glucose production *via* mass action and other mechanisms (1), exerts an earlier temporal influence relative to insulin in maintaining normoglycemia. It has been shown in (2) that glucose effectiveness may be divided into two components: Basal Insulin Effect (*BIE*) and Glucose Effectiveness at Zero Insulin

(*GEZI*). The latter measures the effect of glucose on its own removal in the absence of insulin and thus represents the theoretical insulin-independent glucose disappearance. In normal subjects, it has been reported that glucose effectiveness (independent of dynamic insulin) accounts for 45% to 65% of the total net glucose disposal following an intravenous glucose load (3). In patients with defective insulin action, the impact of insulin on glucose disposal is limited but it is partially compensated by the crucial contribution of glucose effectiveness in the attempt of restoring a good glucose tolerance (1). Given its central role in glucose homeostasis, glucose effectiveness impairment has been proposed as an important indicator of glucose intolerance and as a therapeutic target in the treatment of patients with impaired glucose regulation [Basu et al. (4), Pau et al. (5), Alford et al. (3)]. However, there have been only limited studies aimed at quantifying glucose effectiveness in subjects with normal and impaired glucose tolerance, and there are inconsistencies in those studies (1).

Glucose clamp experiments and the minimal model (MM) approach following an intravenous glucose tolerance test (IVGTT) have been used to quantify glucose effectiveness [Best et al. (6), Ader et al. (7), Dube et al. (1)]. While the glucose clamp method, which involves controlling insulin at near-basal level, is regarded as the gold standard for accessing insulin-mediated glucose disposal, it requires cumbersome experiments and trained research teams. In contrast, the MM analysis is based on a simpler IVGTT or an insulin modified IVGTT (IM-IVGTT) (8), and when coupled with a method for model-based statistical estimation, provides estimates of whole-body glucose disposal indices representing both glucose effectiveness and insulin sensitivity [Bergman et al. (9), Henriksen et al. (10)]. While the many applications of the MM reported in the literature have largely focused on questions related to insulin sensitivity, the MM has also been used to better understand the role of glucose effectiveness in glucose homeostasis in healthy and disease conditions. For example, Henriksen et al. (11) analyzed IVGTT data of 20 normoglycemic first degree relatives of type 2 diabetes (T2D) patients and another 20 matched subjects, where they observed an increased glucose effectiveness in the relatives. The study by Lorenzo et al. (12) assessed whether glucose effectiveness estimated *via* MM analysis in healthy participants could predict the future occurrence of T2D. More recently, Morettini et al. (13) analyzed results from a collection of previous studies in subjects with normal glucose tolerance, focusing on factors associated with differences in glucose effectiveness including body mass index. To explore pathogenic factors in type 2 diabetes, Taniguchi et al. (14) analyzed IM-IVGTT data from 11 healthy subjects and 9 T2D patients, and concluded that diminished glucose effectiveness is partially responsible for glucose intolerance. Similarly, Welch et al. (15) observed a decrease in glucose effectiveness in diabetic subjects based on MM analysis of 21 subjects. These studies using the MM to assess glucose effectiveness have involved either only non-diabetic (ND) subjects [e.g., Henriksen et al. (11), Lorenzo et al. (12), Morettini et al. (13)], or included only a small number of subjects with T2D [e.g., Taniguchi et al. (14) and Welch et al. (15)]. Moreover, these studies analyzed the data from subjects separately, which limits the ability of the analysis to define an overall composite model of the population that incorporates the role of anthropomorphic and pathophysiological factors on MM parameters.

To address these limitations, we conducted a MM analysis of glucose effectiveness using a large set of data obtained from previously conducted studies that included both ND subjects (n=343) and those with T2D (n=154). A hierarchical statistical analysis was performed using the MM, which provides a formal mechanism for a simultaneous modeling analysis of the data from all study subjects, yielding a single composite model that quantifies the role of subject specific characteristics such as weight, height, age, sex, and glucose tolerance status.

MATERIALS AND METHODS

Clinical Study Data

This study involves a pooled analysis of data from previous studies, each performed following the Declaration of Helsinki and upon approval of the respective institutional ethics committees, in which subjects were administered either a regular intravenous glucose tolerance test (IVGTT) or an insulin-modified intravenous glucose tolerance test (IM-IVGTT). A total of 44 study groups was included in the analysis, comprising 497 different subjects as summarized in **Table 1**, which also summarizes sex, age and other anthropometric characteristics. Subjects with type 2 diabetes (T2D) and without diabetes (ND) (assessed by the guidelines of the American Diabetes Association) were incorporated in the analysis, including both obese (body mass index (BMI) > 28 kg/m^2) and non-obese subjects, but not subjects with other conditions that might alter glucose regulation. A standard IVGTT was performed in 268 subjects, while an IM-IVGTT was administered to 229 subjects.

Studies in which some of the characteristics are missing in individual subjects are noted in **Table 1**, with missing values imputed as follows. For studies in which only mean values of age, weight, height or BMI were reported (see table), each subject was assigned the corresponding mean value from that study. In 40 subjects from four of the study groups, the values of height, weight and BMI were missing, and only the mean BMI and its standard deviation (SD) were reported. For these subjects, we applied the virtual population anthropomorphic generator PopGen (39) to produce 40 virtual subjects, using the reported mean BMI ± 2SD as the required BMI range, the reported mean age, and the reported proportion of males (27). The resulting mean body weight of the virtual subjects in each group was then assigned to each of the 40 subjects, with the missing heights calculated as $H = \sqrt{weight/BMI}$ using the mean BMI value. The sex of 18 subjects from two study groups (see **Table 1**) was missing but the proportion of men and woman was reported, and the latter was used to randomly assign the sex of the subjects. For 41 subjects from five studies, no sex was provided, and the sex of these subjects was classified as not available (NA). After missing covariate imputation, characteristics of all 497 subjects are as summarized in **Table 2**, which includes sex, age, weight, height

TABLE 1 | Summary of subject characteristics in the studies (mean ± SD).

Study No.	No. of subjects	Cohort	Sex (F/M/NA)	Age (yrs)	Weight (kg)	BMI (kg/m^2)	Height (cm)	Study type	Reference
1	9	T2D	0/9/0	62.1 ± 5.16	73.1 ± 11.1	28.3 ± 4.48	161 ± 7.95	IM-IVGTT	Avogaro et al. (16)
2	9	ND	3/6/0	27.6 ± 9.44	68.3 ± 10.9	22.3 ± 3.39	175 ± 7.18	IM-IVGTT	Avogaro et al. (17)
3	8	ND	1/7/0	52.5 ± 2.98	85.8 ± 18.1	28.9 ± 6.7	173 ± 4.44	IM-IVGTT	Avogaro et al. (18)
4	8	T2D	1/7/0[a]	64.5 ± 6.26	88.4 ± 10.6	29.3 ± 2.54	173 ± 6.16	IM-IVGTT	Avogaro et al. (18)
5	6	T2D	0/6/0	57.0 ± 7.92	92.1 ± 8.45	29.2 ± 1.9	178 ± 5.05	IM-IVGTT	Ludvik et al. (19)
6	18	T2D	0/18/0	57.7 ± 8.11	88.3 ± 12	27.8 ± 2.72	178 ± 6.65	IM-IVGTT	Ludvik et al. (19)
7	11	ND	1/1/11	29.0 ± 0[b]	67.7 ± 5.88	22.5 ± 0[b]	173 ± 7.56[d]	IVGTT	Trojan et al. (20)
8	31	T2D	10/17/6	50.8 ± 12.9	85.8 ± 19.9	29.5 ± 6.9	171 ± 9.6	IM-IVGTT	O'Gorman et al. (21)
9	10	T2D	7/3/0	50.4 ± 7.24	78.8 ± 20.4	30.0 ± 6.49	162 ± 7.44	IM-IVGTT	Not published
10	2	ND	2/0/0	29.0 ± 9.9	100 ± 17.3	35.2 ± 8.67	170 ± 6.36	IM-IVGTT	Not published
11	2	T2D	2/0/0	36.0 ± 4.24	107 ± 15.3	34.0 ± 4.04	178 ± 2.12	IM-IVGTT	Not published
12	10	T2D	4/6/0	66.0 ± 4.71	64.3 ± 7.45	23.8 ± 0[b]	164 ± 9.45[d]	IVGTT	Viviani and Pacini (22)
13	6	ND	2/4/0	73.2 ± 7.33	63.0 ± 9.25	23.1 ± 0[b]	165 ± 12.2[d]	IVGTT	Viviani and Pacini (22)
14	11	ND	1/10/0	24.6 ± 7.21	71.5 ± 13.7	23.7 ± 0[b]	173 ± 17.7[d]	IVGTT	Viviani and Pacini (22)
15	23	T2D	6/17/0	28.4 ± 7.84	107 ± 20.3	34.8 ± 5.45	175 ± 11.3	IM-IVGTT	McQuaid et al. (23)
16	9	ND	5/4/0	35.2 ± 8.63	66.7 ± 5.24	23.0 ± 1.58	170 ± 5.57	IM-IVGTT	McQuaid et al. (23)
17	10	ND	7/3/0	18.6 ± 3.81	109 ± 14.5	35.8 ± 3.55	174 ± 5.36	IM-IVGTT	McQuaid et al. (23)
18	5	T2D	5/0/0	12.2 ± 1.86	64.8 ± 8.17	27.1 ± 2.94	155 ± 2.79	IM-IVGTT	McQuaid et al. (23)
19	2	ND	1/1/0	27.0 ± 12.7	69.5 ± 7.78	25.6 ± 5.68	166 ± 9.19	IVGTT	Not published
20	15	ND	7/8/0	38.9 ± 10.8	68.8 ± 12.3	24.3 ± 2.6	168 ± 10.6	IM-IVGTT	Pacini et al. (8)
21	10	ND	10/0/0	26.3 ± 2.58	57.0 ± 5.31	20.7 ± 2.3	166 ± 6.51	IM-IVGTT	Gennarelli et al. (24)
22	10	T2D	4/6/0	57.8 ± 8	69.0 ± 9.98	25.3 ± 1.8	165 ± 8.95	IVGTT	Not published
23	10	T2D	4/6/0	54.6 ± 11.2	68.9 ± 9.72	25.3 ± 1.64	165 ± 8.95	IVGTT	Not published
24	13	ND	1/1/13	68.3 ± 5.42	71.7 ± 8.73	24.6 ± 1.96	171 ± 5.33	IVGTT	Pacini et al. (25)
25	10	ND	1/1/10	26.7 ± 2	72.3 ± 9.71	22.9 ± 2.89	178 ± 5.87	IVGTT	Pacini et al. (25)
26	10	ND	2/8/0	36.1 ± 9.61	71.2 ± 7.1	23.8 ± 2.03	173 ± 3.35	IVGTT	Piccardo et al. (26)
27	10	ND	10/0/0	27.0 ± 0[b]	62.1 ± 0[c]	24.9 ± 0[c]	158 ± 0[d]	IVGTT	Ahrén and Pacini (27)
28	10	ND	10/0/0	63.0 ± 0[b]	68.0 ± 0[c]	25.2 ± 0[c]	164 ± 0[d]	IVGTT	Ahrén and Pacini (27)
29	10	ND	0/10/0	27.0 ± 0[b]	74.4 ± 0[c]	24.9 ± 0[c]	173 ± 0[d]	IVGTT	Ahrén and Pacini (27)
30	10	ND	0/10/0	63.0 ± 0[b]	78.6 ± 0[c]	25.2 ± 0[c]	177 ± 0[d]	IVGTT	Ahrén and Pacini (27)
31	9	ND	7/2/0	17.0 ± 2.24	54.2 ± 9.08	19.7 ± 2.5	165 ± 8.37	IVGTT	Cavallo-Perin et al. (28)
32	10	ND	2/8/0[a]	35.6 ± 4.7	75.3 ± 14.3	24.5 ± 3.18	175 ± 8.49	IVGTT	Cavallo-Perin et al. (29)
33	13	ND	10/3/0	13.3 ± 0.63	84.2 ± 10.2	32.5 ± 3.08	161 ± 6.57	IVGTT	Cerutti et al. (30)
34	4	ND	1/3/0	32.2 ± 11.2	75.8 ± 10.7	23.9 ± 1.06	178 ± 9.54	IM-IVGTT	Stingl et al. (31)
35	9	ND	6/4/1	43.9 ± 0[b]	65.7 ± 0 [b]	24.1 ± 0[b]	165 ± 0[d]	IVGTT	Handisurya et al. (32)
36	38	ND	38/0/0	31.5 ± 5.55	68.4 ± 13.3	25.0 ± 5.68	166 ± 5.15	IM-IVGTT	Tura et al. (33)
37	18	ND	9/9/0	44.9 ± 12.8[b]	114 ± 23.3	39.4 ± 3.57[b]	169 ± 12.6[d]	IVGTT	Kautzky-Willer et al. (34)
38	17	ND	10/7/0	33.5 ± 14.3	67.5 ± 13.1	23.0 ± 5.1	172 ± 11.6	IVGTT	Kautzky-Willer et al. (34)
39	7	ND	2/5/0	30.3 ± 6.52	70.0 ± 8.91	23.5 ± 0.835	172 ± 9.56	IVGTT	Kautzky-Willer et al. (35)
40	12	T2D	0/12/0	64.0 ± 5.88[b]	95 ± 19.6	28.6 ± 5.63[b]	182 ± 8.38[d]	IM-IVGTT	Schaller et al. (36)
41	17	ND	17/0/0	38.1 ± 7.85	84.3 ± 11.7	33.4 ± 4.05	159 ± 6.02	IVGTT	Basili et al. (37)
42	13	ND	13/0/0	42.7 ± 11.3	94.1 ± 12.4	37.4 ± 3.59	159 ± 9.86	IVGTT	Basili et al. (37)
43	11	ND	11/0/0	45.9 ± 7.61	111 ± 15.9	44.7 ± 5.82	158 ± 2.66	IVGTT	Romano et al. (38)
44	11	ND	11/0/0	48.2 ± 7.92	95.8 ± 9.46	38.1 ± 3.03	159 ± 3.88	IVGTT	Romano et al. (38)

The values in cells without superscripts are known.
[a]*Individual values randomly assigned as per text.*
[b]*All subjects assigned as the mean value.*
[c]*Determine using anthropomorphic algorithm PopGen.*
[d]*Calculated as described in text.*

TABLE 2 | Characteristics of study subjects.

Characteristic	No.	Mean ± SD	Minimum	Median	Maximum
Study type(IVGTT/IM-IVGTT)	268/229				
Cohort (ND/T2D)	343/154				
Sex (female/male/missing)	239/217/41				
Age (yrs)		41.4 ± 16.9	9.70	40.0	86.0
Weight (kg)		79.7 ± 19.9	40.0	75.0	157
Height (cm)		169 ± 10.1	130	168	196
BMI (kg/m^2)		28.0 ± 6.76	15.9	25.3	53.9

and body mass index. A graphic overview of investigated covariates is provided in **Figure 1**.

Minimal Model

The following parameterization of the minimal model for glucose and insulin was used in the analysis [Bergman et al. (40), Araujo-vilar et al. (41)]:

$$\frac{dG(t)}{dt} = -(GEZI + X(t)) \star G(t) + (GEZI + X_{basal}) \star G_{basal}, \quad G(0) = G_{basal} + \frac{Dose}{V} \tag{1}$$

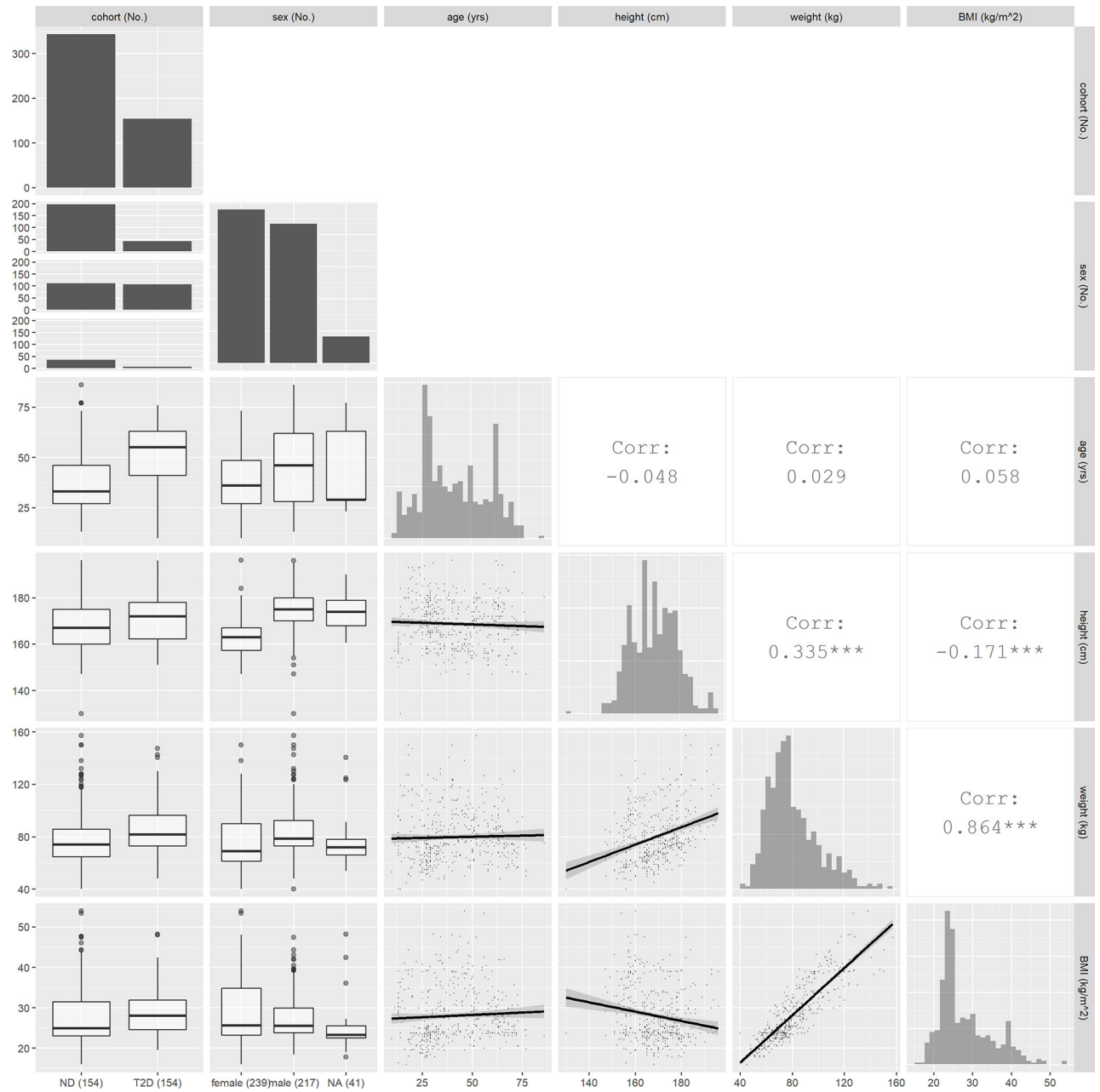

FIGURE 1 | Overview of covariate values and relationships. Histograms plots for continuous covariates and bar graphs for discrete covariates are shown on the diagonal. In the lower triangle, the boxplots between continuous and discrete covariates and scatter plots between continuous covariates are displayed. In the upper triangle, the correlation coefficients between continuous covariates are shown.

$$\frac{dX(t)}{dt} = -p2\star X(t) + p2\star S_I\star I(t), \quad X(0) = S_I\star I_{basal} \qquad (2)$$

where *Dose* denotes the glucose dose (mmol) at time zero, $G(t)$ is the plasma glucose concentration (mmol/L), G_{basal} is basal glucose concentration (measured glucose at the end point), $X(t)$ is the remote insulin action (min^{-1}), $I(t)$ is the measured plasma insulin concentration (pmol/L) and I_{basal} is the basal insulin concentration (measured insulin at the end point). The function $I(t)$ was defined by linearly interpolating the measured insulin concentrations. Model parameters are: glucose effectiveness at zero insulin (*GEZI*, min^{-1}), insulin sensitivity (S_I, min^{-1}/(pmol/L)), remote insulin action parameter ($p2$, min^{-1}) and the volume of glucose distribution (V, L). For IVGTT, a glucose dose of 0.3 g/kg was administrated to the subjects at time zero. The study duration ranged between 180 min and 360 min, while the number of samples ranged from 12 to 30 for each subject. For IM-IVGTT, the same glucose dose was given and a short insulin infusion of between 0.03 to 0.05 U/kg was administered at 20 min. The duration of the IM-IVGTT studies ranged between 180 min and 240 min and number of samples ranged from 12 to 22. The glucose measurements obtained prior to 5 min were excluded from the analysis, since the one-compartment glucose kinetic model does not represent the initial phase of glucose disposal (42).

Hierarchical Modeling Analysis

Hierarchical or population modeling, which is used widely in drug development, provides a formal basis for determining the distribution of model parameters in a population (central tendency and dispersion) and identifying relevant covariates that may explain aspects of the population parameter distribution [see Bonate (43)]. Notable applications of population modeling to the glucose-insulin system include the work of Agbaje et al. (44) using a Bayesian analysis and that of Denti et al. (45) using approximate maximum likelihood methods.

In this work, Eqs (1) and (2) define the first stage of the hierarchical framework, where the residual error (defined as the difference between the measured and predicted glucose concentrations) was assumed to be normally distributed with variance proportional to the predicted glucose concentration. For the second stage of the hierarchy, the vector of model parameters, $\log\theta \equiv \log$ [*GEZI* S_I $p2$ V], is assumed to follow a multivariate normal distribution, $\log\theta \sim N(\mu_{\log\theta}, \Sigma_{\log\theta})$, with the population mean $\mu_{\log\theta}$, covariance $\Sigma_{\log\theta}$, and the conditional mean for each subject $E[\log\theta_i]$, $i = 1,\ldots, n$, are estimated from the pooled study data. The maximum likelihood estimates of $\mu_{\log\theta}$, $\Sigma_{\log\theta}$ and $E[\log\theta_i]$ were obtained using the expectation-maximization (EM) algorithm as applied to solve the nonlinear mixed effects hierarchical modeling problem by Schumitzky (46) and by Walker (47), and as implemented in the MLEM application in ADAPT (Version 5) software (48). The supplemental information contains details regarding the hierarchical modeling framework used in this work.

The following covariates were examined for their influence on model parameters: age, body weight, height, BMI, sex, and glucose tolerance (ND/T2D). We also included test type (IVGTT/IM-IVGTT) as a covariate since some previous studies indicated that there may be a difference in MM parameter estimates between IVGTT and IM-IVGTT experiments (8). Initially, covariate-parameter relationships were identified based on exploratory graphical analysis and mechanistic plausibility. Individual subject conditional mean estimates of model parameters were obtained from the hierarchical model without covariates. All identified covariates for each of the model parameters (S_I, *GEZI*, etc.) were added one-by-one, based on their significance in the exploratory analysis, to generate new hierarchical models. The final explanatory covariates were selected based on estimate precision and objective function value (-2 log likelihood) improvement as accessed using the likelihood ratio test ($p<0.05$) (43). We tested the covariate model for S_I initially, as the importance of S_I for glucose tolerance has been well established and its relationship with BMI has been mentioned in previous studies. Covariate effects on V were then tested, as it was found to correlate with body weight in Denti et al. (45). After accounting for the effects on S_I and V, we then tested the covariate model of *GEZI* to study its relationship with subject characteristics, as this has not been examined in a large population previously. For the continuous covariates considered (age, body weight, height, BMI), power models centered at their median values of the covariates were used. For the categorical covariates considered (sex, glucose tolerance and test type), changes in the covariate model parameters between levels were investigated.

RESULTS

Table 3 (second column) presents the results of the population modeling analysis using the minimal model in Eqs. 1 and 2

TABLE 3 | Population modeling results.

Parameter (Unit)	Without covariates (RSE-CV%)	With covariates (RSE-CV%)
Typical values:		
GEZI (min^{-1})	0.0178 (3.37)	0.0210 (3.73)
S_I (min^{-1}/(pmol/L))	3.59e-5 (5.80)	6.26e-5 (6.33)
$p2$ (min^{-1})	0.0425 (3.62)	0.0420 (3.65)
V (L)	12.4 (1.87)	12.0 (1.56)
Inter-individual variabilities (CV%):		
GEZI	50.9 (4.65)	46.1 (5.09)
S_I	113 (3.83)	83.8 (3.44)
$p2$	44.0 (7.79)	44.9 (7.47)
V	34.4 (3.48)	26.8 (3.11)
Covariate effects:		
T2D on *GEZI*		-0.473 (8.73)
T2D on S_I		-0.479 (9.95)
BMI on S_I		-2.14 (8.43)
IM-IVGTT on S_I		-0.345 (19.4)
weight on V		0.865 (6.49)
Proportional error	0.0706 (0.352)	0.0706 (0.358)
-2 log likelihood	18674	18115

RSE, relative standard error.

Correlation between model parameters: GEZI and S_I: -0.14; GEZI and p2: 0.77; GEZI and p2: -0.07; S_I and p2: -0.05; S_I and V: 0.14; p2 and V: -0.31.

without incorporating covariates in the stage 2 parameter distribution model. The table shows the typical values (TV) of the model parameters as a measure of the central tendency of the parameter population distribution ($TV = e^{\mu_{\log\theta}}$), as well as the parameter inter-individual variability (IIV) as a measure of dispersion of the population distribution $IIV \equiv \{100\sqrt{(\Sigma_{\log\theta})_{ii}}\}$, $i = 1, \ldots, 4$. In the third column of **Table 3**, the corresponding results are presented from the population analysis that included the covariates determined to be significant, as described in MATERIALS AND METHODS.

All model parameters were well estimated, with relative standard errors less than 20 CV%, and the model with covariates (final model) yielded a significant reduction in the log likelihood compared to the base model without covariates (likelihood ratio test, $p<10^{-6}$). The upper row of the goodness-of-fit plots in **Figure 2** shows the population prediction of the base model (**Figure 2A**) and that of the final covariate model (**Figure 2B**), indicating an improved description of the observed data with the later. Plots of the resulting conditional standardized residuals from the final model versus the population predicted glucose concentration (**Figure 2C**) and versus time (**Figure 2D**), indicate that the final population model describes the observed glucose concentrations without significant bias.

GEZI Is Decreased in T2D but Is Not Associated With Other Covariates

In the final population model, the typical value of *GEZI* depends on glucose tolerance category as follows: $GEZI=0.0210*(1-0.473*T2D)$ (min^{-1}), where $T2D=1$ for T2D subjects and $T2D=0$ for ND subjects. The distribution of *GEZI* in the ND population was estimated to have a typical value of 0.021 min^{-1} with inter-individual variability of ± 0.0097 min^{-1}. The corresponding values in the T2D population were estimated to be 0.011 ± 0.0055 min^{-1}. This 47% reduction in the value of *GEZI* in T2D subjects relative to ND subjects was found to be highly significant ($p<10^{-6}$) *via* a likelihood ratio test. The distribution of

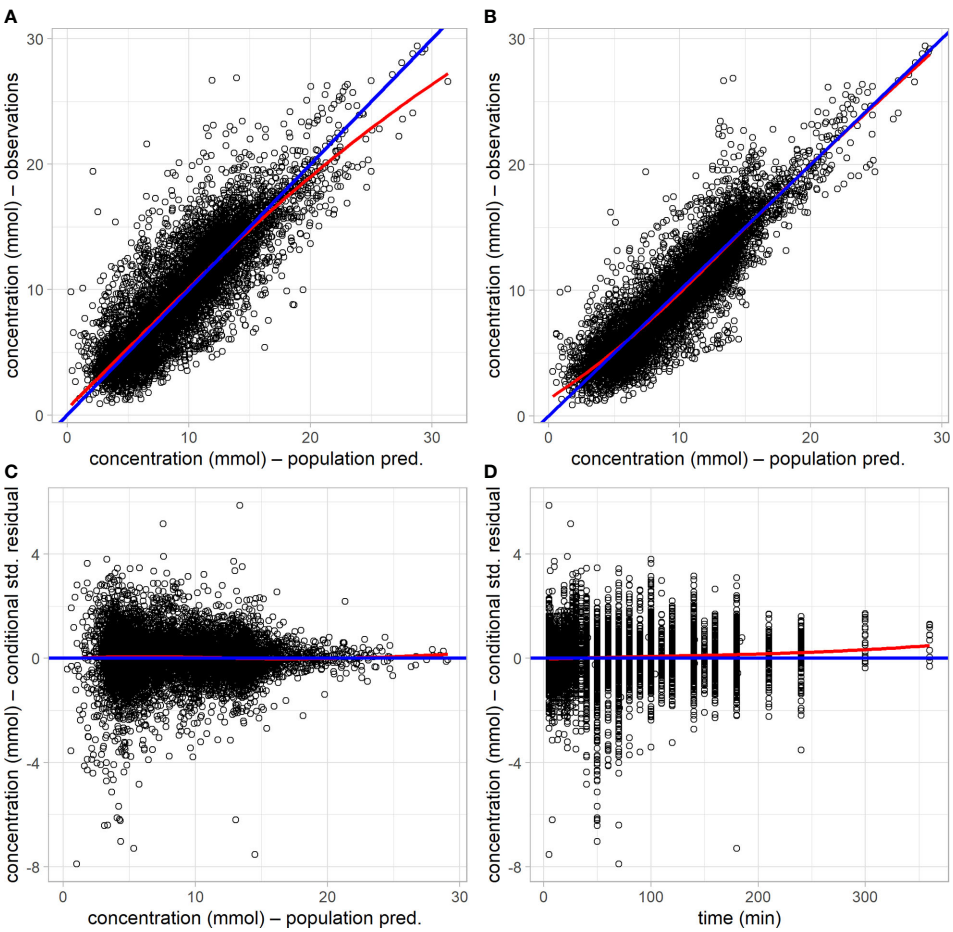

FIGURE 2 | Goodness-of-fit plots of the base model without covariates and the final model with covariates. **(A)** observed glucose concentration versus population prediction from the base model. **(B)** observed glucose concentration versus population prediction from the final model. **(C)** conditional standardized residuals versus population prediction in the final model. **(D)** conditional standardized residual in the final model versus time. Blue lines are the lines of identity or zero value; red lines are loess smooth curves.

individual subject conditional mean estimates of *GEZI* in ND and T2D subjects is shown in **Figure 3**. We also explored possible covariate models relating *GEZI* to *BMI* in both ND and T2D subjects, but no associations were found to be significant. Moreover, the variability in *GEZI* could not be further explained by subjects' age, weight, height or sex; while a decreasing association between *GEZI* and age was noted, this was not statistically significant. No differences in *GEZI* were found between subjects that underwent an IVGTT versus an IM-IVGTT experiment.

S_I Decreases With BMI in Both ND and T2D

In the final population model, S_I was found to be associated with BMI, *a priori* glucose tolerance status, and test type by the following model: $S_I=(6.26e{-}5)*(1{-}0.479*T2D)*(1{-}0.345*IM)*(BMI/25.3)^{-2.14}$, where $IM=1$ for IM-IVGTT and $IM=0$ for IVGTT. **Figure 4** shows the estimated relationships between the typical value of S_I and *BMI* for both ND and T2D subjects from each of the two test types. In both ND and T2D groups, higher BMI values lead to decreased S_I (with a power of -2.14). This is consistent with the conclusions in Bergman and Lovejoy (49), in which they reported a negative association between BMI and S_I. For a given BMI, the population model shows a significant decrease (approximately 48%) in S_I, between the T2D subjects versus those with ND. Our results indicated that IM-IVGTT is associated with significantly lower S_I (approximately 35%) estimate when compared to IVGTT ($p<10^{-5}$). The addition of weight, height, age or sex to the population model was not found to be significant.

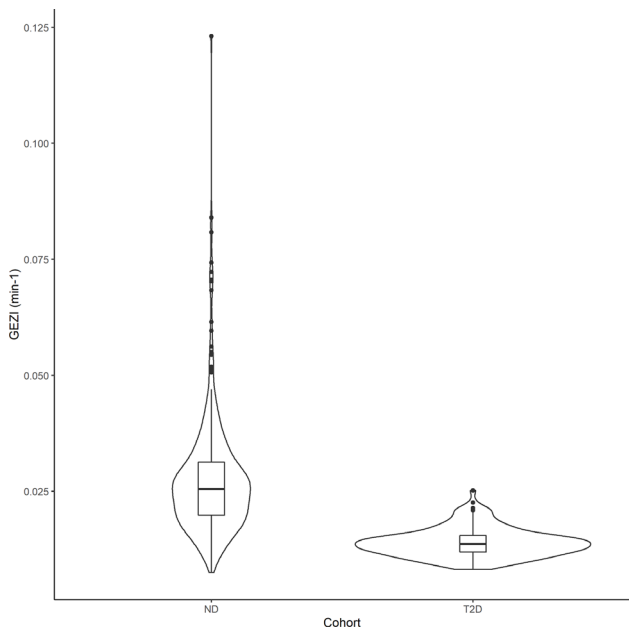

FIGURE 3 | Violin plots showing the distribution of the individual subjects conditional mean estimates of *GEZI* in the ND and T2D cohorts. Boxplots were inserted for each cohort to indicate medians and interquartile ranges.

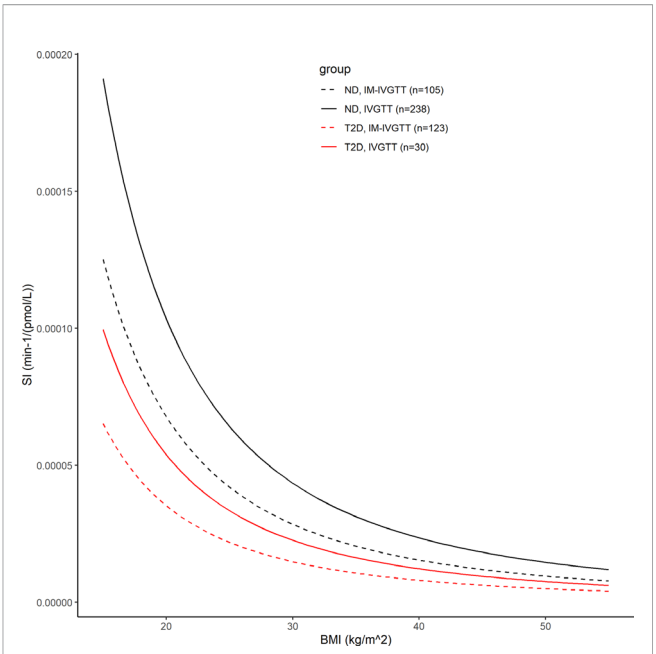

FIGURE 4 | The black lines show the covariate model prediction of the typical value of S_I versus BMI in ND subjects, with the solid line indicating subjects in IVGTT and dash line indicating IM-IVGTT. The red lines are the corresponding curves in T2D patients.

The Significant Non–Insulin-Dependent Contribution to Net Glucose Disposal Is Greater in ND Than T2D Following a Glucose Load

In order to compare the relative contributions of non-insulin- and insulin-mediated pathways to net glucose disposal, we determined the proportion of glucose uptake due to glucose itself and that due to insulin, in ND subjects and those with T2D, in both the basal state and during an IVGTT experiment. Under basal conditions, the fraction of non–insulin-dependent glucose disposal can be calculated using the individual conditional mean estimates of *GEZI* and S_I, together with the measured I_{basal} of each subject: $(GEZI/(\mathrm{GEZI}+S_I I_{basal}))$. In the 343 ND subjects, the non–insulin-dependent pathway accounted for 88.5% ± 7.10% of the total net glucose disposal, and 89.0% ± 10.2% in the 154 T2D subjects. In the IVGTT experiment group (268 subjects), we calculated the net glucose disposal due to the two pathways during the course of the experiment, based on individual subject estimates. The non–insulin-dependent and insulin dependent glucose disposal (*GD-NID*, *GD-ID*) were calculated in each subject as follows: $GD-NID=\int_0^T GEZI*G(t)dt$, $GD-ID=\int_0^T X(t)*G(t)dt$ (T is the last measurement time in the subject's IVGTT experiment). In the 238 ND subjects, the fraction of non–insulin-dependent glucose disposal (*GD-NID*/(*GD-NID* + *GD-ID*)) was 72.8% ± 12.0%, while it was 48.8% ± 16.9% in the 30 T2D subjects in the IVGTT group (**Figure 5**), and this difference was significant ($p<10^{-6}$, unpaired two-samples Wilcoxon test). Our

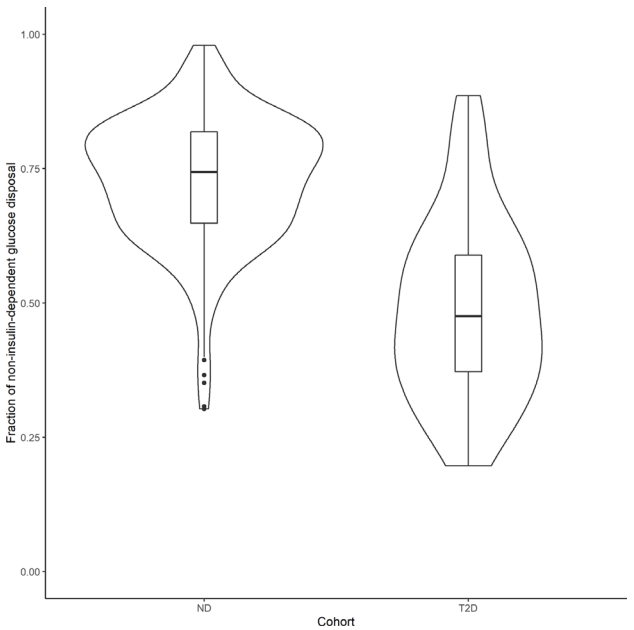

FIGURE 5 | Violin plots showing the distribution of the fraction of non–insulin-dependent net glucose disposal in 238 ND subjects and 30 T2D patients that underwent an IVGTT test. Boxplots were inserted for each cohort to indicate medians and interquartile ranges.

model based analysis indicates that the non–insulin-dependent route accounts for the large majority of the glucose disposal in the ND population, while it is reduced to approximately half of the total in the T2D population.

DISCUSSION

In this work, a hierarchical modeling analysis was conducted to develop a composite population minimal model of glucose-insulin dynamics in ND and T2D subjects, using data from IVGTT and IM-IVGTT studies. The resulting population model was used to quantify the role of subject characteristics (age, body weight, height, BMI, sex, glucose tolerance status) and test type (IVGTT/IM-IVGTT) on glucose effectiveness and other MM parameters. In the final composite population model, glucose tolerance status (ND, T2D) was a significant predictor of glucose effectiveness, as assessed by *GEZI*. The addition of other covariates did not further explain remaining inter-subject variability in *GEZI*, beyond that predicted by glucose tolerance status. Further analysis of the population model indicated that the relative contribution to the total net glucose disposal independent of insulin was significantly greater in ND compared to T2D subjects. As expected, a significant relation between insulin sensitivity, S_I, and BMI was identified in both ND and T2D populations, albeit different in the two groups. Moreover, the estimated S_I-BMI relations were found to depend on test type, with a lower population value of S_I observed in IM-IVGTT versus IVGTT studies, after accounting for BMI.

Based on the composite population model (**Table 3**), glucose effectiveness, as assessed by *GEZI* in this study, is reduced from 0.021 min^{-1} (standard error – 0.00078 min^{-1}) in the ND population to 0.011 min^{-1} (standard error – 0.00045 min^{-1}) in T2D. Moreover, there is less inter-individual variability in GEZI in the T2D population (0.0051 min^{-1}, standard error – 0.00026 min^{-1}) relative to ND (0.0097 min^{-1}, standard error – 0.00049 min^{-1}). This result is qualitatively consistent with other studies that reported a reduction in glucose effectiveness, as assessed by S_G, involving smaller numbers of T2D subjects Welch et al. (15) and Taniguchi et al. (14). We also examined potential associations between *GEZI* and both BMI and age, and while a negative relation was noted with each, neither age nor BMI was found to be significant, when considering all subjects, or separately within the ND and T2D populations. The lack of association with age is consistent with the conclusion in Pacini et al. (25) from their analysis of S_G in 17 elderly healthy subjects. Morettini et al. (13) did, however, find a weak but statistically significant relation between *GEZI* and BMI based on a MM analysis of 204 healthy subjects. While we also noted a negative correlation between *GEZI* and BMI, this was not found to be statistically significant in our study.

In the study in healthy subjects following an IVGTT (50), it was found that the glucose disappearance constant K_G was strongly correlated with *GEZI* and concluded that *GEZI* is a major determinant of glucose disappearance. Further analysis of the population model reported in this work, allows for the calculation of the relative contribution of insulin- and non-insulin-dependent pathways of total net glucose disposal in IVGTT experiments (see **Figure 5**). Although both *GEZI* and S_I are reduced by a similar percent (47%) in T2D and ND subjects, the relative contribution of non–insulin-dependent glucose disposal is lower in T2D subjects (48.8%) compared to that in ND subjects (73.8%). This difference is not unexpected given that *GEZI* directly facilitates plasma glucose disappearance, while S_I influences glucose disposal only indirectly *via* its effect on remote insulin action ($X(t)$). The average fraction of non–insulin-dependent glucose disposal in ND subjects found in this study, 72.8%, is somewhat higher than the range of 45% to 65% reported in Alford et al. (3), but consistent with the reported value of 71% following IVGTT in mice (51). While Best et al. (6) reported that the contribution of glucose effectiveness to glucose disposal is dominant in insulin-resistant subjects (83%) based on an oral glucose tolerance study, our results (**Figure 5**) indicate that the contribution of glucose effectiveness in T2D subjects following IVGTT can range widely (19.7% to 88.6%). Under basal conditions in both ND and T2D subjects, the population modeling analysis found that the fraction of net glucose disposal mediated by the non–insulin-dependent pathway was approximately 89% (see Results section). For comparison, Best et al. (6) reported that at basal insulin levels, glucose effectiveness can account for 60% to 75% of the glucose uptake based on the clamp approach, depending on the basal glucose concentration.

The population modeling results predicting a significantly lower S_I in the T2D population compared to the ND population

(approximately 47.9%, RSE=10%) were expected given the well-documented ability of S_I to predict glucose tolerance (49). The negative association between S_I and BMI quantified in the population model (see **Figure 4**) is also consistent with other studies in ND and T2D populations [Welch et al. (15), Morettini et al. (13)]. However, these results related to BMI should be interpreted cautiously, given the well-known challenges associated with using BMI as independent factor to explain differences in S_I, without incorporating information related to fat distribution (52). The typical glucose distribution volume V was found to depend on body weight following a nonlinear relationship with coefficient and power estimated from the modeling analysis: $V(L)=12.0^{*}(weight/75)^{0.865}$ (weight in kg). The typical glucose distribution volume of 12 L is close to the reported range of 1.65-1.70 dl/kg in Denti et al. (45), but the confidence interval for the power estimate does not include 1. While no relation between $p2$ and any covariates was found to be significant, $p2$ was determined to be positively correlated with *GEZI* (r=0.77) (the ability to estimate all parameter correlations in the population is intrinsic to hierarchical modeling analysis). Thus, any association between $p2$ and glucose tolerance could be reflected in its correlation with *GEZI*. From our analysis, it was also concluded that there is a significant difference in the S_I between subjects administered an IVGTT versus an IM-IVGTT. This results is consistent with the observation in Ward et al. (53) that the MM estimate of S_I depends on the dose and duration of exogenous insulin administration in IM-IVGTT experiments. Since our study used previously collected data from various sites conducted over an extended period of time, the inability to retrieve all the details of the IM-IVGTT experiments precluded us from further exploring any potential effects of the insulin administration profiles on the estimation results.

In this study, a hierarchical modeling analysis was used to develop a composite population minimal model in a diverse collection of subjects who were assessed to either have or not have type 2 diabetes. This modeling analysis allows the complete study data to be used to simultaneously inform the estimation of the population distribution of model parameters (mean and covariance), which provides a mechanism for identifying explanatory subject specific factors (anthropomorphic, pathophysiological, treatment, study, etc.) and quantifying their effects on model parameters. Hierarchical modeling has been applied previously in MM studies, including by Agbaje et al. (44) who used a Bayesian framework to analyze results from IM-IVGTT experiments in 65 T2D subjects, and more recently by Denti et al. (45) using approximate maximum likelihood methods in a study of 204 healthy subjects after IM-IVGTT. An advantage of using hierarchical modeling as implemented in this study, is that it allows for a multivariate assessment of the relative contribution of subject specific characteristics. A limitation of the approach, beyond the additional computational difficulties associated with implementing the EM algorithm to obtain the analytically exact maximum likelihood estimates, is that the MM parameters are assumed to follow a defined distribution in the population (specifically, $\log[GEZI\ S_I\ p2\ V] \sim N(\mu_{\log\theta}, \Sigma_{\log\theta})$). Also, as with any multivariate analysis, identifying the explanatory covariates depends on the specific statistical procedure and the associated criteria for including and excluding covariates, which can be particularly challenging when covariates are not independent. While this work used glucose tolerance tests conducted at different sites, we did not find any systematic differences in model parameter estimates across study sites.

The role of glucose effectiveness as a predictor of glucose intolerance and diabetes has been suggested in several studies [Martin et al. (54), Lorenzo et al. (12)], which have reported that reduced glucose effectiveness may precede diabetes development even in normoglycemic subjects. Indeed, the modeling analysis in this study suggests *GEZI* may be a predictor of the dysregulated glucose tolerance. Also, glucose effectiveness may be a possible target for glucose-reducing therapies (55). Although the molecular mechanisms of glucose effectiveness in regulating glucose remains to be more fully elucidated, some studies have demonstrated that pharmacological intervention (5) and exercise (56) can improve glucose effectiveness and increase plasma glucose clearance. Recently, the development of sodium glucose cotransporter 2 inhibitors has provided a novel antidiabetic therapy independent of insulin action (57).

In summary, we have conducted a hierarchical minimal model analysis of the glucose-insulin response in ND and T2D subjects given an intravenous glucose load, which allowed us to quantify the influence of diabetes status, BMI and body weight on the glucose metabolic parameters, while accounting for the differences in the study type. The relative contribution of non–insulin-dependent net glucose disposal in ND and T2D populations was determined using the resulting population model, demonstrating the utility of this modeling approach to quantify the fraction of non–insulin-dependent glucose disposal based on an IVGTT. The novel finding that *GEZI* is markedly reduced in T2D, both in its absolute value and the relative contribution to net glucose disposal, represents a further indication of the extensive dysregulated glucose homeostasis induced by diabetes. Although this work was focused on MM analysis of ND and T2D subjects, the hierarchical modeling framework can be applied to investigate glucose effectiveness in populations with other accompanying disease conditions, and to investigate other possible explanatory covariates in future studies.

DATA AVAILABILITY STATEMENT

The raw data supporting the conclusions of this article will be made available by the authors, without undue reservation.

ETHICS STATEMENT

The studies involving human participants were reviewed and approved by multiple institutions and approved by each institution's respective ethics committees (**Table 1** in the manuscript lists each institution). Written informed consent to participate in this study was provided by the participants' legal guardian/next of kin.

AUTHOR CONTRIBUTIONS

SH and DD'A participated in the study design, performed the modeling analysis, and drafted the manuscript. YL participated in data analysis and reviewed the manuscript. GP and AT provided the data, participated in the study design, and critically reviewed and revised the manuscript. GP was a visiting collaborator at the Biomedicine Simulations Resource at the University of Southern California over the course of this project. All authors contributed to the article and approved the submitted version.

FUNDING

This work was supported by grants from National Institutes of Health/National Institute of Biomedical Imaging and Bioengineering (NIH/NIBIB) P41-EB001978 and the Alfred E. Mann Institute at USC (DD'A).

ACKNOWLEDGMENTS

The authors thank the colleagues listed in the Reference column of **Table 1**, who have graciously allowed the further analysis of their data that was collected with GP during the last 35 years.

SUPPLEMENTARY MATERIAL

The Supplementary Material for this article can be found online at: https://www.frontiersin.org/articles/10.3389/fendo.2021.641713/full#supplementary-material

REFERENCES

1. Dube S, Errazuriz-Cruzat I, Basu A, Basu R. The forgotten role of glucose effectiveness in the regulation of glucose tolerance. *Curr Diabetes Rep* (2015) 15:605–10. doi: 10.1007/s11892-015-0605-6
2. Kahn SE, Klaff LJ, Schwartz MW, Beard JC, Bergman RN, Taborsky GJJ, et al. Treatment with a somatostatin analog decreases pancreatic B-cell and whole body sensitivity to glucose. *J Clin Endocrinol Metab* (1990) 71:994–1002. doi: 10.1210/jcem-71-4-994
3. Alford FP, Henriksen JE, Rantzau C, Beck-Nielsen H. Glucose effectiveness is a critical pathogenic factor leading to glucose intolerance and type 2 diabetes: An ignored hypothesis. *Diabetes Metab Res Rev* (2018) 34:e2989. doi: 10.1002/dmrr.2989
4. Basu A, Dalla Man C, Basu R, Toffolo G, Cobelli C, Rizza RA. Effects of type 2 diabetes on insulin secretion, insulin action, glucose effectiveness, and postprandial glucose metabolism. *Diabetes Care* (2009) 32:866–72. doi: 10.2337/dc08-1826
5. Pau CT, Keefe C, Duran J, Welt CK. Metformin improves glucose effectiveness, not insulin sensitivity: Predicting treatment response in women with polycystic ovary syndrome in an open-label, interventional study. *J Clin Endocrinol Metab* (2014) 99:1870–8. doi: 10.1210/jc.2013-4021
6. Best JD, Kahn SE, Ader M, Watanabe RM, Ta-Chen N, Bergman RN. Role of Glucose Effectiveness in the Determination of Glucose Tolerance. *Diabetes Care* (1996) 19:1018–30. doi: 10.2337/diacare.19.9.1018
7. Ader M, Ni TC, Bergman RN. Glucose effectiveness assessed under dynamic and steady state conditions. Comparability of uptake versus production components. *J Clin Invest* (1997) 99:1187–99. doi: 10.1172/JCI119275
8. Pacini G, Tonolo G, Sambataro M, Maioli M, Ciccarese M, Brocco E, et al. Insulin sensitivity and glucose effectiveness: Minimal model analysis of regular and insulin-modified FSIGT. *Am J Physiol* (1998) 274:592–9. doi: 10.1152/ajpendo.1998.274.4.e592
9. Bergman RN, Prager R, Volund A, Olefsky JM. Equivalence of the insulin sensitivity index in man derived by the minimal model method and the euglycemic glucose clamp. *J Clin Invest* (1987) 79:790–800. doi: 10.1172/JCI112886
10. Henriksen JE, Alford F, Ward G, Thye-Rønn P, Levin K, Hother-Nielsen O, et al. Glucose effectiveness and insulin sensitivity measurements derived from the non-insulin-assisted minimal model and the clamp techniques are concordant. *Diabetes Metab Res Rev* (2010) 26:569–78. doi: 10.1002/dmrr.1127
11. Henriksen JE, Alford F, Handberg A, Vaag A, Ward GM, Kalfas A, et al. Increased glucose effectiveness in normoglycemic but insulin-resistant relatives of patients with non-insulin-dependent diabetes mellitus. A novel compensatory mechanism. *J Clin Invest* (1994) 94:1196–204. doi: 10.1172/JCI117436
12. Lorenzo C, Wagenknecht LE, Rewers MJ, Karter AJ, Bergman RN, Hanley AJ, et al. Disposition index, glucose effectiveness, and conversion to type 2 diabetes: The insulin resistance atherosclerosis study (IRAS). *Diabetes Care* (2010) 33:2098–103. doi: 10.2337/dc10-0165
13. Morettini M, Di Nardo F, Ingrillini L, Fioretti S, Göbl C, Kautzky-Willer A, et al. Glucose effectiveness and its components in relation to body mass index. *Eur J Clin Invest* (2019) 49:e13099. doi: 10.1111/eci.13099
14. Taniguchi A, Nakai Y, Fukushima M, Kawamura H, Imura H, Nagata I, et al. Pathogenic factors responsible for glucose intolerance in patients with NIDDM. *Diabetes* (1992) 41:1540–6. doi: 10.2337/diab.41.12.1540
15. Welch S, Gebhart SSP, Bergman RN, Phillips LS. Minimal model analysis of intravenous glucose tolerance test-derived insulin sensitivity in diabetic subjects. *J Clin Endocrinol Metab* (1990) 71:1508–18. doi: 10.1210/jcem-71-6-1508
16. Avogaro A, Miola M, Favaro A, Gottardo L, Pacini G, Manzato E, et al. Gemfibrozil improves insulin sensitivity and flow-mediated vasodilatation in type 2 diabetic patients. *Eur J Clin Invest* (2001) 31:603–9. doi: 10.1046/j.1365-2362.2001.00856.x
17. Avogaro A, Watanabe RM, Gottardo L, De Kreutzenberg S, Tiengo A, Pacini G. Glucose tolerance during moderate alcohol intake: Insights on insulin action from glucose/lactate dynamics. *J Clin Endocrinol Metab* (2002) 87:1233–8. doi: 10.1210/jcem.87.3.8347
18. Avogaro A, Watanabe RM, Dall'Arche A, De Kreutzenberg S, Tiengo A, Pacini G. Acute Alcohol Consumption Improves Insulin Action Without Affecting Insulin Secretion in Type 2 Diabetic Subjects. *Diabetes Care* (2004) 27:1369–74. doi: 10.2337/diacare.27.6.1369
19. Ludvik B, Waldhäusl W, Prager R, Kautzky-Willer A, Pacini G. Mode of action of Ipomoea Batatas (Caiapo) in type 2 diabetic patients. *Metabolism* (2003) 52:875–80. doi: 10.1016/S0026-0495(03)00073-8
20. Trojan N, Pavan P, Iori E, Vettore M, Marescotti MC, Tiengo A, et al. Effect of different times of administration of a single ethanol dose on insulin action, insulin secretion and redox state. *Diabetic Med* (1999) 16:400–7. doi: 10.1046/j.1464-5491.1999.00060.x
21. O'Gorman DJ, Yousif O, Dixon G, McQuaid S, Murphy E, Rahman Y, et al. In vivo and in vitro studies of GAD-antibody positive subjects with Type 2 diabetes: A distinct sub-phenotype. *Diabetes Res Clin Pract* (2008) 80:365–70. doi: 10.1016/j.diabres.2007.12.009
22. Viviani GL, Pacini G. Reduced glucose effectiveness as a feature of glucose intolerance: Evidence in elderly type-2 diabetic subjects. *Aging Clin Exp Res* (1999) 11:169–75. doi: 10.1007/bf03399659
23. McQuaid S, O'Gorman DJ, Yousif O, Yeow TP, Rahman Y, Gasparro D, et al. Early-onset insulin-resistant diabetes in obese caucasians has features of typical type 2 diabetes, but 3 decades earlier. *Diabetes Care* (2005) 28:1216–8. doi: 10.2337/diacare.28.5.1216

24. Gennarelli G, Rovei V, Novi RF, Holte J, Bongioanni F, Revelli A, et al. Preserved insulin sensitivity and β-cell activity, but decreased glucose effectiveness in normal-weight women with the polycystic ovary syndrome. *J Clin Endocrinol Metab* (2005) 90:3381–6. doi: 10.1210/jc.2004-1973
25. Pacini G, Valerio A, Beccaro F, Nosadini R, Cobelli C, Crepaldi G. Insulin sensitivity and beta-cell responsivity are not decreased in elderly subjects with normal OGTT. *J Am Geriatr Soc* (1988) 36:317–23. doi: 10.1111/j.1532-5415.1988.tb02358.x
26. Piccardo MG, Pacini G, Nardi E, Rosa MS, Vito RD. Beta-cell response and insulin hepatic extraction in noncirrhotic alcoholic patients soon after withdrawal. *Metabolism* (1994) 43:367–71. doi: 10.1016/0026-0495(94)90106-6
27. Ahrén B, Pacini G. Age-related reduction in glucose elimination is accompanied by reduced glucose effectiveness and increased hepatic insulin extraction in man. *J Clin Endocrinol Metab* (1998) 83:3350–6. doi: 10.1210/jc.83.9.3350
28. Cavallo-Perin P, Pacini G, Cerutti F, Bessone A, Condo C, Sacchetti L, et al. Insulin resistance and hyperinsulinemia in Homozygous beta-Thalassemia. *Metabolism* (1995) 44:281–6. doi: 10.1016/0026-0495(95)90155-8
29. Cavallo-Perin P, Bergerone S, Gagnor A, Comune M, Giunti S, Cassader M, et al. Myocardial infarction before the age of 40 years is associated with insulin resistance. *Metabolism* (2001) 50:30–5. doi: 10.1053/meta.2001.19501
30. Cerutti F, Sacchetti C, Bessone A, Rabbone I, Cavallo-Perin P, Pacini G. Insulin secretion and hepatic insulin clearance as determinants of hyperinsulinaemia in normotolerant grossly obese adolescents. *Acta Paediatr* (1998) 87:1045–50. doi: 10.1080/080352598750031356
31. Stingl H, Schnedl WJ, Krssak M, Bernroider E, Bischof MG, Lahousen T, et al. Reduction of hepatic glycogen synthesis and breakdown in patients with agenesis of the dorsal pancreas. *J Clin Endocrinol Metab* (2002) 87:4678–85. doi: 10.1210/jc.2002-020036
32. Handisurya A, Pacini G, Tura A, Gessl A, Kautzky-Willer A. Effects of T4 replacement therapy on glucose metabolism in subjects with subclinical (SH) and overt hypothyroidism (OH). *Clin Endocrinol* (2008) 69:963–9. doi: 10.1111/j.1365-2265.2008.03280.x
33. Tura A, Grassi A, Winhofer Y, Guolo A, Pacini G, Mari A, et al. Progression to type 2 diabetes in women with former gestational diabetes: time trajectories of metabolic parameters. *PloS One* (2012) 7:e50419. doi: 10.1371/journal.pone.0050419
34. Kautzky-Willer A, Pacini G, Ludvik B, Schernthaner G, Prager R. β-Cell hypersecretion and not reduced hepatic insulin extraction is the main cause of hyperinsulinemia in obese nondiabetic subjects. *Metabolism* (1992) 41:1304–12. doi: 10.1016/0026-0495(92)90100-O
35. Kautzky-Willer A, Thomaseth K, Clodi M, Ludvik B, Waldhäusl W, Prager R, et al. β-Cell activity and hepatic insulin extraction following dexamethasone administration in healthy subjects. *Metabolism* (1996) 45:486–91. doi: 10.1016/S0026-0495(96)90224-3
36. Schaller G, Kretschmer S, Gouya G, Haider DG, Mittermayer F, Riedl M, et al. Alcohol acutely increases vascular reactivity together with insulin sensitivity in type 2 diabetic men. *Exp Clin Endocrinol Diabetes* (2010) 118:57–60. doi: 10.1055/s-0029-1233453
37. Basili S, Pacini G, Guagnano MT, Manigrasso MR, Santilli F, Pettinella C, et al. Insulin resistance as a determinant of platelet activation in obese women. *J Am Coll Cardiol* (2006) 48:2531–8. doi: 10.1016/j.jacc.2006.08.040
38. Romano M, Guagnano MT, Pacini G, Vigneri S, Falco A, Marinopiccoli M, et al. Association of Inflammation Markers with Impaired Insulin Sensitivity and Coagulative Activation in Obese Healthy Women. *J Clin Endocrinol Metab* (2003) 88:5321–6. doi: 10.1210/jc.2003-030508
39. McNally K, Cotton R, Hogg A, Loizou G. Reprint of PopGen: A virtual human population generator. *Toxicology* (2015) 332:77–93. doi: 10.1016/j.tox.2015.04.014
40. Bergman RN, Ider YZ, Bowden CR, Cobelli C. Quantitative estimation of insulin sensitivity. *Am J Physiol* (1979) 5:667–77. doi: 10.1152/ajpendo.1979.236.6.e667
41. Araujo-Vilar D, Rega-Liste CA, Garcia-Estevez DA, Sarmiento-Escalona F, Mosquera-Tallon V, Cabezas-Cerrato J. Minimal model of glucose metabolism: Modified equations and its application in the study of insulin sensitivity in obese subjects. *Diabetes Res Clin Pract* (1998) 39:129–41. doi: 10.1016/S0168-8227(97)00126-5
42. Vicini P, Caumo A, Cobelli C. Glucose effectiveness and insulin sensitivity from the minimal models: consequences of undermodeling assessed by Monte Carlo simulation. *IEEE Trans Biomed Eng* (1999) 46:130–7. doi: 10.1109/10.740875
43. Bonate P. *Pharmacokinetic-Pharmacodynamic modeling and simulation*. New York: Springer US (2011). doi: 10.1007/978-1-4419-9485-1
44. Agbaje OF, Luzio SD, Albarrak AI, Lunn DJ, Owens DR, Hovorka R. Bayesian hierarchical approach to estimate insulin sensitivity by minimal model. *Clin Sci* (2003) 105:551–60. doi: 10.1042/CS20030117
45. Denti P, Bertoldo A, Vicini P, Cobelli C. IVGTT glucose minimal model covariate selection by nonlinear mixed-effects approach. *Am J Physiol Endocrinol Metab* (2010) 298:E950–60. doi: 10.1152/ajpendo.00656.2009
46. Schumitzky A. EM algorithms and two stage methods in pharmacokinetic population analysis. In: DZ D'Argenio, editor. *Advanced methods of pharmacokinetic and pharmacodynamic systems analysis*, vol. 2 . New York: Plenum Press (1995). p. 145–60.
47. Walker S. An EM Algorithm for Nonlinear Random Effects Models. *Biometrics* (1996) 52:934–44. doi: 10.2307/2533054
48. D'Argenio DZ, Alan S, Wang X. *ADAPT 5 User"s Guide: Pharmacokinetic/Pharmacodynamic Systems Analysis Software*. Los Angeles: Biomedical Simulations Resources (2009).
49. Bergman RN, Lovejoy JC. *The Minimal Model Approach and Determinants of Glucose Tolerance*. Pennington Center Nutrition Series: Louisiana State University Press (1997).
50. Kahn SE, Prigeon RL, McCulloch DK, Boyko EJ, Bergman RN, Schwartz MW, et al. The contribution of insulin-dependent and insulin-independent glucose uptake to intravenous glucose tolerance in healthy human subjects. *Diabetes* (1994) 43:587–92. doi: 10.2337/diab.43.4.587
51. Pacini G, Thomaseth K, Ahrén B. Contribution to glucose tolerance of insulin-independent vs. insulin-dependent mechanisms in mice. *Am J Physiol Endocrinol Metab* (2001) 281:693–703. doi: 10.1152/ajpendo.2001.281.4.e693
52. Klein S, Allison DB, Heymsfield SB, Kelley DE, Leibel RL, Nonas C, et al. Waist circumference and cardiometabolic risk: A consensus statement from shaping America's health: Association for weight management and obesity prevention; NAASO, the obesity society; the American society for nutrition; and the American diabetes associat. *Am J Clin Nutr* (2007) 15:1197–202. doi: 10.1093/ajcn/85.5.1197
53. Ward GM, Walters JM, Barton J, Alford FP, Boston RC. Physiologic modeling of the intravenous glucose tolerance test in type 2 diabetes: A new approach to the insulin compartment. *Metabolism* (2001) 50:512–9. doi: 10.1053/meta.2001.21029
54. Martin B, Warram J, Krolewski A, Bergman R, Soeldner J, Kahn C. Role of glucose and insulin resistance in development of type 2 diabetes mellitus: results of a 25-year follow-up study. *Lancet* (1992) 340:925–9. doi: 10.1016/0140-6736(92)92814-V
55. Ahrén B, Pacini G. Glucose effectiveness: Lessons from studies on insulin-independent glucose clearance in mice. *J Diabetes Invest* (2020). doi: 10.1111/jdi.13446
56. Karstoft K, Clark MA, Jakobsen I, Knudsen SH, van Hall G, Pedersen BK, et al. Glucose effectiveness, but not insulin sensitivity, is improved after short-term interval training in individuals with type 2 diabetes mellitus: a controlled, randomised, crossover trial. *Diabetologia* (2017) 60:2432–42. doi: 10.1007/s00125-017-4406-0
57. Seufert J. SGLT2 inhibitors - an insulin-independent therapeutic approach for treatment of type 2 diabetes: focus on canagliflozin. *Diabetes Metab Syndr Obes* (2015) 8:543–54. doi: 10.2147/DMSO.S90662

Conflict of Interest: The authors declare that the research was conducted in the absence of any commercial or financial relationships that could be construed as a potential conflict of interest.

frontiers in Endocrinology

ORIGINAL RESEARCH
published: 29 March 2021
doi: 10.3389/fendo.2021.621687

Selenium Kinetics in Humans Change Following 2 Years of Supplementation With Selenomethionine

*Blossom H. Patterson[1], Gerald F. Combs Jr[2], Philip R. Taylor[3], Kristine Y. Patterson[4], James E. Moler[5] and Meryl E. Wastney[6]**

[1] Biometry Research Group, Division of Cancer Prevention (DCP), National Cancer Institute, Bethesda, MD, United States, [2] Division of Nutritional Sciences, Cornell University, Ithaca, NY, United States, [3] Division of Cancer Epidemiology and Genetics, National Cancer Institute, Bethesda, MD, United States, [4] Beltsville Human Nutrition Research Center, United States Department of Agriculture-Agricultural Research Service (USDA-ARS), Beltsville, MD, United States, [5] Information Management Services, Inc., Rockville, MD, United States, [6] Metabolic Modeling Services, West Lafayette, IN, United States

OPEN ACCESS

Edited by:
Darko Stefanovski, University of Pennsylvania, United States

Reviewed by:
Consolato Sergi, University of Alberta Hospital, Canada
Katja Hummitzsch, University of Adelaide, Australia

***Correspondence:**
Meryl E. Wastney
wastneym@metabolic-modeling-services.com

Specialty section:
This article was submitted to Systems Endocrinology, a section of the journal Frontiers in Endocrinology

Received: *26 October 2020*
Accepted: *05 January 2021*
Published: *29 March 2021*

Citation:
Patterson BH, Combs GF Jr, Taylor PR, Patterson KY, Moler JE and Wastney ME (2021) Selenium Kinetics in Humans Change Following 2 Years of Supplementation With Selenomethionine. Front. Endocrinol. 12:621687. doi: 10.3389/fendo.2021.621687

Background: Selenium (Se) is a nutritionally essential trace element and health may be improved by increased Se intake. Previous kinetic studies have shown differences in metabolism of organic *vs.* inorganic forms of Se [e.g., higher absorption of selenomethionine (SeMet) than selenite (Sel), and more recycling of Se from SeMet than Sel]. However, the effects on Se metabolism after prolonged Se supplementation are not known.

Objective: To determine how the metabolism and transport of Se changes in the whole-body in response to Se-supplementation by measuring Se kinetics before and after 2 years of Se supplementation with SeMet.

Methods: We compared Se kinetics in humans [n = 31, aged 40 ± 3 y (mean ± SEM)] studied twice after oral tracer administration; initially (PK1), then after supplementation for 2 y with 200 μg/d of Se as selenomethionine (SeMet) (PK2). On each occasion, we administered two stable isotope tracers of Se orally: SeMet, the predominant food form, and selenite ($Na_2{}^{76}SeO_3$, or Sel), an inorganic form. Plasma and RBC were sampled for 4 mo; urine and feces were collected for the initial 12 d of each period. Samples were analyzed for tracers and total Se by isotope dilution GC-MS. Data were analyzed using a compartmental model, we published previously, to estimate fractional transfer between pools and pool masses in PK2.

Results: We report that fractional absorption of SeMet or Sel do not change with SeMet supplementation and the amount of Se absorbed increased. The amount of Se excreted in urine increases but does not account for all the Se absorbed. As a result, there is a net incorporation of SeMet into various body pools. Nine of the 11 plasma pools doubled in PK2; two did not change. Differences in metabolism were observed for SeMet and Sel; RBC uptake increased 247% for SeMet, urinary excretion increased from two plasma pools for Sel and from two different pools for SeMet, and recycling to liver/tissues

increased from one plasma pool for Sel and from two others for SeMet. One plasma pool increased more in males than females in PK2.

Conclusions: Of 11 Se pools identified kinetically in human plasma, two did not increase in size after SeMet supplementation. These pools may be regulated and important during low Se intake.

Keywords: selenium, metabolism, trace elements, selenite, selenomethionine, kinetics

INTRODUCTION

Selenium is an essential nutrient for health, and there are indications that higher Se intakes may prevent certain diseases (1). There are 25 proteins that contain Se, as the amino acid selenocysteine (Sec), distributed in tissues throughout the body (2). These selenoproteins function in many systems including the endocrine, nervous, and immune systems (2). Selenium may have a role in some forms of cancer, cardiovascular disease, and cognitive decline (2) and relationships have been proposed between blood Se concentration and some health effects (1). However, assessing Se status is challenging because the element is typically consumed in several forms that are metabolized differently (3). Specifically, Se exists in nature in organic forms, such as selenomethionine (SeMet). SeMet can be converted to the functional form of Se, Sec, but SeMet can also be incorporated into proteins non-functionally in place of the amino acid methionine (3). An inorganic form of Se, selenite (Sel), often used as a supplement (3), has lower absorption than SeMet (4–6) and is only incorporated into functional selenoproteins (3). As total Se concentration in plasma and tissues includes both functional and non-functional selenoproteins, speciation is necessary for determining functional Se levels in tissues but many selenoproteins are low abundance making their detection challenging (7).

Selenium supplementation has been used to improve Se status in populations where soil Se is low [for a review see (8)]. People in the US are considered to have adequate Se intakes (i.e., >55 μg/d) (to convert μg/d to μmol/d, multiply by 0.0127) (9). Even so, 51% percent of the US population take nutritional supplements, many of which may contain Se (10). Use of Se-containing supplements has likely been increased as a result of findings reported from the Nutritional Prevention of Cancer (NPC) Trial in the US that supplementing skin cancer patients with Se significantly decreased the incidence of several cancers (lung, prostate, and colon) (11).

In part, because of the positive results from the NPC Trial, the Selenium and Vitamin E Cancer Prevention Trial (SELECT) was undertaken in some 35,000 healthy US men (12). The trial was stopped after 5 y because no effect was detected on prostate cancer incidence (13). However, both the choice of participants and form of Se used (SeMet) in SELECT have been questioned. It has been pointed out that the negative results in the SELECT cohort, which had relatively high Se status (average plasma Se >130 ng/ml), were consistent with the NPC results (11), which found no protective effects for subjects with relatively high Se status, e.g., >120 ng/ml (14). In addition, a non-significant association with risk for type-2 diabetes was noted in SELECT subjects supplemented with SeMet (13), although with additional follow up found that association to be further attenuated and remained non-significant (15). The NPC trial showed a significant positive association with self-reported diabetes based on 97 cases in all trial participants (hazard ratio = 1.55; 95% confidence interval 1.03–2.33) that was strongest in participants whose baseline plasma Se levels were highest (hazard ratio = 2.70 [1.30–5.61] among 37 cases with plasma Se >121.6 ng/ml) (16).

In order to target persons who might benefit most from Se supplementation, a better understanding of Se metabolism is needed (17). One approach to investigating metabolism *in vivo* is through the use of kinetic studies with tracers. Kinetic studies have been performed in humans after supplementation with various forms of Se for periods of up to a year (18–21); however, these kinetic studies were conducted for less than 3 wk. The objective of the current study was to compare the kinetics of two Se-forms (selenite [Sel] and SeMet) in healthy participants who were studied for a prolonged period (4 mo) before [published previously (6)] and after long-term (2 y) supplementation with SeMet, the dominant form of Se in foods (22). Kinetics were followed using stable Se isotopes and data were analyzed by compartmental modeling (6). The goal was to gain insight into how the metabolism and transport of Se changes in the whole-body long-term with increased Se intake, by identifying pools and pathways that responded to supplementation.

MATERIALS AND METHODS

Aspects of the study are presented in greater detail in Wastney et al. (6). They described model development and analysis of the first part of the study (see below in *Study Design*), however, the materials and methods were the same for the entire study.

Participants

Participant recruitment and eligibility have been described elsewhere (23). Briefly, participants were non-smoking, healthy men (n = 16) and women (n = 15) aged 20–60 y, within 20% of their ideal weight, consuming regular diets, not taking Se

Abbreviations: C, compartment; DT, compartment with a delay time; GPX, glutathione peroxidase; MeSeCys, methylselenocysteine; NPC, Nutritional Prevention of Cancer; PK1, pharmacokinetic study 1 or baseline study; PK2, pharmacokinetic study 2 or supplemented study; Se, selenium; Sel, selenite; *Sel*, ^{76}Se from Sel; SeMet, selenomethionine; SeMet, *SeMet*, ^{74}Se from SeMet; SeP, selenoprotein P; SeCys, selenocysteine; SELECT, Selenium and Cancer Prevention Trial; TMSe, trimethyselenoselonium ion.

supplements >25 μg/d, who ranked high on a Health Consciousness Scale (24), and whose plasma Se levels were 80–160 ng/ml. For reasons given in Wastney et al. (6), the final analyzable sample consisted of 7 males and 13 females. The study protocol was approved by the NCI Special Studies Institutional Review Board, the Cornell University Committee on Human Subjects, the Johns Hopkins University Human Subjects Committee (for the BHNRC).

Study Design

The study consisted of three periods: an initial pharmacokinetics study of 4 mo duration (PK1); a 2 y period of Se-supplementation with 200 μg of Se/d as SeMet; a second, 4 mo pharmacokinetic study (PK2), identical in design to PK1, during which participants remained on supplement. The study lasted for a total of 32 mo. The objective of the design was to compare parameter values for the same participants before (PK1) and following long-term supplementation (PK2). At the beginning of each pharmacokinetic study, fasted participants were given two 300 μg tracer doses of two stable isotope tracers, 150 μg of Se as SeMet, and 150 μg of Se as Sel, orally, in water, on days 0 and 10. Based on results of previous studies (5, 25), two doses of tracer were given to ensure detection for the entire 4 mo periods of observation, PK1 and PK2. The stable isotopes were ^{74}Se as L-selenomethionine (^{74}SeMet, Amersham Laboratories, Chicago, USA), and ^{76}Se as sodium selenite ($Na_2{}^{76}SeO_3$, Oak Ridge National Laboratory, Oak Ridge, TN, USA) prepared as described in (6).

Supplement

The supplement was produced under an Investigational New Drug Application (IND) obtained by the National Cancer Institute. The capsules were manufactured by University Pharmaceuticals of Maryland, Inc. from a specialty blend of L-SeMet and lactose called l-SeMet 5000 provided by Sabinsa Corp. N.J. Two lots of L-SeMet capsules were tested for appearance, assayed for content, content uniformity, variation in weight and dissolution.

Sampling

Multiple blood, urine, and fecal samples were collected during both PK1 and PK2 (6). Specimens were sampled for 4 mo after administration of the initial doses of tracers. Blood (10 ml) was drawn immediately before, then at increasing intervals after administration of the tracer doses starting at 30 min. Complete urine and fecal collections were obtained for days 2–12 after the initial dosing.

Chemical Analysis

Urine, fecal, RBC, and plasma samples were analyzed for both Se tracers and total Se. Following digestion and chelation, the ^{74}Se, ^{76}Se, and total Se contents of the samples were determined by triple isotope dilution gas chromatography-mass spectrometry using enriched ^{82}Se as the internal standard (26). We measured these tracers but did not determine their chemical forms in our samples. While ^{74}Se was given as SeMet, the measured species was not SeMet, *per se*, but was instead derived from SeMet. Thus, we have noted the measured species in italics, i.e., *SeMet* refers to a Se-containing compound originating as SeMet. Similarly, *Sel*, given as ^{76}Se, refers to a species originating as Sel. Sel includes other Se forms that are metabolized similarly to Sel (e.g., SeCys). We do not make this distinction when reporting on the literature.

Concentrations (ng/g) of total Se, ^{74}Se, and ^{76}Se in plasma were converted to total masses by correcting for plasma specific gravity (assumed to be 1.026) and plasma volume (assumed to be 4% of body weight) (6). The same measurements in RBC were converted by correcting for RBC specific gravity (assumed to be 1.09) and RBC volume (assumed to be 3% of body weight). Urine and fecal data were fitted as the cumulative, or daily, amounts (μg or μg/d) excreted over the collection period.

Kinetic Modeling

Data consisting of tracer and total Se in plasma, RBC, urine, and feces were fitted by a compartmental model (described below) using the WinSAAM software. We assumed that participants were in steady state with respect to Se metabolism for both PK1 and PK2. The model was fitted to PK2 data by changing parameter values while retaining the underlying structure from PK1. Fits of the model to the plasma, RBC, urine, and fecal data were assessed graphically. When the model had been fitted to all participants for ^{76}Se (from *Sel*) and ^{74}Se (from *SeMet*) separately, the following were estimated for each form: transfer coefficient parameters, L(*i,j*) representing the fraction/h of the contents of compartment *j* transferred to compartment *i*, masses of pools of Se in the body, M(*i*), (μg), transport rates between pools, R(*i,j*), (μg/h), delay times, DT (*i*), (h) and turnover times (h) of each pool, calculated as the reciprocal of the sum of all loss pathways from each compartment. The amounts of Sel-exchangeable Se and SeMet-Se consumed were calculated using the model parameters (27), and termed Diet-Sel and Diet SeMet. These values were combined as described (6).

Model Description

The compartmental model developed in PK1 (6) was used to analyze Se data from PK2. The model consists of Se pools in the gastrointestinal tract, plasma, RBC, liver, and tissues with excretion into urine and feces (**Figure 1**).

The full model is shown in **Supplemental Figure 1**. Following ingestion, a small fraction of tracer (~3%) appeared in plasma (Pl-4) after a 7 h delay and could only be fitted by a portion of the dose entering plasma as a bolus. The rest of the tracer moves through six pools in the gastrointestinal tract (labeled GI-1 to GI-6). Absorption occurs from the first three gastrointestinal pools and Se not absorbed passes through either a 26- or 62-h delay into the colon and then into feces. Absorbed Se taken up by enterocytes, goes either directly to a plasma pool (Pl-1), *via* the lymphatics into a second plasma pool (PL-2, after moving through a chain of compartments) or into liver (Liv-1). After a 2 h delay, Se enters a second liver pool (Liv-2) and is then either released back into the intestinal tract *via* the pancreas or bile (Pancr/bile); travels directly into a plasma pool (Pl-3) or moves into a tissue pool (Tissue-1). Some Se moves from this tissue pool *via* delays ranging from 4- to 175-h into one of six plasma pools (labeled Pl-5 to Pl-10). The plasma pools were differentiated by their turnover rates. From the first tissue pool, some Se also moves into a second tissue pool (Tissue-2) and then either moves

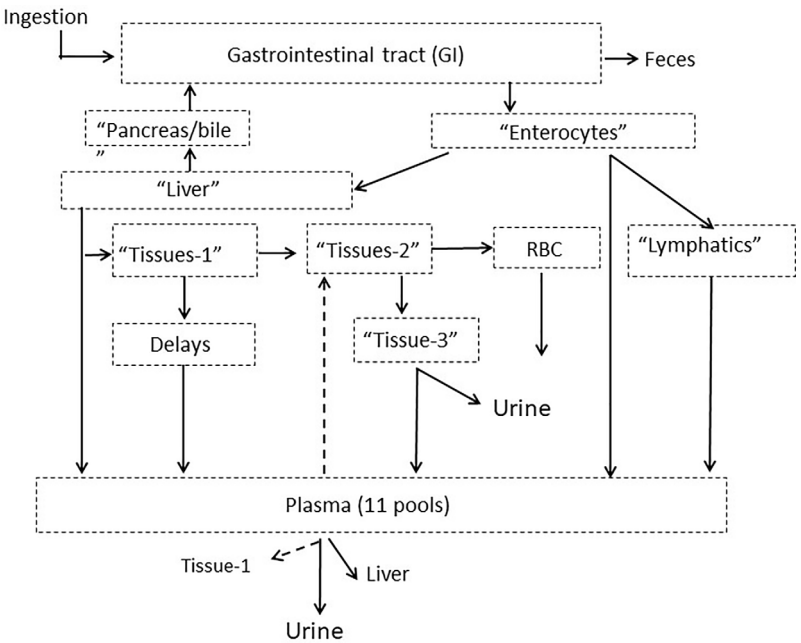

FIGURE 1 | Model schematic for Se metabolism in humans showing compartments grouped into categories with putative physiological labels. Dotted arrows out of plasma indicate pathways that existed for only certain plasma pools. The full model is given in **Supplemental Figure 1**. Published from Wastney et al. (6) by permission of the American Society for Nutrition.

into RBC (RBC-1) after a 1,908 h delay, or into a third tissue pool (Tissue-3) and is excreted into urine. For *SeMet* only, exchange occurs between RBC-1 and a second RBC pool (RBC-2) and some Se moves from the third tissue pool into a plasma pool (Pl-11). Some of the plasma pools recycle Se back to the tissues (Pl-3 into Tissue-1, and Pl-9 into Tissue-2); all plasma pools except Pl-11 recycle Se to the liver; and all plasma pools lose Se *via* the kidneys and into urine.

Statistical Analyses

Results from supplementation were evaluated for changes relative to form and gender and are reported as mean ± SEM. Differences between PK1 and PK2 were calculated as 100 × (PK2 value − PK1 value)/PK1 value. Differences between forms are calculated as [100 × (SeMet − Sel)/Sel] and differences between gender are calculated as [100 × (Female value − Male value)/Male value. Within-subject differences (between *Sel* and *SeMet* and between PK1 and PK2) were tested using two-sided paired t-tests while differences between gender were tested using (unpaired) t-tests, and were considered significant for $p < 0.05$, as in (23). Statistical software used for the analyses was SAS version 9.1.3 (SAS Institute Inc., Cary, NC, USA). For all participants together, as well as by gender, we report on PK1 *versus* PK2 for *SeMet* and *Sel* and for *SeMet versus Sel* within PK2.

RESULTS

Participants and Kinetic Data

Participants ($n = 20$, 7 males, 13 females) were ages 40 ± 3, 39 ± 6, and 40 ± 6 y and weighed 70 ± 3, 77 ± 7, and 66 ± 3 kg for all, males, and females, respectively (**Table 1**). Additional

TABLE 1 | Age, weight, and Se measurements of participants[1].

	All, *n* = 20		Males, *n* = 7		Females, *n* = 13	
	PK1	PK2	PK1	PK2	PK1	PK2
Age, *y*	40 ± 3		39 ± 6		40 ± 6	
Weight,[2] *kg*	70 ± 3		77 ± 7		66 ± 3	
Plasma Se,[3] *μg/L*	134 ± 3	266 ± 11*	141 ± 6	263 ± 16*	131 ± 4	267 ± 14*
RBC Se, *μg/L*	231 ± 7	649 ± 27*	236 ± 13	642 ± 47*	227 ± 8	652 ± 35*
Urine Se, *μg/d*	71 ± 4	193 ± 6*	84 ± 9	209 ± 9*	64 ± 4	184 ± 8*
Fecal Se, *μg/d*	36 ± 2	45 ± 3*	44 ± 4	46 ± 3	31 ± 2	44 ± 4*

[1]*Values are means ± SEM. *Different from PK1, P < 0.01. For females vs. males, PK2, no values were significant.*
[2]*Weight not measured at beginning of PK2.*
[3]*To convert μg to μmol, multiply by 0.0127.*

participants are not reported for the following reasons: five males and one female for data discrepancies (primarily lack of fecal samples submitted for analysis), one male who completed PK1 only, one male excluded due to Hashimoto's disease, and three participants (two males) whose samples were not chemically analyzed but were kept for further analyses (e.g., speciation), but the techniques did not develop before the samples were considered compromised and therefore not retained. Baseline plasma Se concentrations (**Table 1**) were above average US values reported in NHANESIII of 125 ng/ml for men and 122 ng/ml for women (28) indicating that the participants were Se-replete (29). After 2 y of supplementation with 200 μg SeMet/d, plasma Se concentration (i.e., all forms of Se) doubled while RBC Se concentration tripled (**Table 1**). Urinary excretion also nearly tripled, while fecal excretion increased by only 25%. None of the increases in plasma, RBCs, urine, or feces were significantly different in males *vs.* females.

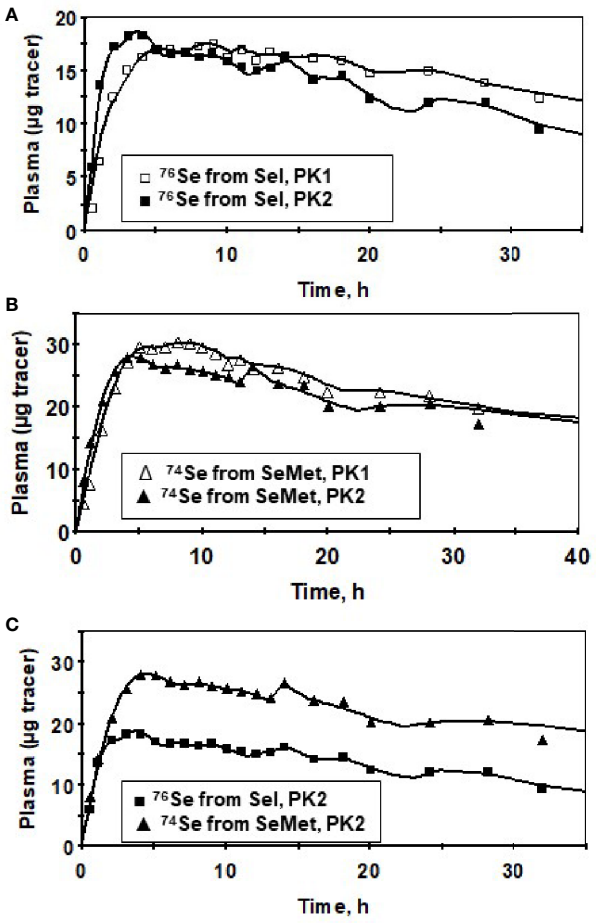

FIGURE 2 | Tracer data for a male subject for *Sel* (^{76}Se-*Sel*) before (PK1, □), and after (PK2, ■) Se supplementation **(A)**, *SeMet* (^{74}Se -*SeMet*) in plasma for PK1 (Δ) and PK2 (▲) **(B)** and for *SeMet* (▲) versus Sel (■) for PK2 showing similar timing of the peaks between the forms **(C)** for the first 40 h after isotope administration. Symbols are observed values; lines are model-calculated values (**Supplemental Figure 1**).

Plasma kinetic curves were similar between PK2 and PK1 for *Sel* (**Figure 2A**) and for *SeMet* (**Figure 2B**). However, as in PK1, the curves for the two forms (*SeMet* vs. *Sel*) differed in PK2 (**Figure 2C**) (6). Tracer curves for *SeMet* in PK2 compared with PK1 were slightly lower in plasma and RBC (**Figures 3A–C**), higher in urine (**Figure 3D**), and lower in feces (**Figure 3E**). Cumulative excretion curves of natural Se followed those of the tracers: higher in PK2 than PK1 for urine, but similar for feces (**Figures 3F–G**). Plots of *Sel* and *SeMet* in PK1 *versus* PK2 and *Sel versus SeMet* in PK1 and PK2 for one male subject are provided in **Supplemental Figures 2–5**. (A plot of *Sel versus SeMet* for PK1 for a female is shown in the previous paper (6)). The appearance times of the pools in plasma in PK1 are given in (6) and for PK2 in **Figure 4**.

Effect of Supplementation on Absorption

With the supplement, Se intake in PK2, estimated as the sum of urinary and fecal excretion, was more than double that in PK1 (**Table 2**). While the percent absorption of both forms remained the same in PK2 as in PK1, because of the increase in SeMet consumed, the Se absorbed more than doubled, from 79 to 202 μg Se/d. As expected, the calculated increase in Se absorbed in PK2 was predominantly from *SeMet*. There were no gender differences in any aspect of absorption in PK2.

Parameter Changes in PK2 versus PK1 and Between Forms in PK2

The turnover times of the pools in PK2 were like PK1 but the turnover of the largest Se pool (Tissue-3) was faster in PK2 than PK1 (7,308 *versus* 10,325 h, **Supplemental Table 1**). Significant parameter changes in PK2 *vs.* PK1 are listed in **Supplemental Table 2** and included on **Supplemental Figure 6** (for *Sel*) and **Supplemental Figure 7** (for *SeMet*) as dotted arrows; values are given for all participants, males, and females. The largest change for both forms in PK2 *versus* PK1 were increases in urinary excretion pathways (**Supplemental Table 2**).

Differences between forms in PK2 (**Supplemental Table 3**) were that RBC uptake of *SeMet* was 247% higher than for *Sel* and *SeMet* excretion from five of the plasma pools was lower than *Sel.*

Effect of Supplementation on Pool Sizes, Recycling, and Excretion

The amount of Se in the pools was calculated by assuming that the ratio of SeMet to Sel in body pools was the same as that calculated for the diet. Total Se in the body was estimated to be 80% higher with supplementation (**Table 2**) and all extravascular pools except for the 9-h delay, increased during supplementation (**Supplemental Table 4**).

The plasma pools of Se, expressed as concentrations (using an average bodyweight of 70 kg and plasma volume of 4%, or 2.8 L) also increased about two-fold, except for two pools, Pl-5 and Pl-6 (**Table 3**). Some increases were significant in females but not males (Pl-1, Pl-8, Pl-9, and Pl-10, **Supplemental Table 5**). One plasma pool that was smaller in females in PK1 (Pl-1) (6), increased in PK2 in females but not males, and another pool increased in males but not females (Pl-4) (**Supplemental Table 5**). The distribution of Se in plasma did not change during PK2 vs

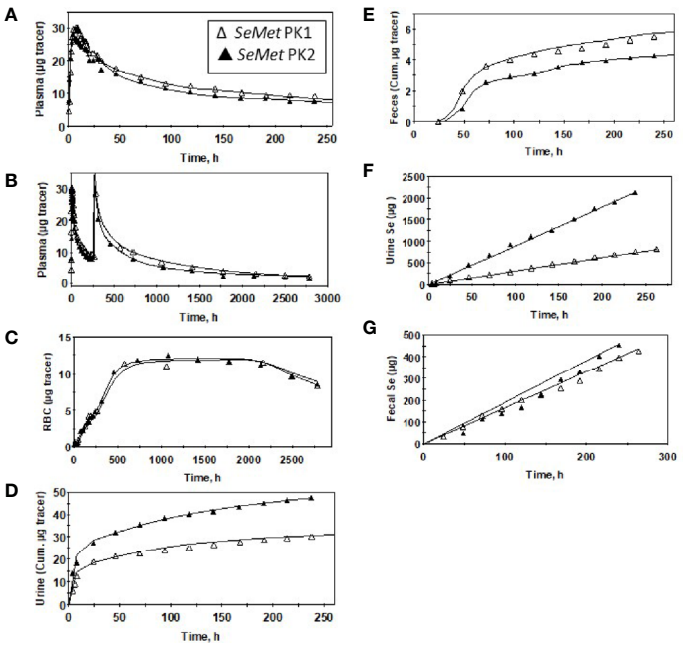

FIGURE 3 | Observed data (Δ,▲) and model-calculated (**Supplemental Figure 1**) values (solid lines) for a male subject before (PK1, Δ) and after (PK2, ▲) Se supplementation for *SeMet* (from ^{74}Se -SeMet) in plasma for 260 h **(A)** or 2,880 h **(B)** after tracer administration, RBC **(C)**, urine **(D)**, and feces **(E)**; and total Se excreted in urine **(F)** and feces **(G)**.

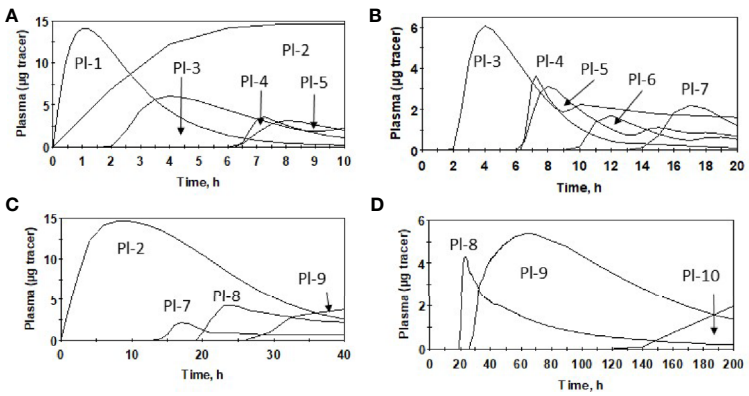

FIGURE 4 | Appearance of oral dose of *SeMet* in plasma pools for males after Se supplementation (PK2), using average parameter values over 0–10 h **(A)**, 0–20 h **(B)**, 0–40 h **(C)** and 0–200 h **(D)** and model (**Supplemental Figure 1**).

PK1 (**Table 3** and **Supplemental Table 5**). Recycling to liver increased from Pl-3 for *Sel* and from two pools (Pl-5 and Pl-7) for SeMet (**Table 3** and **Supplemental Table 2**).

The rates of Se urinary excretion from most pools was greater in PK2 than in PK1 but the rates did not change from four plasma pools, (Pl-4, Pl-6, Pl-7, and Pl-11, **Figure 5**). The relative contributions of each pool, expressed as % of total excreted, remained similar in PK1 and PK2 (**Supplemental Table 6**). There were no differences between genders in PK2, however differences were noted in Se form; for *SeMet* excretion increased from plasma Pl-2 and Pl-9 and decreased from Pl-4, and for *Sel* excretion increased from Pl-8 and Pl-10 (**Supplemental Table 2** and **Table 3**).

DISCUSSION

By comparing Se kinetics before and after 2 yr supplementation with SeMet, we have shown that fractional absorption of SeMet or Sel do not change compared to baseline and, therefore, the amount of Se absorbed increases with supplementation. The

TABLE 2 | Calculated values for Se intake; absorption of Se, *Sel*, and *SeMet*; daily intake of Se, Sel, SeMet, and amount of Se in humans before (PK1) and after (PK2) supplementation with SeMet[1].

	All, *n* = 20		Males, n = 7	Females, n = 13
	PK1	PK2	PK2	PK2
Se intake,[2] *μg/d*	107 ± 6	237 ± 8**	255 ± 11**	228 ± 11**
Se absorption, *%*	73 ± 1	85 ± 0.8**	86 ± 1*	85 ± 1**
Se absorbed, *μg/d*	79 ± 5	201 ± 7**	220 ± 10**	191 ± 8**
Sel : SeMet intake[3]	60:40	36:64	34:66	37:63
Sel intake, *μg/d*	64 ± 5	85 ± 11*	88 ± 26	84 ± 11
Sel absorption, *%*	57 ± 2	58 ± 3	56 ± 5	59 ± 3
Sel absorbed,[4] *μg/d*	36	50	49	50
SeMet intake, *μg/d*	43 ± 5	152 ± 11**	167 ± 22**	144 ± 13**
SeMet absorption, *%*	97 ± 0.2	97 ± 0.2	98 ± 0.3	97 ± 0.3
SeMet absorbed, *μg/d*	42	148	163	140
Total body Se, *mg*	21 ± 1	38 ± 4**	42 ± 5*	35 ± 5*

[1]*Values are means ± SEM of those calculated for each participant by the model (**Figure 1**).*
**Different from PK1, P < 0.05. ** Different from PK1, P < 0.001. There were no significant differences between males and females.*
[2]*To convert g to mol, multiply by 0.0127.*
[3]*Ratio in intake of Sel-exchangeable-Se : SeMet-Se.*
[4]*Calculated as % absorption × SeMet (or Sel) intake.*

amount of Se excreted in urine also increases but does not account for the additional Se absorbed. As a result, there is a net accumulation of Se from SeMet into various body pools. During supplementation, as during baseline *SeMet* is absorbed at a higher rate than *Sel*, and the kinetics of each form are for the most part similar during supplementation to the kinetics during baseline. Only subtle differences were detected between Se forms and these related to the plasma pools contributing Se to urine and recycling to tissues. Some differences were observed between sexes in terms of the size of plasma pools in response to supplementation, the source of Se excreted in urine, and plasma pools that recycle Se to tissues.

Supplementation Amount and Duration

An assumption of our modeling was that a new steady state had been achieved after 2 y of supplementation. This assumption is supported by our own observations as well as those of others. Burk et al. (29) reported that plasma Se levels approached a plateau in Se-replete participants after 4 mo of supplementation with either 158, 338, and 507 μg/d Se as SeMet. Combs et al. (30) reported plasma concentrations plateauing between 9–12 mo. Se concentration increased in whole blood in Danish participants after daily supplementation for 3 mo with the same dose as in our study (200 μg of Se as SeMet) and were still elevated 4 mo after the end of supplementation (31). In the present study, after 3 mo on 200 μg/d, plasma values were within 13% of levels subsequently reached at 9 mo (23).

Metabolism by Form

Se form is probably the most influential factor in determining response to supplementation. In agreement with our (5, 25) and others' studies (19), we found *SeMet* to be almost completely absorbed (97%) while *Sel* absorption was lower (57%); these fractions were the same before and during supplementation. The absolute amount of Se absorbed during supplementation increased, however, as Se intake changed from mainly Sel-like forms to the more readily absorbed SeMet form. The predicted increase in Se intake during supplementation (130 μg/d) was less than the 200 μg/d given as a supplement. The lower-than-expected increase may have been due to reduced dietary Se

TABLE 3 | Concentration and distribution of Se in plasma pools before (PK1) and after (PK2) supplementation with SeMet, description of the metabolism of each pool, and putative identification of the pools.

Plasma pool	Plasma "Diet" concentration (μg/L)[1]		Plasma distribution (%)		Description	Putative identification[2]
	PK1	PK2	PK1	PK2		
1	0.73 ± 0.13	1.47 ± 0.19**	0.5	0.5	Does not pass through liver. Pool size in females 50% of males in PK1	SeMet
2	4.5 ± 0.5	10.2 ± 1.0**	2.7	3.8	Pool size in females 50% of males in PK1. Excretion in urine increased for *SeMet*	Apo B/lipoproteins—from lymphatics
3	2.87 ± 0.62	6.12 ± 1.35**	2.2	2.3	Recycling increased for *Sel*	Selenosugar1
4	0.16 ± 0.05	0.40 ± 0.11*	0.1	0.1	Increased more in males than females in PK2. Excretion in urine decreased for *SeMet*	
5	1.33 ± 0.35	1.87 ± 0.44	1.0	0.7	Recycling increased for *SeMet*	
6	1.06 ± 0.26	1.04 ± 0.23	0.8	0.4		
7	1.28 ± 0.17	2.00 ± 0.31*	1.0	0.7	Recycling increased for *SeMet*	Selenosugar 3
8	4.00 ± 0.52	7.54 ± 0.97**	3.0	2.8	Doubles in females in PK2. Excretion in urine increased for *Sel*	
9	15.8 ± 1.5	29.9 ± 5.3*	11.9	11.1	Increased 71% in females in PK2. Excretion in urine increased for *SeMet*	GPx3
10	30.3 ± 3.5	69.6 ± 6.5**	22.8	25.9	Doubles in females in PK2. Excretion in urine increased for *Sel*	SeP
11	72.0 ± 4.6	138.5 ± 8.1**	54.1	51.5	Turnover time is 30 d	Non-specifically incorporated Se (by definition)-albumin
TOTAL	134.0	269.0	100.0	100.0		

**Increased in PK2 vs. PK1, P < 0.05 or **P < 0.01*
[1]*Values are calculated by the model (**Supplementary Figure 1**). To convert μg to μmol multiply by 0.0127.*
[2]*Some pools were identified in Wastney et al. (6).*

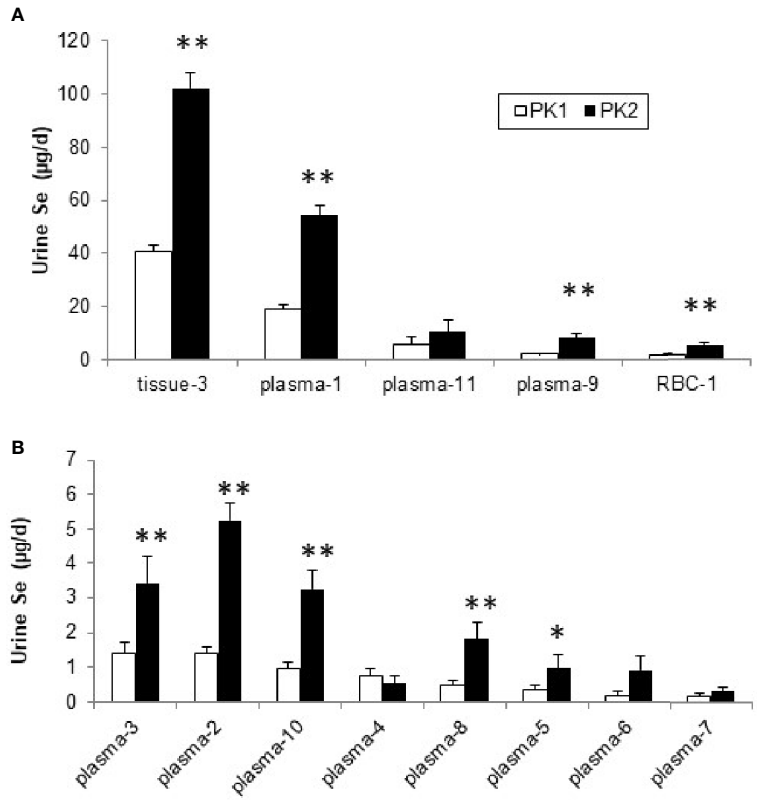

FIGURE 5 | Se (µg/d) excreted into urine from plasma, RBC, and tissue pools before (PK1) and after Se supplementation (PK2) estimated using the model in **Supplemental Figure 1**, for pools with higher excretion rates **(A)** and those with lower rates (<10 µg/d), **(B)**. *Differences are significant for PK2 *vs.* PK1 ($P < 0.05$), or **($P < 0.01$).

intake and/or poor compliance with pill-taking or with excreta collection (27). Losses may have been underestimated due to additional loss of Se in breath or desquamation (32).

Kokarnig et al. (33) administered Se in various forms to volunteers and measured non-protein bound Se, or small Se species, in plasma and urine over several hours. At baseline, only Se from Sel could be measured in plasma, but after a single dose of 200 µg Se/d as SeMet, plasma Se increased from <0.1 to 1.2 µg/L at 1 h, and selenosugar increased from <0.1 to 0.63 µg/L at 3 h. Because the stable isotope tracer dose we administered in PK1 was a similar amount (150 µg SeMet), the timing of the appearance tracer in the pools suggests their identity. i.e., Plasma-1 may be SeMet and Plasma-3 may be selenosugar 1 [See **Figure 2** (6)]. The predicted concentration of these compounds are higher in our study (0.7 µg/L for SeMet and 2.9 µg/L for selenosugar), but the plasma Se concentration was 40% higher in our study [134 µg/L *vs.* 95 µg/L in (33)]. Kokarnig et al. (33) reported measuring traces of trimethyselenoselonium ion (TMSe) and methylselenocysteine (MeSeCys) in plasma. We identified at least three other pools in plasma at concentrations <4 µg/L but are not able, without further biochemical analyses, to identify them. We postulated previously that Pool-9 and Pool-10 could be GPX3 and SeP (6). Based on analyses by Combs et al. (34) in adults with similar plasma Se concentrations as the current study, 20% of plasma Se was in GPx3 and 34% in SeP, which agrees with our predictions of the identity of these pools (Pl-9 has 16% of plasma Se, and Pl-10, 30%).

Urinary excretion of Se increased during supplementation, confirming that the kidneys play a major role in the homeostatic regulation of Se (35). In a high-dose human Se-supplementation study conducted by Burk et al. (29), 60% of the doses given were excreted in urine. In the present study, urinary excretion comprised a similar percentage of the supplement. Others report that after ingestion of a single dose (1 mg) of Se as Sel or SeMet, 80% was excreted over 48 h (36). In basal urine, 30–70% of Se in urine could be identified, as selenosugars (36) while others (33) report identifying only 10–20% of the Se species in background urine. However, following ingestion of 200 µg Se as SeMet up to 92% of the species were identified (33), with more than 80% of the Se excreted in urine was as selenosugar 1, about 4% as SeMet, 12% as selenosugar 3, and a trace of TMSe. Following ingestion of 200 µg Se as Sel, selenosugar 1 also accounted for most of the Se (33).

From the kinetics following 2 yr supplementation, we showed that contributions by four of the 11 plasma pools to urine did not increase. We found differences between the forms with respect to which plasma pools contributed to the changes. During supplementation for Se originating from Sel, urinary losses occurred from plasma pools Pl-8 and Pl-10 while for Se from

SeMet, changes in urinary losses occurred from three other pools (Pl-2, Pl-4, and Pl-9). Biochemical identification of the plasma pools is required to explain these differences in metabolism. Both forms showed increased urinary excretion from the tissue pool that contained the bulk of Se in the body, but only *Sel* showed increased loss from RBC. The lower absorption of *Sel* was considered by Burk et al. to explain in part the lack of response of plasma selenoproteins to Sel supplementation compared with SeMet (29). Fractional uptake of Se by RBC did not change during supplementation, but Se mass in RBC increased due to the higher rate of uptake. When metabolism of the two forms of Se was compared during supplementation, RBC uptake for *SeMet* was 2.5 times greater than for *Sel*, in agreement with other studies (37).

Metabolism by Gender

Combs et al. (30) reported a larger increase in urinary Se excretion with Se supplementation in women than in men. We did not find a gender difference in our smaller population, although we found gender differences in response to supplementation of the pools contributing to urine Se: males showed a five-fold increase in urine excretion of *SeMet* from the plasma pool considered to be associated with lipoproteins while females had an almost four-fold increase in loss from the third largest plasma pool. We noted an additional gender difference during supplementation in that the smallest plasma pool, where the bolus entered directly, increased more in males than females. Burk et al. (29) reported a higher level of SeP in males compared to females at baseline, but did not report any gender differences after supplementation (if Plasma Pool-10 is SeP, we also report no gender difference after supplementation). We found that recycling of Se from Sel was increased with supplementation in a gender-specific way; recycling from one plasma pool increased ~2-fold in males but did not change in females, while recycling from another pool increased by 80% in females but did not change in males.

A strength of the present study was that it enrolled healthy non-smokers, examined two tracer forms before and after supplementation, and was able to separate changes in Se metabolism by form and gender and ascribe differences to specific pools and pathways. Previous studies showed increases in plasma and RBC Se concentrations and in urinary and fecal Se excretion during Se-supplementation (18, 29) but were affected by Se form, supplement amount, duration of supplementation, and subject gender and lifestyle characteristics, such as smoking (38). Together these factors limited both the direct comparison and interpretation of studies of Se supplementation as well as the identification of biomarkers of Se status (38). The repeated measures design of this study in which each participant was compared to themselves (i.e., before and following supplementation) eliminated between-subject variance. A repeated-measures design lacks a control group, so effects due to secular trends, such as change in dietary intake, or age-related effects, cannot be evaluated. However, both kinetic studies were conducted in groups of four to five participants over the course of 16 mo, thereby reducing or eliminating seasonality as a potential confounder. A limitation of the current study was the number of males studied compared to females and that speciation was not performed.

Future Studies

Future studies would identify biochemically the purported plasma pools. Through kinetics we have identified the labeling patterns of these pools, i.e., the time after dosing that each plasma pool has the maximum amount of tracer. By sampling the pools at those times, the identification of the contents of the pools could be determined by speciation analyses. The current studies were in Se-replete participants. Future studies could examine changes in participants with low Se-status. Results from the NPC trial showed that Se supplementation was associated with a significant reduction in total cancer incidence among former smokers (39). This observation suggests that kinetic studies in former smokers may show which pools and pathways of Se metabolism are altered in this population, when compared to our study of non-smokers.

In conclusion, the present study found that supplementation with SeMet increased recycling of Se from specific plasma pools to tissues, and changes in the amount and source of Se excreted in urine. Some changes were Se form- and gender-specific. As expected, the Se mass of most pools increased with SeMet supplementation, because SeMet is incorporated into proteins in place of methionine. Some plasma pools did not increase in mass and these may represent proteins with few methionine residues, or selenoproteins that are regulated, and these proteins may be important in metabolism as they would be expected to respond to supplementation when Se intake is low. All selenoproteins are expected to be identified through the expanding field of selenoproteomics (40).

DATA AVAILABILITY STATEMENT

The datasets analyzed for this study can be found in the Cancer Data Access System of the Division of Cancer Prevention, National Cancer Institute at https://cdas.cancer.gov/publications/1138/.

ETHICS STATEMENT

The studies involving human participants were reviewed and approved by the NCI Special Studies Institutional Review Board, the Cornell University Committee on Human Subjects, and the Johns Hopkins University Human Subjects Committee (for the BHNRC). The patients/participants provided their written informed consent to participate in this study.

AUTHOR CONTRIBUTIONS

BP, GC, and PT designed research. GC conducted research. KP supervised sample analysis. JM, BP, and MW analyzed data. BP and MW wrote the paper. MW had primary responsibility for final content. All authors contributed to the article and approved the submitted version.

FUNDING

Supported by Interagency Agreement Y1-SC-0023 between the National Cancer Institute and USDA. This research was supported in part by the Intramural Research Program of the National Institutes of Health, the National Cancer Institute, and the Division of Cancer Epidemiology and Genetics.

ACKNOWLEDGMENTS

We thank Dr. Orville Levander, Beltsville Human Nutrition Research Center, USDA for contributing his expertise in selenium metabolism and his thoughts on supplementation, Dr. Wes Canfield, Division of Nutritional Sciences, Cornell University, who served as the study physician for this project and performed most of the venipunctures, and A. David Hill, Beltsville Human Nutrition Research Center, USDA, for assistance in sample analysis. We gratefully acknowledge the expert technical assistance of Ms. Mary Brindak, and the recruiting assistance of Dr. David Levitsky, both of the Division of Nutritional Sciences, Cornell University.

SUPPLEMENTARY MATERIAL

The Supplementary Material for this article can be found online at: https://www.frontiersin.org/articles/10.3389/fendo.2021.621687/full#supplementary-material

REFERENCES

1. Fairweather-Tait SJ, Bao Y, Broadley MR, Collings R, Ford D, Hesketh JE, et al. Selenium in human health and disease. *Antioxid Redox Signal* (2011) 14:1337–83. doi: 10.1089/ars.2010.3275
2. Avery JC, Hoffmann PR. Selenium, Selenoproteins, and Immunity. *Nutrients* (2018) 10. doi: 10.3390/nu10091203
3. Burk RF, Hill KE. Regulation of Selenium Metabolism and Transport. *Annu Rev Nutr* (2015) 35:109–34. doi: 10.1146/annurev-nutr-071714-034250
4. Patterson BH, Zech LA. Development of a model for selenite metabolism in humans. *J Nutr* (1992) 122:709–14. doi: 10.1093/jn/122.suppl_3.709
5. Swanson CA, Patterson BH, Levander OA, Veillon C, Taylor PR, Helzslouer K, et al. Human 74.selenomethionine metabolism: a kinetic model. *Am J Clin Nutr* (1991) 54:917–26. doi: 10.1093/ajcn/54.5.917
6. Wastney ME, Combs GFJr., Canfield WK, Taylor PR, Patterson KY, Hill AD, et al. A human model of selenium that integrates metabolism from selenite and selenomethionine. *J Nutr* (2011) 141:708–17. doi: 10.3945/jn.110.129049
7. Cardoso BR, Ganio K, Roberts BR. Expanding beyond ICP-MS to better understand selenium biochemistry. *Metallomics* (2019) 11:1974–83. doi: 10.1039/C9MT00201D
8. Navarro-Alarcon M, Cabrera-Vique C. Selenium in food and the human body: a review. *Sci Total Environ* (2008) 400:115–41. doi: 10.1016/j.scitotenv.2008.06.024
9. Institute of Medicine (US) Panel on Dietary Antioxidants and Related Compounds. *Dietary Reference Intakes for Vitamin C, Vitamin E, Selenium, and Carotenoids*. Washington (DC: National Academies Press (US (2000).
10. Wallace TC, McBurney M, Fulgoni VL. 3rd, Multivitamin/mineral supplement contribution to micronutrient intakes in the United States, 2007-2010. *J Am Coll Nutr* (2014) 33:94–102. doi: 10.1080/07315724.2013.846806
11. Clark LC, Combs GFJr., Turnbull BW, Slate EH, Chalker DK, Chow J, et al. Effects of selenium supplementation for cancer prevention in patients with carcinoma of the skin. A randomized controlled trial. Nutritional Prevention of Cancer Study Group. *JAMA* (1996) 276:1957–63. doi: 10.1001/jama.1996.03540240035027
12. Klein EA, Thompson IM, Lippman SM, Goodman PJ, Albanes D, Taylor PR, et al. SELECT: the selenium and vitamin E cancer prevention trial. *Urol Oncol* (2003) 21:59–65. doi: 10.1016/s1078-1439(02)00301-0
13. Lippman SM, Klein EA, Goodman PJ, Lucia MS, Thompson IM, Ford LG, et al. Effect of selenium and vitamin E on risk of prostate cancer and other cancers: the Selenium and Vitamin E Cancer Prevention Trial (SELECT). *JAMA* (2009) 301:39–51. doi: 10.1001/jama.2008.864
14. Rayman MP, Combs G, Waters DJ. Selenium and vitamin E supplementation for cancer prevention. *JAMA* (2009) 301:1876. author reply 1877. doi: 10.1001/jama.2009.625
15. Klein EA, Thompson IMJr., Tangen CM, Crowley JJ, Lucia MS, Goodman PJ, et al. Vitamin E and the risk of prostate cancer: the Selenium and Vitamin E Cancer Prevention Trial (SELECT). *JAMA* (2011) 306:1549–56. doi: 10.1001/jama.2011.1437
16. Stranges S, Marshall JR, Natarajan R, Donahue RP, Trevisan M, Combs GF, et al. Effects of long-term selenium supplementation on the incidence of type 2 diabetes: a randomized trial. *Ann Intern Med* (2007) 147:217–23. doi: 10.7326/0003-4819-147-4-200708210-00175
17. Hatfield DL, Gladyshev VN. The outcome of Selenium and Vitamin E Cancer Prevention Trial (SELECT) reveals the need for better understanding of selenium biology. *Mol Interv* (2009) 9:18–21. doi: 10.1124/mi.9.1.6
18. Robinson MF. 1988 McCollum award lecture. The New Zealand selenium experience. *Am J Clin Nutr* (1988) 48:521–34. doi: 10.1093/ajcn/48.3.521
19. Bugel S, Larsen EH, Sloth JJ, Flytlie K, Overvad K, Steenberg LC, et al. Absorption, excretion, and retention of selenium from a high selenium yeast in men with a high intake of selenium. *Food Nutr Res* (2008) 52. doi: 10.3402/fnr.v52i0.1642
20. Finley JW. The retention and distribution by healthy young men of stable isotopes of selenium consumed as selenite, selenate or hydroponically-grown broccoli are dependent on the isotopic form. *J Nutr* (1999) 129:865–71. doi: 10.1093/jn/129.4.865
21. Finley JW, Duffield A, Ha P, Vanderpool RA, Thomson CD. Selenium supplementation affects the retention of stable isotopes of selenium in human subjects consuming diets low in selenium. *Br J Nutr* (1999) 82:357–60. doi: 10.1017/S0007114599001592
22. Schrauzer GN. Selemethionine: A review of its nutritional significance, metabolism and toxicity. *J Nutr* (2000) 130:1653–6. doi: 10.1093/jn/130.7.1653
23. Combs GFJr., Midthune DN, Patterson KY, Canfield WK, Hill AD, Levander OA, et al. Effects of selenomethionine supplementation on selenium status and thyroid hormone concentrations in healthy adults. *Am J Clin Nutr* (2009) 89:1808–14. doi: 10.3945/ajcn.2008.27356
24. Gould SJ. Health consciousness and health behavior: the application of a new health consciousness scale. *Am J Prev Med* (1990) 6:228–37. doi: 10.1016/S0749-3797(18)31009-2
25. Patterson BH, Levander OA, Helzlsouer K, McAdam PA, Lewis SA, Taylor PR, et al. Human selenite metabolism: A kinetic model. *Am J Physiol* (1989) 257(Reg. Integr. Comp. Physiol. 26):R556–67. doi: 10.1152/ajpregu.1989.257.3.R556
26. Reamer DC, Veillon C. A double isotope dilution method for using stable selenium isotopes in metabolic tracer studies: analysis by gas chromatography/mass spectrometry (GC/MS). *J Nutr* (1983) 113:786–92. doi: 10.1093/jn/113.4.786
27. Patterson BH, Wastney ME, Combs GF. (2006). Calculation of the amounts of organic and inorganic selenium in the diet from kinetic studies, in: Mathematical Modeling in Nutrition and Agriculture. Proceedings of the Ninth International Conference on Mathematical Modeling in Nutrition, Roanoke, Virginia, Virginia Tech, Roanoke, VA Virginia Tech, August 14-17, 2006, pp. 213–22.

28. Niskar AS, Paschal DC, Kieszak SM, Flegal KM, Bowman B, Gunter EW, et al. Serum selenium levels in the US population: Third National Health and Nutrition Examination Survey, 1988-1994. *Biol Trace Elem Res* (2003) 91:1–10. doi: 10.1385/BTER:91:1:1
29. Burk RF, Norsworthy BK, Hill KE, Motley AK, Byrne DW. Effects of chemical form of selenium on plasma biomarkers in a high-dose human supplementation trial. *Cancer Epidemiol Biomarkers Prev* (2006) 15:804–10. doi: 10.1158/1055-9965.EPI-05-0950
30. Combs GFJr., Jackson MI, Watts JC, Johnson LK, Zeng H, Idso J, et al. Differential responses to selenomethionine supplementation by sex and genotype in healthy adults. *Br J Nutr* (2012) 107:1514–25. doi: 10.1017/S0007114511004715
31. Clausen J, Nielsen SA. Comparison of whole blood selenium values and erythrocyte glutathione peroxidase activities of normal individuals on supplementation with selenate, selenite, L-selenomethionine, and high selenium yeast. *Biol Trace Elem Res* (1988) 15:125–38. doi: 10.1007/BF02990131
32. Combs GF, Combs SB. "Absorption, excretion, and metabolism of selenium". In: GF Combs and SB Combs, editors. *The role of selenium in nutrition*. Orlando: Academic Press (1986). p. 179–204.
33. Kokarnig S, Tsirigotaki A, Wiesenhofer T, Lackner V, Francesconi KA, Pergantis SA, et al. Concurrent quantitative HPLC-mass spectrometry profiling of small selenium species in human serum and urine after ingestion of selenium supplements. *J Trace Elem Med Biol* (2015) 29:83–90. doi: 10.1016/j.jtemb.2014.06.012
34. Combs GF Jr, Watts JC, Jackson MI, Johnson LK, Zeng H, Scheett AJ, et al. Determinants of selenium status in healthy adults. *Nutr J* (2011) 10:75. doi: 10.1186/1475-2891-10-75
35. Sanz Alaejos M, Diaz Romero C. Urinary selenium concentrations. *Clin Chem* (1993) 39:2040–52. doi: 10.1093/clinchem/39.10.2040
36. Kuehnelt D, Kienzl N, Traar P, Le NH, Francesconi KA, Ochi T. Selenium metabolites in human urine after ingestion of selenite, L-selenomethionine, or DL-selenomethionine: a quantitative case study by HPLC/ICPMS. *Anal Bioanal Chem* (2005) 383:235–46. doi: 10.1007/s00216-005-0007-8
37. Thomson CD, Robinson MF, Campbell DR, Rea HM. Effect of prolonged supplementation with daily supplements of selenomethionine and sodium selenite on glutathione peroxidase activity in blood of New Zealand residents. *Am J Clin Nutr* (1982) 36:24–31. doi: 10.1093/ajcn/36.1.24
38. Ashton K, Hooper L, Harvey LJ, Hurst R, Casgrain A, Fairweather-Tait SJ. Methods of assessment of selenium status in humans: a systematic review. *Am J Clin Nutr* (2009) 89:2025S–39S. doi: 10.3945/ajcn.2009.27230F
39. Duffield-Lillico AJ, Reid ME, Turnbull BW, Combs GFJr., Slate EH, Fischbach LA, et al. Baseline characteristics and the effect of selenium supplementation on cancer incidence in a randomized clinical trial: a summary report of the Nutritional Prevention of Cancer Trial. *Cancer Epidemiol Biomarkers Prev* (2002) 11:630–9.
40. Peeler JC, Weerapana E. Chemical Biology Approaches to Interrogate the Selenoproteome. *Acc Chem Res* (2019) 52:2832–40. doi: 10.1021/acs.accounts.9b00379

Conflict of Interest: JM was employed by the company Information Management Services, Inc., and MW was employed by Metabolic Modeling Services.

The remaining authors declare that the research was conducted in the absence of any commercial or financial relationships that could be construed as a potential conflict of interest.

frontiers in Endocrinology

ORIGINAL RESEARCH
published: 28 June 2021
doi: 10.3389/fendo.2021.656054

Modeling Challenge Data to Quantify Endogenous Lactate Production

Darko Stefanovski[1]*, *Pamela A. Wilkins*[2] *and Raymond C. Boston*[3]

[1] Department of Clinical Studies – New Bolton Center, School of Veterinary Medicine, University of Pennsylvania, Kennett Square, PA, United States, [2] Department of Veterinary Clinical Medicine, College of Veterinary Medicine, University of Illinois, Urbana-Champaign, IL, United States, [3] Department of Clinical Studies- New Bolton Center, School of Veterinary Medicine, University of Pennsylvania, Kennett Square, PA, United States

With the intention of isolating the susceptibility of modeling methodology to influence our investigation of the infusion data, we used three kinetic approaches to our models: a simple approach, a unit approach, and a novel approach. The simple approach used exclusively built-in modeling features of the software in terms of units of the infusion dilution (mmol/L), as well as in terms of the precision of switching the infusion on and off. The unit approach used the same switching mechanism as the simple approach, but the units were modeled in those of the infusion (e.g., mmol/kg). Thirdly with the novel approach, we used an automated approach to controlling the infusion, in the sense that as the modeling mechanism sensed the slowdown of the infusion, it was gradually turned off. The units of the analysis for the novel approach were exactly the same as those deployed in the unit approach. Our objective here was to see if common pharmacokinetic parameters were seriously impacted by the particular modeling method.

Keywords: lactate, mathematical model, horse, metabolism, infusion, units

OPEN ACCESS

Edited by:
Chiara Dalla Man, University of Padua, Italy

Reviewed by:
Nicola Santoro, Yale University, United States
Andrea Tura, Institute of Neuroscience, National Research Council (CNR), Italy

***Correspondence:**
Darko Stefanovski
sdarko@vet.upenn.edu

Specialty section:
This article was submitted to Systems Endocrinology, a section of the journal Frontiers in Endocrinology

Received: *20 January 2021*
Accepted: *07 June 2021*
Published: *28 June 2021*

Citation:
Stefanovski D, Wilkins PA and Boston RC (2021) Modeling Challenge Data to Quantify Endogenous Lactate Production. Front. Endocrinol. 12:656054. doi: 10.3389/fendo.2021.656054

INTRODUCTION

Recent times have seen a rapid expansion in the use of challenge studies to help quantitate endogenous production of metabolites. The reasons for this are clear: unlike steady-state investigations, they are not as time costly as there is no need to equilibrate multiple analytes by leveraging others (e.g., establishing a new steady state for glucose while infusing insulin) that often takes several hours, the results are relatively easy to interpret, and they need not necessarily focus kinetically to beyond the specific metabolite of interest. L-lactate (LAC) is one such key cellular metabolite, produced by every cell and oxidized by those containing mitochondria; its metabolism is central to energy homeostasis and the cellular redox state. LAC has both beneficial and even essential functions in several metabolic disorders (1–4).

LAC is well recognized as a prognostic indicator in many severe disease states, both in humans and animals, and it is not necessarily a detrimental factor. Clinically, initially, in many disease states, aberrations in circulating LAC concentrations (blood LAC) are assumed to result from perfusion disturbances, resulting in increased production. Changes in blood LAC in later stages of diseases such as sepsis are thought to result from continued increased production, aberrant metabolism, including decreases in elimination, or both. While the majority of LAC produced by the body is metabolized in the liver (converted back to glucose and then stored as glycogen), 20-30% is removed by the kidney (5). Of this, only 10-12% is thought to be eliminated *via* urinary excretion, the rest removed by uptake and metabolism within the kidney (6).

Single or serial measurement of blood [LAC] is considered a reliable prognostic indicator in critically ill foals and adult horses (7–11). Endogenous LAC clearance has been similarly used, relying on various techniques employing changes in [LAC] over time (10–18). The various estimates of lactate 'clearance' (decrease or disappearance from the blood) used in earlier studies suggested that estimates of [LAC] 'clearance' is more useful than single measurements of [LAC] (10, 12, 15, 19). Calculation of true clearance of exogenously administered L-lactate (ExLC) in hemodynamically stable septic human patients was shown in 2 studies to be a useful prognostic indicator (4, 13). The technique allowed for a determination of true clearance -in addition to the production of LAC- with utility in interrogating the underlying processes of hyperlactatemia in critically ill human and veterinary patients. An equine species-specific ExLC test has been developed for use in horses (20).

The specific aim of this report is, using a study, and data, outlined earlier (20), to introduce an array of approaches enabling us to readily characterize the disposition of lactate subsequent to a brief infusion. We will explore how a selection of the units in which the infusion is modeled and the modeling approach per se (e.g., modeling elements used) to portray the infusion itself, and each may have evident consequences in our investigation and the interpretation of an infusion-based challenge to a system. As a consequence of our novel modeling approaches described here, we will capitalize on the WinSAAM software (www.winsaam.org) (21) and we will use the opportunity here to explain some less well-known features of this computational tool for compartmental analysis.

MATERIALS AND METHODS

Institutional approval: All procedures were approved by the Institutional Animal Care and Use Committee.

L-lactate infusion: The LAC infusion protocol has been described in detail elsewhere (20). Briefly, 500 ml sterile 0.9% NaCl solutions containing 1 $mmol.kg^{-1}$ body weight of lactate were infused into the jugular vein of 5 healthy adult horses using an infusion pump over 15 min. The opposite jugular vein was sampled at various times, with blood [LAC] determined using a YSI lactate meter (**Figure 1**). No other analytes such as glucose, insulin or triglycerides were collected during this experimental protocol.

Pattern of Lactate Disposition

In **Figure 2**, using classical exploratory methods (22), we present two perspectives of the lactate disposition: the pattern of lactate (for each horse) from the time immediately prior to the lactate infusion (**Figure 2**, left) until the lactate level returned to its value prior to the infusion; and, the pattern of lactate (**Figure 2**, right, again for each horse) from the cessation of the infusion until the lactate returned to its mean baseline value (20). Three features of these graphs are as follows: 1) in both cases there is considerable variation in aspects of the disposition, 2) the mean baseline lactate value is slightly higher than the lactate value just prior to the infusion, and 3) a semilog pattern, evident in each graph, is strongly suggestive of a biphasic disposition, with irreversible loss, of lactate from the horses.

Each of the points motivates the utilization of kinetic modeling software (21) to help explore these responses.

Modeling the Lactate Disposition

There are now three relatively common approaches to building and using pharmacokinetic kinetic (PK) models to explore systems: 1) Gabrielsson and Weiner's (22) approach uses clearances (within the system), volumes of distribution, and drug or metabolite blood levels to fabricate accounts of systems for an array of challenging and significant reasons. While the basis for this approach is undeniably sound, the manipulation of this subset of modeling objects can seem quite foreign to the PK

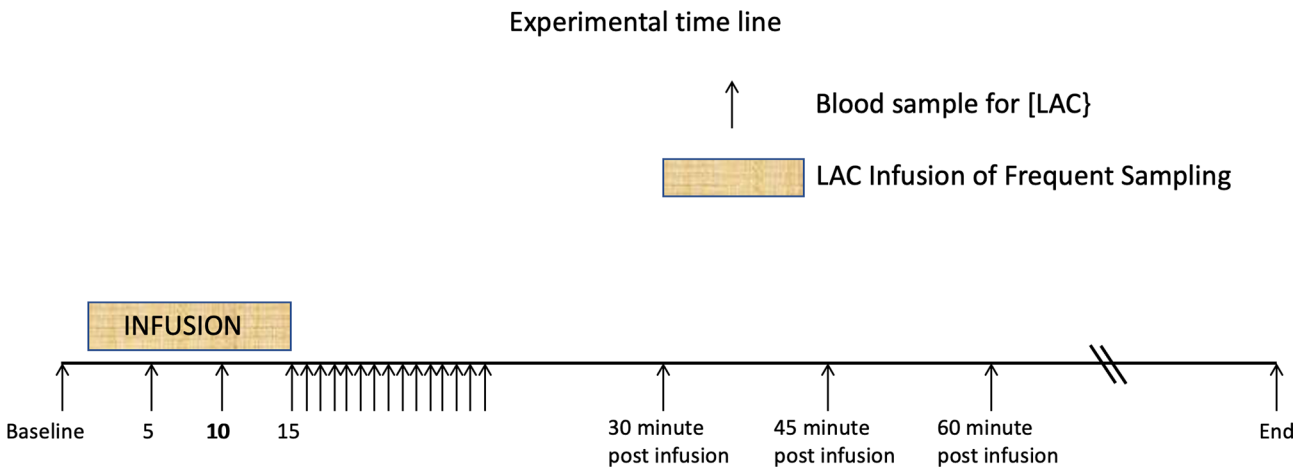

FIGURE 1 | Time line showing 15 minute periods one of L-Lactate infusion, and the other of rapid sampling. These are followed by the postinfusion sampling strategies. Additional samples were drawn until the baseline lactate was reached. From Figure 1 from P De Pedro et al. J. Vet. Emerg. Crit. Care 22 (5)2012. pp 564-572 (20).

FIGURE 2 | Pattern of lactate disposition, by horse, from sample immediately prior to infusion to the final observation (Left), and also shown (Right) the pattern of lactate disposition from the completion of the infusion to the final observation.

investigator [Pharmacokinetic: meaning the study of the time course of drug or metabolite concentrations in different body spaces, e.g. blood, plasma, cerebrospinal fluid, and tissues (22)], and hence may quite likely not be readily embraced.

2) A strong case seems to have been made by Rowlands and Tozer (23) for the advantages offered by the ubiquitous Macro Constant model. Their reason for promoting this line of investigation is essentially linked to the principle that all of the information in linear PK data is actually encapsulated in the indices, A, alpha, B, beta etc., of the Macro Models. Thus, creative use can be advanced by accessing this information as a tool for extending our third model structures, 3) Micro Rate Models. We have actually developed a novel approach to enhancing Micro Rate model data using a form of Kinetic Imputation. Here, using modeling software (21) it is possible to extend the kinetic data using added time predictions based on the Macro model. Our reason though, in promoting Micro Rate constant models, is because they are susceptible to manipulation of the model topology (inputs, outputs, and exchanges) to meet the needs of, otherwise unavailable, approaches, without disrupting the system eigenvalues.

Throughout this report we will be referring to Micro Rate constant models and these will be solved, and fitted to data using the WinSAAM modeling software, see **Supplementary Data 1** (essentially, explaining the WinSAAM syntax) and, an allied account, **Supplementary Data 2** (for a breakdown of the semantics of the WinSAAM modeling elements used in this investigation). Finally, **Supplementary Data 3** outlines the critical elements in the models used and the manipulation of their units.

The Units of Models and Modeling Objects

There are essentially three layers of modeling elements and their units falling under the investigator's control for the manipulation of the system. The first is the system inputs, e.g. infusions, and allied external controls, the second relates to the internal modeling objects impacting the various determinations called for by the system's investigation, and, finally, the third layer of manipulations amounts to transforming our intermediate determinations from the second layer to match the requirements of the external objects. The last array of objects usually serve as precursors to data or measurements reflecting the rationale for our investigation.

Consider the lactate infusion administered in this study. Setting up the infusion calls for selection of its units e.g. $mmol.min^{-1}$, or $mmol.kg^{-1}.min^{-1}$. Motivating our choice here could be susceptible to a) keeping numbers manageably small, or b) simplifying the algebra associated with the second level of our processing, or c) ensuring that the unit choice blends our analysis to be ready for the final, third, step in preparing for the observation, or measurement, units.

There is also some back-wash from our units. The units of any object do not exist in isolation. Each object abuts other objects and these interfaces need to match one another unit-wise or take on a critical, possibly final, step in a chain, gradually assuring completeness in the end.

We consider an example: assume that we allow the unit of the infusion to be $mmol.kg^{-1}.min^{-1}$.

So long as the responses and inputs are linear we can write [see Common equations, **Supplementary Data 2** and (24)]

$$UF1 = L(1,2)\,.\,F2 - L(2,1)\,.\,F1 - L(0,1)\,.\,F1 + G1 + G2 \quad (1)$$

$$F2\,` = L(2,1)\,.\,F1 - L(1,2)\,.\,F2 \quad (2)$$

See (**Supplementary Data, 1, 2** and **3**) for an account of the nomenclature.

Here we will breakdown the equations to illustrate how the units of our infusion impact our state variables (F1, and F2). Since UF1 is

the net rate of accumulation of lactate in compartment 1, L (1,2).F2 is the fractional rate of return of lactate from compartment 2 (F2) back into F1, and L (2,1).F1 is the fractional rate of movement of lactate from compartment 1 to compartment 2. G1 and G2 are inputs, G1, from the lactate infusion, and G2 from metabolism. If, as specified, our infusion is in the units of $mmol.kg^{-1}.min^{-1}$ then UF1 must also be of those units. Note that UF1 is a rate whereas F1, and F2 are amounts with the units of $mmol.kg^{-1}$. The solutions to eq (1) and eq (2) are obtained by numerical integration from the modeling software.

Note from (**Supplementary Data 1** and **Supplementary Data 2**) the units of L (1,2), L (2,1), and L (0,1) are min^{-1} and their contexts are as fractional rates. Since these equations are linear all additive terms have the same units, and, of course, L (2,1).F1 and L (1,2).F2 have the same units, as well as do, G1 and G2 ($mmol.kg^{-1}.min^{-1}$).

To ease the ease the understanding of the two equations the reader is referred to **Supplementary Data 1** and **Supplementary Data 2**.

Portraying Lactate Infusions

There have been considerable variations in the modeling of infusions explored over the years, and this seems to have emanated from the confidence investigators have had in their infusion pumps, or, in other mechanical devices to help administer infusions both completely, and smoothly. For example, one early approach, was to simply assert that infusions ran for the time intended (e.g. 15 minutes, in our case), and, in so doing, delivered the entire infusate within this allotted time (25–27). Other procedures (26) take a somewhat more realistic approach allowing the infusion to start slowly, gather speed, and then slow down again towards their climax (i.e. a sort of rhomboidal pattern of delivery and passage).

We have considered a novel approach here in which the speed of infusion delivery and the duration of delivery are each sensed and estimated using a multi-cell delay system which turns the infusion off soon after detecting that the administration of the content is reached. Since our model does not rely on any assumptions in regards to the state of perturbation of the system, or in other words, whether the system is in steady state or not, it is equally applicable in both states.

Indeed, we propose to examine the responses of three infusion delivery systems on aspects of the lactate kinetics as follows: A Simple Model (S) using rigid modeling tools to confer infusion design and limitations (e.g. infusion duration and amount) on the infusion units (e.g. $mmol.min^{-1}$), A Unit Model (U) with the same infusion machinery as the S model but allowing the infusion units to maintain those of the study design (i.e. $mmol.kg^{-1}.min^{-1}$, in our case), a Novel Model (N) using the software delay machinery (21) to automatically detect completeness of the infusion delivery, and the infusion duration. The N model will use the same units as those for the U model.

To ensure that there is no disruption from the novel infusion machinery we simultaneously evaluated several of the common PK dependencies discussed by Gabrielsson and Weiner (22), (e.g. Volumes of distribution, Clearance rates, Macro rate constants, and their half-lives, along with others) using both the U model and the N model. Then we ran concordance tests (28) to confirm that the pattern of dependencies among the N model calculations were not significantly different, or divergent, from those of the U model (which we recall used simplified methods for infusion modeling). To confirm the differential equation solution estimates of the dependencies we also calculated these using the WinSAAM matrix equation facility where appropriate.

Finally, to emphasize the significance of the basal lactate level in regard to its prominence in our kinetic analysis, and, to recognize that it was based on an average of many more (13, typically) observations we used Bayesian methods here (21, 24, 29) based on the distribution of the basal lactate values.

RESULTS

Five horses successfully completed the lactate infusion (20) and we compared the stability of the common indices of the PK disposition among some of these to judge the consistency of our results across the study.

In our **Supplementary Data 1** and **Supplementary Data 2**, we provide a comprehensive guide to the common indices, or model elements, that we intend to investigate in regard to their susceptibility to vary in association with our choice among the three lactate infusion models (S, U, and N).

In **Table 1** and **Figure 2** we present the macro constant models for each horse with dispositions displayed. An outstanding feature of the table, and these plots, is the very stable estimates of the Macro constants in spite of the quite substantial range in horse weights.

Figure 3 shows 4 dispositions plots for horse 5 with the upper left relating to the S model, and upper right relating to the U model, lower left to the N model and lower right all three models.

Figure 4 a similar collection of plots but for horse 1 here.

In **Figure 5** we demonstrate how the N model, applied to the infusion for horse 5, is able to detect the completion of the infusion allowing isolation of duration and net lactate administered.

Table 2 presents the final estimates, their errors, for the adjustable parameters for horse 5, and for each of the 3 models

TABLE 1 | Independently estimated macro constants and their standard errors are shown along with the respective horse weights.

Horse	A	CV	a	CV	B	CV	b	CV	Weight [kg]
1	0.694	13%	0.247	30%	1.492	5%	0.008	17%	484
2	1.041	12%	0.092	23%	0.735	17%	0.002	74%	588
3	0.738	10%	0.101	16%	1.104	7%	0.006	17%	450
4	0.604	7%	0.269	17%	1.183	3%	0.007	8%	503
5	0.698	16%	0.202	35%	1.337	8%	0.011	19%	480

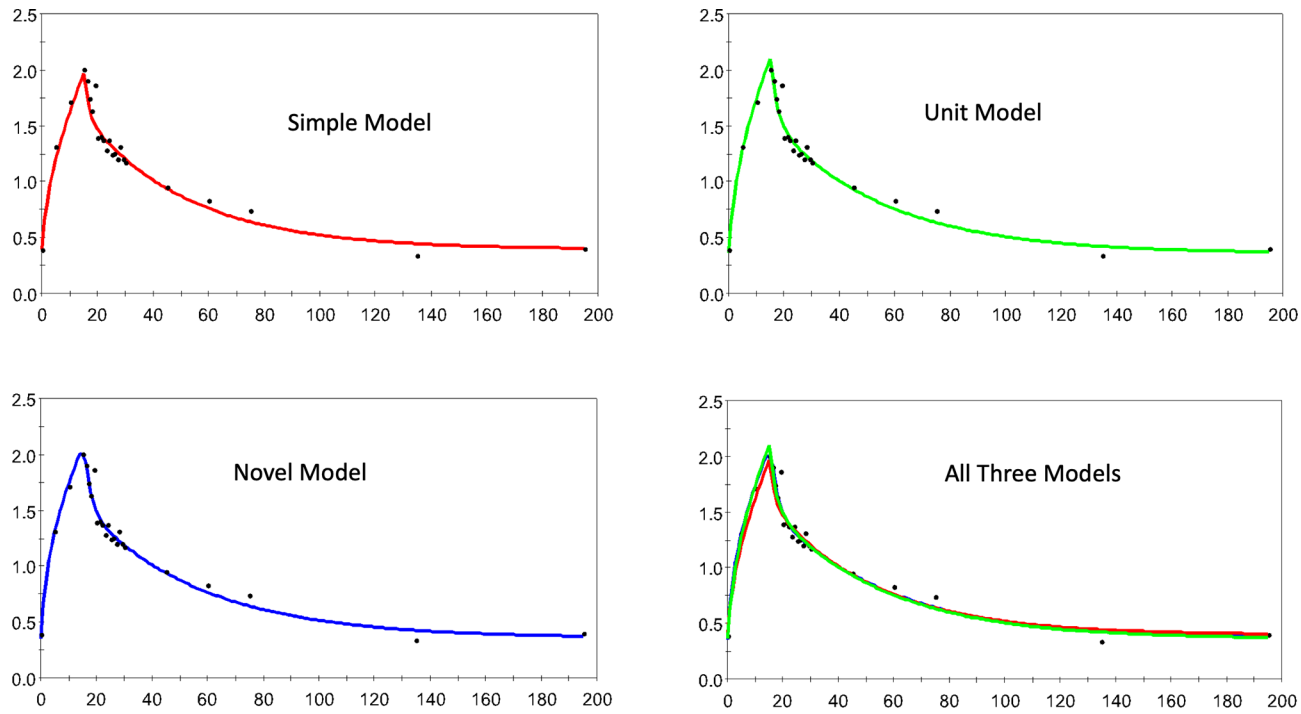

FIGURE 3 | The estimated and observed lactate disposition for the S, U, and N models separately, and all models together are shown for horse 5. Note uniform offset to pre-infusion mean lactate level.

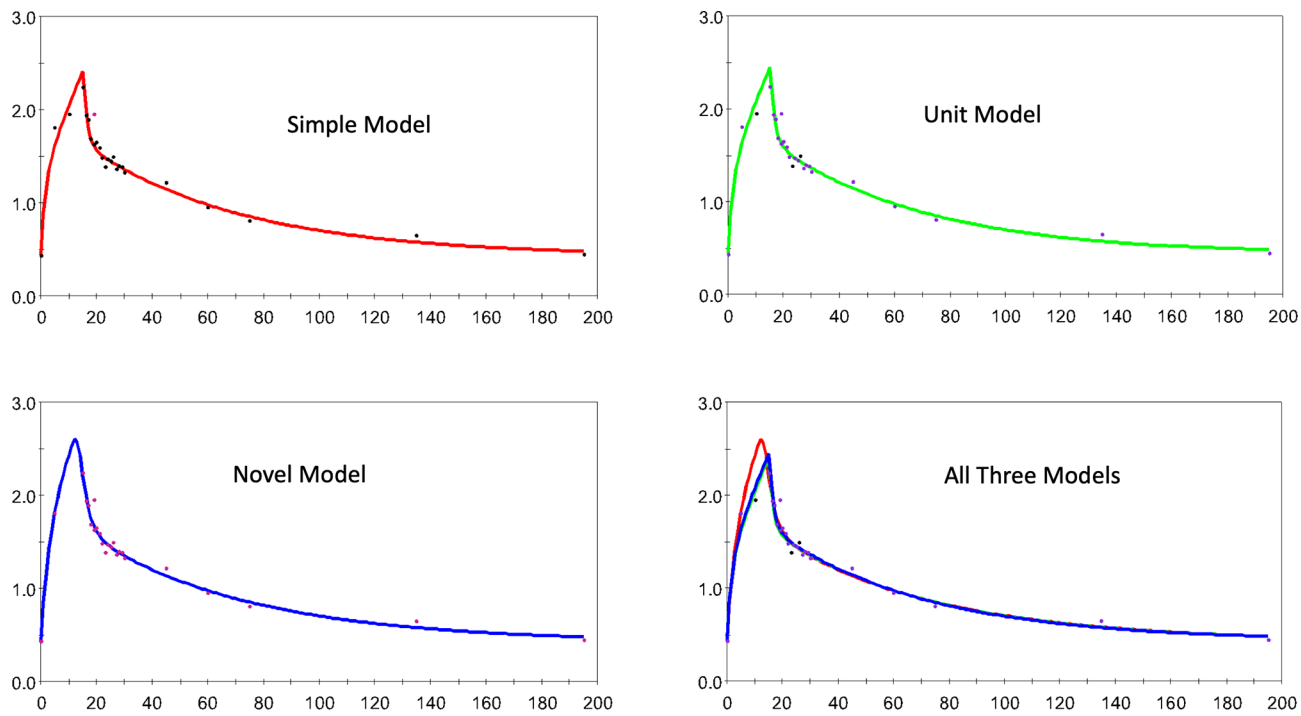

FIGURE 4 | The estimated and observed lactate disposition for the S, U, and N models separately, and all models together are shown for horse 1. Note uniform offset to pre-infusion mean lactate level.

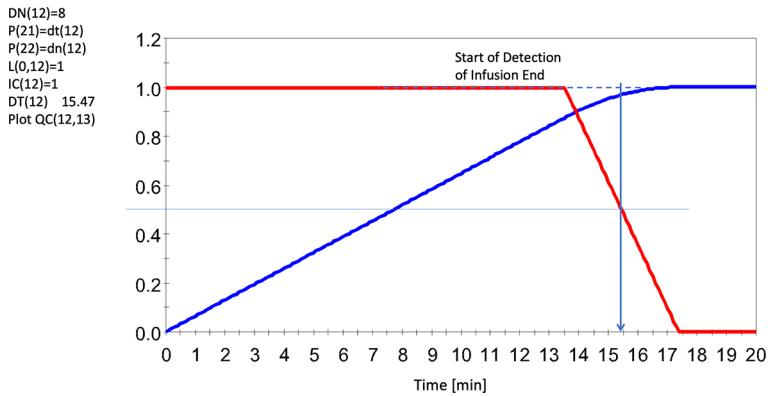

FIGURE 5 | Sensing the End of the Infusion Using an 8 Cell Delay System (red line), and accumulated input lactate infusion UF (13) = 1.F (12)/DT (12) (blue line). Note dashed line regarding agreements of results. Note this infusion seemed to run for slightly over 15 mins (albeit slowly here) whereas the average for all infusions was ~14 min. Red line represents the solution to F (12). Horse 5 shown here. All levels were scaled to invoke generalizability. For further details, see **Supplementary Data 2** and **Supplementary Data 3**.

TABLE 2 | The estimates of the adjustable parameters (and their errors) for horse 5 using the SU, and N models (top to bottom).

PARAMETER	VALUE	ERROR	CV
Simple Model			
P (1, 0)	0.419	0.020	5%
K (1, 0)	0.009	0.001	6%
L (0, 1)	0.072	0.003	5%
L (2, 1)	0.280	0.013	5%
L (1, 2)	0.189	0.012	7%
Unit Model			
P (1, 0)	0.357	0.003	1%
P (2, 0)	0.215	0.007	3%
L (0, 1)	0.070	0.002	3%
L (2, 1)	0.209	0.014	7%
L (1, 2)	0.137	0.005	3%
Novel Model			
DT (12, 0)	15.400	0.187	1%
P (1, 0)	0.356	0.003	1%
P (2, 0)	0.181	0.014	8%
L (0, 1)	0.081	0.006	7%
L (2, 1)	0.266	0.034	13%
L (1, 2)	0.133	0.005	4%

*P (1) is the mean pre-infusion baseline (mmol.kg^{-1}). K (1) is the inverse of the lactate pool size (L) (See **Supplementary Data 2** and **Supplementary Data 3** for model S). P (2) is the lactate pool size (L.kg^{-1}) (See **Supplementary Data 2** and **Supplementary Data 3** for model U and N). L(I,J) are fractional transfer rates (min^{-1}) (See **Supplementary Data 1**). Please ignore the zeros ('0') in the right subscript. That is, for example, P (1,0) = P (1).*

explored. It is quite clear that in spite of the differences in numbers of adjustable parameters there is very little change in parameter value estimates by model form (S, U, or N).

In **Figure 6**, we present concordance plots (and measures) for horses 1 (left) and 5 (right), using their respective dependencies. In each of these plots the N model (is the vertical axis) and the U model (the horizontal axis). The goal here was to determine how well the dependencies were preserved in regard to the respective infusion models. The values for the concordances (28, 30) were 0.980 (± 0.05) for horse 1, and 0.997 (± 0.001) for horse 5.

DISCUSSION

Bearing in mind the array of complicated decisions investigators need to negotiate as they prepare for the kinetic analysis of challenge data we have here explored two critical questions. First, is there a convenient and consistent way of managing the units of the information that comes from challenge studies? Second and final, could there be a way of assessing the implication of system infusions lending itself to tracking and compensating for unfortunate issues that arise in association with this type of challenge?

To address these questions, we mounted a series of partial modeling approaches: indeed, we proposed three models to help us here, a Simple Model (S), a Unit Model (U), and a Novel model (N). The S model took a path enabling us to accurately and systematically build a model of the system (infusion, mixing and clearance, for example) using as many of the prefabricated modeling elements as the simulation and analysis exercise called for. The U model followed the S model in regard to appropriating software tools as called for by the modeling purpose but it deviated from the S model when it came to specifying the units of the modeling objects. Most significantly here, the U model called for specification of the units of the investigation to be created around the units of the infusion, in our case mmol.kg^{-1} (or mmol.kg^{-1}.min^{-1}). This single maneuver made it extremely easy to specify the array of units for all objects in the model, and to perform verifiable steps in possibly implicating dependencies.

But units were just one of the issues we intended to address, the other was to see if our N model (with Novel approaches to tracking infusions) was able to help us to discover 1) whether we could capitalize on the modeling software, this time allowing the manipulation of a multicell delay detection system enabling us to automatically find the best guides as to what transpired as our infusion advanced. And, 2) at what cost would this type of service present in regard to offsetting (possibly corrupting) the evaluation of common pharmacokinetic dependencies (22) as a potential collateral consequence of their operation. Armed with

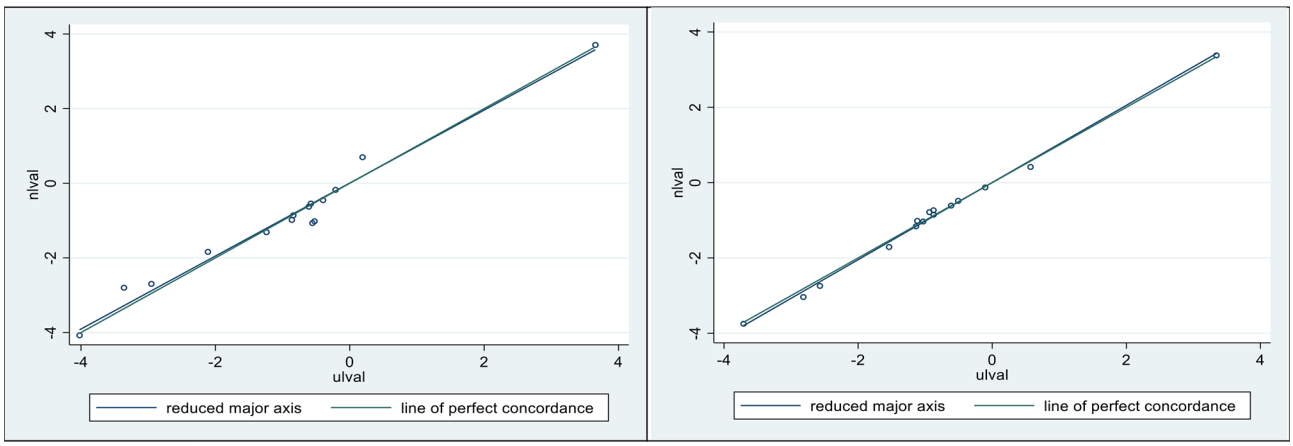

FIGURE 6 | Lin's concordance correlation coefficient (CCC) was 0.98 ± 0.05 for horse 1 (Left), and 0.997 ± 0.001 for horse 5 (Right). Plotted sloping lines represent estimated concordances (identified as the reduced major axis) and a line of perfect concordance, passing, as nearly as possible, through all pairs of observations.

15 common dependencies and our U and N models we were able to present preliminary evidence that the invocation of the delay machinery presented relatively few adverse consequences for these determinations. Indeed, the concordance of dependencies between the U and N-based models revealed that there were minimal corrupting side effects emanating within the N system.

CONCLUSION

Problems with infusion pumps are ubiquitous, and it is far from commonly an operator error leading to this situation. It can be extremes in fluid viscosity and/or heterogeneity, and clumps among the infusate. Indeed, based on one experimental failure (20) (one of our 6 original horses had to be withdrawn due to pump problems), this report was undertaken to explore the possibility of software modeling tools providing quantitative backup of our administration efforts. We cannot categorically state that we have the solution to the issue at this point, but we do believe that we have created a case for at least considering exploring our ideas, and that the more investigators try the methods discussed in this paper the stronger may be the information assembling to endorse this style of operation.

Besides providing a backup for the clinical investigators in terms of administration efforts outlined above, our methodologies offer several additional clinical benefits. First, modeling infusions using the actual units in which the infusion was administered leads to the accurate and straightforward specification of all subsequent system elements from within our PK account. Second and final, the current lactate kinetic models offer a better understanding of how a possible plasma increase in lactate can be attributed to increased production and the extent to which it results from a change in the kinetics of lactate.

One single and clear-cut recommendation we can offer though, is that modeling infusions using the actual units in which the infusion was administered leads to the simple and accurate specification of all subsequent system elements from within our PK account.

DATA AVAILABILITY STATEMENT

The raw data supporting the conclusions of this article will be made available by the authors, without undue reservation.

ETHICS STATEMENT

The animal study was reviewed and approved by the Institutional Animal Care and Use Committee (IACUC) of the University of Illinois at Urbana-Champagne.

AUTHOR CONTRIBUTIONS

DS reviewed and edited the text. PAW conducted the experimental study, reviewed the text. RCB conducted the analysis, wrote, reviewed, edited the article, and produced the figures. All authors contributed to the article and approved the submitted version.

SUPPLEMENTARY MATERIAL

The Supplementary Material for this article can be found online at: https://www.frontiersin.org/articles/10.3389/fendo.2021.656054/full#supplementary-material

REFERENCES

1. Leverve X, Mustafa I, Novak I, Krouzecky A, Rokyta R, Matejovic M, et al. Lactate Metabolism in Acute Uremia. *J Ren Nutr* (2005) 15:58–62. doi: 10.1053/j.jrn.2004.09.023
2. Hernandez G, Bellomo R, Bakker J. The Ten Pitfalls of Lactate Clearance in Sepsis. *Intensive Care Med* (2019) 45:82–5. doi: 10.1007/s00134-018-5213-x
3. Brooks GA. Cell-Cell and Intracellular Lactate Shuttles. *J Physiol* (2009) 587:5591–600. doi: 10.1113/jphysiol.2009.178350
4. Levraut J, Ciebiera JP, Chave S, Rabary O, Jambou P, Carles M, et al. Mild Hyperlactatemia in Stable Septic Patients Is Due to Impaired Lactate Clearance Rather Than Overproduction. *Am J Respir Crit Care Med* (1998) 157:1021–6. doi: 10.1164/ajrccm.157.4.9705037
5. Bellomo R. Bench-to-Bedside Review: Lactate and the Kidney. *Crit Care* (2002) 6:322–6. doi: 10.1186/cc1518
6. Hohmann B, Frohnert PP, Kinne R, Baumann K. Proximal Tubular Lactate Transport in Rat Kidney: A Micropuncture Study. *Kidney Int* (1974) 261:5–11. doi: 10.1038/ki.1974.35
7. Armstrong BA, Betzold RD, May AK. Sepsis and Septic Shock Strategies. *Surg Clin North Am* (2017) 97:1339–79. doi: 10.1016/j.suc.2017.07.003
8. Rosenstein PG, Tennent-Brown BS, Hughes D. Clinical Use of Plasma Lactate Concentration. Part 2: Prognostic and Diagnostic Utility and the Clinical Management of Hyperlactatemia. *J Vet Emerg Crit Care* (2018) 28(2):106–21. doi: 10.1111/vec.12706
9. Tennent-Brown BS, Wilkins PA, Lindberg S, Russell G, Boston RC. Assessment of a Point-of-Care Lactate Monitor in Emergency Admissions of Adult Horses to a Referral Hospital. *J Vet Intern Med* (2007) 21:1090–8. doi: 10.1892/0891-6640(2007)21[1090:aoaplm]2.0.co;2
10. Tennent-Brown BS, Wilkins PA, Lindborg S, Russell G, Boston RC. Sequential Plasma Lactate Concentrations as Prognostic Indicators in Adult Equine Emergencies. *J Vet Intern Med* (2010) 24:198–205. doi: 10.1111/j.1939-1676.2009.0419.x
11. Borchers A, Wilkins PA, Marsh PM, Axon JE, Read J, Castagnetti C, et al. Admission L-Lactate Concentration in Hospitalized Equine Neonates: A Prospective Multicenter Study. *Equine Vet J* (2012) Suppl(41):57–63. doi: 10.1111/j.2042-3306.2011.00509.x
12. Bakker J, Gris P, Coffernils M, Kahn RJ, Vincent JL. Serial Blood Lactate Levels Can Predict the Development of Multiple Organ Failure Following Septic Shock. *Am J Surg* (1996) 171:221–6. doi: 10.1016/S0002-9610(97)89552-9
13. Nguyen HB, Rivers EP, Knoblich BP, Jacobsen G, Muzzin A, Ressler JA, et al. Early Lactate Clearance is Associated With Improved Outcome in Severe Sepsis and Septic Shock. *Crit Care Med* (2004) 32:1637–42. doi: 10.1097/01.ccm.0000132904.35713.a7
14. Corley KTT, Donaldson LL, Furr MO. Arterial Lactate Concentration, Hospital Survival, Sepsis and SIRS in Critically Ill Neonatal Foals. *Equine Vet J* (2005) 37(1):53–9. doi: 10.2746/0425164054406856
15. Wotman K, Wilkins PA, Palmer JE, Boston RC. Association of Blood Lactate Concentration and Outcome in Foals. *J Vet Intern Med* (2009) 23:598–605. doi: 10.1111/j.1939-1676.2009.0277.x
16. Henderson ISF, Franklin RP, Wilkins PA, Boston RC. Association of Hyperlactatemia With Age, Diagnosis Survival Equine Neonates. *J Vet Emerg Crit Care* (2008) 18:496–502. doi: 10.1111/j.1476-4431.2009.00384.x
17. Castagnetti C, Pirrone A, Mariella J, Mari G. Venous Blood Lactate Evaluation in Equine Neonatal Intensive Care. *Therio* (2010) 73:343–57. doi: 10.1016/j.theriogenology.2009.09.018
18. Moore JN, Owen RR, Lumsden JH. Clinical Evaluation of Blood Lactate Levels in Equine Colic. *Equine Vet J* (1976) 8:49–54. doi: 10.1111/j.2042-3306.1976.tb03289.x
19. Vink EE, Bakker J. Practical Use of Lactate Levels in the Intensive Care. *J Intensive Care Med* (2018) 33:159–65. doi: 10.1177/0885066617708563
20. De Pedro P, Wilkins PA, McMichael MA, Dirikolu L, Lascola LM, Clark-Price SC, et al. Exogenous L-Lactate Clearance in Adult Horses. *J Vet Emerg Crit Care* (2012) 22:564–72. doi: 10.1111/j.1476-4431.2012.00800.x
21. Stefanovski D, Moate PJ, Boston RC. Winsaam: A Windows-Based Compartmental Modeling System. *Metabolism* (2003) 52(9):1153–66. doi: 10.1016/S0026-0495(03)00144-6
22. Gabrielsson J, Weiner D. *Pharmacokinetics & Pharmacodynamics: Concepts and Applications. 4th Edn*. Stockholm, Sweden: Swedish Pharmaceutical Press (2006).
23. Rowland M, Tozer T. *Clinical Pharmacokinetics: Concepts and Applications. 3rd Edn*. Baltimore: Williams and Wilkins (1995).
24. Dalla Man C, Caumo A, Cobelli C. The Oral Glucose Minimal Model: Estimation of Insulin Sensitivity From a Meal Test. *IEEE Tans BioMed Eng* (2002) 49:419. doi: 10.1109/10.995680
25. Levraut J, Ichai C, Petit I, Ciebiera J-P, Perus O, Grimaud D. Low Exogenous Lactate Clearance a an Early Predictor of Mortality in Normolactatemic Critically Ill Septic Patients. *Crit Care Med* (2003) 31:705–10. doi: 10.1097/01.CCM.0000045561.85810.45
26. Connor H, Woods HF, Ledingham JGG, Murray JD. A Model of L(+)-Lactate Metabolism in Normal Man. *Ann Nutr Metab* (1982) 26:254–63. doi: 10.1159/000176571
27. Grip J, Falkenstrom T, Promsin P, Wernerman J, Norberg A, Ryackers O. Lactate Kinetics in ICU Patients Using a Bolus of 13C-Labeled Lactate. *BMC Crit Care* (2020) 24:46. doi: 10.1186/s13054-020-2753-6
28. Lin LI-K. A Concordance Correlation Coefficient to Evaluate Reproducibility. *Biometrics* (1989) 45:255–68. doi: 10.2307/2532051
29. Lyne A, Boston R, Pettigrew K, Zech L. Emsa; A SAAM Service for the Estimation of Population Parameters Based on Model Fits to Identically Replicated Experiments. *Comp Meth Prog BioMed* (1992) 38:117–51. doi: 10.1016/0169-2607(92)90082-i
30. Bland JM, Altman DG. Statistical Methods for Assessing Agreement Between Two Methods of Clinical Measurement. *Lancet I* (1986) 8476:307–10. doi: 10.1016/S0140-6736(86)90837-8

Conflict of Interest: The authors declare that the research was conducted in the absence of any commercial or financial relationships that could be construed as a potential conflict of interest.

frontiers in Endocrinology

PERSPECTIVE
published: 16 July 2021
doi: 10.3389/fendo.2021.611512

Adapting Protocols or Models for Use in Insulin-Requiring Diabetes and Islet Transplant Recipients

Glenn M. Ward[1,2,3]*, *Jacqueline M. Walters*[1,3], *Judith L. Gooley*[1,3] *and Raymond C. Boston*[1,3,4]

[1] Department of Endocrinology and Diabetes, St. Vincent's Hospital, Fitzroy, VIC, Australia, [2] Department of Clinical Biochemistry, St. Vincent's Hospital, Fitzroy, VIC, Australia, [3] University of Melbourne Department of Medicine, St. Vincent's Hospital, Fitzroy, VIC, Australia, [4] School of Veterinary Medicine, University of Pennsylvania, Philadelphia, PA, United States

The authors' perspective is described regarding modifications made in their clinic to glucose challenge protocols and mathematical models in order to estimate insulin secretion, insulin sensitivity and glucose effectiveness in patients living with Insulin-Requiring Diabetes and patients who received Pancreatic Islet Transplants to treat Type I diabetes (T1D) with Impaired Awareness of Hypoglycemia. The evolutions are described of protocols and models for use in T1D, and Insulin-Requiring Type 2 Diabetes (T2D) that were the basis for studies in the Islet Recipients. In each group, the need for modifications, and how the protocols and models were adapted is discussed. How the ongoing application of the adaptations is clarifying the Islet pathophysiology in the Islet Transplant Recipients is outlined.

Keywords: mathematical modeling, type 1 diabetes mellitus, islet transplantation, insulin secretion, insulin sensitivity, minimal model, C-peptide model

OPEN ACCESS

Edited by:
Susanna Röblitz,
University of Bergen, Norway

Reviewed by:
Kyle C. A. Wedgwood,
University of Exeter, United Kingdom
Thomas Linn,
University of Giessen, Germany

***Correspondence:**
Glenn M. Ward
gmward@unimelb.edu.au

Specialty section:
This article was submitted to Systems Endocrinology, a section of the journal Frontiers in Endocrinology

Received: *29 September 2020*
Accepted: *28 June 2021*
Published: *16 July 2021*

Citation:
Ward GM, Walters JM, Gooley JL and Boston RC (2021) Adapting Protocols or Models for Use in Insulin-Requiring Diabetes and Islet Transplant Recipients. Front. Endocrinol. 12:611512. doi: 10.3389/fendo.2021.611512

INTRODUCTION

In this article we describe the evolution of the modifications we made in our clinic to glucose challenge protocols or mathematical models of insulin secretion, insulin sensitivity and glucose effectiveness, in order to study these parameters in patients with Insulin-Requiring Type2 Diabetes (T2D) and Type 1 diabetes (T1D), including T1D patients who have received Islet Transplants to treat their severe recurrent hypoglycemia and impaired awareness of hypoglycemia. This includes fitting of the Minimal Model of Bergman et al. (1) to Intravenous Glucose Tolerance Tests (IVGTT), and of the ISEC model to Oral Glucose Tolerance Tests (OGTT). We revisit the adaptations that were made for use in T1D, and Insulin-Requiring Type 2 Diabetes (T2D) as it helps to build a cohesive account of the work in our clinic aimed at studying the pathophysiology of insulin secretion and insulin action in the Islet Transplant Recipients. In each group we consider what issues were encountered, how we overcame them, and why we chose to adapt the protocols or models.

ESTIMATION OF INSULIN SENSITIVITY FROM INTRAVENOUS GLUCOSE TOLERANCE TESTS IN T1D

Modification of Minimal Model to Apply to Stepped Insulin-Modified IVGTT in T1D

The Minimal Model of Bergman et al. (1) consists of a Minimal Model of Glucose Disappearance (the "Glucose Minimal Model", gMM) [2, Equations 1 & 2] and a Minimal Model of Insulin Kinetics (the "Insulin Minimal Model", iMM) [3, Equation 3].

The gMM can be fitted to plasma glucose and insulin data from an IVGTT to simultaneously estimate Insulin Sensitivity (Si, increase in fractional glucose disappearance per unit increase in plasma insulin) and Glucose Effectiveness (Sg, ability of glucose per se to enhance its own disappearance independent of an increment in plasma insulin above basal).The iMM can be fitted to a IVGTT to estimate beta-cell responsiveness to glucose: first-phase responsivity (Phi1, amount of insulin (per unit volume) that can be accounted for by an assumed initial injection, per unit change in plasma glucose); and, second-phase responsivity (Phi2, the proportionality factor between glucose and the rate of rise of insulin secretion). Software to fit both models to IVGTT data includes Minmod (4). An alternative method used in our laboratory utilizes the SAAM modeling program to fit the model equations 1 to 3 as described (5).

$$dG/dt = -(p1 + X(t))*G(t) + p1*Gb \quad 1$$

$$dX/dt = -p2 \,.\, X(t)*p3(I(t) - Ib) \quad 2$$

$$dI/dt = -nI(t) + \gamma(G(t) - h) \,.\, t \quad 3$$

Where: G(t) and I(t) are the time courses of glucose and insulin in plasma following a rapid intravenous injection of glucose; Gb and Ib are basal levels; X(t) is the insulin effect on net glucose disappearance; p1 is glucose-mediated glucose disposal; p2 is insulin degradation; p3 is insulin action; n is the insulin clearance; γ is the proportionality factor between glucose concentration and the rate of increase of second phase insulin secretion for plasma glucose levels G(t) that exceed h, the threshold glucose level.

Although this method successfully accommodated data from healthy subjects and a variety of pathological states in fitting the gMM, we found it could not fit data from many patients with Type 1 diabetes (T1D) because: there was insufficient insulin input into the model as commented by Pacini and Bergman (4); and, insulin antibodies in many T1D interfered with the measurement of plasma insulin. In addition, Godsland and Walton showed that the success rate of minimal model analysis is reduced if the glucose does not return to baseline (6). We subsequently applied a modification of the gMM, which included a model of the exogenous insulin infusions, to IVGTT data from T1D subjects who had undergone a modified exogenous insulin protocol (7). This aimed to achieving sufficient insulin input to the model to regularize the glucose disappearance curves with sufficient features in the glucose curves to enable successful identification of the parameters (4). We also addressed the frequent presence in T1D of insulin antibodies which interfere with the insulin radioimmunoassay, by measuring plasma free-insulin after precipitation of bound insulin according to the method of Nakagawa et al. (8) using polyethylene glycol precipitation before freezing in order to avoid disturbing the equilibrium between free and antibody-bound insulin (9). In a recent study using a dextran-coated charcoal insulin assay (10) in our clinic, insulin antibodies were detected in a very low percentage in non-diabetic subjects, but in 50% of T1D, and 74% of Islet Transplant Recipients (manuscript in preparation).

To simulate a more physiological insulin profile during the IVGTTs in T1D, stepped exogenous insulin was infused with the total dose modified to achieve near-normal glucose disappearance (K_g). The stepped protocol aimed at approximating the insulin profile seen during an IVGTT in healthy normal weight subjects, derived by simulation of insulin disappearance kinetics. The final pattern of insulin infusion (analogous to **Figure 2**) was: 2-4 min = 14 mU of insulin per kg; 7-16min = 1 mU/min/kg; 17-50 min = 0.5 mU/min/kg; 51-180 min = rate estimated to maintain basal euglycemia based on the previous overnight insulin requirement. A model of the insulin infusion was added to the Minimal Model to estimate Si and Sg (**Figure 1**) (7), in 8 T1D subjects (age 21-38 y, BMI 20-26 kg/m^2) *versus* 17 healthy control subjects(20-37 y, 19-25 kg/m$^{2)}$)'.

The exogenous insulin protocol in T1D IVGTTs achieved near-normal plasma free-insulin levels: first-phase = 62 ± 9 SE mu/L; second-phase = 34 ± 9 mu/L, and K_g was normal at 1.3 ± 0.29 min^{-1} x 10^2 (7). Using the modified model and protocol as described (7) (**Figure 1**), we found T1D v controls: Si = 2.5 ± 0.6 v 8.3 ± 1.5 min^{-1}.mU^{-1}.L^{-1} x 10^4; Sg = 1.6 ± 0.5 v 2.6 ± 0.2 min^{-1} x 10^2; P <.05 Mann-Whitney, Fractional Standard Deviation < 0.5. Given that protocols used in the diabetic subjects were different from the normal subjects, it must be carefully considered whether the estimates are robust to structural perturbations. Nevertheless we examined the robustness by the following experiments. Using IVGTT during basal insulin infusion as described by Ader et al. (12), Sg was verified to be similar by this technique in the same T1D subjects (1.0 min^{-1} x 10^2, p = NS, Mann-Whitney) (7). We verified Si by comparison to a previous euglycemic clamp study where Si was 4.2 ± 1.0 min^{-1}.mU^{-1}.L^{-1} x 10^4 in a similar T1D group (p =NS, Mann-Whitney) (13). Therefore we concluded that the estimates were sufficiently robust to structural protocol perturbations, particularly if experiments could be designed using subjects as their own controls with the same protocol, as will be exemplified in the next three sections.

Alternatives to Stepped Insulin-Modified IVGTT in T1D

With regard to the stepped insulin infusions in the protocol, there can be alternative approaches that may not require as significant overhauls to the protocol. With the increasing use of continuous subcutaneous insulin pumps, a basal intravenous insulin infusion from 51 to 180 minutes may not be necessary

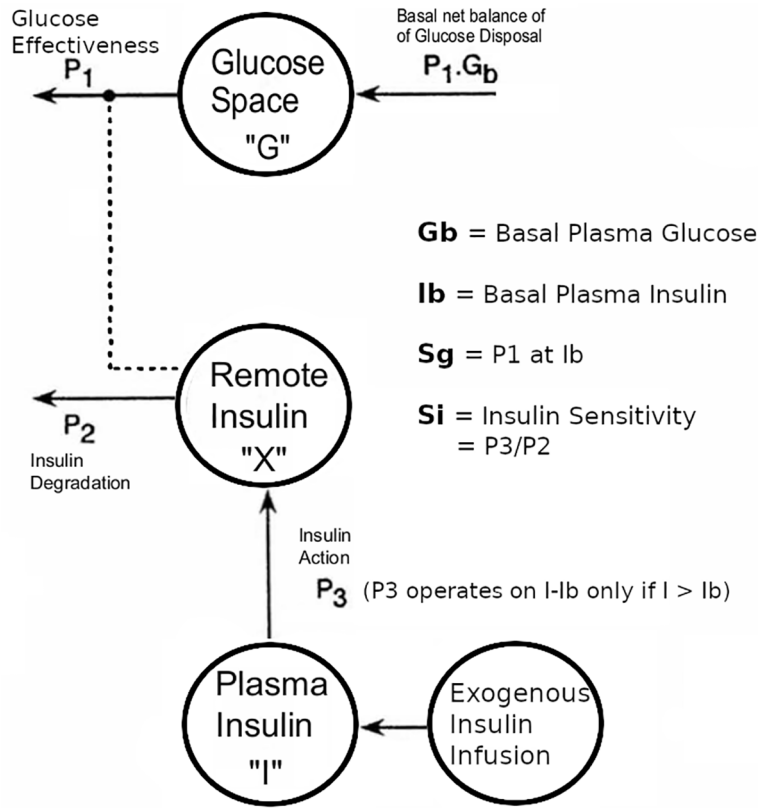

FIGURE 1 | Modifications to the Bergman minimal model of the intravenous tolerance test, aimed at enabling the model to be applied to data from T1D subjects in whom endogenous insulin secretion was minimal compared with the exogenous insulin infusion. Note that the endogenous coupling of the plasma insulin response to plasma glucose that was used in our modeling of non-diabetic subjects (5) was replaced with an external insulin supply represented by an additional compartment, as described in reference 7. This figure has been reproduced in a modified form from 7 with permission.

during the IVGTT if the basal pump rate is continued, providing insulin assays are used with specificity for analogue insulin (14, 15), such as research-grade assays with defined cross-reactivity with analogue insulin. The alternative approach of cessation of insulin pumps and switching to a long acting insulin prior to IVGTT may see unpredictable declines in plasma insulin (16) and may risk hypoglycemia while fasting. Another alternative regimen has been switching to a night-time dose of intermediate insulin, but this is sometimes associated with the need for an intravenous basal insulin infusion during the IVGTT.

Stepped Insulin-Modified IVGTT Protocol With Epinephrine in T1D

A practical example and test of the robustness of the use of the Stepped IVGTT protocol (A.1) was our study to explore the relative roles of Sg and Si in the observed impairment of glucose disposal with epinephrine infusion in T1D (17). An eight-fold rise in plasma epinephrine was achieved by intravenous delivery at 25ng/kg/min for 5.5 hours (EPI), in 7 non-obese young adult T1D patients, none of whom were on insulin pumps, but who had a basal overnight insulin infusion (12mU/kg/hr) with euglycemia maintained by adjustment of intravenous glucose. At 2.5 hours the IVGTT was performed with the stepped exogenous insulin protocol and analyzed as described (A.1) (7). Each subject had in random order a control (CTR) infusion of basal insulin prior to the IVGTT. Elevation of plasma epinephrine caused: impaired glucose disposal (Kg) (EPI 0.59 ± 0.1 *vs* CTL 1.91 ± 0.33 min^{-1} x 10^2, p<0.02 Mann-Whitney), associated with a marked impairment of Si (EPI 0.9 ± 0.5 *vs* CTR 7.03 ± 3.2 $min^{-1}.mU^{-1}.L \times 10^4$, p<0.05 Mann-Whitney); but, no impairment of Sg (EPI 2.5 ± 0.2 *vs* CTR 3.1 ± 0.5 $min^{-1} \times 10^2$) [p=NS Mann-Whitney]. These experiments indicated that physiological epinephrine elevation in T1D impairs Si but not Sg (17). Therefore, even in patients not on insulin pumps, the baseline insulin infusion during the IVGTT is able to effectively maintain basal glucose levels despite perturbation by Epinephrine.

Stepped Insulin-Modified IVGTT Protocol With Pulsatile Insulin Infusions in T1D

Another practical example of the robustness of protocol A.1 in T1D subjects, is our study of pulsatile insulin infusions in which, therapeutic levels of intravenous pulsatile insulin were compared with continuous intravenous insulin, at matching levels in T1D subjects (18). Of the 11 young non-obese T1D subjects, 4 had detectable fasting plasma C-peptide (40 ± 20SE pmol/L) and 5

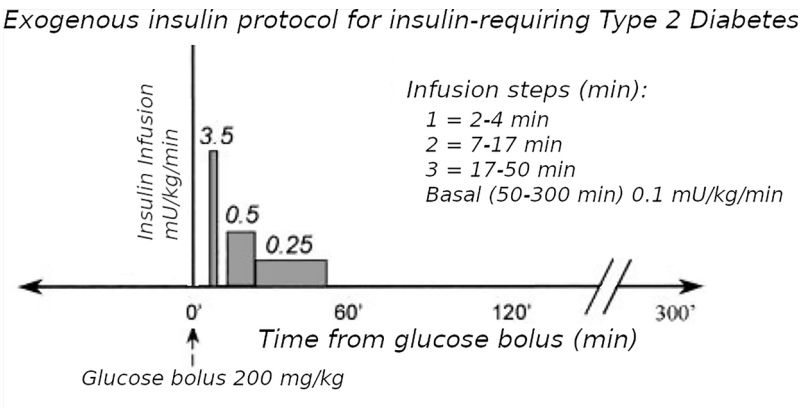

FIGURE 2 | Exogenous insulin protocol in T2D. This figure has been reproduced in a modified form from 11 with permission. It shows the steps of insulin infusion used in the T2D protocol, but also is similar in principle to the stepped protocol used for T1D.

had diabetes-duration above 10 years. Insulin was delivered intravenously at 12 mU/kg/h overnight for 17h, either as 40-second pulses every 13 minutes (PI) or continuously (CI), and euglycemia was maintained during the overnight fast by adjustable intravenous glucose. The next morning a fasting IVGTT was performed and analyzed as above (A.1).

The hypoglycemic effect of PI *versus* CI, estimated by glucose infusion rates, was approximately doubled in the 6 subjects with duration less than 10 years, (PI *vs* CI, 7.5 ± 2.7 *vs* 3.2 ± 0.6 μmol/kg/min p <0.05 Mann-Whitney) but did not differ in the 5 subjects with duration over 10 years (PI *vs* CI, 5.8 ± 2.4 *vs* 4.7 ± 2.2 μmol/kg/min). Insulin sensitivity from analysis of the IVGTT data was uniformly increased after PI *versus* CI with duration under 10 years (PI *vs* CI, 4.9 ± 1.4 *vs* 3.0 ± 1.0 $min^{-1}.mU^{-1}$. L x104). After 10 years diabetes duration insulin sensitivity was uniformly greater with CI than with PI (PI *vs* CI, 0.3 ± 0.1 *vs* 2.9 ± 1.6 $min^{-1}.mU^{-1}$. L x104, p <0.05 Mann-Whitney).

We concluded that, prolonged pulsatile *versus* continuous intravenous insulin resulted in a significant increase in hypoglycemic effects and insulin sensitivity in T1D with diabetes duration up to 10 years the differential effect of PI was dependent on duration of diabetes. This indicates that the use of a basal insulin infusion during the IVGTT in T1D patients who are not on insulin pumps, is effective in maintaining the constant pattern of glucose levels at the end of the IVGTT, despite pulsatile insulin infusions being used.

ESTIMATION OF INSULIN SECRETION AND INSULIN SENSITIVITY IN T1D AFTER ISLET TRANSPLANTATION

Pancreatic Islet Transplantation in T1D

Pancreatic islet transplantation (IT) is an established clinical treatment for people with T1D, who suffer with severe hypoglycemia unawareness. Islets are obtained from the pancreas of a deceased organ donor, purified and then transfused into the portal vein of the recipient. Restoring natural islet function improves glycemic control and can markedly reduce hypoglycemia. Transplant recipients need life-long immunosuppression to prevent rejection-mediated cell loss.

In order to apply both iMM and gMM to analyze IVGTTs in Islet Transplant Recipients (ITR), we found there was a need to further modify the protocol and model compared to the T1D analyses, building on the investigations done on T2D IVGTTs discussed below.

Extension of Modifications of Protocol and Model to T2D

The Minimal Model of Bergman et al. could only be used in early studies of T2D subjects if they had sufficient endogenous insulin secretion. An adequate increase during the IVGTT in the AUC of insulin levels was necessary to be able to fit the Minimal Model. To overcome this limitation, exogenous insulin protocols have been used in IVGTTs in T2D to enable the Minimal Model to estimate Si and Sg (19, 20). Also, in insulin-requiring T2D, the baseline insulin levels may need to be maintained during the IVGTT when insulin secretion is low. Therefore we adapted protocol A.1 with basal insulin infusion during the IVGTT for use in insulin-requiring T2D. However, we found (11) that the estimates were affected by the doses of insulin used: either Welsh et al. (19) or Taniguchi et al. (20). Because of this, we developed a "minimal disturbance" approach to estimating Si and Sg in T2D. To avoid supra-physiological peak glucoses in T2D with elevated fasting glucose, we used a reduced glucose load (200 mg/kg). In order to compensate for endogenous insulin secretion in T2D the T1D Stepped insulin infusion rates (A.1) were reduced by 50% (**Figure 2**). In a series of 8 T2D patients, 5 of whom were insulin-requiring, data from this approach were analyzed either using the unmodified Minimal Model of Bergman (BMM), or a modified model (MMD) with an additional element (in this case DT18 in SAAM terminology) representing a time delay in the transfer of insulin into the remote insulin compartment (X). As described in (11) (**Figure 3**), the program SAAM compiles the model "deck" and generates and numerically solves the differential

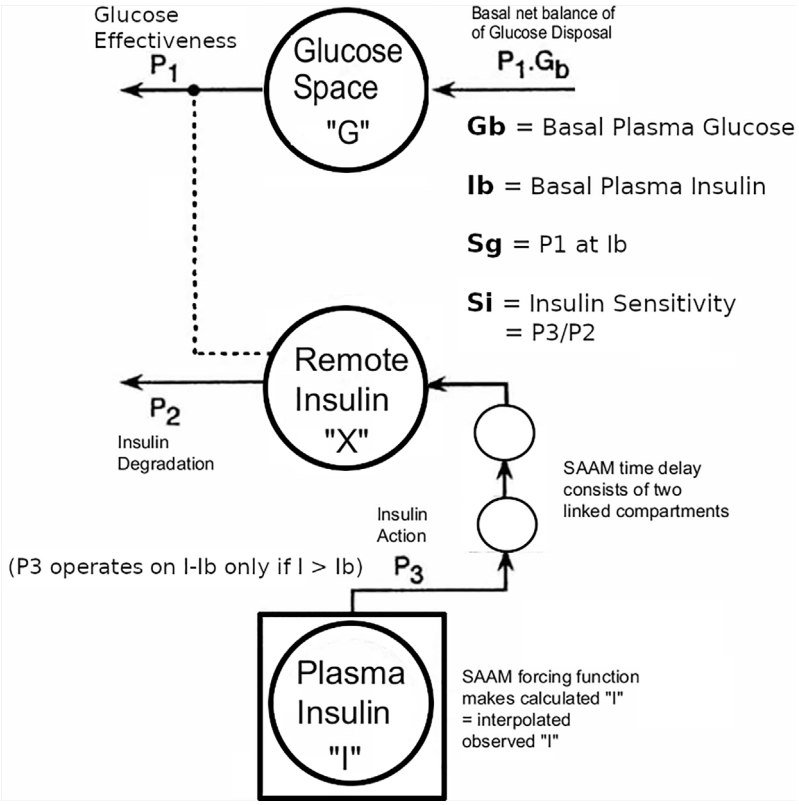

FIGURE 3 | Modification of Minimal Model to accommodate T2D data with the physiological exogenous insulin protocol. This figure has been reproduced in a modified form from 11 with permission. The IVGTT glucose and insulin data were analyzed using the glucose model of Bergman et al. as described (5) using the simulation, analysis, and modeling program SAAM (6). Except there were the following modifications: The square around compartment "I" indicates that the observed plasma insulin concentrations drive the system, and an additional element that is the equivalent of two linked compartments represents a time delay in the transfer of insulin into the remote insulin compartment (X). The program SAAM generates and numerically solves the differential equations without the need to supply explicit differential equations representing the time delay element.

equations without needing explicit differential equations representing DT18.

Adaptation by adding the delay element improved identification of Si and Sg from 37.5% (BMM) to 100% (MMD) in this largely insulin-requiring T2D group. Si in these T2D subjects was lower than normal(1.86 ± 0.60 v 8.65 ± 2.27 $min^{-1}.mU^{-1}.L \times 10^4$,p <.01 Mann-Whitney). The reduced Si values were confirmed in this T2D group with 2-stage euglycemic clamps (Si CLAMP = 2.02 ± 0.42 $min^{-1}.mU^{-1}.L \times 10^4$, p > 0.4 *vs* IVGTT Mann-Whitney). Sg was not significantly reduced (2.00 ± 0.25 T2D v 1.55 ± 0.26 normal, $min^{-1} \times 10^2$). Use of the delay in normal subjects did not improve the fit.

These results suggest that insulin action at physiological insulin levels in insulin-requiring T2D may not be a single phase, possibly due to impaired trans-capillary endothelial transfer.

In the process of protocol selection, we found that, since our protocol could accommodate insulin requiring T2D, some needed free insulin assay, and some may need basal insulin infusions during the IVGTT. These studies indicate that, in T2D with minimal insulin secretion such as insulin-requiring T2D, we would recommend using an IVGTT protocol with basal insulin infusion during the IVGTT.

Delay in Insulin Secretion During IVGTT and OGTT After Islet Transplantation in T1D

Selection of the exogenous insulin protocol for IVGTT for Islet Transplant Recipients (ITR) in our clinic was informed by our previous adaptations in T1D and T2D. Free insulin assays were used if insulin antibodies were detected in individual subjects, and this was necessary in about 75% of cases. Although ITRs have features similar to T2D, their insulin sensitivity was more similar to T1D so that a more standard exogenous insulin protocol could be used, and without the need for a delay element in the modeling. Approximately 50% of ITRs became insulin independent and had better homeostasis of the basal glucose and insulin. In these subjects we were able to model IVGTTs without exogenous insulin supplementation as described (5). Alternatively, many insulin dependent ITRs used

insulin pump therapy, enabling stabilization of the baseline state by continuing the insulin pump together with the Taniguchi exogenous insulin protocol (20).

In the ITRs we chose also to model plasma C-peptide responses during the glucose challenges to estimate Insulin Secretion Rates by the ISEC methodology (21). We aimed to maximize the information to further investigate the pathophysiology of insulin secretion by the transplanted islets. We reported deficient first-phase insulin secretion (Phi1) during IV glucose tolerance tests and greater restoration of second compared with first phase insulin secretion after successful islet transplantation, with maintained Si despite being on immunosuppression regimens after islet transplantation (22), indicating that comprehensive estimates of insulin secretion capacity (first and second phases, and DI) with the Non-insulin modified IVGTT (NIM-IVGTT) have an significant role in metabolic monitoring after islet transplantation in subjects who are insulin independent. This finding contrasted with other studies using IVGTT which showed that islet transplantation can restore first-phase insulin secretion to the normal range (23, 24). Further studies of the insulin independent ITR patients included C-peptide ISEC analyses and our preliminary data confirms a reduction in first phase insulin secretion rates (**Figure 4**), and this would also indicate that our previous results with plasma insulin Phi1 (22) were not reduced secondary to binding of secreted insulin by circulating insulin antibodies.

We extended our studies of the delays of early secretion of insulin to include Oral Glucose Tolerance Tests (OGTT) because this test included the incretin effects (25, 26) which is a potentially important element in the ITR group, and we found that the incretin effect was reduced in our cohort of ITR (25, 26). We found however that one practical drawback, was the difficulty of using OGTTs in the insulin-dependent subset of ITRs because of the lack of standardization of exogenous insulin protocols during the OGTT, which would be needed to avoid undesirable hyperglycemia during the tests in the insulin-dependent group. It is also difficult to model the insulin responses in this group because of the low insulin responses limit the ability to fit the model to the data (6). We therefore focused our OGTT studies on the insulin-independent ITRs which make up about 50% of the ITRs in our clinic in accordance with other clinics who use the standard Edmonton Islet Transplant Protocol (27).

Our studies using OGTTs in Islet Transplant recipients (25) indicated that there is a delay in insulin secretion rates which may be related to factors such as incretin function (26). Our OGTT studies also demonstrated a normalized suppression of free fatty acids in islet transplant recipients despite this delay in insulin secretion (28).

Our ITR subjects were 7 T1D patients (Group A, gender 7F, age 56 ± 4 SE yr, BMI 19.8 ± 1.0 kg/m2, T1D duration 46 ± 10 yr.) who had achieved insulin-free status following IT as described in our Multicenter Trial (29). The detailed exclusion and inclusion criteria for the transplants were as described (29) but the key criteria were T1D patients with life-threatening severe recurrent hypoglycemia and impaired awareness of hypoglycemia, but who were suitable for immunosuppression. They were compared to 9 matched non-diabetic controls as described (25). (Group B, 7F:2M, 53 ± 4 yr., BMI 24.8 ± 1.0 kg/m2). All subjects had both OGTTs and IVGTTs. The clinical investigations described here were carried out with the approval

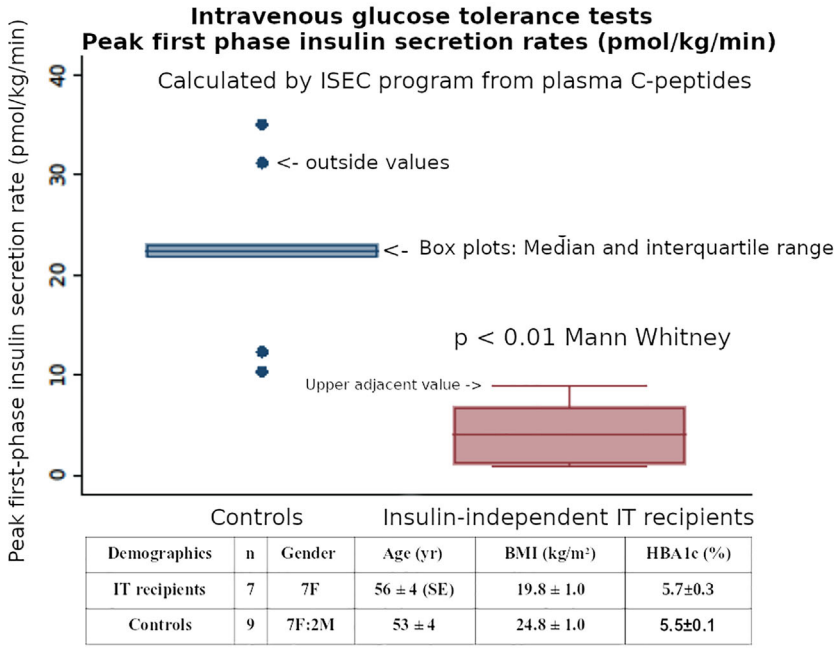

Demographics	n	Gender	Age (yr)	BMI (kg/m²)	HBA1c (%)
IT recipients	7	7F	56 ± 4 (SE)	19.8 ± 1.0	5.7±0.3
Controls	9	7F:2M	53 ± 4	24.8 ± 1.0	5.5±0.1

FIGURE 4 | The post-transplant first-phase insulin secretion (Phi1) during an IVGTT, when calculated by ISEC analysis of plasma C-peptide levels, was reduced in insulin independent Islet Transplant recipients - compared with matched healthy controls.

of the Institutional Human Research Ethics committee at St Vincent's Hospital Melbourne. Within 6 months of gaining insulin-independence, 75-gram 4-hour OGTTs and 200mg/kg IVGTTs were performed in the 7 insulin-independent T1D islet transplant recipients and compared to the similar non-diabetic healthy subjects who had both an OGTT and an IVGTT within 6 months of each other. The groups A & B had similar glucose levels (transplant recipients *vs* healthy non-diabetic subjects: mean HBA1c 5.7 ± 0.3SE *vs* 5.5 ± 0.1% p=NS; and similar insulin sensitivity HOMA2-S% 117 ± 28 *vs* 83 ± 8 p=NS Mann-Whitney).

Plasma glucose, insulin and C-peptide were measured at 30 minute intervals during the OGTTs, and as previously described (7) during the IVGTTs.

Insulin secretion rates were calculated by using ISEC to fit a model of C-peptide kinetics to the plasma C-peptide concentrations during both IVGTTs and OGTTs (21). Using these Insulin Secretion Rates (ISR) during the IVGTTs, the initial post-transplant first-phase insulin secretion (Phi1, peak value in first 10 minutes) was reduced in recipients compared with healthy non-diabetic subjects (median [Interquartile Range] 4.1 [1.1-6.78] *vs* 22.4 [21.8-23.1] pmol/kg/min, respectively, p<0.01 Mann Whitney). (**Figure 4**). Using the ISR during the first 30 minutes of the OGTT to calculate first-phase insulin secretion (oPhi1, as the increment in ISR per increment in glucose) also showed a reduction in the recipients *versus* healthy non-diabetic subjects (0.43 [0.26-1.11] *vs* 2.32 [1.41-2.59] pmol/kg/min per mmol/L, respectively, p<0.01 Mann Whitney). The above data on Phi1 and oPhi1 were not normally distributed so non-parametric tests were used.

Although the transplant recipients' mean OGTT 2-hour glucose was elevated (13.8 ± 1.7 mmol/L), 2 recipients were classified as non-diabetic (<11.1), and all recipients' glucoses returned to baseline (5.8 ± 1.2) by 4-hours. (**Figure 5**).

ISEC analysis of the plasma C-peptide allowed estimation of Insulin Secretion Rates (**Figure 6**), showing a delay in early insulin secretion with clear improvement in the latter half of the OGTT. The relationship of this improvement to incretin effects requires further investigation.

Only measuring early insulin release during OGTTs could underestimate later secretion by ~30% in islet transplantation, correlating with our previous report using IVGTTs (22). The good control of HBA1c in the recipients despite the delayed early secretion could be related to the portal route of transplantation, or might reflect the dietary preferences of the recipients.

However, our findings support a role for also testing the early secretion using IVGTT. When C-peptide-derived Insulin Secretion Rates during the IVGTTs were estimated using ISEC, the initial post-transplant first-phase insulin secretion was reduced in recipients compared with healthy non-diabetic subjects. This confirms our previous conclusion based on plasma insulin concentrations (22), indicating that the reduced Phi1 was not caused by binding of secreted insulin by insulin antibodies.

Reduced IVGTT Phi1 after islet transplantation could reflect the same factors as the delayed insulin secretion during OGTT.

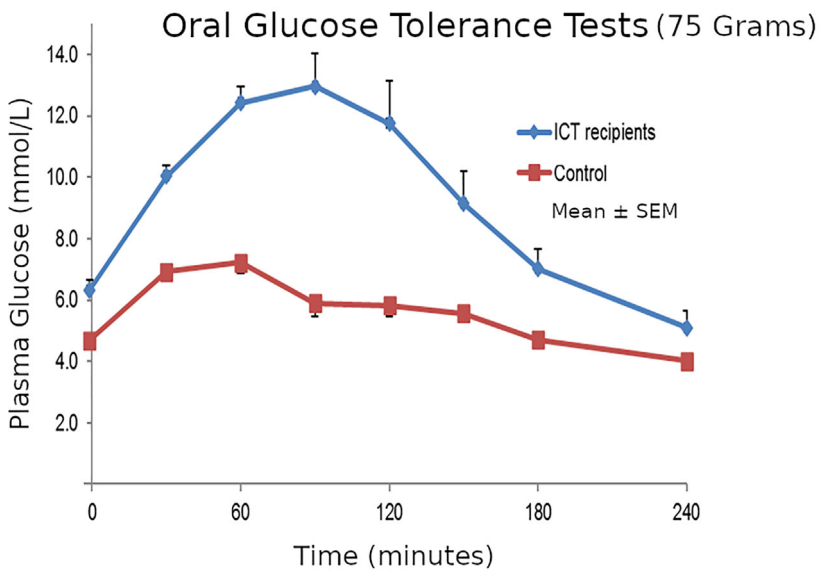

Demographics	n	Gender	Age (yr)	BMI (kg/m²)	HBA1c (%)
IT recipients	7	7F	56 ± 4 (SE)	19.8 ± 1.0	5.7±0.3
Controls	9	7F:2M	53 ± 4	24.8 ± 1.0	5.5±0.1

FIGURE 5 | Mean ± SE plasma glucose concentrations during 75g OGTTs in the 7 Insulin-independent Islet Transplant Recipients, and in the 9 Nondiabetic Controls.

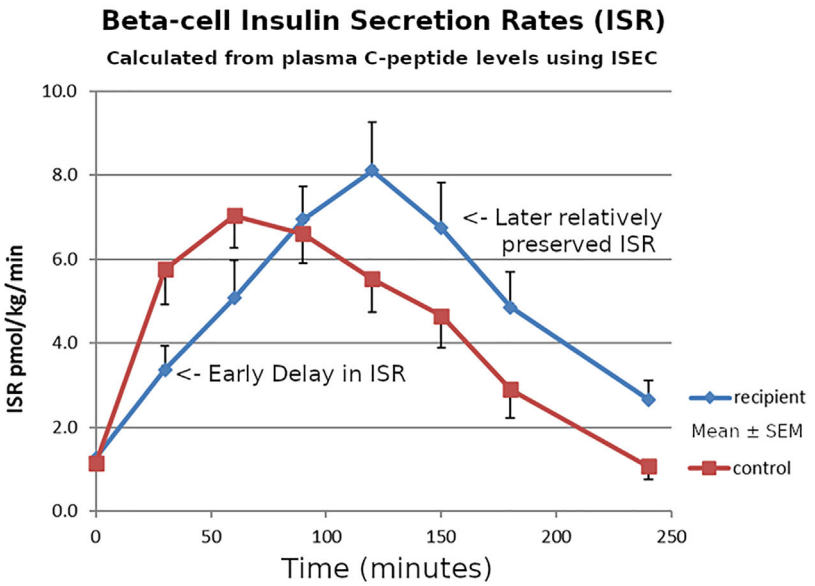

Demographics	n	Gender	Age (yr)	BMI (kg/m²)	HBA1c (%)
IT recipients	7	7F	56 ± 4 (SE)	19.8 ± 1.0	5.7±0.3
Controls	9	7F:2M	53 ± 4	24.8 ± 1.0	5.5±0.1

FIGURE 6 | Mean ± SE Pre-hepatic insulin secretion rates estimated from the plasma C-peptide concentrations by deconvolution using the program ISEC, during 75g OGTTs in the 7 Insulin-independent Islet Transplant Recipients, and in the 9 Nondiabetic Controls.

For example it has been suggested that increased beta-cell overdrive could cause depletion of readily-releasable insulin stores. This marker of beta cell dysfunction provides a parameter that could be monitored in addition to indices of beta cell mass. Alternatively, these reduced insulin responses could represent recurrence of autoimmune beta cell damage similarly to that observed with reduced first phase insulin responses in pre-type 1 diabetes patients (30). Further studies are underway in our clinic with greater number of patients to clarify the significance of this delay in insulin secretion and its relationship of the pathophysiology of the decline in islet function after ITR.

Future Directions in IVGTT and OGTT After Islet Transplantation in T1D

Future evaluation of beta cell function in islet transplant recipients would be improved by better understanding of the interaction of insulin sensitivity, glucose effectiveness and the parameters of beta cell secretion of insulin. It is well accepted that insulin secretion and sensitivity are best interpreted together, because of the hyperbolic relationship between these two parameters (31), and that an improved measure of beta cell function is obtained by calculating the "disposition index" (i.e. the "insulin sensitivity-adjusted beta cell function") (31). The other less well-understood interaction is the degree to which exogenous insulin given during IVGTTs can directly suppress endogenous insulin secretion, independent of the impact upon glucose levels, due to the feedback loop of circulating insulin on its own secretion (32). The current methods to correct for this effect mainly involve omitting of data during exogenous insulin supplementation but would benefit from standardization. Other methods of data analysis such as Bayesian hierarchical analysis could be explored that could improve parameter estimation (33), although it would need to be confirmed whether this would avoid the need for optimized exogenous insulin protocols during the IVGTT. Alternatively algorithms developed for closed-loop subcutaneous insulin pumps (34) and successfully used in exercise perturbation studies (35), may allow adaptation to intravenous glucose monitoring and insulin delivery, which may allow real-time adjustment of insulin infusions during IVGTT or OGTTs. This would optimize the glucose decay curves and therefore the ability to identify parameters for Sg and Si (6).

OVERALL SUMMARY

We have presented our perspective of the application of the Mathematical Models to the analysis of intravenous and oral glucose challenges in Type I diabetes. The modifications of the protocols necessary to apply these models also to Type I diabetes patients who have received Islet Transplants were elaborated. Islet Transplant Recipients represent a pathophysiological state that is similar to T2D, but has some distinct differences. These

differences are exposed by application of the modified protocols and models of insulin secretion and action. In our preliminary studies, IVGTT *versus* OGTT parameters provided additional insights into the pathophysiology of transplanted islets, reflecting beta cell dysfunction rather than only monitoring beta cell mass (23) in Islet Transplant Recipients. Further evaluation with greater numbers of ITR is required to explore the relevance of delayed early insulin secretion in determining survival of transplanted islets.

DATA AVAILABILITY STATEMENT

The raw data supporting the conclusions of this article will be made available by the authors, without undue reservation.

ETHICS STATEMENT

The studies involving human participants were reviewed and approved by St Vincent's Hospital Human Research Ethics Committee. The patients/participants provided their written informed consent to participate in this study.

AUTHOR CONTRIBUTIONS

GW, JG, JW, and RB collaborated on the investigations that form the basis of this perspective. GW wrote the initial draft based on previous discussions with the coauthors, and JG, JW, and RB made substantial contributions to revisions of it. All authors contributed to the article and approved the submitted version.

FUNDING

The work discussed in this manuscript was supported by grants from Diabetes Australia Research Foundation, St Vincent's Hospital Research Foundation, National Health and Medical Research Council of Australia, and the Juvenile Diabetes Research Foundation.

ACKNOWLEDGMENTS

We acknowledge the support of St Vincent's Hospital Melbourne, St Vincent's Pathology, University of Melbourne, and Directors of the Department of Endocrinology and Diabetes, Prof. F. Alford, Prof. K. W. Ng, and Prof. R. MacIsaac.

REFERENCES

1. Bergman RN, Phillips LS, Cobelli C. Physiologic Evaluation of Factors Controlling Glucose Tolerance in Man: Measurement of Insulin Sensitivity and Beta-Cell Glucose Sensitivity From the Response to Intravenous Glucose. *J Clin Invest* (1981) 68(6):1456. doi: 10.1172/JCI110398
2. Bergman RN, Ider YZ, Bowden CR, Cobelli C. Quantitative Estimation of Insulin Sensitivity. *Am J Physiol-Endocrinol Metab* (1979) 1236(6):E667. doi: 10.1152/ajpendo.1979.236.6.E667
3. Toffolo G, Bergman RN, Finegood DT, Bowden CR, Cobelli C. Quantitative Estimation of Beta Cell Sensitivity to Glucose in the Intact Organism. *Diabetes* (1980) 29:12. doi: 10.2337/diabetes.29.12.979
4. Pacini G, Bergman RN. MINMOD: A Computer Program to Calculate Insulin Sensitivity and Pancreatic Responsivity From the Frequently Sampled Intravenous Glucose Tolerance Test. *Comput Methods Progr Biomed* (1986) 23(2):113–22. doi: 10.1016/0169-2607(86)90106-9
5. Martin IK, Weber KM, Ward GM, Best JD, Boston RC. Application of the SAAM Modeling Program to Minimal Model Analysis of Intravenous Glucose Tolerance Test Data. *Comput Methods Progr BioMed* (1990) 33 (4):193–203. doi: 10.1016/0169-2607(90)90070-P
6. Godsland IF, Walton C. Maximizing the Success Rate of Minimal Model Insulin Sensitivity Measurement in Humans: The Importance of Basal Glucose Levels. *Clin Sci* (2001) 101(1):1. doi: 10.1042/CS20000250
7. Ward GM, Weber KM, Walters JM, Aitken PM, Lee B, Best JD, et al. A Modified Minimal Model Analysis of Insulin Sensitivity and Glucose-Mediated Glucose Disposal in Insulin-Dependent Diabetes. *Metabolism* (1991) 40(1):4–9. doi: 10.1016/0026-0495(91)90183-W
8. Nakagawa S, Nakayama H, Sasaki T, Yoshino K, Yu YY, Shinozaki K, et al. A Simple Method for the Determination of Serum Free Insulin Levels in Insulin-Treated Patients. *Diabetes* (1973) 122(8):590–600. doi: 10.2337/diab.22.8.590
9. Hanning I, Home PD, Alberti KGMM. Measurement of Free Insulin Concentrations: The Influence of the Timing of Extraction of Insulin Antibodies. *Diabetologia* (1985) 28(11):831–5. doi: 10.1007/BF00291073
10. Albano JDM, Ekins RP, Maritz G, Turner RC. A Sensitive, Precise Radioimmunoassay of Serum Insulin Relying on Charcoal Separation of Bound and Free Hormone Moieties. *Acta Endocrinol (Copenh)* (1972) 70 (3):487–509. doi: 10.1530/acta.0.0700487
11. Ward GM, Walters JM, Barton J, Alford FP, Boston RC. Physiologic Modeling of the Intravenous Glucose Tolerance Test in Type 2 Diabetes: A New Approach to the Insulin Compartment. *Metabolism* (2001) 50(5):512–9. doi: 10.1053/meta.2001.21029
12. Ader M, Pacini G, Yang YJ, Bergman RN. Importance of Glucose Per Se to Intravenous Glucose Tolerance. *Diabetes* (1985) 34:12. doi: 10.2337/diabetes.34.11.1092
13. Nankervis A, Proietto J, Aitken P, Alford F. Impaired Insulin Action in Newly Diagnosed Type 1 (Insulin-Dependent) Diabetes Mellitus. *Diabetologia* (1984) 27(5):497–503. doi: 10.1007/BF00290383
14. Heurtault B, Reix N, Meyer N, Gasser F, Wendling M-J, Ratomponirina C, et al. Extensive Study of Human Insulin Immunoassays: Promises and Pitfalls for Insulin Analogue Detection and Quantification. *Clin Chem Lab Med CCLM* (2014) 52(3):355–62. doi: 10.1515/cclm-2013-0427
15. Parfitt C, Church D, Armston A, Couchman L, Evans C, Wark G, et al. Commercial Insulin Immunoassays Fail to Detect Commonly Prescribed Insulin Analogues. *Clin Biochem* (2015) 48(18):1354–7. doi: 10.1016/j.clinbiochem.2015.07.017
16. McAuley SA, Ward GM, Horsburgh JC, Gooley JL, Jenkins AJ, MacIsaac RJ, et al. Asymmetric Changes in Circulating Insulin Levels After an Increase Compared With a Reduction in Insulin Pump Basal Rate in People With Type 1 Diabetes. *Diabetes Med* (2017) 34(8):1158–64. doi: 10.1111/dme.13371
17. Walters JM, Ward GM, Kalfas A, Best JD, Alford FP. The Effect of Epinephrine on Glucose-Mediated and Insulin-Mediated Glucose Disposal in Insulin-Dependent Diabetes. *Metabolism* (1992) 41(6):671–7. doi: 10.1016/0026-0495(92)90062-F
18. Ward GM, Walters JM, Aitken PM, Kalfas A, Alford FP. Pulsatile Insulin Administration in Insulin-Dependent Type 1 Diabetes. *Diabetologia* (1990) 33 (S1):A35. doi: 10.1007/BF00401950
19. Welch S, Gebhart SSP, Bergman RN, Phillips LS. Minimal Model Analysis of Intravenous Glucose Tolerance Test-Derived Insulin Sensitivity in Diabetic Subjects. *J Clin Endocrinol Metab* (1990) 71(6):1508–18. doi: 10.1210/jcem-71-6-1508
20. Taniguchi A, Nakai Y, Fukushima M, Kawamura H, Imura H, Nagata I. Pathogenic Factors Responsible for Glucose Intolerance in Patients With NIDDM. *Diabetes* (1992) 41(12):1540–6. doi: 10.2337/diabetes.41.12.1540
21. Hovorka R, Soons PA, Young MA. ISEC: A Program to Calculate Insulin Secretion. *Comput Meth Prog BioMed* (1996) 50:253–64. doi: 10.1016/0169-2607(96)01755-5
22. Vethakkan SR, Jenkins AJ, Kay TWH, Goodman DJ, Walters JM, Gooley JL, et al. Improved Second Phase Insulin Secretion and Preserved Insulin

Sensitivity After Islet Transplantation. *Transplantation* (2010) 89(10):1291–2. doi: 10.1097/TP.0b013e3181d45ab3
23. Rickels MR, Naji A, Teff KL. Acute Insulin Responses to Glucose and Arginine as Predictors of Beta-Cell Secretory Capacity in Human Islet Transplantation. *Transplantation* (2007) 84(10):1357–60. doi: 10.1097/01.tp.0000287595.16442.a7
24. Rickels MR, Schutta MH, Mueller R, Markmann JF, Barker CF, Naji A, et al. Islet Cell Hormonal Responses to Hypoglycemia After Human Islet Transplantation for Type 1 Diabetes. *Diabetes* (2005) 54(11):3205–11. doi: 10.2337/diabetes.54.11.3205
25. Ward GM, Walters JM, Gooley JL, Vethakkan SR, Krishnapillai M, Boston RC, et al. Delay in Insulin Secretion Following an Oral Glucose Load After Islet Transplantation in Human Type 1 Diabetes. *Proc Aust Diabetes Soc Annu Sci Meeting* (2017).
26. Vethakkan SR, Walters JM, Gooley JL, Boston RC, Kay TW, Goodman DJ, et al. The Incretin Response After Successful Islet Transplantation. *Transplantation* (2014) 97(2):e9–e11. doi: 10.1097/01.TP.0000437565.15965.67
27. *Collaborative Islet Transplant Registry (Citr). Citr Tenth Annual Report. [Internet]* (2017). Available at: https://citregistry.org/system/files/10th_AR.pdf.
28. Vethakkan SR, Walters JM, Gooley JL, Boston RC, Kay TWH, Goodman DJ, et al. Normalized NEFA Dynamics During an OGTT After Islet Transplantation. *Transplant J* (2012) 94(7):e49–51. doi: 10.1097/TP.0b013e3182696a39
29. O'Connell PJ, Holmes-Walker DJ, Goodman D, Hawthorne WJ, Loudovaris T, Gunton JE, et al. On Behalf of the Australian Islet Transplant Consortium. Multicenter Australian Trial of Islet Transplantation: Improving Accessibility and Outcomes: Multicenter Trial of Islet Transplantation. *Am J Transplant* (2013) 13(7):1850–8. doi: 10.1111/ajt.12250
30. Eisenbarth GS. Type I Diabetes Mellitus. *N Engl J Med* (1986) 314(21):1360–8. doi: 10.1056/NEJM198605223142106
31. Bergman RN, Ader M, Huecking K, Van Citters G. Accurate Assessment of -Cell Function: The Hyperbolic Correction. *Diabetes* (2002) 51(Supplement 1):S212–20. doi: 10.2337/diabetes.51.2007.S212
32. Elahi D, Nagulesparan M, Hershcopf RJ, Muller DC, Tobin JD, Blix PM, et al. Feedback Inhibition of Insulin Secretion by Insulin: Relation to the Hyperinsulinemia of Obesity. *N Engl J Med* (1982) 306(20):1196–202. doi: 10.1056/NEJM198205203062002
33. Godsland IF, Agbaje OF, Hovorka R. Evaluation of Nonlinear Regression Approaches to Estimation of Insulin Sensitivity by the Minimal Model With Reference to Bayesian Hierarchical Analysis. *Am J Physiol-Endocrinol Metab* (2006) 291(1):E167–74. doi: 10.1152/ajpendo.00328.2004
34. Hovorka R. Continuous Glucose Monitoring and Closed-Loop Systems. *Diabetic Med* (2006) 23(1):1–12. doi: 10.1111/j.1464-5491.2005.01672.x
35. Jayawardene DC, McAuley SA, Horsburgh JC, Gerche AL, Jenkins AJ, Ward GM, et al. Closed-Loop Insulin Delivery for Adults With Type 1 Diabetes Undertaking High-Intensity Interval Exercise Versus Moderate-Intensity Exercise: A Randomized, Crossover Study. *Diabetes Technol Ther* (2017) 19(6):340–8. doi: 10.1089/dia.2016.0461

Conflict of Interest: The authors declare that the research was conducted in the absence of any commercial or financial relationships that could be construed as a potential conflict of interest.

Advantages of publishing in Frontiers

OPEN ACCESS
Articles are free to read for greatest visibility and readership

FAST PUBLICATION
Around 90 days from submission to decision

HIGH QUALITY PEER-REVIEW
Rigorous, collaborative, and constructive peer-review

TRANSPARENT PEER-REVIEW
Editors and reviewers acknowledged by name on published articles

Frontiers
Avenue du Tribunal-Fédéral 34
1005 Lausanne | Switzerland

Visit us: www.frontiersin.org
Contact us: frontiersin.org/about/contact

REPRODUCIBILITY OF RESEARCH
Support open data and methods to enhance research reproducibility

DIGITAL PUBLISHING
Articles designed for optimal readership across devices

FOLLOW US
@frontiersin

IMPACT METRICS
Advanced article metrics track visibility across digital media

EXTENSIVE PROMOTION
Marketing and promotion of impactful research

LOOP RESEARCH NETWORK
Our network increases your article's readership